Philipps-Universität Marburg

Fachbereich Biologie

Development of novel orthogonal genetic circuits, based on extracytoplasmic function (ECF) σ factors

Dissertation
zur
Erlangung des Doktorgrades
der Naturwissenschaften
(Dr. rer. nat.)

vorgelegt von

Stefano Vecchione

Aus Neapel

Marburg, Juli 2019

Die Untersuchungen zur vorliegenden Arbeit wurden von Dezember 2015 bis Juni 2019 am LOEWE-Zentrum für Synthetische Mikrobiologie (SYNMIKRO) der Philipps-Universität Marburg unter der Leitung von Dr. Georg Fritz durchgeführt.

Erstgutachter: Dr. Georg Fritz
Zweitgutachter: Prof. Dr. Anke Becker
Am Fachbereich angenommen am: 03.09.2019
Tag der mündlichen Prüfung: 10.09.2019

Eidesstattliche Erklärung

Hiermit erkläre ich, dass die vorliegende Dissertation:
“Development of novel orthogonal genetic circuits, based on extracytoplasmic function (ECF) σ factors” von mir selbstständig und ohne unerlaubte Hilfsmittel angefertigt wurde. Es wurden keine anderen als die von mir angegebenen Quellen verwendet. Zudem versichere ich, dass die Dissertation in dieser oder ähnlicher Form noch bei keener anderen Hochschule eingereicht wurde.

……
Stefano Vecchione, Marburg, 11 Juli 2019

Publications

[I] Mauri M., Vecchione S., Fritz G. Deconvolution of luminescence cross-talk in high-throughput gene expression profiling. *ACS Synthetic Biology* (2019)

[II] Vecchione S., Fritz G. CRIMoClo plasmids for modular assembly and orthogonal chromosomal integration of synthetic circuits in *Escherichia coli* (under review in Journal of Biological Engineering)

[III] Pinto D*., Vecchione S*., Wu H., Mauri M., Mascher T., Fritz G. Engineering orthogonal synthetic timer circuits based on extracytoplasmic function σ factors. *Nucleic Acids Research* (2018)

*First author contribution

Selected talks and posters

[I] Poster at the VAAM conference in Jena (2016): Vecchione S., Mauri M., Fritz G. Development of novel orthogonal genetic circuits based on Extracytoplasmic function (ECF) σ factors.

[II] Poster at the VAAM conference in Wuerzburg (2017): Mauri M., Vecchione S., Fritz G. Deconvolution of luminescence cross-talk in high-throughput gene expression profiling.

[III] Talk at the Systems Biology meets Synthetic Biology conference in Frankfurt (2017): Vecchione S., Pinto D., Wu H., Mauri M., Mascher T., Fritz G. Engineering orthogonal synthetic timer circuits in bacteria.

[IV] Poster at the GASB I - conference on Synthetic Biology in Marburg (2017): Vecchione S., Diehl A., Fritz G. CRIMoClo: conditional-replication, integration, and modular cloning plasmids for synthetic biology applications in *Escherichia coli*.

[V] Poster at the international conference How microorganisms see their world in Marburg (2018): Vecchione S., Diehl A., Fritz G. CRIMoClo: conditional-replication, integration, and modular cloning plasmids for synthetic biology applications in *Escherichia coli*.

[VI] Talk at iGEM meetup Germany in Marburg (2018): Vecchione S., Pinto D., Wu H., Mauri M., Mascher T., Fritz G. Engineering orthogonal synthetic timer circuits in bacteria.

[VII] Talk at VAAM conference in Mainz (2019): Vecchione S., Diehl A., Fritz G. Design and characterization of synthetic ECF σ/anti-σ threshold gate genetic circuit in *Escherichia coli*.

Table of contents

Acknowledgements

I want to thank my supervisor Dr. Georg Fritz for giving me the opportunity to work on this interesting project. Georg, I would like to thank you for your support, your unlimited enthusiasm the helpful discussions and for pushing my limits. It has been a real pleasure to work with you.

I am grateful to Prof. Dr. Anke Becker for her support and for giving me the opportunity to conduct the first year of my PhD thesis in her laboratory at the SYNMIKRO in Marburg.

I am thankful to my thesis committee members for the advice they provided during our meetings. In particular, I would like to thank Prof. Dr. Thorsten Waldminghaus for providing some of the plasmids and bacterial strains used in this study and for his advice and the interesting discussions during the German lunch hour.

I would like to thank Dr. Marco Mauri, Luis M. Oviedo Bocanegra, and Delia Casas Pastor for the insightful discussions during the Italian lunch hour.

Many thanks to Daniel Schindler, Johannes Döhlemann and Doreen Meyer for their precious scientific advice and Calin C. Guet and Anna Staroń for sharing the CRIM plasmids.

I'm thankful to Dr. Marco Mauri, Andre Sim, Delia Casas Pastor and Benjamin Daniel for the constructive criticism on the draft of this dissertation.

My thanks also go to our project collaborators Prof. Dr. Anke Becker, Prof. Dr. Carol A. Gross, Prof. Dr. Mark J. Buttner, and Prof. Dr. Thorsten Mascher, Prof. Dr. Alexander Goesmann that are part of the ERA-SynBio consortium "ECFexpress" that founded this project.

Zusammenfassung

Das Feld der synthetischen Biologie zielt darauf ab die Ingenieursprinzipien des „Design-Build-Test-Learn“ Kreislaufs auf die Implementierung synthetischer genetischer Schaltkreise, welche das Verhalten biologischer Systeme beeinflussen, anzuwenden. Um dieses Ziel zu erreichen verwenden Projekte der synthetischen Biologie eine Reihe komplett charakterisierter biologiescher Bauteile. Diese können nach rationalen, Modell gestützten Gesichtspunkten, stufenweisen zu komplexen synthetischen Schaltkreisen kombiniert werden. Die Konstruktion aus einfachen, charakterisierten Bauteilen stellt einen optimalen Startpunkt für das Testen synthetischer Schaltkreise dar. Deren Design ist allerdings durch die beschränkte Verfügbarkeit von DNA-Bausteinen limitiert. Für gewöhnlich bestehen sie nur aus einer Handvoll von Transkriptionsregulatoren, welche zusätzlich häufig aus natürlichen Systemen entliehen wurden. Dies kann zu Kreuzreaktionen zwischen den implementierten Schaltkreisen und Wirt, und damit einem Verlust der Funktion führen. Eine der Herausforderungen der synthetischen Biologie ist daher die Entwicklung solcher synthetischen Systeme mit minimalen Kreuzreaktionen (Orthogonalität).

Das Ziel dieses Projektes ist es, die Einschränkungen verbreiteter transkriptioneller Regulatoren durch die Anwendung von Extra-Zytoplasmischen σ-Faktoren (ECF) zu überwinden. ECFs sind die kleinsten und einfachsten alternativen σ-Faktoren welche Promotoren mit hoher Spezifität erkennen. Sie stellen einen der wichtigsten Mechanismen der Signalübertragung in Bakterien dar. Ihre Aktivität ist häufig von Anti σ-Faktoren kontrolliert. Auch wenn gezeigt wurde, dass Anti-σ-Faktoren negative Effekte auf den Wirt haben können stellen sie eine attraktive Möglichkeit dar ECFs zu regulieren. Zu diesem Zeitpunkt kennen wir tausende ECF σ-Faktoren aus einem Großteil der Bakterien-Phyla. Durch bioinformatische Analysen sind sie und auch das dazugehörige Anti-σ-Faktoren identifizierbar.

All diese Eigenschaften machen ECFs zu optimalen Kandidaten für das Design orthogonaler, synthetischer Schaltkreise. Um ECF σ-Faktoren als Standardbausteine in der synthetischen Biologie zu etablieren, haben wir zuerst eine Methode für Hochdurchsatzmessungen entwickelt. Diese basiert auf Mikro-Plate-Reader Experimenten, bei denen hochsensible Lumineszenz-Reporter verwendet werden. Dank ihres niedrigen Hintergrundrauschens sind sie Fluoreszenz-Reportern überlegen, da sie eine größere dynamische Spanne abdecken können. Von Nachteil ist das Durchscheinen emittierten Lichts von einem Töpfchen in die benachbarten, was die dort gemessenen Werte beeinflusst. Um diese Einschränkung zu überwinden haben wir einen computergestützten Algorithmus entwickelt der dieses Durchscheinen aus dem Signal herausrechen kann um die tatsächlichen Werte zu erhalten.

In dieser Arbeit zeigen wir, dass der Algorithmus auch Signale knapp über dem Hintergrund erhält und universell für verschiedene experimentelle Bedingungen einsetzbar ist. Um die Assemblierung großer, ECF basierter Schaltkreise zu vereinfachen haben wir eine Sammlung von ECF Bausteinen in *E. coli* konstruiert. Diese Sammlung ermöglicht, in Kombination mit einer anderen Sammlung kompatibler Bausteine, eine die Kombination quasi aller ECFs in großen Schaltkreisen. Zusätzlich ermöglicht es die Integration der so gebauten synthetischen Schaltkreise in vier verschiedenen Phagen-Insertions-Loci (*att*) im *E. coli* Genom. Das erlaubt den direkten Übergang zwischen Plasmid basierter Expression und Expression von gnomisch integrierten Schaltkreisen. Dadurch wird die Zahl der möglichen Konfigurationen jedes Schaltkreises erheblich

erhöht. Zusätzlich konnten wir zeigen, dass die vier *att*-Loci sich bezüglich der Expression integrierter synthetischer Schaltkreise zueinander orthogonal verhalten.

Um ECF basierte, synthetische Schaltkreise rational Planen zu können haben wir das dynamische Verhalten von 15 ECF σ-Faktoren, sowie deren Anti-σ-Faktoren und zugehörigen Promoter, charakterisiert. Abschließend können wir feststellen, dass ECFs funktionieren, unterschiedliche Affinitäten zu ihren zugehörigen Promotoren haben und dabei nicht Toxisch wirken. Unsere Ergebnisse zeigen, dass die dynamische Spanne sowie die Stärke des Eingangs und Ausgangssignals, der ECF-basierten Schalter abhängig von der Kopienzahl der ECF und Zielpromotor eingestellt werden kann. Durch die Kombination von bis zu drei ECF-Schaltern konnten wir genetische Zeitmesser bauen. Dies waren die ersten synthetischen Schaltkreise mit mehreren ECFs. Die ECF Zeitmesser können eine Auswahl von Zielgenen zeitversetzt aktivieren und ihr verhalten kann mittels eigens entwickelter mathematischer Modelle vorhergesagt werden. Um die dynamische Spanne der ECF Konstrukte zu erhöhen fügten wir Anti-σ-Faktoren hinzu. Dabei vielen uns schnell negative Effekte auf das Wachstum von *E. coli* auf für die wir nach Lösungen suchten. Wir konnten demonstrieren, dass diese negativen Effekte teilweise verringert werden können, wenn gekürzte, lösliche Varianten der Anti-σ-Faktoren verwendet werden. Darauf aufbauend fanden wir, dass die Toxizität komplett behoben werden kann, wenn diese chromosomal integriert werden. Abschließend, nachdem wir zeigen konnten, dass Anti-σ-Faktoren verwendet werden können um einstellbare Verzögerungen in der ECF Expression zu erreichen, konstruierten wir ECF/AS-Selbstmord Schalter. Diese Schaltkreise erlauben das Einstellen eines Zeitverzögerten Zelltods in *E. coli* und können als Prototypen für die zukünftige Entwicklung von ECF/AS-basierten Autolyse-Schaltkreisen dienen.

Abstract

The synthetic biology field aims to apply the engineering 'design-build-test-learn' cycle for the implementation of synthetic genetic circuits modifying the behavior of biological systems. In order to reach this goal, synthetic biology projects use a set of fully characterized biological parts that subsequently are assembled into complex synthetic circuits following a rational, model-driven design. However, even though the bottom-up design approach represents an optimal starting point to assay the behavior of the synthetic circuits under defined conditions, the rational design of such circuits is often restricted by the limited number of available DNA building blocks. These usually consist only of a handful of transcriptional regulators that additionally are often borrowed from natural biological systems. This, in turn, can lead to cross-reactions between the synthetic circuit and the host cell and eventually to loss of the original circuit function. Thus, one of the challenges in synthetic biology is to design synthetic circuits that perform the designated functions with minor cross-reactions (orthogonality).

To overcome the restrictions of the widely used transcriptional regulators, this project aims to apply extracytoplasmic function (ECF) σ factors in the design novel orthogonal synthetic circuits. ECFs are the smallest and simplest alternative σ factors that recognize highly specific promoters. ECFs represent one of the most important mechanisms of signal transduction in bacteria, indeed, their activity is often controlled by anti-σ factors. Even though it was shown that the overexpression of heterologous anti-σ factors can generate an adverse effect on cell growth, they represent an attractive solution to control ECF activity. Finally, to date, we know thousands of ECF σ factors, widespread among different bacterial phyla, that are identifiable together with the cognate promoters and anti-σ factors, using bioinformatic approaches.

All the above-mentioned features make ECF σ factors optimal candidates as core orthogonal regulators for the design of novel synthetic circuits. In this project, in order to establish ECF σ factors as standard building blocks in the synthetic biology field, we first established a high throughput experimental setup. This relies on microplate reader experiments performed using a highly sensitive luminescent reporter system. Luminescent reporters have a superior signal-to-noise ratio when compared to fluorescent reporters since they do not suffer from the high auto-fluorescence background of the bacterial cell. However, they also have a drawback represented by the constant light emission that can generate undesired cross-talk between neighboring wells on a microplate. To overcome this limitation, we developed a computational algorithm that corrects for luminescence bleed-through and estimates the “true” luminescence activity for each well of a microplate. We show that the correcting algorithm preserves low-level signals close to the background and that it is universally applicable to different experimental conditions.

In order to simplify the assembly of large ECF-based synthetic circuits, we designed an ECF toolbox in *E. coli*. The toolbox allows for the combinatorial assembly of circuits into expression vectors, using a library of reusable genetic parts. Moreover, it also offers the possibility of integrating the newly generated synthetic circuits into four different phage attachment (*att*) sites present in the genome of *E. coli*. This allows for a flawless transition between plasmid-encoded and chromosomally integrated genetic circuits, expanding the possible genetic configurations of a given synthetic construct. Moreover, our results demonstrate that the four *att* sites are orthogonal in terms of the gene expression levels of the synthetic circuits.

With the purpose of rationally design ECF-based synthetic circuits and taking advantage of the ECF toolbox, we characterized the dynamic behavior of a set of 15 ECF σ factors, their cognate promoters, and relative anti-σs. Overall, we found that ECFs are non-toxic and functional and that they display different binding affinities for the cognate target promoters. Moreover, our results show that it is possible to optimize the output dynamic range of the ECF-based switches by changing the copy number of the ECFs and target promoters, thus, tuning the input/output signal ratio. Next, by combining up to three ECF-switches, we generated a set of "genetic-timer circuits", the first synthetic circuits harboring more than one ECF. ECF-based timer circuits sequentially activate a series of target genes with increasing time delays, moreover, the behavior of the circuits can be predicted by a set of mathematical models.

In order to improve the dynamic response of the ECF-based constructs, we introduced anti-σ factors in our synthetic circuits. By doing so we first confirmed that anti-σ factors can exert an adverse effect on the growth of *E. coli*, thus we explored possible solutions. Our results demonstrate that anti-σ factors toxicity can be partially alleviated by generating truncated, soluble variants of the anti-σ factors and, eventually, completely abolished via chromosomal integration of the anti-σ factor-based circuits. Finally, after demonstrating that anti-σ factors can be used to generate a tunable time delay among ECF expression and target promoter activation, we designed ECF/AS-suicide circuits. Such circuits allow for the time-delayed cell-death of *E. coli* and will serve as a prototype for the further development of ECF/AS-based lysis circuits.

1. Introduction

In this introductory chapter, we briefly introduce one the major challenge in synthetic biology, defining the principle of "orthogonality". Then, we illustrate different DNA manipulation strategies that are currently used for the generation of synthetic circuits, highlighting their advantages and limitations. Finally, we introduce Extracytoplasmic function (ECF) σ factors and their regulators, anti-σ factors, as a strategy to enhance the context-independency of synthetic circuits.

1.1 Facing the unpredictability of the living systems: a major challenge in synthetic biology

Synthetic biology is described as a field that aims to apply engineering principles (such as standardization, modularity, and simplicity) to the biological systems, with the aim of engineering them to perform new tasks[1]. To date, even though the engineering of the biological systems has brought impressive accomplishments[2–4], synthetic biology projects are frequently frustrated when engineering faces the complexity of the living cell[5]. Such complexity arises from the interconnection of all the compounds within the living cell that generates context-dependences and poses a challenge in the development of synthetic circuits[6]. Indeed, context-dependences can affect both the host and the performance of the heterologous genetic circuit, leading ultimately to the unpredictability of the system behavior[7]. For instance, the expression of a synthetic circuit can lead to toxic side effects on the host cell, due to competition for shared cellular resources, such as metabolites, RNA polymerase or ribosomes[8]. At the same time, the natural cellular processes, such expression of endogenous transcription factors, as well as different genetic backgrounds, can affect the functionality and the stability of a heterologous genetic circuit[5]. Hence, one of the major challenges in synthetic biology consists in the development of truly context-independent (i.e. orthogonal) genetic circuits that perform their function with minor cross-reactions. To achieve this goal, the synthetic biology field aims to apply a rational, model-driven design that allows for a robust characterization of the individual genetic parts. This allows their combination in complex circuits that feature a predictable response under certain conditions[9]. However, only by combining the rational design approach, together with the development of strategies that limit the context-dependence, the SynBio field will ultimately succeed in minimizing the undesired cross-reactions with the host cell and increase the orthogonality of the genetic circuits.

1.2 DNA manipulation strategies for the design of synthetic circuits

In synthetic biology, the rational design of genetic circuits can be facilitated by implementing engineering principles, such as standardization, modularity, and simplicity. Indeed, the use of standardized, modular DNA parts, will improve the engineering 'design-build-test-learn' cycle in biology, encouraging, at the same time, the sharing of genetic parts and facilitating automated processes[10]. In the design of synthetic circuits applying a bottom-up approach, each DNA-encoded component such as a promoter or an open reading frame can be considered as an isolated part[1]. Ideally, a robust characterization of these individual parts allows their combination in increasingly complex circuits. Within this vision, simple genetic parts (such as promoters, ribosome binding sequences, coding sequences, and terminators) are combined in transcription units, which are further combined to assemble biosynthetic pathways, that can ideally lead to the generation of synthetic genomes[9]. Thus, another challenge for synthetic biology consists in the establishment of standardized assembly methods that allow for a hierarchical assembly and ideally, for the

generation of part libraries. Such libraries allow a combinatorial approach in the circuit assembly and simplify the sharing of the genetic parts within the SynBio community.

Along the years the scientific community established a plethora of DNA manipulation strategies to achieve modularity and standardization goals. The BioBrick standard was established more than a decade ago and represented one of the first attempt to standardize a restriction enzyme-based DNA assembly method. In the Biobrick standard, DNA parts have standardized flanking sequences that are useful for the assembly by traditional restriction/ligation methods[11,12]. With BioBrick it became possible to create a series of modular biological parts that could be shared and easily assembled in different combinations[9]. The reusability and simplicity of BioBricks make them popular, thus helping the augmentation of the genetic parts encoded in this standard. However, despite the standardization advantages, Biobricks have some drawbacks. For instance, the length of the fusion scar (that is generated by the assembly of two BioBricks parts), can act as a destabilizing sequence in *E. coli*[13], and the presence of an in-frame stop codon in the fusion scar is problematic when assembling fusion proteins[9]. Moreover, the DNA sequences need to be cured for eventual restriction sites, relative to the endonucleases used in the digestion procedure. Even though the scientific community attempted to alleviate these issues -e.g. by shortening the fusion sites[14], creating standards to assist assembly of fusion proteins[9] and using enzymes with rare restriction sites[15] no Biobrick-based method allows scar-less assembly of the genetic parts. Moreover, the BioBrick parts can only be assembled in pairs, and the digestion and ligation processes take place in separate reactions. This makes the construction of multipart constructs time-consuming and labor-intensive.

There are different techniques that allow for scar-less assembly of DNA fragments and that do not require classic digest-ligation reactions, such as overlap extension polymerase chain reaction (OE-PCR)[16] and its evolution: Circular Polymerase Extension Cloning (CPEC)[17]. However, the assembly of DNA parts with these techniques relies on PCR-amplification, which is prone to errors when applied to large genetic constructs[18].

A major innovation in the scar-less DNA assembly techniques came with the development of the Isothermal Assembly Reaction (Gibson assembly)[19] and the Ligase cycling Reaction (LCR)[20]. These methodologies allow for ordered assembly of multiple genetic parts and do not strictly depend on PCR-amplification. In particular, Gibson assembly relies on overlapping sequences encoded on the genetic parts and three enzymes (5' exonuclease, DNA polymerase and DNA ligase) that work in a one-pot reaction (Figure 1.1). During the assembly procedure, the 5' exonuclease digests the 5' end of double-stranded DNA fragments and generates 3' single-stranded overhangs. Thus, two or more DNA fragments that have 20-40bp of homology at their ends can anneal to each other thanks to the resulting complementary overhangs. The polymerase fills in any remaining regions of single-stranded DNA and then the ligase fuses the nicks, generating a single DNA fragment. A major benefit of this method is that it allows the assembly of large DNA constructs, even bacterial artificial chromosomes (BACs)[19]. However, one of the drawbacks of the Gibson assembly is that it does not enable the assembly of more than four DNA parts with more than 50% of clones being correct[20].

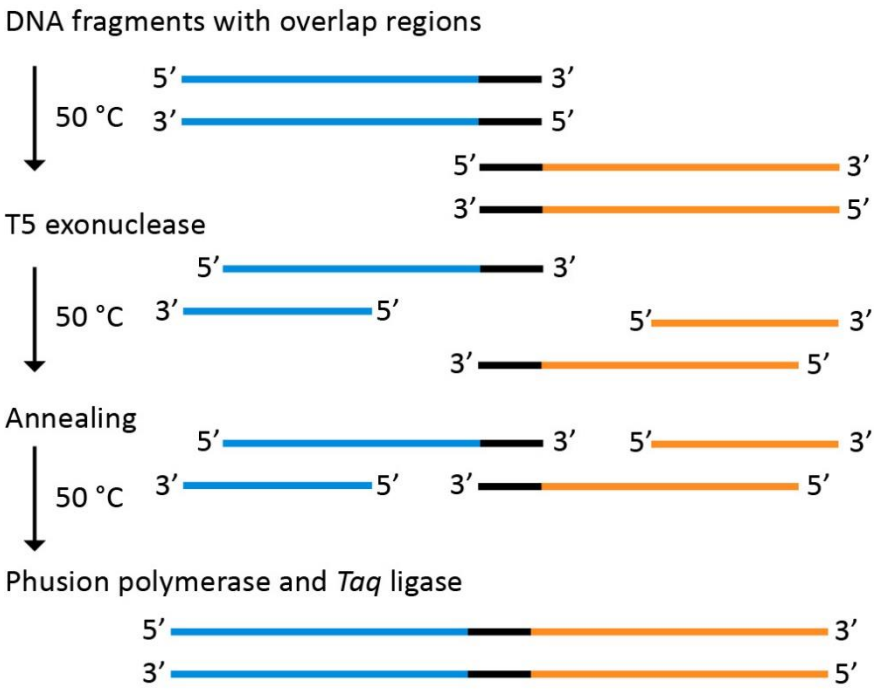

Figure 1.1. Gibson assembly. Two DNA fragments (blue and orange) sharing terminal sequence overlaps (black) are joined into a covalently sealed molecule in a one-step isothermal reaction. T5 exonuclease removes nucleotides from the 5' ends of double-stranded DNA molecules, complementary single-stranded DNA overhangs anneal, Phusion DNA polymerase fills the gaps and Taq DNA ligase seals the nicks. T5 exonuclease is heat-labile and is inactivated during the 50 °C incubation.

A solution to this problem was given by de Kok and collaborators, that developed the DNA assembly via LCR that allows the assembly of up to 12 DNA parts, with 60−100% of correct individual clones[20]. The one-step, scarless DNA assembly via LCR uses single-stranded bridging oligos that are complementary to the ends of DNA parts to be assembled. The procedure includes an initial denaturation at high temperature followed by a temperature downshift that allows the annealing of the upper (or lower) strands of neighboring DNA, on both halves of the provided bridging oligo. Then a thermostable ligase joins the neighboring DNA parts via a phosphodiester bond without the introduction of any scar sequence. In the subsequent denaturation−annealing−ligation temperature cycles, the assembled strand serves as a template for the assembly of the other strand from neighboring DNA parts. Finally, by applying multiple temperature cycles, many DNA parts are assembled into complex DNA constructs (Figure 1.2).

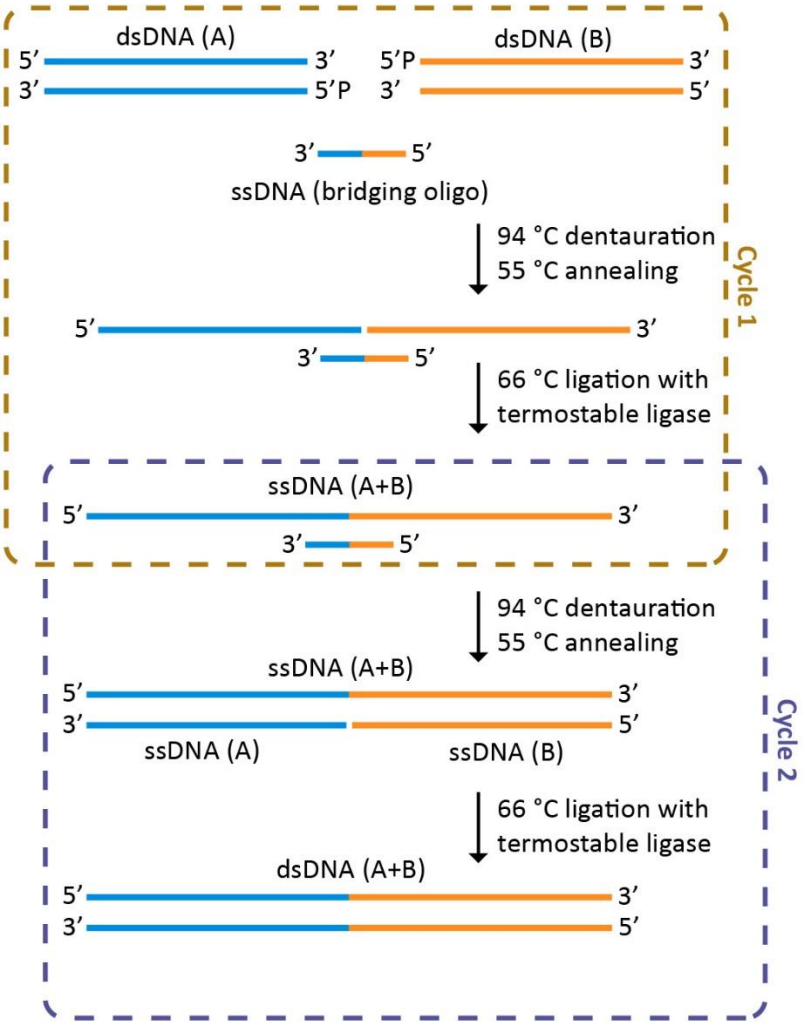

Figure 1.2. LCR assembly. In the first temperature cycle custom single-stranded bridging oligos, complementary to the ends of neighboring DNA parts, serve as a template to bring the upper strands of denatured DNA parts together, after which a thermostable ligase joins the DNA fragments. In the second and subsequent temperature cycles, the assembled upper strand serves as a template for ligation of the lower strand. Multiple denaturation−annealing−ligation temperature cycles are used for assembly of many DNA parts into complex DNA constructs.

Both LCR and Gibson assembly, do not require the restriction/digestion step, thus increasing the speed of the assembly and facilitating the generation of complex synthetic DNA constructs. Hence, both methodologies have great advantages, for instance speeding up the construction or modification of plasmids[21]. However, even though in both methodologies the assembly of the genetic parts does not rely on PCR-amplification, the generation of the DNA parts involved in the reaction is often achieved with this technique. This implies the limitation in the DNA fragment sizes described above and even though the chemical synthesis of the genetic fragments represent a solution, to date, it is still a costly and slow process. Finally, both LCR and Gibson assembly do not favor the storage of the single genetic parts, thus limiting the combinatorial assembly and the sharing of the parts on a large scale.

The need for assembly techniques that allow for scaling-up the combinatorial assembly, led to the development of new methods based on Type IIs restriction enzymes. These enzymes have the peculiarity of cutting outside their recognition sequence, generating 4 bp overhangs[22,23]. The

utilization of Type IIs restriction enzymes led to the invention of the Golden Gate assembly method, in which the customization of the 4bp overhangs allows for the assembly of neighboring fragments. Indeed, the design of DNA parts with compatible overhangs allows their directional cloning and since Type IIS restriction sites are eliminated during the cloning procedure, digestion and ligation reactions can take place in the same tube at the same time. Thus, Golden Gate cloning allows fast and reliable multi-part DNA assembly, but it also requires the accurate design cloning vectors. Indeed, the destination vector must have the appropriate Type IIS restriction sites and overhangs, in order to be compatible with the other DNA fragments involved in the assembly reaction.

1.2.1 The Modular Cloning (MoClo) system

A major enhancement of the original Golden Gate Assembly framework came with the development of the Modular Cloning (MoClo) system that enables not only the hierarchical assembly of multigene constructs but also the combinatorial assembly of large (33kb in the original publication) genetic circuits from a library of fully reusable parts[24]. The design of synthetic circuits greatly benefits from a combinatorial approach in the circuit assembly allowing, for instance, to randomize the topology of a circuit[25]. Thus, the MoClo system represents a precious resource for the circuit design in the synthetic biology field. The MoClo system provides a series of vectors that are equipped with a *lacZa* fragment (for blue/white selection) flanked by two pairs of different Type IIS restriction sites (BpiI and BsaI), for the generation of pre-defined 4bp overhangs called fusion sites (Figure 1.3). The DNA sequences of the fusion sites determine the order of the multi-part assembly and, different resistance cassettes, together with the positioning of the two pairs of Type IIS restriction sites, define different hierarchically organized MoClo levels (0, 1, M and P)[24,26]. Thus, by the addition of the appropriate Type IIS restriction site and compatible fusion sites, a given DNA fragment can be cloned into the MoClo vector system, generating a MoClo part. Subsequently, the design characteristics of the MoClo, allow for the assembly of several parts encoded within a MoClo level, into a MoClo destination vector belonging to a higher level.

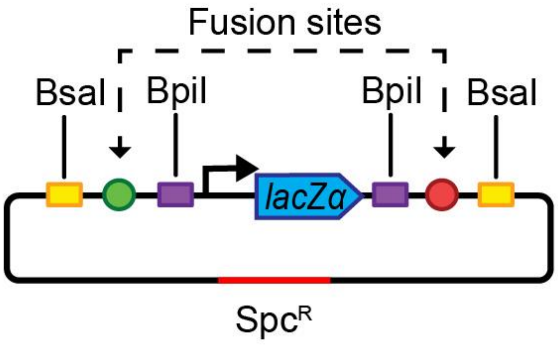

Figure 1.3. Level 0 MoClo destination vector. The positioning of the two pairs of Type IIs restriction sites (BpiI and BsaI) allows the generation of pre-defined 4bp overhangs (fusion sites). In level 0 vectors, BpiI restriction sites are used for cloning a DNA fragment into the destination vector, while BsaI restriction sites allow the combination of multiple level 0 parts into level 1 destination vectors. The *lacZa* fragment allows the screening for successful cloning events, through blue/white colony selection.

The entry vectors of the MoClo system are defined as level 0 (Figure 1.3). Upon PCR amplification, oligo annealing, or gene synthesis, a genetic part can be easily cloned in one of 16 different level 0 vectors, via Golden Gate cloning, generating a level 0 part. Up to 8 level 0 parts can be then assembled in any level 1 destination vector, generating transcription units (TUs) (Figure 1.4).

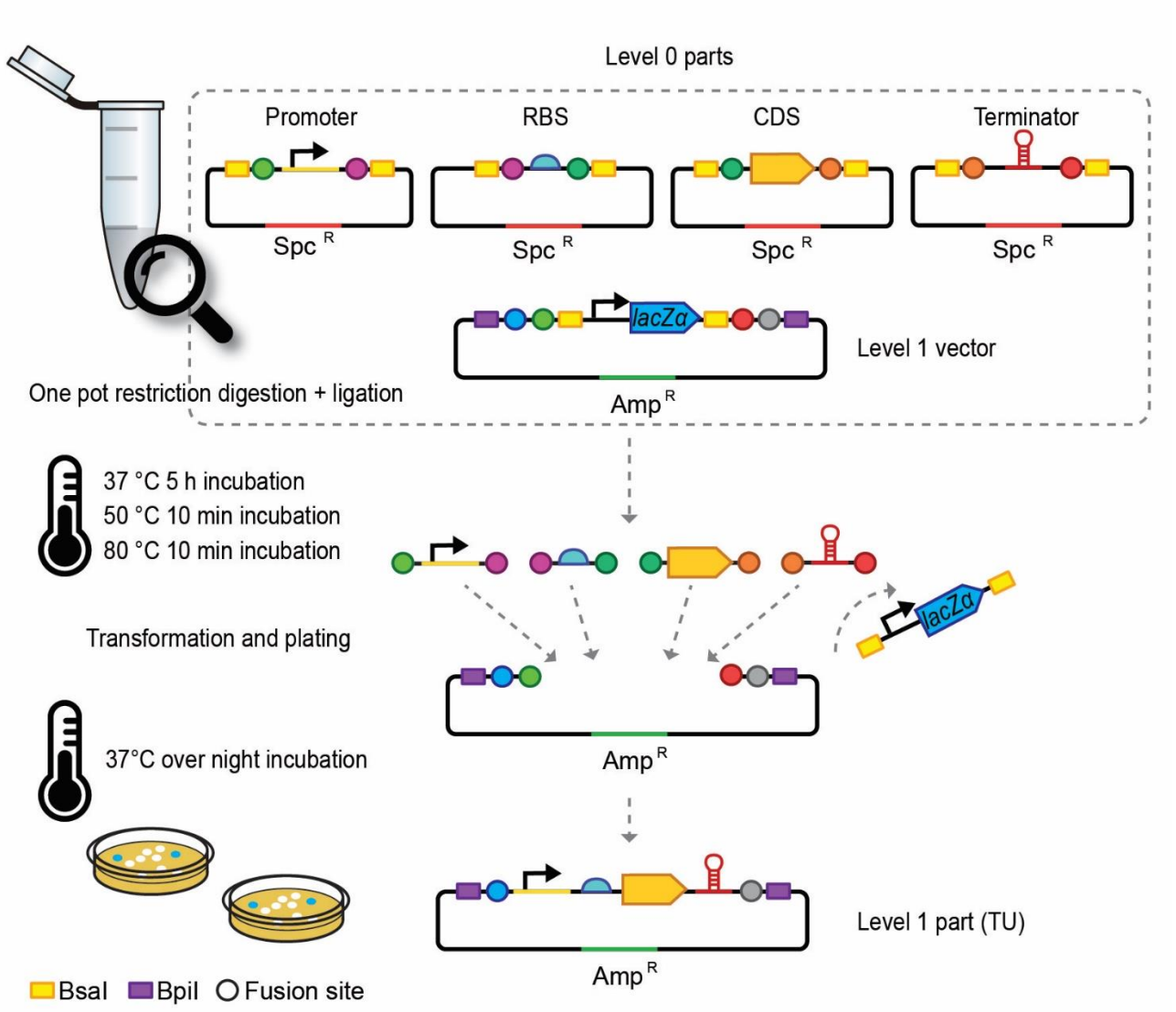

Figure 1.4. Assembly of multiple level 0 parts into a level 1 destination vector. Up to 8 levels 0 parts can be assembled in a level 1 destination vector via Golden Gate cloning. The simultaneous digestion of the genetic parts and of the destination vector, using the same Type IIs restriction enzyme (BsaI), generates compatible fusion sites, determining the order of the multi-part assembly. The digestion and ligation reactions take place in the same tube at the same time in a 5 h reaction. The deactivation of the enzymes is induced by two temperature shift steps (50° C and 80° C) lasting 10 min each. The selection for successful cloning events is facilitated by the presence of the *lacZa* fragment in the destination vector, that is eliminated during the cloning procedure. A different pair of Type IIs restriction sites (BpiI), present in the destination vector, allows, in a further reaction, for the assembly of multiple level 1 parts into a level M destination vector.

There are two sets of level 1 destination vectors (each one including 7 vectors) that can be used for cloning the TUs in forward or in reverse orientation, starting from the same set of level 0 parts. Independently from the orientation, up to six level 1 TUs can be then cloned into level M vectors, and subsequently, up to 6 level M parts can be assembled into level P vectors. Finally, the system allows for a continuous assembly of parts from level P to level M and *vice versa*, allowing the design of complex genetic pathways (Figure 1.5). The possibility of continuous cycling between level M and level P assembly was not available in the original MoClo system, in which the final destination vectors for the circuits assembly were defined as level 2. However, a further revision of the system, by their own inventors, introduced this possibility, using a novel set of destination vectors (level M and level P), together with a series of so-called "end-linkers". For a detailed explanation of the end-linkers and their utilization for cloning the constructs in level M and P vectors, we recommend consulting the original publication[26].

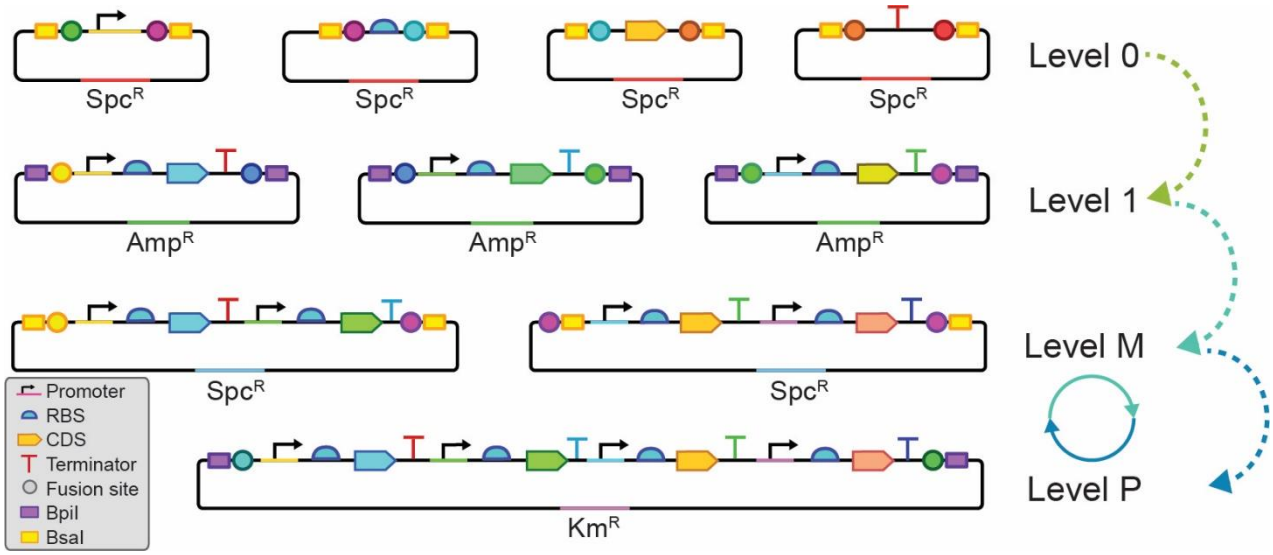

Figure 1.5 Hierarchal assembly of multiple genetic parts within the MoClo framework. Up to 8 fragments, from a library of level 0 parts, can be assembled in transcription units encoded in level 1 vectors, which in turn serve to generate level M genetic circuits. Up to six level M genetic circuits can be combined in level P destination vectors, generating complex genetic pathways. The MoClo system allows for continuous cycling between level M and level P assembly.

With the availability of 16 levels 0 entry vectors and the above-described features, the MoClo represent an optimal choice to generate a library of genetic parts, that can then be used to generate complex synthetic circuits in a fast and reliable way. Indeed, the one-pot assembly reaction is performed within 5 hours and the different antibiotic resistances of the destination vectors in combination with the blue/white selection guarantee a high cloning efficiency (99% of white colonies per reaction[24]). Moreover, the scars left between the parts after the assembly (fusion sites), are relatively short (4bp), thus limiting the impact on the design of the genetic constructs. In addition, some MoClo vectors are specifically designed to accommodate coding sequences, by having the fusion site "AATG". This can match the canonical start codon of a gene, allowing, for instance, the establishment of a precise nucleotide spacing between the start codon and the upstream RBS sequence. Finally, in case the genetic parts need to be cured for eventual Type IIs restriction

sites, this can be easily performed simultaneously when cloning the parts in level 0 vectors, as described by Weber *et al*.,[24].

Concluding, simple library generation and combinatorial assembly from reusable parts make the MoClo a valuable tool for synthetic biology application. Indeed, to date, MoClo-based strategies are used for the generation of libraries of genetic parts[27,28]. Moreover, the MoClo system is being further implemented and optimized[29,30]. This will inevitably lead to a further increase of the MoClo capabilities and promote the sharing of MoClo-encoded standard parts. While synthetic synthesis of the genetic constructs will probably represent the definitive solution for synthetic DNA circuit design, at the moment the cost and the speed of this approach still limit its utilization. Hence, to date, all the characteristics described above, make the MoClo and derived methodologies one of the best DNA manipulation strategies for the bottom-up design of synthetic circuits.

1.3 Reducing the cross-talk between the synthetic circuits and the host cell: chromosomal integration

As mentioned in Section 1.2, the generation of complex synthetic circuits and metabolic pathways can count on the utilization of several DNA assembly methods mainly based on Gibson Assembly[19], Ligase cycling reaction[20] and Golden Gate cloning[31]. However, even though these systems allow for complex genetic circuit generation[13], the constructs are ultimately assembled on expression vectors. The use of such vectors as chassis for encoding the genetic circuits is advantageous in terms of speed of circuit generation and manipulation, however, the presence of medium and high-copy plasmids in the bacterial host can generate undesired [32,33]. Indeed, plasmid maintenance as well as, high expression of heterologous genetic constructs, can cause a metabolic burden to the cell and therefore toxic effects[34–36]. Hence, lowering the copy number of the constructs using low copy number plasmids, or via chromosomal integration is often a solution to reduce the impact of the heterologous circuits on the host cell. To this end, different methods for integrating DNA from plasmids into the *E. coli* chromosome have been developed[37–41].

The most widely used integration methodologies are based on the λ Red recombinase-mediated integration (Recombineering)[42]. Recombineering in *Escherichia coli* relies on short (50 base pairs) homology regions, that are used to target any position in the genome, and on the expression of three genes of the bacteriophage λ Red (*gam*, *bet,* and *exo*). The integration procedure involves the electroporation of linear DNA molecules, usually in the form of PCR products, and the expression of the genes of the bacteriophage λ Red. Thus, *gam* gene product, Gam, prevents an *E. coli* nuclease, RecBCD, from degrading linear DNA fragments, allowing preservation of transformed linear DNA in vivo. The *bet* gene product, Beta, is an ssDNA binding protein that promotes annealing of two complementary DNA molecules, and together with the *exo* gene product, Exo, (5′ to 3′ dsDNA exonuclease) insert the linear DNA at the target locus, defined by the homology regions[43].

Even though the method allows for efficient gene knockouts, deletions, and point mutations, it was not designed with the intent of generating and integrating large synthetic circuits. To circumvent this limitation, different Recombineering-based strategies such as KIKO vectors[37], and a two-plasmid system[38] have been developed, allowing the integration of high molecular weight DNA (up to 50kb) into the *E. coli* chromosome. However, these strategies often rely on PCR-amplification and traditional restriction digest and ligation, which limit the speed of circuit

construction/integration and do not allow for recycling of genetic parts. Recently an innovation was developed by Schindler *et. al.*, providing a series of MoClo-compatible vectors that facilitate the generation of large genetic constructs and their integration via lambda Red-based recombination[30]. However, all recombineering-based strategies still suffer from another limitation, which is the lack of well-characterized orthogonal loci. For instance, it was shown that protein expression and metabolite production in *E. coli* may be influenced by the location of their integrations sites on the genome[44] and even though five novel open reading frames were identified as suitable integration loci for synthetic circuits in *E. coli*, the integration efficiency and expression of genetic constructs in these loci varied significantly[45].

An alternative way to perform chromosomal integration is represented by strategies based on site-specific recombination[46]. Conditional-replication, integration, and modular (CRIM)-based plasmids carry different phage attachment (*attP*) sites and can be used to insert large DNA fragments at bacterial phage-attachment (*attB*) sites. The site-specific recombination is driven via expression of phage-derived integration (*int*) gene encoded on a helper plasmid. The integration procedure is very simple, requiring only the transformation of the bacterial strain with a CRIM plasmid, the relative helper plasmid, and a temperature shift that induces the phage-derived integrase. Since the helper plasmid is also temperature sensitive for replication, the integration of the CRIM and the cure of the helper plasmid are simultaneous (Figure 1.6). Moreover, CRIM plasmids possess the γ conditional origin of replication of R6K that depends on the trans-acting π protein (encoded by *pir*) for replication. Hence, successful integration events can easily be selected by transforming CRIM plasmids in *pir*$^-$ host in the presence of antibiotic selection[39].

The described characteristics make CRIM plasmids a fast and reliable strategy for chromosomal integration in *E. coli*. However, even though the system was further improved[40], so far CRIM-based integration methods lacked standardization, limiting the speed of DNA assembly/integration and not allowing for the reusability of genetic parts. Moreover, the *att* sites used for the chromosomal integration has, so far, never been characterized in terms of orthogonality of the genetic circuits expression.

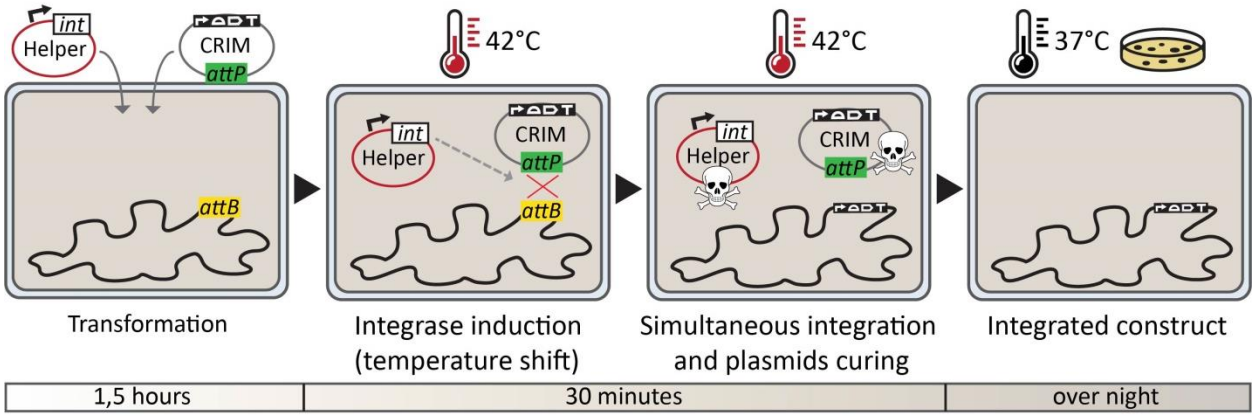

Figure 1.6. Chromosomal integration framework using Conditional-replication, integration, and modular (CRIM) plasmids in *E. coli*. The co-transformation of a CRIM-based plasmid and the cognate helper plasmid is followed by a temperature shift that induces the expression of the integrase, driving the site-specific recombination event at the specific phage attachment site. The proprieties of the system allow for the integration and curing of the helper plasmid in the same incubation step and easy selection for recombinant clones after overnight incubation.

1.4 Extracytoplasmic function (ECF) σ factors, as novel orthogonal regulators

Synthetic circuit components interact with the host organism at different levels[47]. This can lead to unexpected behavior of the synthetic circuit or even loss of its functionality[6]. One of the reasons for such cross-interactions between the heterologous circuit and the host cell is the usage of transcriptional factors (TFs) as core building blocks of complex synthetic circuits. For instance, commonly used transcriptional regulators, such as LacI[48], AraC[49], and TetR[50] are borrowed from natural regulatory systems and thus particularly prone to cross-interact with the host, leading ultimately to context-dependences. Moreover, even though bacterial TFs are well-characterized, they are limited in number, thus, narrowing the possibility of designing complex synthetic circuits that feature orthogonality. Finally, commonly used TFs are generally specific for the different bacterial species, thus limiting the functionality of a given synthetic circuit, when placed in different genetic backgrounds. The synthetic biology field would then highly benefit from the development of a new class of orthogonal, universal, transcriptional regulators[51]. To this end, in recent years orthogonal regulators were derived from natural systems, including dCas9[52], small transcription-activating RNAs[53], translational riboswitches[54], as well as extracytoplasmic function (ECF) σ factors.

The ECF σ factors family has been identified 25 years ago as a distinct group of σ^{70}-like factors[55]. Initially, ECF σ factors were found to regulate genes with extracytoplasmic functions in response to extracytoplasmic signals, thus inspiring the name of the group[55] (Figure 1.7A, B). However, currently, there are members of the family that are known to sense also intra-cellular signals and control responses that primarily influence the cytoplasm[56].

The distinct characteristic of ECFs is that they are the smallest and simplest alternative σ-factors. Indeed, they only possess the conserved domains σ_2 and σ_4, lacking domain 1 and domain 3, that in σ^{70}-like factors recognize sequences present downstream and upstream the −10 promoter element, respectively[57]. Thus, ECF σ_2 and σ_4 domains are sufficient to recruit the RNA polymerase to highly specific promoters. In particular, ECF σ_2 is responsible for the recognition of the -10 element and promoter melting[58], while ECF σ_4 recognize the -35 elements (Figure 1.7C).

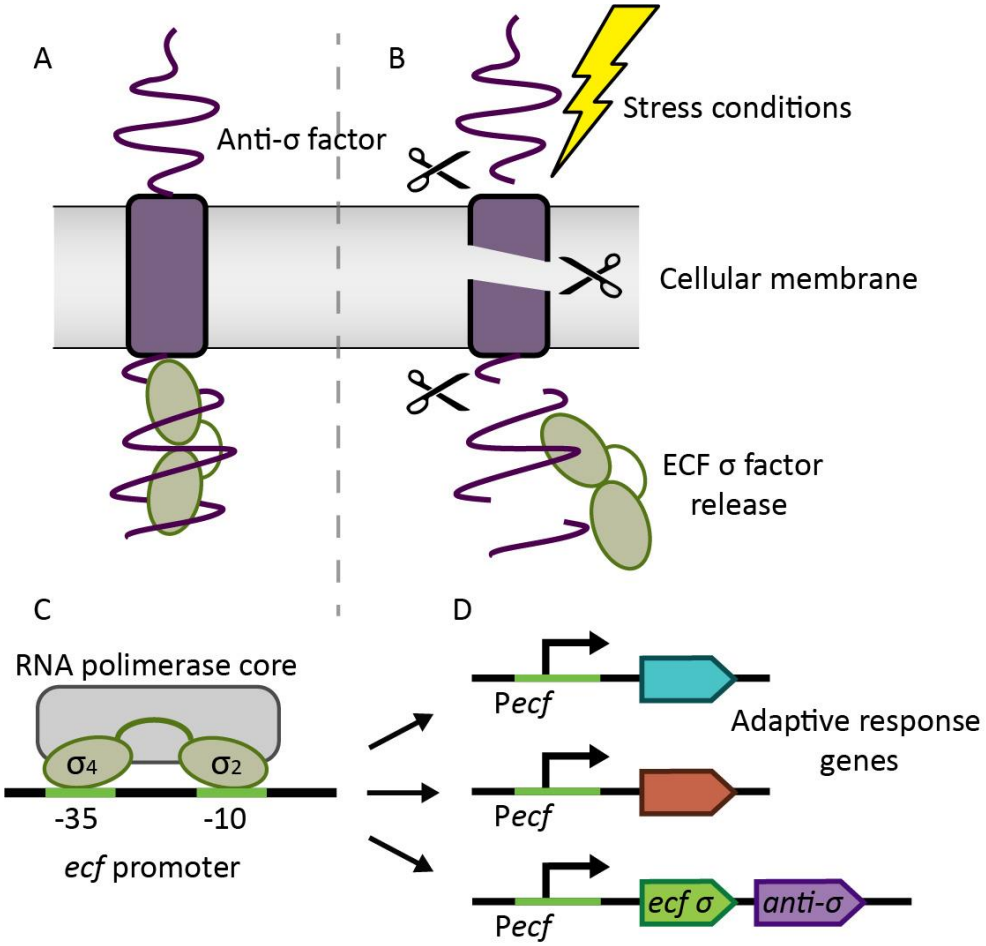

Figure 1.7. ECF σ and signal transduction. (A) the ECF σ factor (green) is kept inactive by a cognate anti-σ factor (purple). (B) A stressful signal triggers the release of the ECF σ factor. The Figure shows the regulated proteolysis of the anti-σ factor, one of the mechanisms of ECF σ release (Section 1.5). (C) The ECF σ factor recruits the RNA polymerase to the *ecf* promoter. ECF σ_4 and ECF σ_2 subunits recognize the -35 and -10 promoter elements respectively. (D) The ECF σ factors up-regulate the expression of genes involved in the adaptive response and, often, of an *ecf* operon encoding *ecf* and *anti-σ* factor genes.

To date, we know that there are, on average, 6 ECFs per genome[59], moreover ECFs have been classified into 56 major and 32 minor phylogenetically distinct ECF subgroups, based on sequence similarity[59–62]. Since the majority of ECFs are regulated by positive feedback (Figure 1.7D), it is possible to identify their target promoter sequences by genetic context analysis[59,63]. *Ecf* promoters appear to be group specific, therefore, the consensus promoter sequence of an ECF group is distinct from the one of the other ECF groups. Moreover, the *ecf* promoters are different from the promoters recognized by σ^{70} and since bioinformatic approaches allow the identification of ECF σ and cognate promoters, the increase of available annotated genomes will lead to an expansion of their number. Finally, since the core RNA polymerase is strongly conserved among different bacteria, ECF σs are potentially functional in different bacterial species.

All the described features make ECFs exceptional candidates as novel orthogonal regulators for SynBio applications. Indeed, in 2013, Rhodius and collaborators demonstrated that at least 20 heterologous ECF σ factors in *E. coli* specifically activate their target promoters – with minor cross-activation of native, or other ECF target promoters[63](Figure 1.8A). Moreover, ECF σ_4 and σ_2 domains appear to be modular, being able to recognize the -35 and the -10 elements independently.

Indeed, the combination of σ_4 and σ_2 from two different sigma factors, along with the respective −35 and −10 promoter sequences, allowed the construction of chimeric σ-factors with new promoter specificity[63](Figure 1.8B). This pioneering study confirmed that heterologous ECFs, in combination with their cognate promoters, are functional in *E. coli* and that they exhibit orthogonal characteristics. However, in order to extensively use ECF σ factors, they now have to be precisely characterized, identifying their advantages and potential limitations when embedded in synthetic circuits. Moreover, prior to this study, ECFs have only been used to design ECF-promoter genetic switches[63,64], or regulatory circuits[65], featuring only one ECF, while the possibility of combining them in more complex synthetic circuits has never been explored.

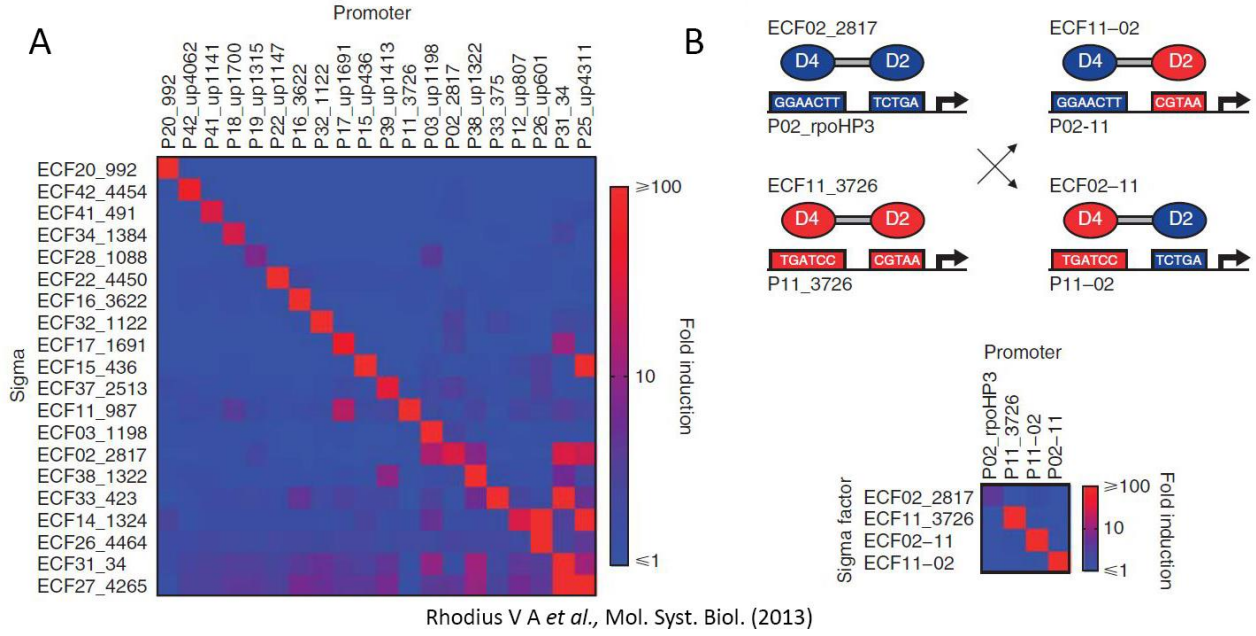

Rhodius V A *et al.*, Mol. Syst. Biol. (2013)

Figure 1.8. Activity and orthogonality of ECF σ factors in *E. coli*. Orthogonality matrix of 20 ECF-promoter pairs (A) and 2 chimeric ECF-promoter pairs (B) tested in *E. coli*. The Figure was adapted from[63], distributed under the terms of the Creative Commons Attribution Non-Commercial License CC BY-NC.

1.5 Anti-σ factors, as ECF σ factors regulators

The ability to control the activity of transcriptional regulators is a fundamental characteristic in synthetic circuit engineering[51]. In nature, ECF σ factors represent one of the mechanisms of signal transduction in bacteria[59], thus precise control of their activation state in response to external signals represent one of their key features. ECF σ factors belonging to group ECF41 and ECF42, are known to possess a C-terminal extension that seems to be fundamental to regulate the state of these ECFs[66]. However, this is a rare mechanism for controlling ECF activity. Indeed, in the majority of cases, ECFs are encoded in an operon together with an anti-σ (AS) factor[59]. Anti-σ factors are transmembrane or cytosolic proteins that bind and block the cognate ECF-σ factor forming an inactive complex. Upon the arrival of a stressful stimulus AS factor releases the ECF that can then activate target promoters expressing genes that are involved in the stress response. In membrane-anchored AS factors, the N-terminus resides in the cytoplasm and contains a σ-factor binding domain, followed by a transmembrane domain (TM) and a periplasmic C-terminus responsible for sensing extracellular stimuli. Soluble AS factors show a significant degree of sequence and

structural similarity to membrane-anchored AS factors, at least in the domain that binds the cognate σ-factor[67] nevertheless the mechanisms of their release is generally different. Currently, there are four known mechanisms to release an ECF from the bind with its cognate AS[68]. We can distinguish between mechanisms that belong to membrane-anchored AS factors and the ones that belong to soluble AS factors.

For membrane-anchored AS factors, regulated proteolysis represents the best-understood mechanism of ECF releasing and it has been studied in great detail for two of the paradigmatic ECF/AS: σ^E-RseA from *E. coli*, and σ^W-RsiW of *B. subtilis*[69]. In both cases, the accumulation of misfolded proteins in the periplasm triggers the proteolytic cleavage of the extracellular domain of the AS factor and its single transmembrane helix, releasing the ECF/AS pair into the cytoplasm. The remaining soluble portion of the AS factor is then degraded by the ClpXP protease[70,71]. Another mechanism of ECF releasing from membrane-anchored AS is given by protein-protein interaction cascades. This is a mechanism in which the paradigm is represented by FecI/FecR like proteins, that are usually involved in regulating iron-siderophore uptake[59]. In this case, the AS FecR keeps the ECF inactive, while the activation of the ECF is triggered by the binding of the substrate (Fe^{3+}) to an outer membrane porin (FecA). The presence of the substrate is then signaled with a protein-protein interaction cascade via FecR, to the intracellular σ factor FecI, triggering its activation. In some cases, FecR-like proteins are also required for ECF activity, even though the mechanism of this positive role is not fully understood[72,73]. The third mechanism of ECF releasing involves conformational changes in the AS factor. The conformational changes in the AS factor can be triggered in response to the binding of cobalt and nickel ions to an extracellular sensor protein, as it has been shown for the transmembrane AS factor CnrY[74]. However, conformational changes are mainly known for being the main mechanism of ECFs release from soluble AS factors, in response to redox or oxidative stress[75,76]. The fourth known mechanism of ECF release applies only to soluble AS factors and is represented by partner-switching based on σ factor mimicry[77]. In this mechanism, a response regulator possesses a receiver domain at the C-terminus that interacts with a cognate transmembrane histidine kinase. In contrast, the N-terminus of the response regulator has a sequence similarity to the regulated ECF σ factor. Under stressful conditions, the transmembrane sensor kinase phosphorylates the response regulator, causing its conformational change. The new conformation allows the N-terminal domain to bind the soluble AS factor, therefore releasing the cognate ECF σ[78].

Despite the described release mechanisms, AS factors represent one of the best options to control ECF activity, making them a valuable tool to modulate the response of ECF-based genetic circuits. Indeed, Rhodius and collaborators identified at least 12 anti-σ factors that were able to repress the activity of cognate ECF σs, with minor cross-reactions[63](Figure 1.9). However, the variety of stimuli that trigger ECF release from the ECF/AS complex poses a challenge in the development of context-independent AS factors. Moreover, it has been shown that AS factors overexpression in *E. coli*, can lead to growth defects[63]. Hence, these issues must be addressed in order to extensively use AS factors and enhance the control of ECF-based synthetic circuits.

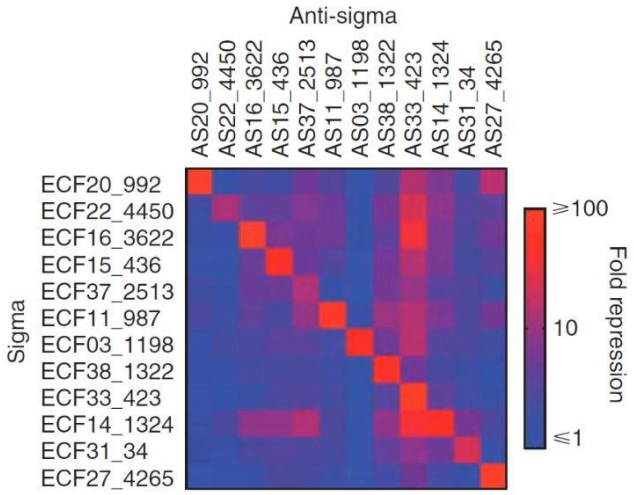

Figure 1.9. Activity and orthogonality of anti-σ factors in *E. coli.* The crossreactivity of 12 anti-σ factors on a set of 12 cognate ECF σ factors, assayed in *E. coli*. The Figure was taken from[63], distributed under the terms of the Creative Commons Attribution Non-Commercial License CC BY-NC.

1.6 Aim of the project

The aim of this project resides in using Extracytoplasmic function (ECF) σ factors to design novel, orthogonal, synthetic circuits in *Escherichia coli*. ECF σ factors are the smallest and simplest alternative σs. Briefly, ECFs differ from σ^{70}-factors, having just two domains, σ_4 and σ_2, that are enough to recruit the RNA polymerase to orthogonal target promoters[63,79]. ECFs are widespread among different bacterial phyla, and they are identifiable together with the cognate promoters and anti-σ factors, using bioinformatic approaches[59]. Thus, the increase of available annotated genomes will lead to the expansion of their number. Moreover, ECF σ_4 and σ_2 domains are modular, thus, their combination from two different σ factors allows the construction of chimeric σ-factors, that recognize specific chimeric promoters, that does not exist in nature[63]. This approach eventually allows for increasing ECF specificity and orthogonality. Finally, since the core RNA polymerase is strongly conserved among bacteria, ECF σ-based circuits are potentially functional in different bacterial species. Thus, for all the above-mentioned features, ECF σ factors represent optimal candidates as core orthogonal regulator for the design of novel synthetic circuits.

In order to establish ECF σ factors as standard building blocks in the synthetic biology field, in this study we aim to characterize them in the context of synthetic circuit design, identifying their features, advantages and potential limitations. To do so, we first aim to establish a high throughput experimental setup that allows for a precise quantitative characterization of the genetic circuits. Thus, we aim to establish an easy and reliable cloning framework that allows for the modular assembly of multiple, reusable, genetic parts, following a bottom-up approach. With the purpose of rationally design ECF-based synthetic circuits, we want to assemble a set of ECF σ factors-switches and evaluate the impact of ECF σ expression on the growth of *E. coli*. The ECF-switches will also serve to characterize the dynamics of activation of *ecf* target promoters in our experimental conditions. Next, we aim to generate the first synthetic circuit harboring more than one ECF, verifying if ECF σs feature a robust and predictable quantitative behaviour. Moreover, we aim to explore the possibility of implementing anti-σ factors in ECF-based circuits. To do so, we will analyze the impact of their expression on cellular growth and isolate them from the variety of

extracellular stimuli that trigger their activation. Finally, we aim to combine ECF and anti-σ factors in order to design threshold gate circuits, that allow for a time tunable control of ECF σ factors activation and, in turn, delayed downstream protein expression.

2. Establishment of a highly sensitive reporter system for synthetic circuit evaluation

This chapter introduces the experimental settings that we extensively used in this work. First, we introduce the *E. coli* strain that served as reporter system. Next, we present a luminescence reporter as an alternative to the widely used fluorescent reporters, for the evaluation of genetic circuit output. Finally, we introduce a novel computational method for the correction of luminescence bleed-through and the estimation of the "true" luminescence activity, in microplate-reader experiments.

2.1 *E. coli* reporter strain SV01

In this project, we aim to explore the possibility of using ECFs factors as core regulators for novel synthetic circuits. However, to date, ECF activity can be regulated mainly through AS factors. There are a variety of stimuli that trigger ECF release from ECF/AS complexes (as described in the introductory Section 1.5) and most of them are related to stressful conditions. Thus, the inherent complexity in reproducing the signals that trigger ECFs activation poses a challenge in using AS factors to control of ECF activity. We then reasoned that commonly used transcriptional regulators (such as TetR[50], LacI[48], and AraC[49]) represent, to date, the best mechanism to control ECF σ expression in novel synthetic circuits.

In designing synthetic circuits the synthetic biology field uses extensively the above-mentioned well-characterized transcriptional regulators. These regulators are part of the natural regulatory system, thus, they are prone to context-dependencies. In order to reduce the cross-interactions between these regulators and the host, the scientific community has engineered a variety of *E. coli* strains. In particular, due to the exogenous nature of TetR and CI parts, there are many *E. coli* strains that are suitable for harboring synthetic regulatory networks built from these parts. However, the choice is limited for the networks that use the LacI and AraC parts, as they are endogenous to *E. coli*[80]. For instance, the majority of *E. coli* strains lead to an all-or-none response by the *araBAD* promoter (P_{BAD}), in which cells both display full expression or only basal expression, while gradual induction cannot be achieved[81]. This all-or-none phenomenon occurs because the expression of the inducer transporter (encoded by *araE*) is also controlled by the inducer itself through a positive feedback mechanism[81]. This, in combination with the stochastic expression of *araE* prior to the induction, determines the heterogeneous response of the cell population especially at low concentrations of the inducer L-arabinose[81]. Moreover, it has been shown, that the positive feedback control, together with the stochastic expression of *araE,* leads, at intermediate arabinose concentrations, to a highly variable time delay in the induction of the arabinose promoter, within the cell population[82]. Finally, the majority of *E. coli* strains contain arabinose-metabolizing genes, which results in a decrease in the effective concentration of L-arabinose as the cells utilize it.

A solution to these problems is represented by the *E. coli* strain MK01 generated by M. Kogenaru and S. Tans[80]. This strain is a derivative of BW27783[83] and it is suitable for gene regulatory networks involving both the AraC and LacI transcription factors. Indeed, it carries a deletion for the arabinose metabolizing genes, and abolished the all-or-none response, with a copy of the low-affinity high-capacity transporter, AraE, under the control of an arabinose-independent promoter. Moreover, the endogenous *lacI* copy is knocked out, thus allowing precise control of genetic circuits containing the LacI regulator as well[80]. For the proprieties described above, this strain represented an optimal candidate as reporter strain for our synthetic circuits, however, MK01 carries a chloramphenicol cassette in the *lacI* locus, flanked by *LoxP* sites. In order to allow maximum flexibility for further applications presented in this study, we recombined the

chloramphenicol cassette from MK01, using the Cre recombinase[84] (as described in Section 7.3) and generated the strain SV01 (Table 2.1). This strain, with all the appealing characteristics described above, represent the reporter strain used in all the experiments that will follow.

Strain	**Genotype**
SV01	F- λ- *rph-1* DE(araD-araB)567, *lacZ*4787(del)::rrnB-3 DE(rhaD-rhaB)568, hsdR514 DE(araH-araF)570(::FRT) *araEp*-532(del)::FRT Phi P_cp8 araE535, *lacI*(del)::Lox

Table 2.1 *E. coli* SV01 strain genotype. The strain was generated by removing the chloramphenicol cassette from MK01.

2.2 A luciferase reporter for a high sensitive circuit dynamic evaluation

Many applications in synthetic biology require a precise quantification of gene expression at a high time resolution. High throughput methodologies such time-course microplate reader experiments are then fundamental tools in the field since they allow for the simultaneous, real-time monitoring of growth and reporter gene activity of multiple bacterial cultures distributed over the wells of a microplate[85]. Using these methodologies it is possible to resolve minute differences in gene expression dynamics and to measure simultaneously many strains and experimental conditions. For these reasons, we reasoned that microplate reader experiments represent the best strategy to analyze and characterize the behavior of novel synthetic circuits.

In order to characterize synthetic circuits dynamic in microplate experiments, it is necessary to use a sensitive reporter to monitor the output signal of the genetic circuits. The reporters used for microplate experiments ranges from fluorescent proteins to luciferase enzymes, both of which present advantages and disadvantages. Fluorophores absorb energy from a light source at a certain wavelength and emit light at a different wavelength, therefore having the advantage of possessing different spectral characteristics. This allows, for instance, the combination of different fluorophores in a given strain to monitor the activity of different promoters or the expression of different genes. However, one of the biggest disadvantage using fluorophores is given by the auto-fluorescence of bacterial cells[86,87] and of certain commonly used media such LB medium. This can lead to increased background noise, therefore limiting the dynamic range. Bioluminescence, on the other hand, is produced by luciferase enzymes during the oxidation of the substrate luciferin[88] and presents the advantage of having virtually zero background signal in organisms not harboring luciferase genes[89]. This feature makes luciferase an attractive reporter system that is widely used to monitor gene expression dynamics[90–95]. To show the potential of the luciferase operon as reporter system, we compared, in microplate experiments, the kinetic response of a strain harboring a plasmid-borne arabinose-inducible promoter fused with a *gfp* reporter gene[96], or with the *luxCDABE* operon from *Photorhabdus luminescens*[97]. We assayed both strains in transparent MOPS minimal media (as described in Section 7.1 and 7.10) for 10 h, inducing the cultures at time t=0 hour (h) with different arabinose concentrations (Figure 2.1).

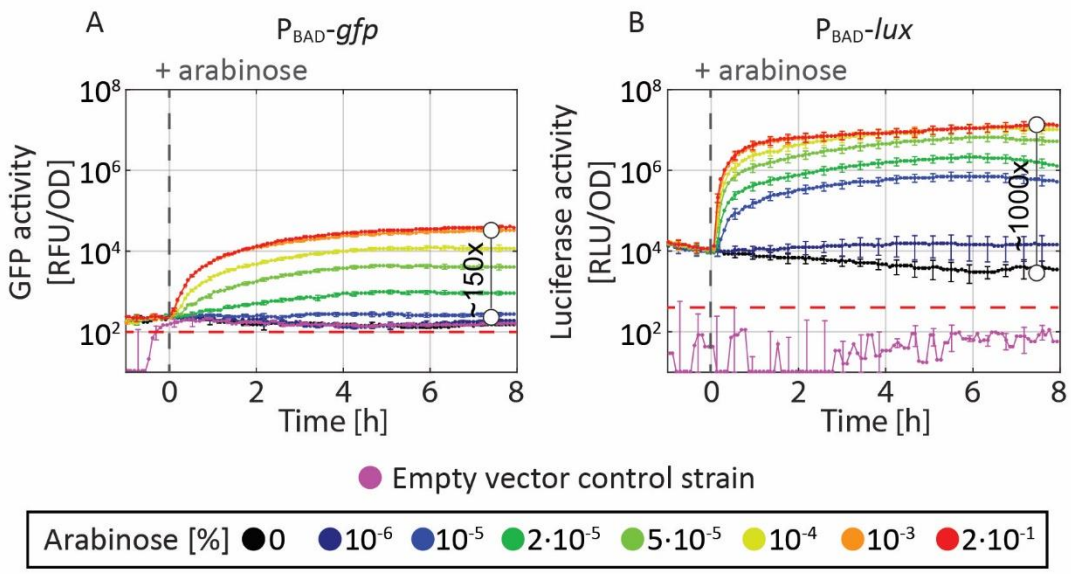

Figure 2.1. Comparison of the dynamical response of GFP activity and luciferase activity. P_{BAD}-*gfp* (A) and P_{BAD}-*lux* (B) constructs dynamical responses are compared after the addition of various concentrations of arabinose at t=0 h. The reporter activities are shown in relative fluorescent units (A) and relative luminescence units (B), normalized by the optical density measured at 600 nm. The maximal fold induction for each construct is indicated. The red dashed line represents the low detection limit of the plate reader for fluorescent (A) and luminescent (B) signals. The results are averaged from at least two independent biological assays and error bars denote standard deviations.

The results show, for the uninduced P_{BAD}-*gfp* construct (Figure 2.1A, black curve), a background activity ~$2x10^2$ Relative Fluorescent Units normalized by the optical density measured at 600 nm (RFU/OD_{600}), which is close to the minimal sensitivity of the machine – defined as three times the standard deviation of the fluorescence signal registered in a well filled with media, divided by the averaged OD_{600} values registered in the same well (~10^2 RFU/OD_{600}; Figure 2.1A, red dashed line). This can actually mask any signal below this threshold (e.g. in the case of the construct encoded on low copy plasmids or chromosomally integrated). Moreover, the empty vector control strain also showed a signal ~$2x10^2$ RFU/OD_{600} (Figure 2.1A, purple curve), due to the autofluorescence of *E. coli* described above, and this could actually mask the P_{BAD} promoter basal activity. Indeed, the same promoter fused with the luciferase reporter showed a basal activity ~10^4 Relative Luminesce Units (RLU)/OD_{600} (Figure 2.1B, black curve), while the non-luminescent control strain displayed values <100 RLU/OD_{600} (Figure 2.1B, purple curve), which are below the detection limit of the machine – defined as three times the standard deviation of the luminescence signal registered in a well filled with media, divided by the averaged OD_{600} values registered in the same well (~$4x10^2$ RLU/OD_{600}; Figure 2.1B, red dashed line). Therefore, the use of the luciferase reporter revealed a basal activity of the P_{BAD} promoter, in absence of inducer, ~50-fold higher than the one registered using the fluorescent reporter GFP, thus increasing the resolution. Moreover, P_{BAD}-*lux* showed a higher dynamic range (~1000x between the uninduced and the fully-induced strain) when compared to P_{BAD}-*gfp* (~150x between the uninduced and the fully-induced strain). Finally, when comparing qualitatively the temporal response of the two reporters upon induction, we noticed that the luciferase reporter signals reached the maximum values prior than the GFP reporter, for each inducer concentration (Figure 2.1A, B). This is due to the slower chromophore maturation times when compared with luciferase enzymes, which folds cotranslationally and are enzymatically active

upon folding[98]. Therefore, using the luciferase operon it is possible to increase resolution, dynamic range, and temporal response of the circuit output – properties that can be beneficial to evaluate more complex synthetic circuits. For these reasons, we extensively adopted the luciferase cassette as a reporter system to monitor the output signal in our novel synthetic circuits.

2.3 Deconvolution of luminescence cross-talk in high-throughput experiments

The results of this section are published in Paper I (Mauri *et al*., 2019)

In the previous section, we showed that the luciferase cassette is an optimal candidate as a reporter system to evaluate complex synthetic circuits. However, the luminescent reporters have the draw-back represented by the constant light emission, that often leads to undesired cross-talk between neighboring wells on a microplate[99]. This is due to the fixed distance between the microplate surface and the detector that allows the light emitted from neighboring wells to be detected as a false-positive signal. Although manufacturers produced black, light-absorbing microplates that limit such luminescence "bleed-through", we found that a light emitting strain placed in a single well of the plate illuminated more than 50% the other empty wells (Figure 2.2A). The bleed-through can then significantly bias the measurement of luminescent signals, especially in a scenario where positive and negative controls are placed in neighboring wells. To circumvent this problem, many labs either fill their microplates only sparsely or discard reading wells clearly affected by luminescence cross-talk[100] and thus lose significant throughput in their analyses. In our laboratory, in order to utilize extensively luminescent reporters, we developed a computational method that corrects for luminescence cross-talk and to estimate the "true" luciferase activity in each well of a microplate. The method, developed by Dr. Marco Mauri, is inspired by computational approaches in super-resolution microscopy, in which the point-spread function of the microscope setup is used to infer the accurate positions and intensities of light-emitting molecules[101]. Similarly, the algorithm uses the measurements of a calibration plate (in which only a single high luminescent strain is present) to estimates the "light-spread function" of the microplate reader setup. Subsequently, the algorithm uses a deconvolution strategy to estimate the most likely configuration of true luminescence activities that can explain the observed light intensities in all wells of the microplate.

2.3.1 Deconvolution procedure

Convolution is a mathematical operation on two functions to produce a third function that expresses how the shape of one is modified by the other[102]. Deconvolution on the opposite is an algorithm-based process that reverses the effects of convolution on recorded data. In the case of a microplate reader experiment, the signal generated by multiple luminescent strains represents the convolved data recorded by the detector. In order to deconvolve these data, we estimated the luminescence bleed-through. To do so, we analyzed a so-called "calibration plate" in which only a single well (positioned in well *E5*) of a black 96-well was inoculated with a luminescent *Escherichia coli* strain (GFC153). The other wells of the microplate instead, were inoculated with cells of a non-luminescent *E. coli* strain SV01. The luminescent strain (GFC0153) harbors a plasmid-borne, copy of the *luxCDABE* operon from *Photorhabdus* luminescens[97] fused to an arabinose-inducible promoter (Table 9.1). After two hours of incubation (referred to as t=0 h), expression of the *lux* operon was fully induced by adding arabinose at a final concentration of 0.2%

and luminescence activity was monitored over time in a Tecan Infinite F200 PRO microplate reader (Figure 2.2B).

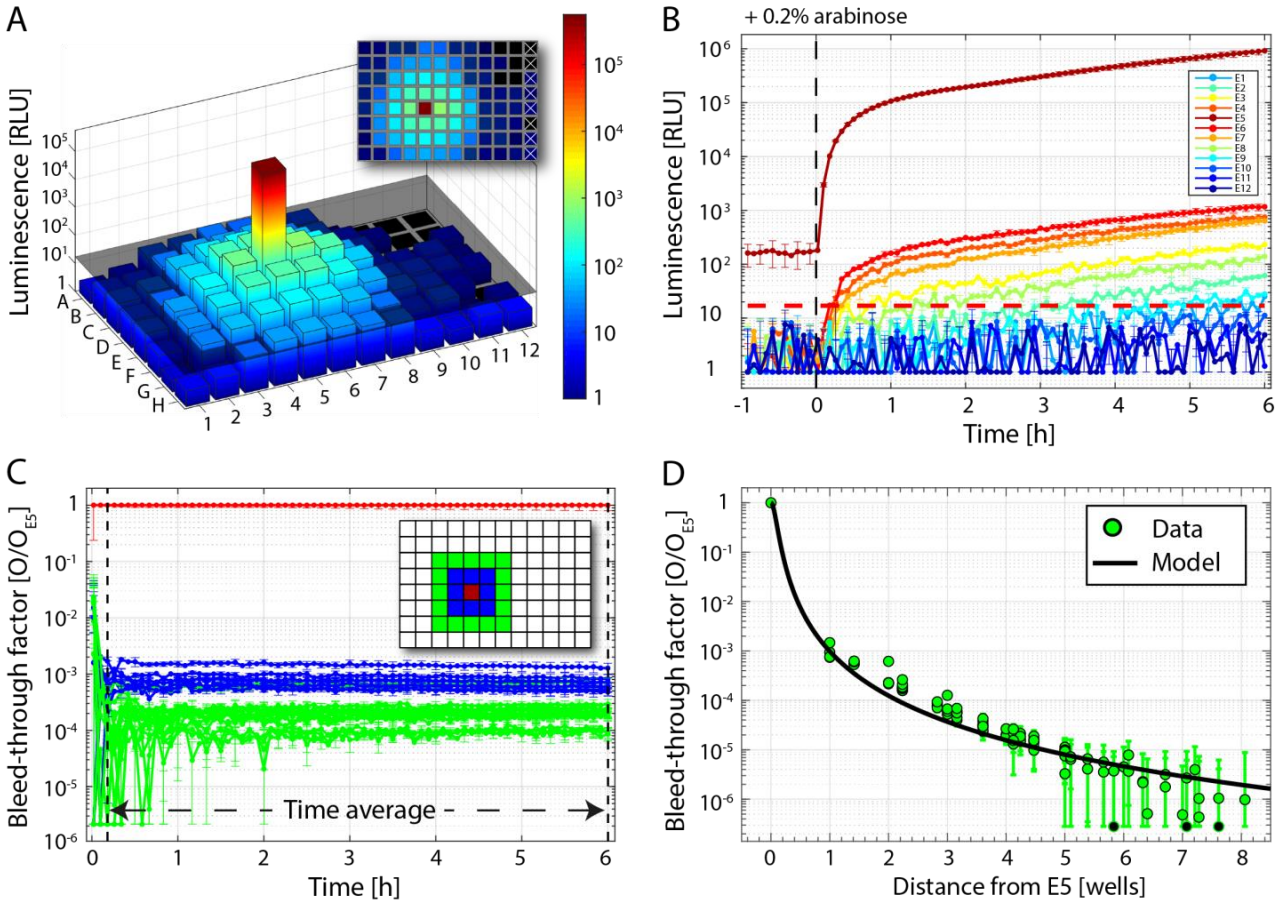

Figure 2.2. Quantification of luminescence bleed-through in the calibration microplate. (A) The calibration plate was prepared with a single highly luminescent spot in the well E5. All data are background-subtracted and averaged over three experimental replicates. The background was obtained by averaging the signal of the wells indicated by the white crosses in the inset over the time before addition of arabinose (induction time). The 3D-plot shows the observed luminescence signal at 270 minutes after the induction. (B) Time evolution of the observed luminescence signal of the E-row. The red line represents the instrument sensitivity value, defined as three times the standard deviation of the background value. (C) Luminescence bleed-through factor of the two shells closest to E5, in blue and green. Values were obtained dividing the observed signal from a specific well by the signal recorded in E5. The dashed lines indicate the time range over which the bleed-through was averaged to obtain in (D) the bleed-through factor as a function of the distance from E5 (green dots). The black solid line is the parameter-free prediction of the bleed-through. *This figure was adapted with permission from Paper I* (Mauri *et al*., 2019). Copyright 2019 American Chemical Society.

This concentration of arabinose allows full saturation of the arabinose promoter as shown in Figure 2.1B. After induction, luminescence activity in the well *E5* increased about 10.000-fold from 10^2 to 10^6 RLU. At the same time, we observed a significant increase of apparent luminescence activities in a radius of three to four wells surrounding *E5*, with the highest values of 10^3 RLU reached in closest proximity to the light-producing strain (Figure 2.2A and B). This value is about 600-fold above the average background luminescence of the non-luminescent strain (1.8 ± 0.6 RLU). We also defined an instrument sensitivity $s = 17$ RLU given by three times the standard

deviation of the background luminescence (black plate in Figure 2.2A and red dashed line in Figure 2.2B). Any signal below the instrument sensitivity cannot be statistically distinguished from the background value. Next, we analyzed the calibration plate, looking at the correlation between the luminescence bleed-through and the magnitude of light-emission from well *E5*. To this end, we defined the bleed-through factor *B* in a given well (m,n) at time *t* as the ratio between the observed, background-subtracted luminescence intensities *O* in well (m,n) and in well (E5)

$$B_{m,n}(t) = \frac{O_{m,n}(t)}{O_{5,5}(t)}. \quad (1)$$

Here m = 1, 2, … , 8 indicates the row of the microplate and n = 1, 2, …, 12 the column. From this we can then obtain, the entries of a bleed-through matrix *B* with values that can range between the background-subtracted luminescence intensity over *E5* signal (no bleed-through) and 1 (full bleed-through). The experimental data plotted in Figure 2.2C show that as soon as the intensity in a well exceeds the instrument sensitivity of *s* (Figure 2.2C dashed line), the bleed-through factor becomes almost constant in time and only dependent on the distance from the emitting well. To quantify this dependency, we time-averaged the bleed-through factor and plotted it as a function of the distance from the emitting well (Figure 2.2D). As noted before, we can observe a 1000-fold initial decrease of the time-averaged bleed-through factor in the wells immediately neighbouring the emitting well, followed by a slower decline – still exceeding machine sensitivity up to four wells away from the emitter. The relationship between the bleed-through and the distance from the emitting well can be elucidated with a mathematical model that depends only from the height of the detector and the distance between the centers of neighbouring wells. The mathematical model allows for a parameter-free prediction of the bleed-through factor and agrees well with the experimental data (black line in Figure 2.2D).

Given that luminescence bleed-through can be described by a simple, distance-dependent factor, Dr. Marco Mauri developed an algorithm that was able to estimate bleed-through factors on a more complex plate, with many different luminescent wells of different intensities. The algorithm by estimating the "light spread function" from the calibration plate (where only a single luminescent strain is present) generates a deconvolution matrix (D_{best}). The algorithm then uses the matrix D_{best} to correct the bleed-through of any other measurement obtained under the same technical conditions.

2.3.2 Experimental evaluation of the bleed-through correction algorithm

To evaluate the robustness of the algorithm we first corrected the bleed through of the calibration plate, in which all wells except for E5 do not emit luminescence (Figure 2.3). After applying the deconvolution strategy, the luminescence bleed-through visible in the raw data (Figure 2.3A, B) was removed (Figure 3C, D), revealing the "true" experimental setup.

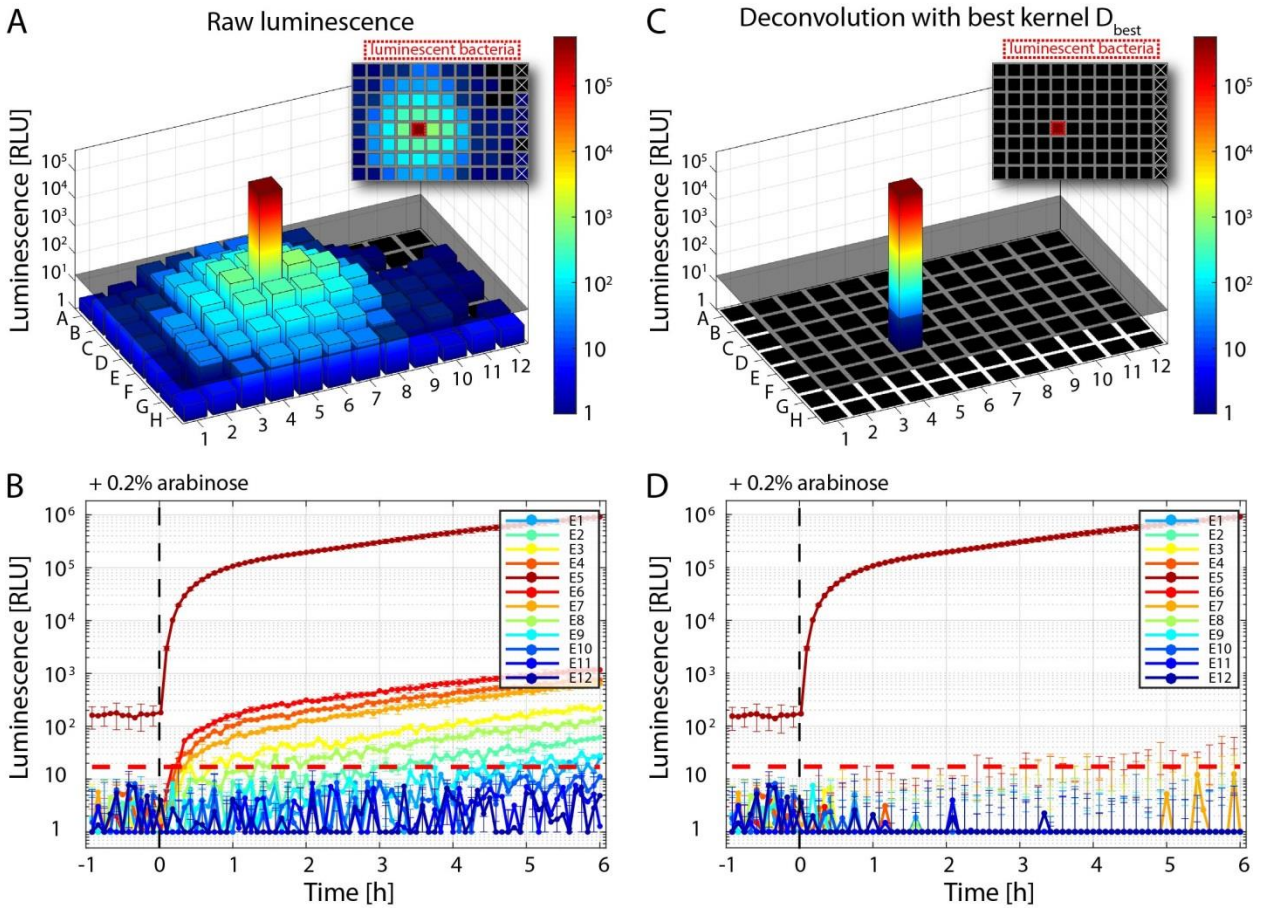

Figure 2.3. Deconvolution of luminescence signals in the calibration microplate. Luminescence values on the calibration plate 270 minutes after the induction of *E. coli* strain GFC0153 (in well E5) with 0.2% arabinose (A, C) and its time evolution in the wells of row E (B, D) for raw signal (A, B) and after applying the deconvolution algorithm (C, D). *This figure was adapted with permission from Paper I* (Mauri *et al*., 2019). Copyright 2019 American Chemical Society.

To test if the algorithm was able to remove bleed-through signals and at the same time preserving true luminescence signals close to the background, we designed a microplate experiment with the configuration illustrated in Figure 2.4.

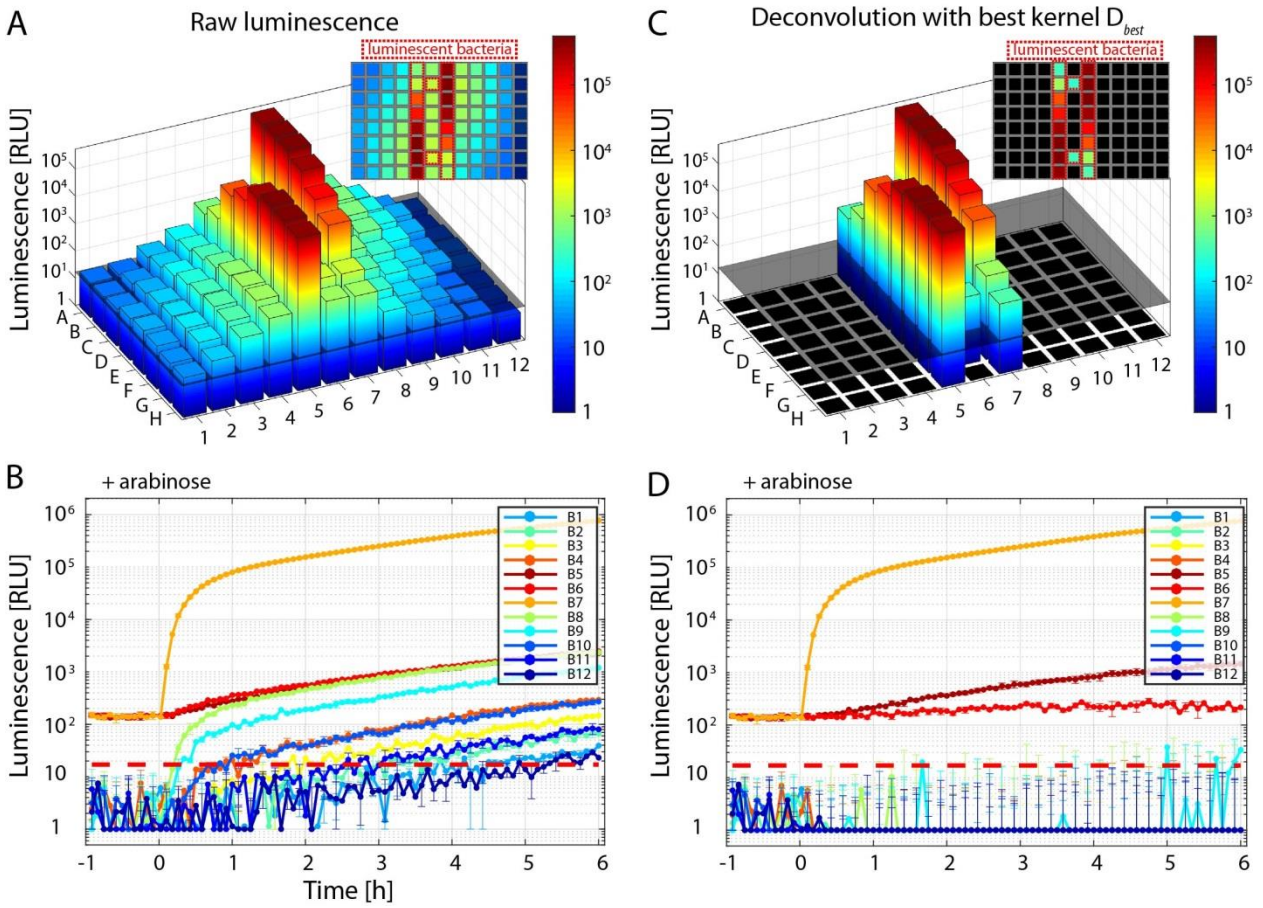

Figure 2.4. Deconvolution of luminescence signals in the test microplate. Luminescence values on the test plate 270 minutes after the induction of *E. coli* strain GFC0153 with varying concentrations of arabinose (in wells A5-H5: 0%, 10^{-6}%, 10^{-5}%, $2x10^{-5}$%, $5x10^{-5}$%, 10^{-4}%, 10^{-3}%, $2x10^{-1}$%; in wells A7-H7: $2x10^{-1}$%, 10^{-3}%, 10^{-4}%, $5x10^{-5}$%, $2x10^{-5}$%, 10^{-5}%, 10^{-6}%, 0%; in wells B6 and G6: 0%) (A, B). The time evolution of luminescence values is shown in the wells of row B (B, D) for raw signal (A, B), after applying the deconvolution algorithm (C, D). *This figure was adapted with permission from Paper I* (Mauri *et al*., 2019). Copyright 2019 American Chemical Society.

This arrangement simulates a typical experimental condition were two wells (B6 and G6) were filled with weakly luminescent cultures resulting from the basal activity of a plasmid-borne, arabinose-inducible promoter (P_{BAD}) fused with the luciferase reporter. Strong luminescent signals (obtained with the full induction of the arabinose promoter) were placed in the immediate neighborhood (wells A5-H5 and A7-H7). In this way, the signals of the weakly luminescent strains were completely masked by bleed-through from the strongly luminescent strains (Figure 2.4A). Moreover, comparing the luminescence of the second raw of the plate (B1-B12; Figure 2.4B) it is evident that the raw signal of the weakly luminescent strain (B6) is almost identical to the raw signal of a non-luminescent strain (B8). Applying the deconvolution algorithm, most of the spurious signals were removed and low-level luminescence in wells B6 and G6 could be clearly discriminated from the non-luminescent wells (Figure 2.4C, D and Figure 2.5A). Moreover, performing an independent measurement of the weak signals in the absence of bleed-through (Figure 2.5B), we obtained a signal that was strikingly identical (within the error tolerances), to the one recovered in presence of bleed-through (Figure 2.5C). This clearly shows that the

deconvolution procedure faithfully removes spurious bleed-through signals while preserving true luminescence signals close to background values.

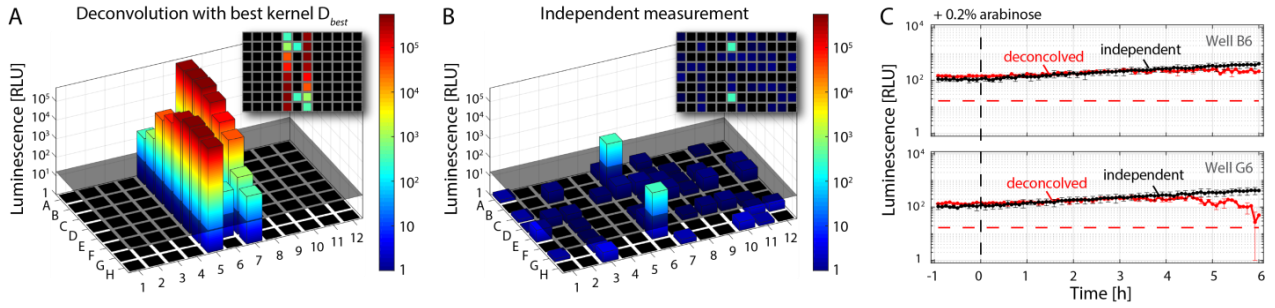

Figure 2.5. Comparison between deconvolution results and independent measurement. The luminescence values of wells B6 and G6 of the deconvolved test plate (A) as compared to independent measurements in the absence of bleed-through, for which *E. coli* strain GFC0153 in wells B6 and G6 was not induced with arabinose (B). Black and red lines in (C) represent the independently measured and the deconvolved signal, respectively. *This figure was reprinted with permission from Paper I* (Mauri *et al.*, 2019). Copyright 2019 American Chemical Society.

In order to evaluate the robustness of the algorithm, we then analyzed different experimental setups. First, we evaluated if the correction algorithm was affected by a lower luminescence value in the calibration plate. To this end, we used a modified calibration plate with 6-fold weaker luminescence signal than in Figure 2.3 (Figure 2.6A) and corrected the raw data showed in Figure 2.4A.

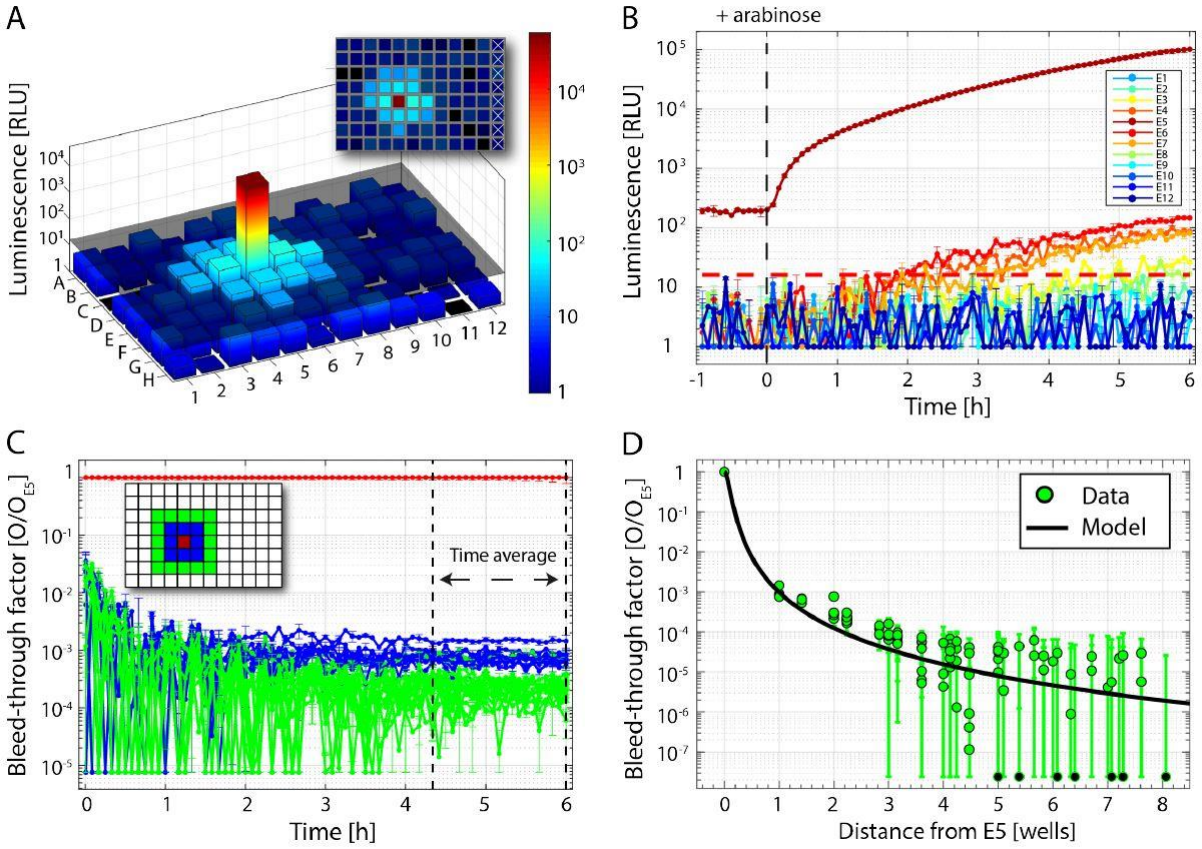

Figure 2.6. Quantification of luminescence bleed-through in the black calibration microplate for a calibration plate with low luminescence intensity. (A) The black calibration plate was prepared with a single mildly luminescent spot in the well E5. All data are background-subtracted and averaged over two experimental replicates. The background was obtained by averaging the signal of the wells indicated by the white crosses in the inset over the time before the addition of arabinose (induction time). The 3D-plot shows the observed luminescence signal at 270 minutes after the induction with $2x10^{-5}$% arabinose. (B) Time evolution of the observed luminescence signal of the E-row. The red line represents the instrument sensitivity value, defined as three times the standard deviation of the background value. (C) Luminescence bleed-through factor of the two shells closest to E5, in blue and green. Values were obtained dividing the observed signal from a specific well by the signal recorded in E5. The dashed lines indicate the time range over which the bleed-through was averaged to obtain in (D) the bleed-through factor as a function of the distance from E5 (green dots). The black solid line is the parameter-free prediction of the bleed-through. *This figure was reprinted with permission from Paper I* (Mauri *et al*., 2019). Copyright 2019 American Chemical Society.

The results show almost identical values to the deconvolution obtained with the original calibration plate (Figure 2.7A, B, C). If we compare the bleed-through factors of the two calibration plates (strong and weak luminescence intensities) we can notice that they appear to be equal within error tolerances in a radius of 3 wells around the light-emitting well (Figure 2.7D). Beyond this distance, the bleed-through factors in the calibration plate with weak luminescence signal are slightly overestimated because the signal intensity drops below background levels. Thus, although the most accurate estimate for the deconvolution kernel is obtained with the strongest possible luminescence signal on the calibration plate, the deconvolution approach is robust with respect to (limited) variations in the maximal signal intensity on the calibration plate.

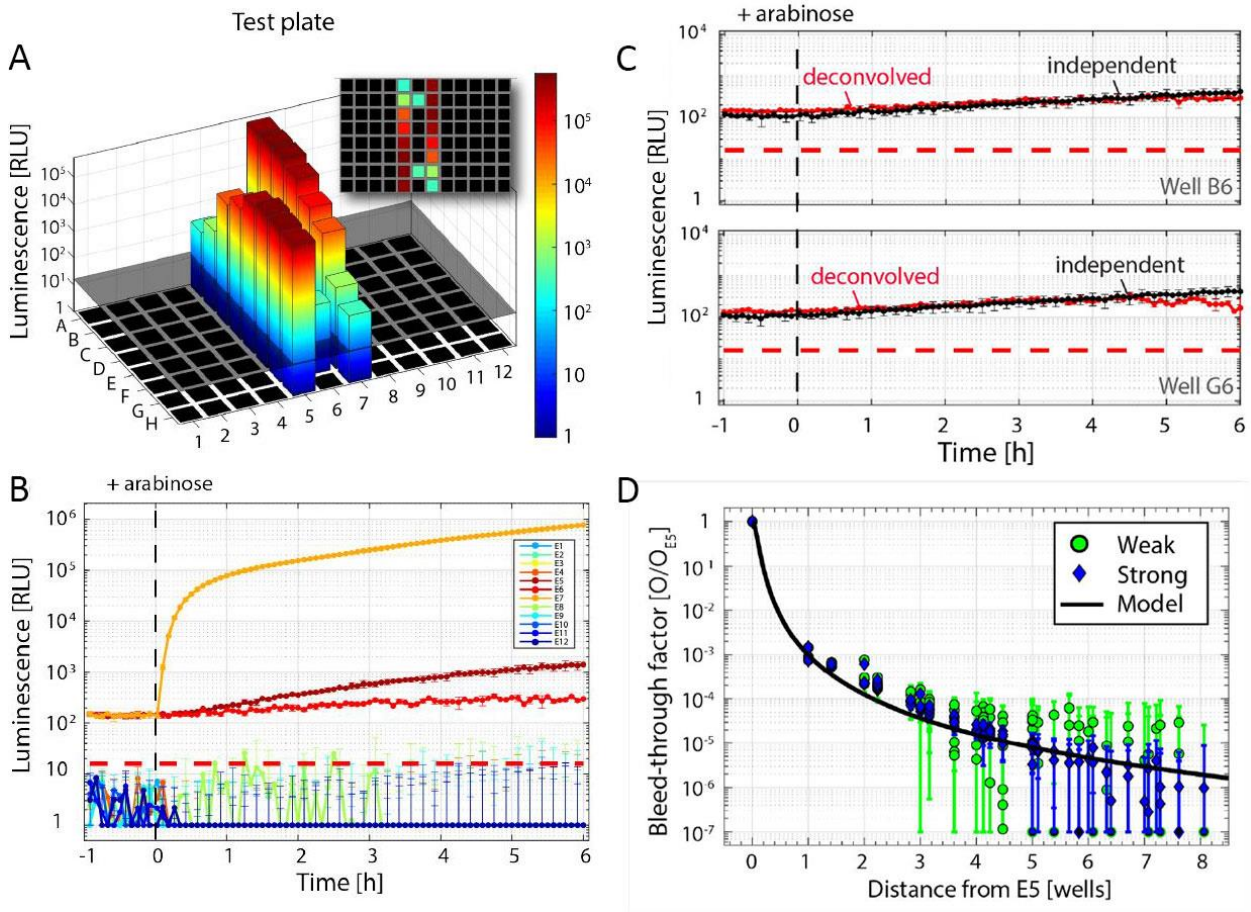

Figure 2.7. Deconvolution procedure using a calibration plate with low luminescence intensity. (A) Deconvolution of luminescence signals in the test microplate by using the calibration plate with low luminescence intensity. Luminescence values on the test plate 270 minutes after the induction of *E. coli* strain GFC0153 with varying concentrations of arabinose (in wells A5-H5: 0%, 10^{-6}%, 10^{-5}%, $2x10^{-5}$%, $5x10^{-5}$%, 10^{-4}%, 10^{-3}%, $2x10^{-1}$%; in wells A7-H7: $2x10^{-1}$%, 10^{-3}%, 10^{-4}%, $5x10^{-5}$%, $2x10^{-5}$%, 10^{-5}%, 10^{-6}%, 0%; in wells B6 and G6: 0%). (B) The time evolution of luminescence values is shown in the wells of row B after applying the deconvolution algorithm. (C) the luminescence values of wells B6 (top) and G6 (bottom) of the deconvolved test plate as compared to independent measurements in the absence of bleedthrough, for which *E. coli* strain GFC0153 in wells B6 and G6 was not induced with arabinose, as described in the main text. Black and red lines represent the independently measured and the deconvolved signal, respectively. (D) Comparison between bleed-through factor generated from the strongly induced luminescent strain (induced with 0.2% arabinose), from Figure 2.2 and the weakly induced luminescent strain (induced with $2x10^{-5}$% arabinose), from Figure 2.6 as a function of the distance from E5 as blue diamonds and green points, respectively. *This figure was adapted with permission from Paper I* (Mauri *et al*., 2019). Copyright 2019 American Chemical Society.

Next, we analyzed how wells with different optical density influence bleed-through over the plate. To do so, we designed a calibration plate were on one half (columns 1 to 5) was filled with the non-luminescence *E. coli* strain SV01 and the and on the other half (columns 6 to 12) with water (Figure 2.8A, B). The results show that the bleed-through factors are not influenced by the OD of surrounding wells (Figure 2.8C), indicating that the optical properties within individual wells do not critically affect bleed-through.

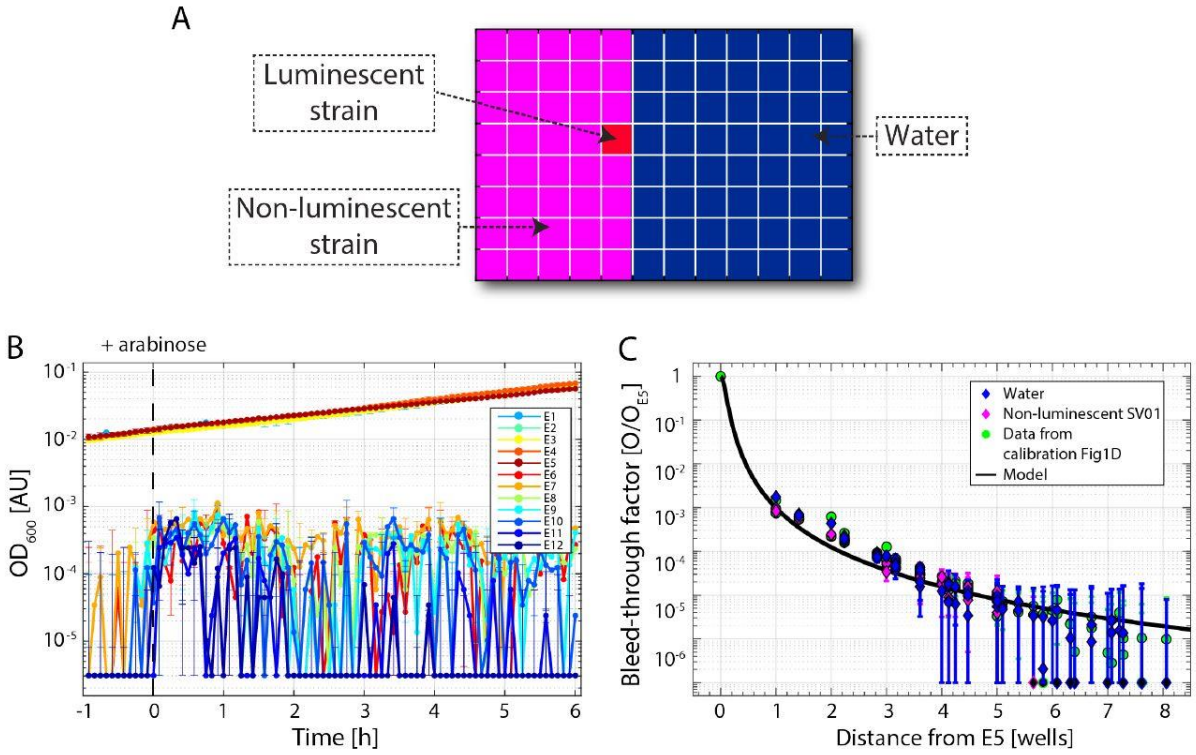

Figure 2.8. Optical density influence on the luminescence bleed-through. (A) Arrangement of the calibration plate: left half (columns 1 to 5) was filled with the non-luminescent *E. coli* strain SV01 and right half (columns 6 to 12) with water. Water and bacterial strain SV01 have two orders of magnitude difference in the measured OD_{600} (10^{-4} and 10^{-2}, respectively), as shown from the OD_{600} measured along row E of the plate (B). (C) Bleed-through factors of water (blue diamonds), SV01 (magenta diamonds) and from the original calibration plate in Figure 2.2D (green diamonds). *This figure was reprinted with permission from Paper I* (Mauri *et al*., 2019). Copyright 2019 American Chemical Society.

To further assess the robustness of the algorithm, we tested how different levels of luminescence bleed-through would affect the results of the deconvolution process. To this end, we designed a test plate (Figure 2.9), in which low, medium and strong luminescence signals (in columns 2, 7 and 12) were positioned adjacent to identical gradients of luminescence intensities (in columns 1, 6 and 11). Luminescence gradients were obtained by inducing a chromosomally integrated P_{BAD}-*luxCDABE* reporter construct (strain GFC0214), while the low, medium and strong luminescence signals were obtained by non-luminescent *E. coli* strain, and *E. coli* strain GFC0153 induced with medium and high arabinose levels respectively. 170 minutes after induction with arabinose the raw data for the luminescence gradients are biased by the bleed-through strengths of the other luminescent strains (Figure 2.9A). This can be appreciated plotting dose-response curves of the (raw) luminescence gradients (Figure 2.9C), that show a 100-fold increase of the apparent basal promoter activity at 0% arabinose ranging from 5 RLU at low bleed-through (column 1) to 500 RLU at high bleed-through (column 11). Strikingly, after deconvolution, the dose-response curves at different bleed-through strength collapse on the curve with low bleed-through (Figure 2.9D). Furthermore, all wells loaded with media and the non-luminescent strain (Figure 2.9B) are also corrected for the apparent luminescence that appeared in the raw data (Figure 2.9A). This demonstrates that independently of the strength of the luminescence bleed-through that affects the plate, our algorithm is able to recover the real signals within error accuracy.

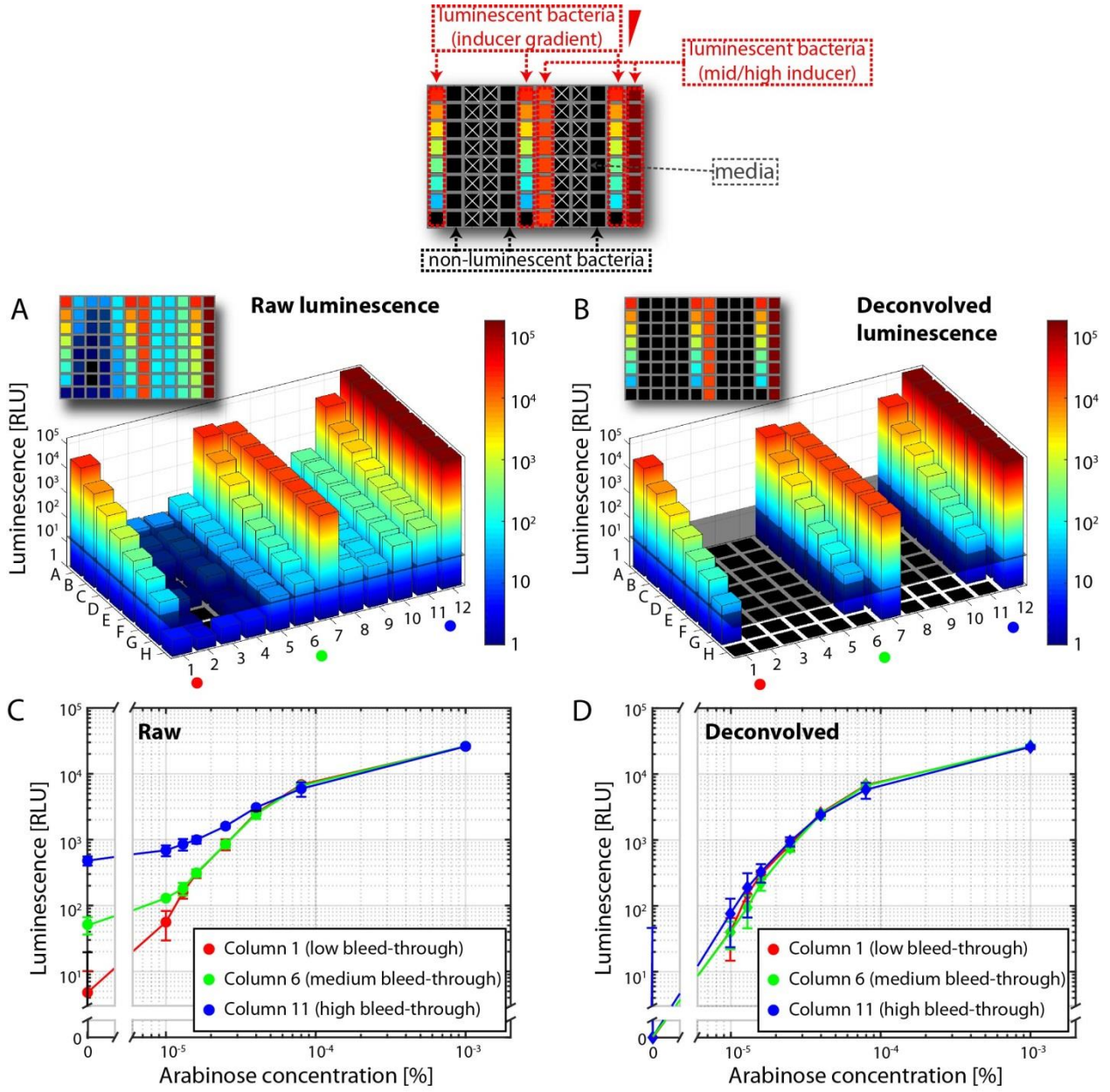

Figure 2.9. Effect of different bleed-through strengths on deconvolution. Luminescence values on the plate 170 minutes after the induction of *E. coli* strain GFC0214 (columns 1, 6 and 11), and of non-luminescent *E. coli* strain SV01 (columns 2, 5 and 10) with varying concentrations of arabinose (in rows 1-7: 10^{-2}%, $8x10^{-5}$%, $4x10^{-5}$%, $2.5x10^{-5}$%, $1.6x10^{-5}$%, $1.3x10^{-5}$%, 10^{-5}%, 0%). Luciferase expression in *E. coli* strain GFC0153 (columns 7 and 12) was induced with 2 $x10^{-5}$% and 0.2% arabinose. Raw and deconvolved luminescence intensities in (A) and (B), respectively, were obtained from three independent biological replicates. (C) The comparison of luminescence intensities in column 1 (red dots), 6 (green dots) and 11 (blue dots) at 170 minutes after induction with arabinose. (D) After deconvolution of the luminescence signals from (C), the three dose-response curves collapse on each other. Data points and error bars represent mean and standard deviations from three experimental replicates. *This figure was reprinted with permission from Paper I* (Mauri *et al*., 2019). Copyright 2019 American Chemical Society.

To ultimately test the deconvolution algorithm we designed a test plate where highly luminescent strains of different intensities were arranged to yield the letters “LUX” in the well of a transparent plate (Figure 2.10A). This kind of plate does not protect against luminescence bleed-through at all, indeed, a single highly luminescent strain illuminates the whole microplate (Figure 2.10C, D) with

highest values of 10^4 RLU reached in the closest wells to the light-producing strain. Figure 2.10B illustrates the raw data of the test plate were bleed-through (in grey) masked real signals (green and blue lines representing "L" and "U", respectively), which are not even close to the background value. However, after generating a new correction plate (Figure 2.10C) and applying the deconvolution algorithm described above, we were able to recover the "true" signals composing the letters "LUX" ($2.5x10^4$ RLU, $8x10^4$ RLU and $2x10^5$ RLU respectively) on the plate and reduce spurious bleed-through signals, as shown in Figure 2.10F.

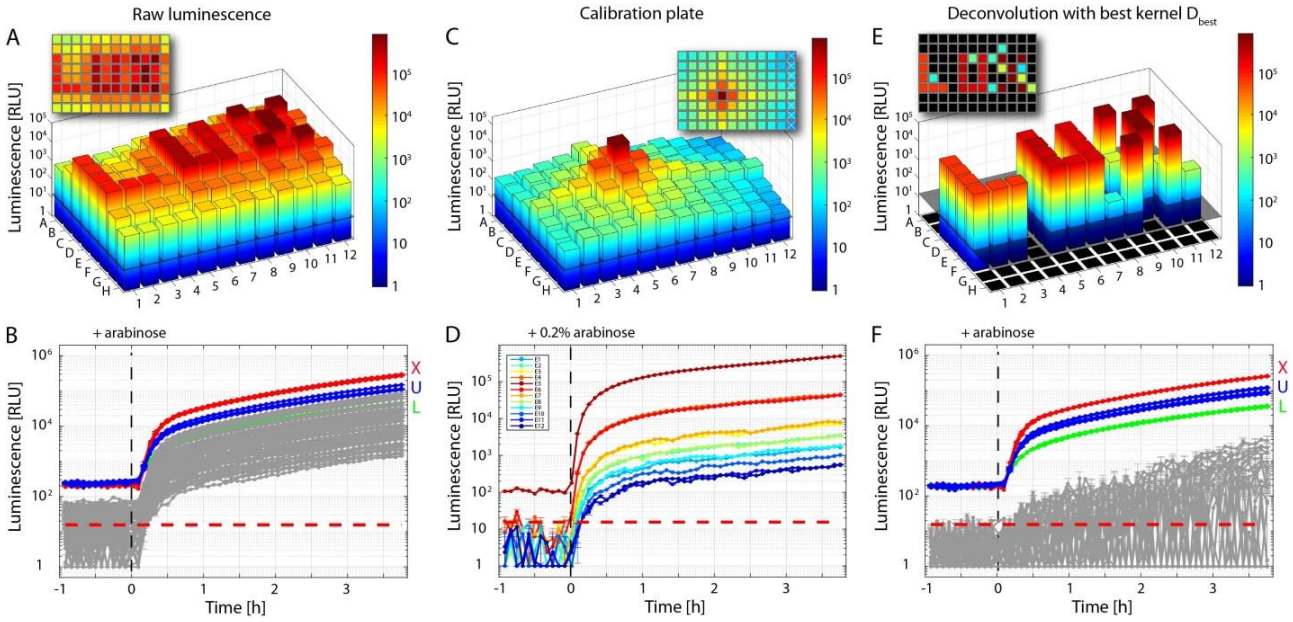

Figure 2.10. Deconvolution of luminescence signals in a transparent microplate. Luminescence values at 137 minutes and time evolution of the calibration plate, raw test plate and deconvolved test plate in (A, B), (C, D) and (E, F), respectively. In the test plate, we arranged luminescent *E. coli* strain GFC0153 to compose the word "LUX". All wells in the letter "L" were induced with 10^{-5}% arabinose, those in the letter "U" with $2x10^{-5}$% arabinose and those in "X" with $5x10^{-5}$% arabinose. Panel (B) shows the time evolution of luminescence in row E in the calibration plate. Panels (D) and (F) show the time evolution of the wells in (C) and (E), respectively, that contribute to "L" (green), "U" (blue), "X" (red), as well as the remaining wells (grey). Data points and error bars represent mean and standard deviations from three experimental replicates. *This figure was adapted with permission from Paper I* (Mauri *et al.*, 2019). Copyright 2019 American Chemical Society.

Overall, the results of all experiments showed the precision and reliability of our bleed-through correction algorithm. Indeed, we were able to correct the data obtained from different experimental setups involving high and low luminescent strains, placed in close proximity in the well of a microplate. In all cases, we were able to recover the otherwise masked weak luciferase signal, within error tolerance.

2.4 Summary

In this chapter, we introduced the *E. coli* strain SV01, as reporter strain to characterize novel synthetic circuits. This strain has the endogenous *lacI* copy knocked out, to allow for networks containing LacI. Moreover, it allows for a graded, arabinose-dependent induction of P_{BAD} promoter.

These modifications make SV01 a perfect candidate for the utilization of circuits encoding classical transcriptional regulators, like the lactose operon regulator (LacI[48]) and the arabinose operon regulator (AraC[49]), in addition to the tetracycline operon regulator (TetR[50]), due to its exogenous nature. In this study, the use of such regulators is fundamental, due to the complexity of the natural mechanisms that control ECF σ factor activation.

High throughput methodologies such plate reader experiments, represent an optimal choice to characterize multiple synthetic circuits at the same time, in a single experiment. In order to extensively use microplate experiments for the characterization of our synthetic circuits, we introduced a luciferase reporter to measure the circuit output. We showed that this reporter increases both resolutions, time response and dynamic range of the circuit output, when compared with the widely used GFP fluorophore (Figure 2.1). However, in microplate experiments, the finite distance between photodetector and microplate leads to the false positive detection of luminescence activities from neighboring wells on the microplate. As demonstrated in Section 2.3, the luminescence bleed-through clearly biases results and therefore limits the otherwise exquisite signal-to-background ratio of luminescence reporters. Hence, we developed a deconvolution method to estimate the true luminescence intensities in all wells of a fully filled microplate. Since our method successfully applied to luminescence data obtained from several different experimental setups, we applied our correction algorithm to all the microplate reader experiments, performed with strains harboring a luciferase reporter, presented in this study.

3. ECF toolbox: a modular framework for fast ECF σ-based circuit generation, from a library of genetic parts

This chapter illustrates the generation of an ECF toolbox, that represents a framework for the fast modular assembly of ECF σ-based, synthetic circuits. The toolbox, based on the MoClo system, contains novel MoClo compatible vectors, that we designed for the expression and the chromosomal integration of the genetic circuits in *E. coli*. Moreover, it contains a library of genetic parts, encoded in the MoClo standard, that we precisely characterized in order to generate ECF σ-based synthetic circuits.

3.1 A novel MoClo expression vector: pSVM-mc

In Section 1.2.1, we introduced the MoClo framework[24,26] as one of the finest DNA manipulation strategies for the bottom-up design of synthetic circuits. The system, based on Golden gate assembly[31], includes a series of vectors organized in levels (0-1-M and P), for the assembly of the genetic parts in circuits with increasing complexity. Thus, a library of level 0 part, can be combined into a level 1 destination vector, generating a transcription unit (TU). Multiple TUs can then be assembled into level M and subsequently, from level M to level P generating more complex genetic pathways (Figure 1.5). However, since the MoClo was mainly designed to simplify the multi-part assembly, the majority of MoClo vectors possess a high copy number origin of replication (pMB1 or ColE1 ori). This allows for high plasmid yield during the cloning process but can lead to cellular stress when the plasmid is used as reporter vector. Indeed, the maintenance of such a high copy number plasmid can generate metabolic burden to the cell[103]. However, the MoClo toolbox also provides a level P destination vector (pICH82094) that features a high copy number origin of replication (ColE1) before cloning and a medium origin of replication (p15A) after cloning[26]. Hence, this plasmid represents a suitable medium copy reporter vector, however, existing only in level P, it limits the speed of circuit generation when starting from level 1 parts. Indeed, due to the characteristics of the system, level 1 parts have first to be cloned into a level M destination vector, to then be sub-cloned in a level P vector.

In order to address this problem, we created a variant of this medium copy vector, possessing level M fusion sites. To do so, we used Gibson assembly, PCR-amplifying the plasmid backbone from pICH82094, including the kanamycin resistance cassette and the medium copy number origin of replication. We then amplified the multicloning site of pICH82094, using primers that provide the homology region necessary for the Gibson assembly and at the same time allowed the exchange of the MoClo fusion sites from level P to level M. Finally we fused the two PCR products, generated the new MoClo reporter plasmid pSVM-mc, possessing two origins of replication and level M compatibility (Figure 3.1 and Section 7.4).

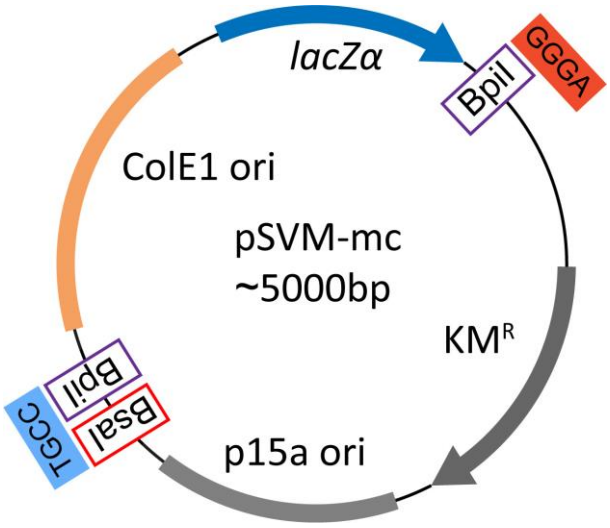

Figure 3.1. Blueprint of MoClo compatible reporter vector pSVM-mc. The vector possesses a double origin of replication (ColE1 and p15a) and a kanamycin resistance cassette (KM^R). During the cloning procedure, the use of the Type IIs restriction enzyme BpiI allows the generation of level M compatible fusion sites (TGCC-GGGA) and simultaneous excision of a DNA fragment containing *lacZα* and the high copy number origin of replication ColE1. Like the original MoClo level M and P destination vectors, pSVM-mc must be used in combination with the appropriate end-linker, (see Section 1.2.1) that will add a second BsaI site for further cloning of the parts in level P-compatible destination vectors (see main text for compatibility with level P vectors).

The majority of the complex synthetic circuits, analyzed in this study, are assembled, on average, by a combination of 5 level 1 TUs. Thus, encoding the genetic circuits into the original level P medium copy vector would have required, for each assembly, an extra intermediate cloning step using level M destination vectors. Hence, the novel pSVM-mc vector offers the fastest way for assembling MoClo encoded level 1 parts onto a medium copy expression plasmid. However, since this vector possess the same resistance cassette of level P vectors (kanamycin), a genetic circuit encoded on pSVM-mc does not allow, in principle, cycling between level M and level P. The usage of the same resistance cassette, in pSVM-mc and level P vectors, is due to the fact that during the vector construction we were not able to implement the original level M resistance cassette (spectinomycin), in combination with the medium origin of replication p15A. This is probably due to the promoter characteristics of the spectinomycin cassette, that did not allow the proper expression of the antibiotic gene when the construct was encoded on a lower copy plasmid. However, this represents a minor limitation, mainly because the genetic constructs encoded on pSVM-mc represent the finalized version of a circuit that, usually, do not require further expansion. Moreover, we further developed a new class of level M and P MoClo compatible vectors (presented in the following section) possessing additional resistance cassettes. Even though these vectors are meant to be used for the chromosomal integration of MoClo compatible genetic constructs, they can also be used as classic MoClo cloning vectors.

3.2 Expanding the MoClo: CRIMoClo vectors

The results of this section are included in Paper II (under review in Journal of Biological Engineering)

As illustrated in the introductory Section 1.2, the MoClo system represents a valuable tool for synthetic biology, allowing for simple library propagation and combinatorial assembly from reusable parts[24]. However, even though the system allows for complex genetic circuit generation, to date all circuits are assembled on low and multi-copy plasmids. Encoding the genetic constructs on multi-copy plasmids presents certain advantages (e.g. amplification of the output signal of a synthetic circuit, or increasing the production yield of a recombinant protein), however, it may also lead to overproduction of proteins. This can, in turn, generate adverse effects on growth and stress responses that are not present at lower levels of expression[104]. To circumvent these issues, a general strategy consists in lowering the copy number of the genetic constructs via chromosomal integration. As introduced in Section 1.3, currently there are different strategies for integrating DNA from plasmids into the *E. coli* chromosome, mainly based on recombineering-based strategies[37,38,42] and bacteriophage integrases[39,40]. However, these methodologies are normally limited in terms of speed and modularity of the circuits assembly. Thus, it would be desirable, to have a system that combines the advantages of the combinatorial assembly, with a highly efficient chromosomal integration strategy. While a lambda Red-based recombination framework, that facilitated the generation and the integration of multi-part genetic constructs, was provided by Schindler *et. al*.[30], a similar system has never been developed for strategies that rely on bacteriophage integrases.

The principal system that utilizes bacteriophage integrases for the chromosomal integration is based on "Conditional-replication, integration, and modular" (CRIM) plasmids[39], which features were described in detail in Section 1.3. Briefly, these plasmids allow for the insertion of large DNA fragments at different bacterial phage-attachment (*attB*) sites. The integration is due to site-specific recombination and it is driven via expression of phage-derived integrase (*int*) encoded on a helper plasmid. Thanks to the proprieties of the system the integration of the CRIM and the cure of the helper plasmid occur simultaneously. Moreover, since CRIM plasmids can only replicate in a host carrying the *pir* gene, the integrant clones can be easily selected by transforming a *pir*$^-$ host with CRIM plasmids, under antibiotic selection[39] (Figure 1.6). These characteristics make CRIM plasmids a fast and reliable strategy for *E. coli* chromosomal integration, however, as introduced above, CRIM-based methods lack standardization, thus limiting the speed of DNA assembly/integration. Moreover, the phage attachment (*att*) sites have never been characterized in terms of gene expression orthogonality. Hence, in order to increase the speed of circuit generation and integration, allowing at the same time the recycling of the genetic parts, we decided to combine the most valuable CRIM features with the modularity of the MoClo system. By doing so, we created a set of 32 novels CRIMoClo plasmids that facilitate the generation and the integration of synthetic circuits, built from reusable MoClo genetic parts. Further, we compared the expression levels of various reporter constructs, when integrated, using CRIMoClo plasmids, into 4 different phage attachment sites, thus assaying the suitability of the 4 *att* sites for the orthogonal expression of synthetic circuits.

3.2.1 CRIMoClo features

As illustrated previously, the MoClo system provides a series of vectors that are organized in different levels (0. 1, M and P) defined by a specific resistance cassette and different 4bp overhangs. Since in the MoClo system the basic DNA parts and the transcription units are encoded in level 0 and level 1 vectors[24,26], we generated CRIMoClo plasmids possessing level M (pAGM8031) and level P (pICH75322) fusion sites. Thus, like in the original MoClo framework, up to six level 1 TUs can be cloned in CRIMoClo level M destination vectors, as well as in MoClo level M destination vectors. Subsequently, up to six level M parts (encoded on MoClo or CRIMoClo plasmids) can be assembled to level P destination vectors of both systems. Thus, since both CRIMoClo M and CRIMoClo P plasmids can also be integrated into the genome of *E. coli*, the system allows for a seamless transition between MoClo destination vectors, MoClo compatible expression vectors and chromosomal integration (Figure 3.2).

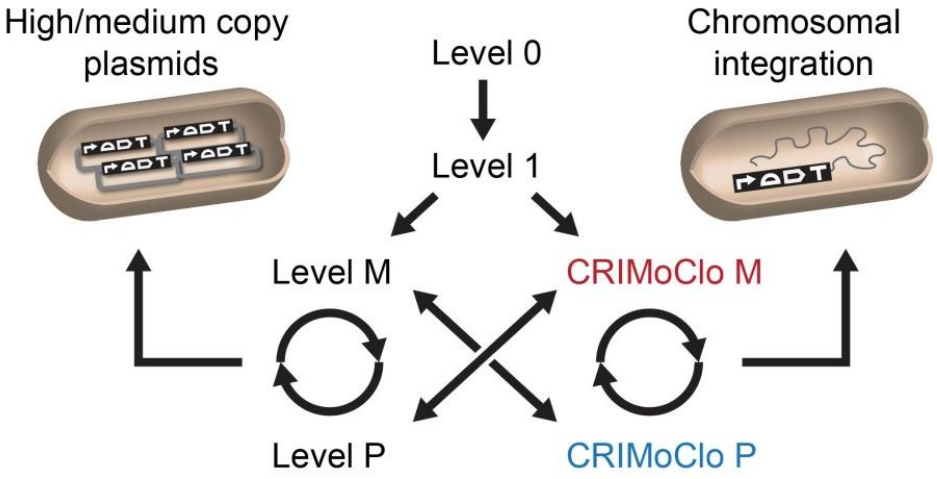

Figure 3.2. Joint use of CRIMoClo plasmids (level M and P) with other vectors in the MoClo system. Any transcription unit generated in Level 1 can be cloned into high/medium copy number MoClo plasmids or be chromosomally integrated using CRIMoClo plasmids. The design of CRIMoClo plasmids allows for a seamless transition between the two systems.

Within the level M and P cloning sites of CRIMoClo plasmids, we maintained the *lacZ* gene from *E. coli*, for blue/white selection and added a high copy number origin of replication (ColE1) derived from MoClo vector pICH8209[24]. CRIMoClo plasmids also possess the γ conditional origin of replication of R6K, which requires the *trans*-acting π protein (encoded by *pir*) for replication, allowing them to replicate at a medium (15 per cell) plasmid copy number in *pir*$^{+}$ *E. coli* hosts, but not in normal (non-*pir*) hosts[105]. This setup with dual origins of replication allows propagation of the CRIMoClo vectors at high copy number before cloning a construct (relying on ColE1), and their conversion into suicide vectors after cloning (relying on R6K), which in turn allow efficient chromosomal integration in non-*pir* hosts (see below). Moreover, in our design, the MoClo cloning module is flanked by bacterial (*rgnB*) and phage λ (*tL3*) terminators to insulate the insert from transcriptional read-through. Last, each CRIMoClo vector exists in four variants that differ in the selectable resistance markers, allowing high flexibility while maintaining the capability of switching between level M and level P. CRIM plasmids can be integrated efficiently in different phage attachment sites into the chromosome of *E. coli* and other bacteria[39]. To maintain this feature,

CRIMoClo plasmids possess four phage attachment sites (att_{HK022}, att_{P21}, $att_{\phi 80}$, att_{λ}) that showed the highest integration efficiency before[39](Figure 3.3A). A detailed description of the strategies used for the generation of CRIM plasmids is available in Section 7.5.

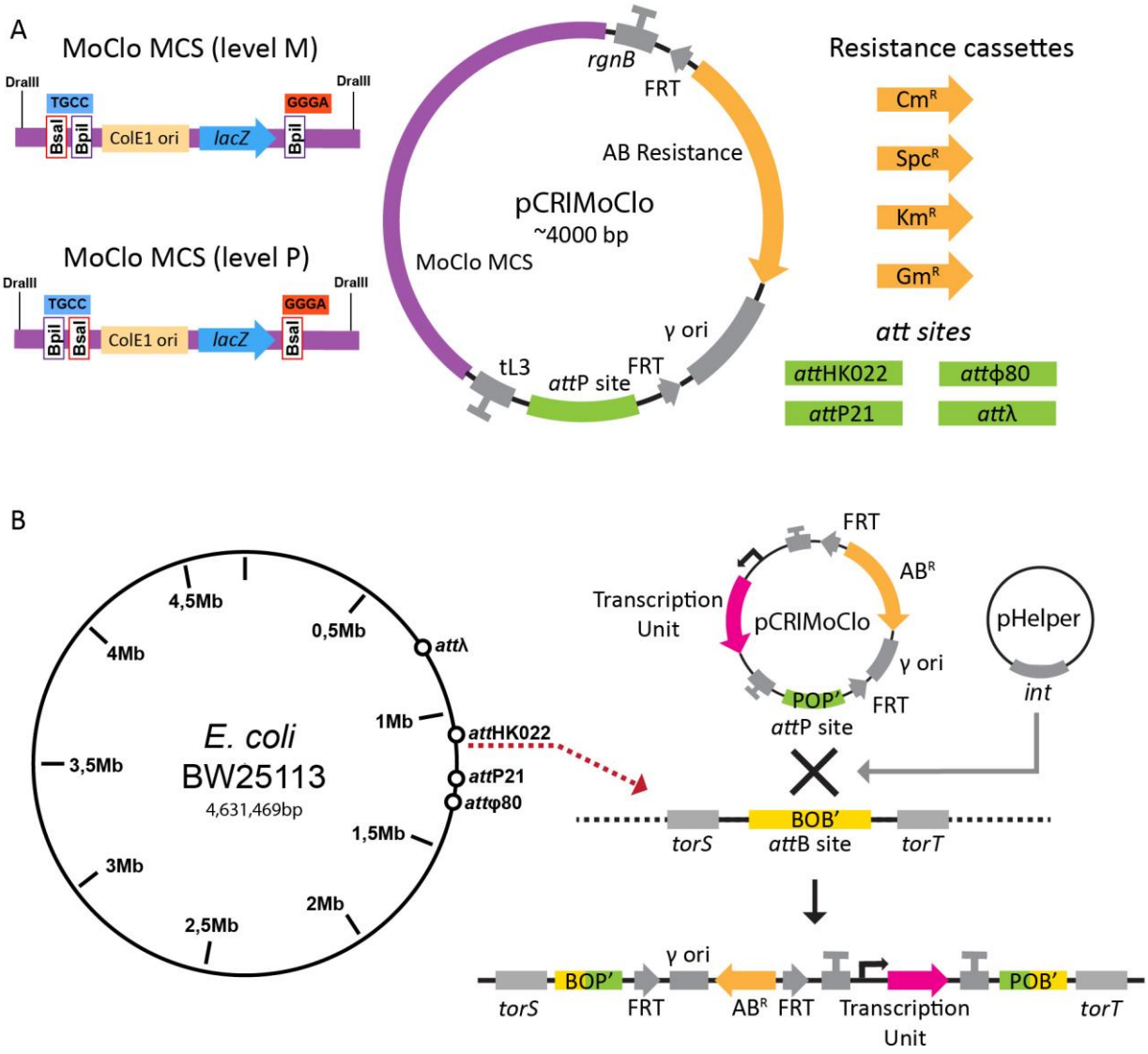

Figure 3.3. CRIMoClo vectors and chromosomal integration. (A) Blueprint of CRIMoClo plasmids. Each plasmid has a MoClo-compatible cloning cassette (purple box), flanked by two terminators (*RGB* and *tL3* depicted in grey) and followed by a selectable resistance marker (orange arrows), a γ conditional-replication origin (grey box), both enclosed between two FRT sites (grey arrows). All CRIMoClo plasmids have one of four different phage attachment sites (green boxes) for the integration into the chromosome by site-specific recombination. (B) Locations of chromosomal *attB* sites into the annotated genome of *E. coli* BW25113 (left) and site-specific recombination of CRIMoClo-based plasmid into the att_{HK022} (right).

The chromosomal integration into one of the *attB* sites follows the same strategy of CRIM plasmids (Figure 3.3B), where a non-*pir E. coli* strain carrying a CRIM helper plasmid (expressing the integrase specific to the respective *attB* site on the chromosome[39]) is transformed with the CRIMoClo-based plasmid. Alternatively, CRIMoClo and helper plasmids can be efficiently co-transformed (see Section 3.2.3) using the transformation and storage solution (TSS)

methodology[106]. Independent of the preferred strategy, expression of the integrase gene encoded in the helper plasmid is induced at elevated temperatures during the transformation procedure (as described in Section 7.6), and since the helper plasmids are also temperature-sensitive for replication, integration and curing of the helper plasmid occur in the same incubation step. Single integration events can be then screened by colony PCR with four primers (P1-P2-P3-P4; see Table 3.1) that allow the distinction between single, multiple, and no integration events (as described previously[39]). Like the original CRIM plasmids, CRIMoClo plasmids can also be excised efficiently from the chromosome by another round of helper plasmid transformation and excisionase (*Xis*) expression[39].

attB site	PCR fragment size (bp)			
	P1-P2	P2-P3	P3-P4	P1-P4
HK022	499	583	824	740
P21	767	881	620	506
ϕ80	611	797	732	546
λ	787	712	666	741

Table 3.1. The predicted size of PCR fragments for *attB* sites, using primers P1-P2-P3-P4. Successful integration events at each *attB* site are revealed by two fragments generated by P1-P2 and P3-P4 (highlighted in green). Recombinants with two (or more) CRIMoClo plasmids at the *attB* site show, in addition, a third fragment generated by P2-P3. False positives (non-integrants) are revealed by the PCR product generated by P1 to P4 (highlighted in red).

Based on this design we created a combinatorial set of 32 CRIMoClo plasmids featuring all permutations of four phage attachment sites (att_{HK022}, att_{P21}, $att_{\phi 80}$, att_{λ}), four resistance cassettes (chloramphenicol, kanamycin, spectinomycin, gentamicin) and compatibility with two MoClo levels (M and P). In theory, this now allows efficient assembly and chromosomal integration of synthetic genetic circuits in only four days, starting from level 1 transcription units. Moreover, the availability of each plasmid with one of four resistance cassettes should allow, in principle, sequential integration in different *att* sites without the necessity of recombining the resistance cassette after each integration step.

3.2.2 Insulation and robustness of gene expression at *attB* sites

To demonstrate the versatility of CRIMoClo plasmids for synthetic biology applications, we evaluated the modularity of chromosomal integration into the four *attB* sites. To this end, we compared the expression of the same reporter constructs integrated into each of the *attB* sites. The position of the integration sites (*attB*) in the chromosome of *E. coli* BW25113 (the closest parental strain of our reporter strain SV01 with an annotated genome) is shown in Figure 3.3B. Since essential chromosomal genes lie between the different integration sites and since all CRIMoClo plasmids are integrated into the same relative orientation, recombination among them does not lead

to genome instability, as previously described[39]. In order to evaluate the gene expression of the four *attB* sites, we used the P_{BAD}-*lux* reporter construct illustrated in the previous sections. We, therefore, sub-cloned this transcription unit, encoded on MoClo level 1 vector, in all 16 CRIMoClo M plasmids (all combinations of four different *att* sites and four selection markers) simultaneously in 1 day. After construct verification and plasmid isolation (day 2) we integrated them in the four different phage attachment sites (att_{HK022}, att_{P21}, $att_{\phi 80}$, att_{λ}) of *E. coli* strain SV01 (day 3). On day 4 we tested the clones with colony PCR and strikingly, single integration events showed a success rate of 97% for all *att* sites and selection markers.

The expression of the luciferase cassette was benchmarked by growing strains in defined minimal media and assaying luciferase activity continuously for 8 h after the addition of the inducer (Figure 3.4A). We found that in all *loci* the luciferase signal was not detectable in the absence of the inducer, while, after induction, the luciferase operon was expressed from all promoters (~10,000- to 100,000-fold over empty vector control depending on the inducer concentration). Strikingly, in all *loci*, the expression dynamics (corresponding to different inducer levels) measured in the different *att* sites, are almost identical. In fact, when quantitatively comparing the luciferase activities between the different loci, we find a striking correlation of the detected signals for each arabinose concentration at individual time points (Figure 3.5A). This shows that integration into the four *att* sites leads to highly reproducible gene expression behavior, suggesting that the loci can be used in an interchangeable and orthogonal manner for the chromosomal integration of synthetic circuits.

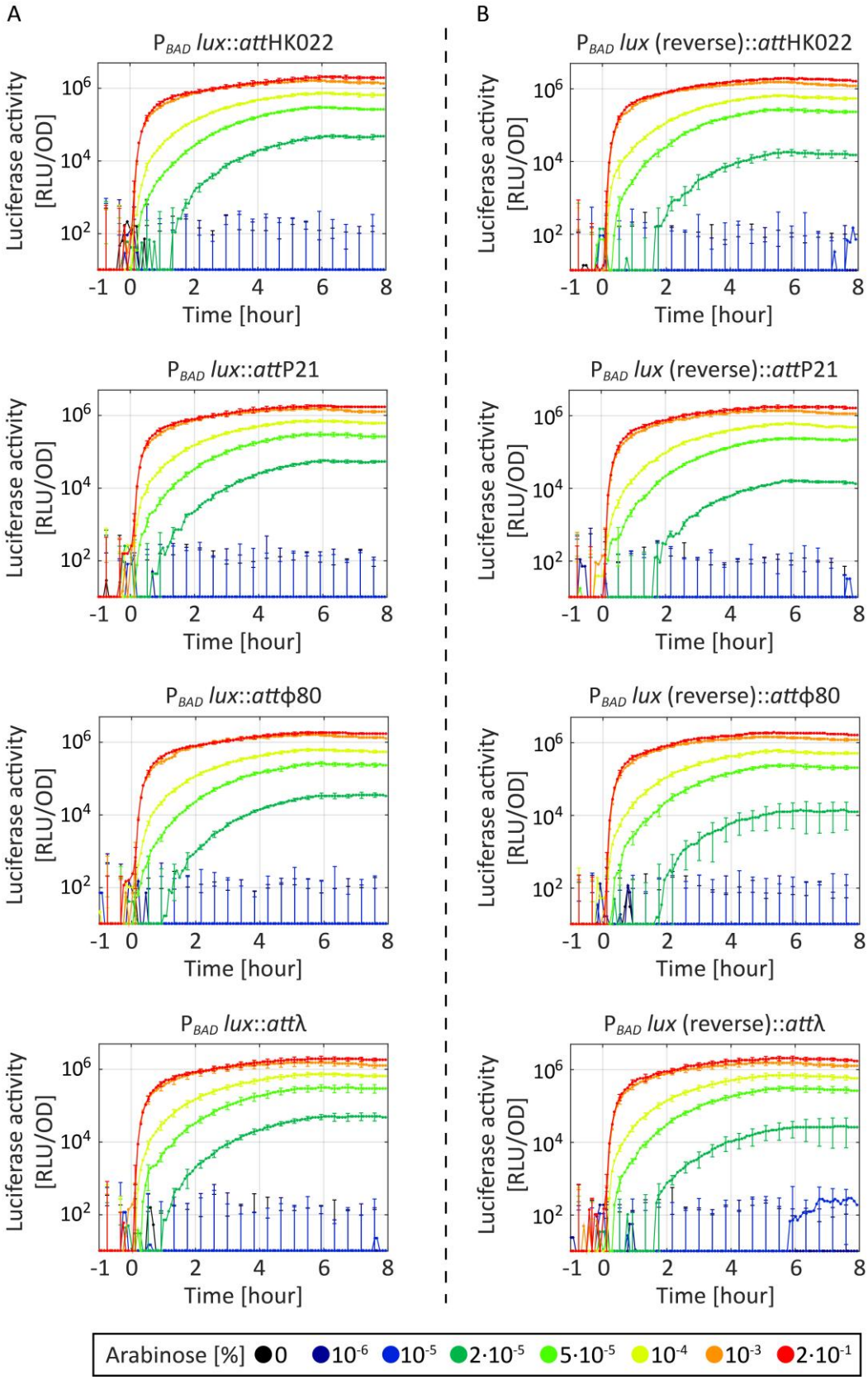

Figure 3.4. Dynamical response of luciferase activity measured from four phage attachment sites. Comparison of the dynamical response of luciferase activity of the P_{BAD}-*lux* construct integrated into att_{HK022}, att_{P21}, $att_{\phi 80}$, att_{λ} in forward (A) and reverse (B) orientation, after the addition of indicated concentrations of arabinose at t=0 h. The results are averaged from at least two independent biological assays and error bars denote standard deviations.

Since each CRIMoClo plasmid exists with four different resistance cassettes (Figure 3.3A), we wanted to test the potential influence of the resistance cassettes on reporter activity after chromosomal integration. To this end, we integrated and measured the expression level of P_{BAD}-*lux* integrated into all *att* sites, using CRIMoClo plasmid possessing different selection markers (Figure 3.5B and Appendix Figure 9.1-9.3). The results show again virtually any difference in the expression level, suggesting that also the different resistance cassettes can be used interchangeably.

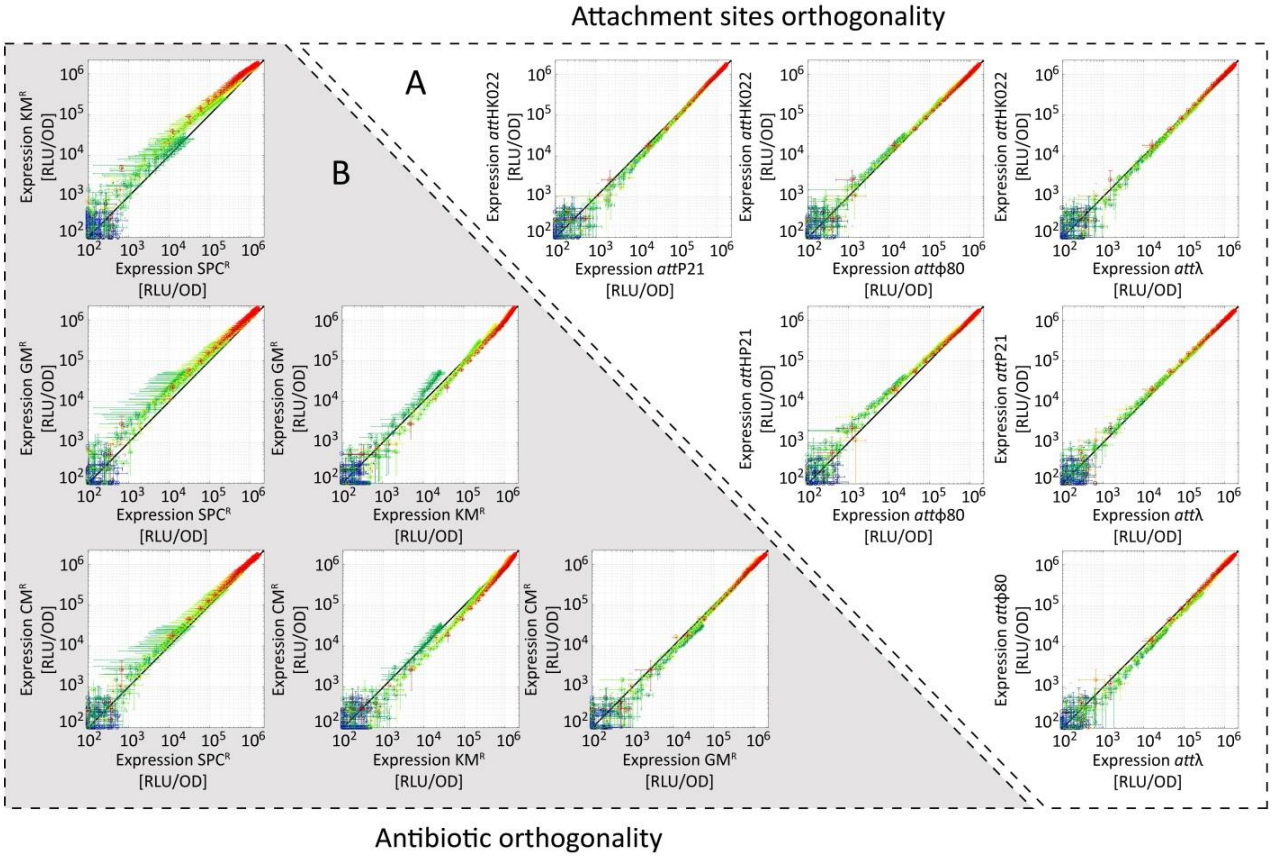

Figure 3.5. Orthogonality of reporter gene expression between different integration sites and between different resistance cassettes used for integration. (A) Correlation graphs between the luciferase activities in Figure 3.4A, obtained from P_{BAD}-*lux* integrated into different *att* sites. Each data point represents mean and standard deviation measured at a the same time point in Figure 3.4A, while the color code indicates the inducer concentration as in Figure 3.4 (B) Correlation graphs between luciferase activities obtained from P_{BAD}-*lux* integrated into att_{HK022}, using CRIMoClo plasmids with four indicated resistance cassettes (chloramphenicol, kanamycin, spectinomycin, gentamicin). All data indicate averages from at least two independent biological assays and error bars denote standard deviations.

The position and orientation of genes on the chromosome may affect the expression pattern of a neighboring transcription unit (TU), e.g., due to transcription-induced DNA supercoiling, affecting the activity of neighboring promoters[107]. Even though the different CRIMoClo plasmids are integrated into the same relative direction, the orientation of the cloned construct can be easily inverted using the proprieties of the MoClo system (e.g. starting with level 1 parts cloned in reverse orientation). To test whether the expression of a TU is influenced by its orientation in the four *att* sites on the genome, we integrated P_{BAD}-*lux* in reverse orientation in all loci (Figure 3.4B). The results show again no difference in the expression level of the construct from the different *att* sites. Moreover, the expression levels of constructs cloned in forward and reverse orientation are virtually

identical (Figure 3.4A and 3.4B), indicating that the circuits are well insulated from the genetic context and that the *att* sites are not affected by effects such DNA supercoiling.

Overall, these results show that the four phage attachment sites are well-insulated from their genetic context and that the different positions and orientations of the transcription units on the chromosome do not influence the dynamics of reporter gene expression. Therefore, our experiments demonstrate orthogonality of the four phage attachment sites of the CRIMoClo system, which makes them ideally suited for synthetic biology applications.

3.2.3 Multi-locus integrations

The high-efficiency of site-specific recombination combined with the availability of four different resistance cassettes should, in principle, enable fast and reliable multi-locus integrations. To demonstrate this, we sequentially integrated four different reporter cassettes into the *E. coli* chromosome, without removing the selectable marker after each integration step. The novel transcription units were built fusing the inducible P_{BAD} promoter with different reporter genes (*gfp*, *mCherry*, *mTurquoise*). To achieve sequential multi-integration, we used the *E. coli* strain harboring P_{BAD}-*lux* in att_{HK022} (GFC0214) characterized above, and integrated P_{BAD}-*gfp* in att_{P21}, as described in Section 7.7. The newly generated strain (GFC0505) was then used for the integration of P_{BAD}-*mCherry* in $att_{\phi80}$ (GFC0533) and subsequently P_{BAD}-*mTurquoise* in the last available *att* site (att_{λ}), generating strain GFC0547. We analyzed the expression level of the different reporter constructs expressed in the newly generated strains (single, double, triple and quadruple integration) and compared them with single integration strains, were each reporter construct was integrated in one of the four phage attachment sites individually (GFC0214, GFC0514, GFC0531, GFC0544 harboring P_{BAD}-*lux*::att_{HK022}, P_{BAD}-*gfp*::att_{P21}, P_{BAD}-*mCherry*::$att_{\phi80}$, P_{BAD}-*mTurquoise*::att_{λ}, respectively). All the strains were monitored within time course experiments for optical density (measured at 600 nm) and the four reporter activities (also when one or more of the reporters were absent) following the expression of the reporters, in presence and absence of the inducer. The histogram in Figure 3.6 shows the dynamic range (reporter signal of induced strain, divided by reporter signal of uninduced strain), measured after 10 h, of all single integrant strains in comparison with strains generated with single, double, triple or quadruple integration events.

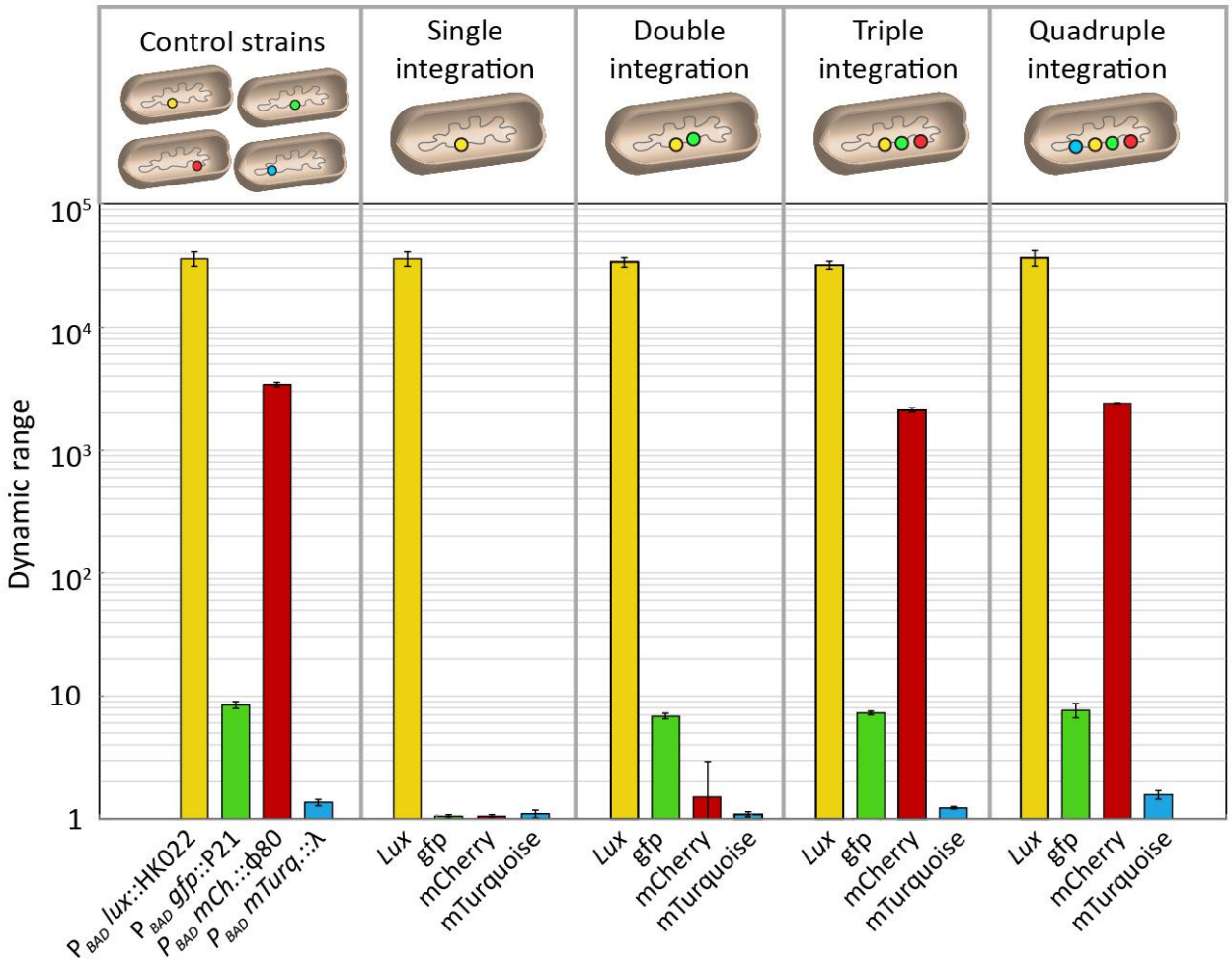

Figure 3.6. Dynamic range of four reporter constructs measured from four phage attachment sites. The dynamic range of four different arabinose-inducible reporter constructs, integrated sequentially into the genome of *E. coli* in four phage attachment sites (att_{HK022}, att_{P21}, $att_{\phi 80}$, att_{λ}) and control strains in which the same reporter systems are integrated singularly in one of four phage attachment site. The dynamic range is measured as the luminescence induced with 0.2% of arabinose, divided by the basal activity of the promoter in the absence of arabinose. All data indicate averages from at least two independent biological assays and error bars denote standard deviations.

Overall, we found that the transcription units were functional after the integration (Figure 3.6). The luciferase construct showed the highest dynamic range (~$3.8x10^4$-fold induction), followed by mCherry (~$3.5x10^3$-fold induction), GFP (~8.9-fold induction) and mTurquoise (~1.4-fold induction). Moreover, the signal measured in the strains that lack one or more reporter system (single, double, and triple integration), was not detectable in case of GFP and mCherry, or close to the lower detection limit for mTurquoise, indicating the absence of cross-talk among different reporters. Strikingly the dynamic range values for single integrant strains are identical (within the error tolerances) to the one calculated for single, double triple and quadruple integration strains (Figure 3.6), showing that the sequential integration of each reporter construct does not affect the expression level of the previously integrated ones. Also, the simultaneous presence of multiple copies of P_{BAD} in the same strain does not lead to instability or change in reporter expression levels, suggesting that the potential recombination among the loci does not occur. Finally, these results

show that the multi-integration strategy using CRIMoClo plasmids is highly flexible and does not require time-consuming removal of resistance cassettes after the individual integration steps.

Overall, our experiments showed that the CRIMoClo system allows for the generation of genetic circuits from reusable, MoClo-compatible parts and their reliable integration into 4 *att* sites into the genome of *E. coli*. We showed that the expression levels of a reporter construct from each locus is highly similar and independent by the orientation. Moreover, utilizing four different resistance module CRIMoClo system allows for easy, fast, and reliable multiple integrations. With these features the CRIMoClo system brings the combinatorial assembly to the next step, making possible a flawless transition between plasmid-encoded and chromosomally integrated genetic circuits. Finally, used together, MoClo and CRIMoClo systems, allow for the generation and simultaneous utilization of plasmid-borne and chromosomally integrated genetic modules. We will extensively use this possibility in the next chapters, showing how the combination of the two systems allows fine-tuning the stoichiometry of the different components of a synthetic circuit, maximizing the downstream output signal dynamic.

3.3 A library of parts encoded according to the MoClo standard

In the previous sections, we presented our expansions to the MoClo system, that now can count on a novel medium copy number expression vector, as well as on a set of 32 modular CRIMoClo plasmids for fast and reliable chromosomal integration. As mentioned above the MoClo framework represent an attractive solution to perform combinatorial assembly from a library of genetic parts. Hence, in this section, we present our MoClo-encoded part library that served as a base for the construction of all the genetic circuits analyzed in this study.

As mentioned previously, the entry vectors of the MoClo system are defined as level 0, thus we encoded our library of basic genetic parts within different destination vectors belonging to this level. As illustrated in Section 1.2.1, upon PCR amplification with primers that include the Type IIS restriction site BpiI and the appropriate fusion sites, a genetic part can be easily cloned in one of 16 different level 0 vectors, generating a level 0 part. It is important to notice that this is the only step in the MoClo system that requires PCR amplification, indeed, the next cloning steps only require the level 0 parts generated by the user and an empty MoClo vector belonging to the next level. According to the proprieties of the MoClo framework, any transcription unit assembled in level 1 must begin with a part cloned in a level 0 vector having the left fusion site “GGAG” and end with a part cloned in a level 0 vector having the right fusion site “CGCT”[24](Figure 3.7). In order to fulfill this requirement, we cloned the different genetic parts of the library (promoters, ribosome binding sequences, coding sequences, and terminators) in specific level 0 vectors (pICH41233, pICH41246, pICH41308, pICH41276 respectively[24]) as illustrated in Figure 3.7.

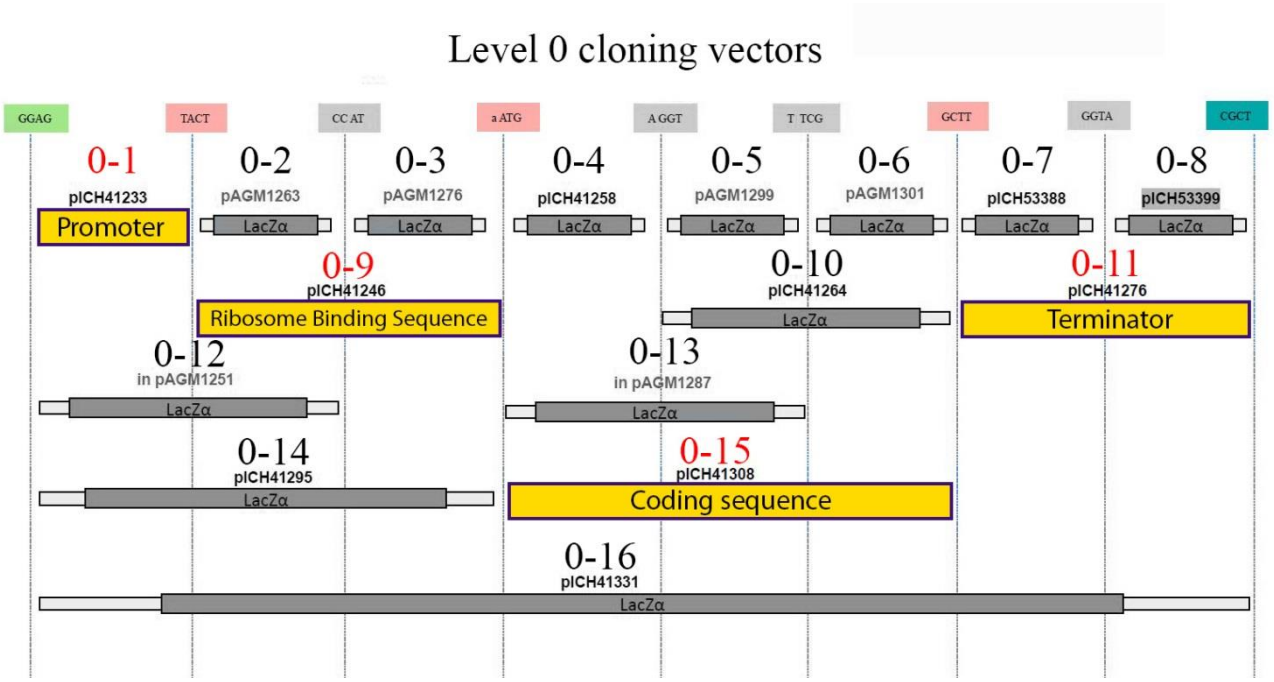

Figure 3.7. MoClo level 0 vectors and positioning of MoClo-encoded library parts. Yellow boxes indicate the position (within different level 0 destination vectors) and the category of different library parts. The original names of the MoClo vectors (pICH and pAGM series) and the sequence of the 4bp fusion sites are indicated. We assigned codes from 0-1 to 0-16 to the MoClo vectors in order to simplify the identification of specific MoClo-encoded parts within the library. The complete list of our level 0 part library is reported in Table 9.3.

We selected these vectors in order to maintain maximum flexibility for future expansion of the library. For instance, a coding sequence that is normally cloned in the vector pICH41308 can be also cloned in the vector pAGM1287 and fused with a protein tag cloned in the vector pAGM1301 (Figure 3.7). In this way is still possible to join the newly generated tagged sequence with the promoters, ribosome binding sequences and terminators already present in the library. We also cloned short (15bp) and long (300bp) random DNA sequences that cover each level 0 position. We refer to these sequences as dummy (Du) sequences, as they can be used to substitute any part in a transcription unit. In this way we facilitate, for instance, the creation of an operon, using transcription units that lack the promoter or the terminator. Dummy sequences are also suitable for the generation of insulator elements, especially in combination with terminators (see Section 3.3.4). Finally, for easy identification of the library parts, we named the level 0 vectors from 0-1 to 0-16, as indicated in Figure 3.7. Thus, for instance, all the parts encoded in the vector pICH41233 will be named pXX0-1, where "XX" represents the initials of the creator of the part and 0-1 identifies the position of the part within the library (Figure 3.7).

Promoters, ribosome binding sites (RBS), coding sequences (CDS) and terminators are the basic DNA components that serve for the generation of genetic circuits. Hence, we selected these DNA parts from different sources in order to build our library encoded in MoClo level 0 vectors. In order to precisely control the transcription in the synthetic circuit, the library includes three inducible promoter parts (P_{BAD}[108], P_{tet}[109], $P_{Llac0\text{-}1}$[110]) together with their regulatory proteins (AraC[49] TetR[50], LacI[48]) encoded in divergent orientation. In this way, we ensured to maintain the stoichiometry between the promoter and the regulatory protein (see Section 3.3.1). In addition, the library contains two members of the iGEM Anderson constitutive promoter collection, having low and medium

strength (BBa_J23117, BBa_J23108; http://parts.igem.org/Promoters/Catalog/Anderson). Finally, the library includes 15 *ecf* promoters that previously showed high fold induction and high orthogonality in *E. coli*[63](see Section 3.3.3).

In order to tune the translational efficiency of the mRNA, we included in the library 12 ribosome binding sites (RBS) possessing different strengths[111](see Section 3.3.2). Moreover, we also added 12 synthetic terminators, to mediate transcriptional termination. These terminators have sufficient sequence diversity to reduce homologous recombination when used together in a design[112], a fundamental characteristic in order to combine them in complex synthetic circuits (see Section 3.3.4). To monitor gene expression we added to the library five different reporters, including four fluorophores (GFP mut-3[96], YFP[113], mCherry[80], mTurquoise[114]) and the luciferase cassette from *Photorhabdus luminescens*[97]. Finally, to control the expression of the synthetic circuits the library contains 15 ECF σ factors, 14 anti-σ factors[63], and 21 truncated (soluble) anti-σ factors variants that we created in this study (see Section 3.3.3 and Section 5.2).

Upon their incorporation in the library, all the genetic parts were sequenced. Moreover, in some cases, we also performed some modifications, prior to their insertion into the library. For instance, we added a different strong terminator sequence at the end of each gene encoding the regulatory proteins TetR, AraC, and LacI (see Section 7.8). This allows the usage of these parts in complex genetic circuits, limiting the interference with the expression of neighboring genes. Further, some coding sequences required the removal of BpiI or BsaI restriction sites (Table 9.3). In this case, we ensured to perform synonymous mutations generating, at the same time, a codon with the same, or enhanced translation efficiency in *E. coli*. A detailed description of the strategies used for the generation of the parts included library is available in Section 7.8. The complete list of the level 0 part library is available in Table 9.3.

3.3.1 Part characterization: Promoters

Most of the synthetic regulatory circuits built to date are based on classic transcriptional regulators such as TetR, AraC or LacI. These regulators and the relative inducible promoters allow for precise tuning of the expression level, upon different inducer concentrations. Another advantage is represented by the fact that different inducers can also be used at the same time, allowing for the combination of these promoters in a single bacterial cell[110]. Finally as introduced in Section 2.1, the usage of such regulators is also essential to control the expression of ECF σ factors. For the above-mentioned reasons, we decided to include the three mostly orthogonal inducible promoters, that are controlled by these regulators, in our library.

In case of TetR, we included the natural cognate promoters P_{tet}, that in the "OFF-state" (absence of the inducer) is tightly repressed and can be activated, over a broad dynamic range, by tuning the amounts of the non-toxic inducer anhydrotetracycline (ATc)[50]. Indeed, the repression of P_{tet} by TetR is very efficient and orthogonal, due to a high binding constant of TetR to the operator sequence *tet*O and its low affinity for non-operator sequences when compared with other repressors[115,116]. In case of AraC, we also included the natural cognate promoter P_{BAD}, since it was recently demonstrated, by Kogenaru and Tans, that this promoter modulates the gene expression with a high (up to 898-fold) output dynamic range[80]. Moreover, the authors measured the promoter activity using the SV01 closely related strain MK01 (see Section 2.1), thus enhancing our chances of obtaining a similarly high fold-induction, by using this promoter in our experimental conditions.

In the same work, the authors also show that the natural P_{lac} promoter, controlled by the LacI repressor, modulates the gene expression only up to 23-fold[80]. For this reason, in the case of LacI, we selected the IPTG inducible promoter $P_{Llac0\text{-}1}$ created by Lutz and Bujard[110]. In their work, they used the phage lambda promoter $P_{L,}$ that is commonly induced by inactivating the repressor cI 857 via a temperature shift, and replaced the cI binding sites with sequences encoding the operator of the *lac* operon (*lac*O1). In this way, they obtained an IPTG inducible promoter whose activation was not dependent by temperature shift (like in the case of P_L), nor by the activating complex CRP/cAMP (like in the case of P_{lac}) and that displayed a dynamic range ~600 fold[110].

To extensively use these promoters and control gene expression in our synthetic circuits, we characterized their dynamic response to the inducers, in our experimental conditions. These include the MOPS minimal medium that we use for our assays (see Section 7.1), and our reporter systems (plasmid-borne with an average copy number of 50 per cell, or chromosomally integrated) expressed in the strain SV01. In order to characterize the three inducible promoters, we generated three different TUs, where each of the promoters was fused with the luciferase cassette (P_{BAD}-*lux*, P_{tet}-*lux*, and $P_{Llac0\text{-}1}$-*lux*). We tested these constructs encoded on the medium copy plasmid pSVM-mc and when chromosomally integrated, assaying the response of the luciferase upon the addition of the relative inducers (arabinose, ATc, IPTG) at increasing concentrations (Figure 3.8).

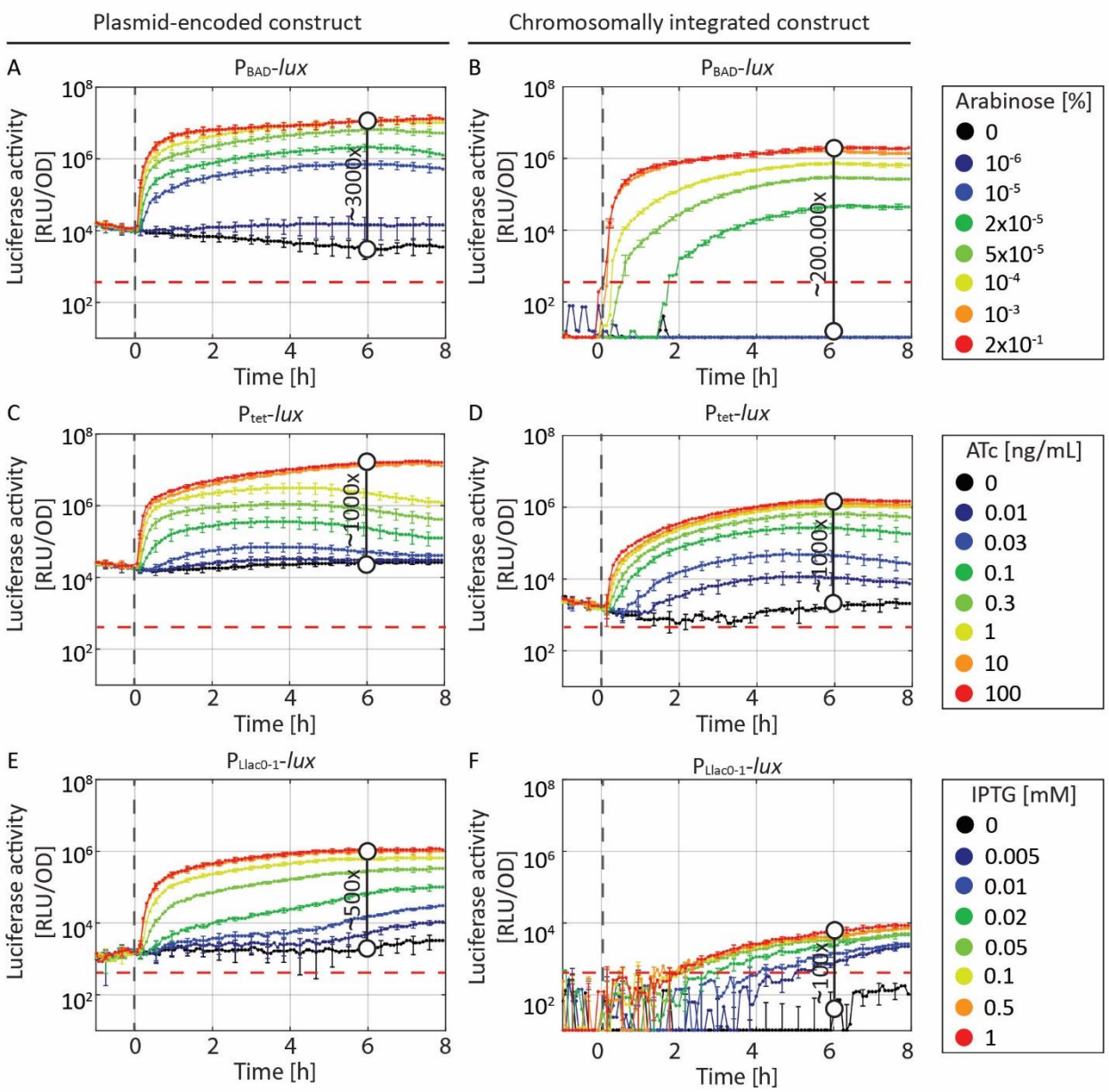

Figure 3.8. Comparison of the dynamical response of three inducible promoters measured in two genetic configurations. Comparison of the dynamical response of luciferase activity, expressed from three inducible promoters in two genetic configurations, after the addition of the indicated concentrations of inducers at t=0 h (grey dashed line). The reporter activities are shown in relative luminescence units, normalized by the optical density measured at 600 nm. The red dashed line represents the low detection limit of the plate reader. The constructs indicated in A, C, E are encoded on the medium copy number plasmid pSVM-mc, while the constructs indicated in B, D, F are integrated at the phage HK022 attachment site into the genome of *E. coli*. The indicated fold inductions are measured as the luminescence induced with the highest inducer concentration indicated, divided by the basal activity of the promoter in the absence of inducer at time t = 6 h. The results are averaged from at least two independent biological assays and error bars denote standard deviations.

Overall we found that all the promoters are inducible with the TUs encoded in both configurations (plasmid-borne; Figure 3.8A, C, E and chromosomally integrated; Figure 3.8B, D, F). Interestingly, the plasmid-borne P_{tet} promoter, showed, for ATc inductions below 10ng/mL, ~2 fold decay in luciferase signal from t = 5h to the end of the measurement (Figure 3.8C). Since the

ATc is light sensitive[117], we reasoned that the signal decay may be caused by the relatively low ATc concentrations, together with the high levels of light produced by the strains. This seems to be confirmed by the fact that the signal decay is less pronounced (<2 fold) in the chromosomally integrated construct, that show ~2 fold lower RLU/OD_{600} signal for the same inducer concentrations (Figure 3.8C, D). Moreover, the signal decay is completely absent for the two highest, induction levels (ATc 10 ng/mL and ATc 100 ng/mL) that allow full saturation of the P_{tet} promoter in both genetic configurations (Figure 3.8C, D).

To compare the characteristics of all promoters, we reported, in Figure 3.8, the fold inductions (calculated taking the luciferase signal relative to the highest induction level divided by the basal activity of the uninduced constructs) of all strains, 6 hours after inducer addition. The promoters display marginal differences in the dynamic range when encoded on medium copy plasmid (~500-3000-fold induction; Figure 3.8A, C, E), while the dynamic ranges show more variability when the constructs are integrated into the chromosome (~100-200000-fold-induction; Figure 3.8B, D, F). In particular, the P_{tet} promoter presents the same dynamic range when encoded on plasmid or chromosomally integrated, due to the fact that in the two configurations the luciferase signals in both ON (ATc 100 ng/mL) and OFF (ATc 0 ng/mL) states scale ~10-fold (Figure 3.8C, D; red and black curves). In contrast, the constructs driven by P_{BAD} and $P_{Llac0-1}$ did not show a proportional shift of the luciferase signals of the ON and the OFF states, when going from multi-copy to single copy. Indeed, when chromosomally integrated, $P_{Llac0-1}$ shows, 6 hours after inducer addition, a signal in the OFF state ~50 RLU/OD_{600} (Figure 3.8F; black curve), generating a 40-fold reduction, when compared with the signal of the plasmid-encoded construct in the same conditions (Figure 3.8E; black curve ~$2x10^3$ RLU/OD_{600}). In contrast, by comparing the two ON states of the plasmid-borne and the chromosomally integrated constructs (Figure 3.8E, F; red curves), we found a signal ~10^6 RLU/OD_{600} and ~$5x10^3$ RLU/OD_{600} respectively. This generates a 200-fold signal reduction, between the ON states, when the construct is expressed in single copy. This apparent lack of proportional shift of the OFF and ON signals (40-fold and 200-fold, respectively), when going from multi-copy circuit to single copy circuit, could arise by the plate reader detection limit. Indeed, the baseline signal of the chromosomally integrated $P_{Llac0-1}$-*lux* construct (from the beginning to the end of the measurement) is below the detection limit of the instrument (~$4x10^2$ RLU/OD_{600}; Figure 3.8; red dashed lines). We can then assume that the "true" baseline signal of the chromosomally integrated construct is also reduced by 100-fold (like in the case of the ON signal), but masked by the instrument sensitivity. This would bring the baseline signal value from ~$2x10^3$ RLU/OD_{600} (plasmid-encoded construct) to ~10 RLU/OD_{600} (chromosomally integrated construct) and, as result, to an identical dynamic range for the two genetic configurations (~500-fold-induction; Table 3.2).

Comparing the plasmid-borne and the chromosomally integrated P_{BAD}-*lux* constructs, 6 hours after inducer addition, we observed a signal reduction of 300-fold for the OFF state (from ~$3x10^3$ RLU/OD_{600} to ~10 RLU/OD_{600}; black lines in Figure 3.8A, B) and of 5-fold for the ON state (from ~10^7 RLU/OD_{600} to ~$2x10^6$ RLU/OD_{600}; red lines in Figure 3.8A, B). Therefore, the surprisingly low signal values obtained for chromosomally integrated P_{BAD} promoter in the OFF state (below the detection limit), confers to this promoter the highest dynamic range (200000-fold induction) among all inducible promoters in both configurations (Figure 3.8 and Table 3.2). The precise molecular reasons for this severe baseline down-shift remain elusive. However, a possible explanation involves the formation of the DNA loop, required for P_{BAD} repression in the absence of arabinose[118].

Indeed, even though the formation of the DNA loop needs the presence of supercoiling tension[118], the loop could be less stable when the promoter is encoded on medium copy plasmid, due to hypersupercoiling of the plasmid DNA[119,120]. This, in turn, would lead to a tighter P_{BAD} regulation when the P_{BAD}-*lux* construct is chromosomally integrated and, consequently, to the higher dynamic range displayed by the construct in this genetic configuration.

Summarizing, the results of the experiments performed using the highly sensitive luciferase reporter, showed for all inducible promoters a certain level of leakiness when the reporter construct is encoded on medium copy plasmids (Figure 3.8 A, C, D), from ~10^3 RLU/OD_{600} ($P_{Llac0-1}$-*lux*) to ~10^4 RLU/OD_{600} (P_{BAD}-*lux*). This must be taken into account, especially in the evaluation of genetic switches and more complex circuits, driven by these promoters. However, since P_{BAD} promoter displayed virtually zero basal activity when chromosomally integrated (baseline below the instrument detection limit), and it has the highest dynamic range in both configurations (Table 3.2), we conclude that it represents the first choice to induce genes expression in our synthetic circuits.

Promoter	Plasmid (fold induction)	Chromosome (fold induction)
P_{BAD}	~3000x	~200000x
P_{tet}	~1000x	~1000x
$P_{Llac0-1}$	~500x	~500x*

Table 3.2. Dynamic ranges of three inducible promoters fused with a luciferase reporter in two genetic configurations. The dynamic range is measured as the luminescence signal obtained using the highest inducer concentration (Arabinose 0.2%, ATc 100 ng/mL, IPTG 100 mM), divided by the basal activity of the promoter in the absence of inducer at t=6 h. *The value was calculated assuming a baseline signal in the absence of inducer=10 RLU/OD_{600}.

3.3.2 Part characterization: Ribosome binding sequences

The initiation of protein synthesis in *Escherichia coli* and other bacteria involves the recognition by the 30S ribosomal subunit of specific elements in the mRNA near the start codon of a coding region. These elements, represented by the initiation codon and the Shine-Dalgarno (S/D) sequence, define the ribosome-binding sequence (RBS). Between these two elements lies a spacer region which has variable length and nucleotide composition[111]. In previous work, R. Vellanoweth and J. Rabinowitz generated a series of synthetic RBSs varying the length of the spacer between the S/D sequence and the initiation codon. Hence, starting from a strong (-UAAGGAGG- ΔG = -99.1 kJ mol^{-1}) and weak (-AAGGA- ΔG = -53.8 kJ mol^{-1}) S/D sequence, they generated and measured a library of 11 strong and 10 weak RBSs[111].

In the generation of the synthetic circuit, the ability to tune protein production is a valuable feature, hence, we decided to clone 6 strong and 6 weak RBSs, from the previously generated collection[111], and include them in our library. In the original work of R. Vellanoweth and J. Rabinowitz the different RBSs were tested using a β-Galactosidase activity assay[121], however, a characterization of the dynamic response of the different RBSs, at a higher resolution, was missing. Hence, to characterize the RBSs that we included in the library, we used them to drive the translation of the luciferase operon, fused with the P_{BAD} promoter and assayed the constructs in time course experiments. To compare their dynamic response upon different arabinose concentrations, we plotted dose-response curves at time point 2 h after induction (Figure 3.9).

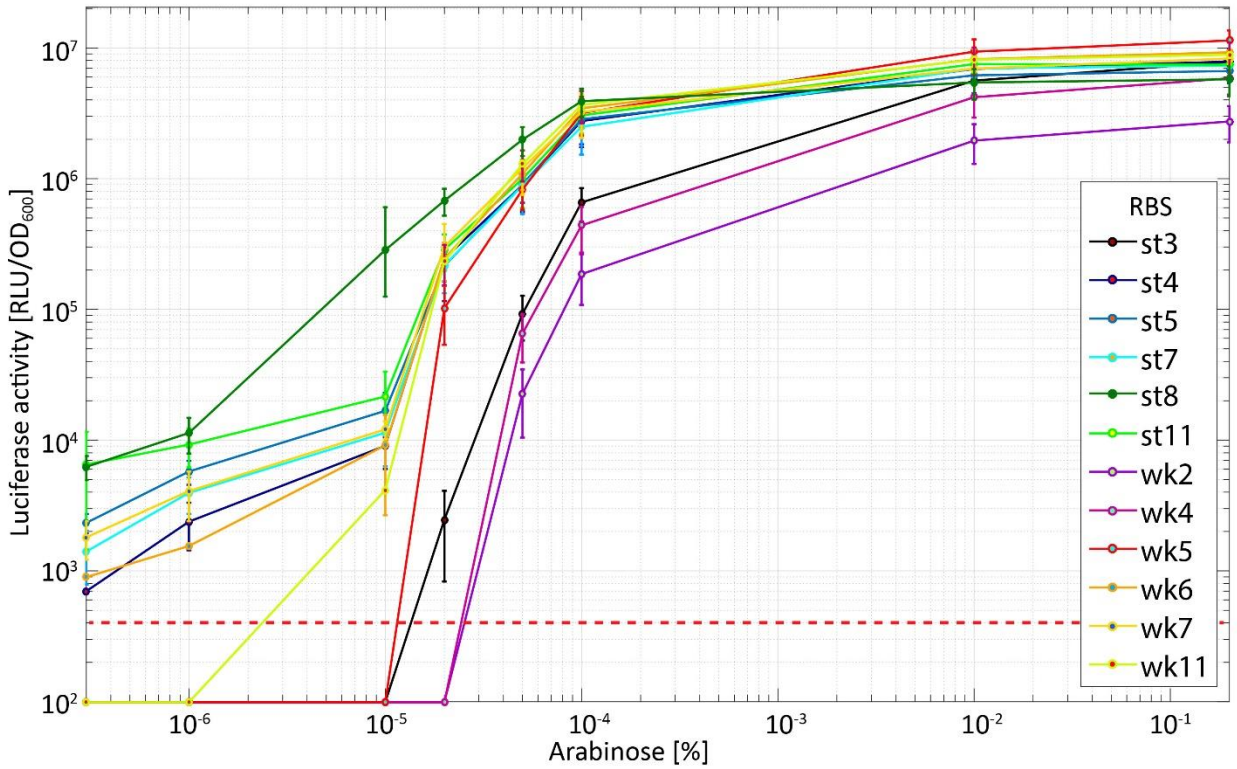

Figure 3.9. Translation efficiency of 12 RBSs, in the function of increasing arabinose induction levels. The different constructs harbor an arabinose-inducible P_{BAD} promoter, fused with a luciferase operon using one of 12 different RBSs. The strong (st) and weak (wk) RBSs posses different translational strength and are listed according to increasing strength, as reported by R. Vellanoweth and J. Rabinowitz[111]. The luciferase activity (reported as relative luminescence units normalized by optical density measured at 600 nm) is reported 2 h after the addition of the indicated arabinose concentrations. The red dashed line represents the low detection limit of the plate reader. The results are averaged from at least two independent biological assays and error bars denote standard deviations.

Overall the results in Figure 3.9 show, for the strong RBSs (st3, st4, st5, st7, st8), a similar luciferase level (between $5x10^6$ and 10^7 RLU/OD_{600}), obtained using the two higher arabinose concentrations (10^{-2}% and $2x10^{-1}$%). In contrast, for mild arabinose inductions ($2x10^{-5}$% and 10^{-4} %) RBS st3 shows values that are 10-300-fold lower than the one obtained for the other strong RBSs (Figure 3.9). We observed similar behavior, when comparing the signal relative to these RBSs, in presence low arabinose inductions (10^{-5}% and 10^{-6}%) and in the uninduced condition. Indeed, for low arabinose inductions, RBS st3 displays values below the detection limit ($<4x10^2$ RLU/OD_{600}), while the other strong RBSs have values that range between $2x10^3$ RLU/OD_{600} (RBS st4) and $2x10^5$ RLU/OD_{600} (RBS st8). Moreover, in the uninduced condition, we can observe that the signal for the RBSs st4, st5, st7, st8, and st11 is overall similar, ranging from $6.5x10^2$ RLU/OD_{600} (RBS st4) to $7x10^3$ RLU/OD_{600} (RBS st8) while the one obtained for RBS st3 is again below the detection limit ($<4x10^2$ RLU/OD_{600}).

Analyzing the dynamic response of the weak RBSs (Figure 3.9; wk2, wk4, wk5, wk6, wk7, wk11), we found an overall similar behavior to the one observed in the strong RBSs (Figure 3.9; "st" series). Indeed, all weak RBSs displayed a similar luciferase level for the two higher arabinose concentrations (between $3x10^6$ and 10^7 RLU/OD_{600} for 10^{-2}% and $2x10^{-1}$% respectively), while for mild arabinose inductions ($2x10^{-5}$ % and 10^{-4} %) two RBSs (Figure 3.9; wk2, wk4) display values ~10-100-fold lower than others. Interestingly, in the uninduced condition, only RBS wk6 and wk7

presented a detectable signal (~10^3 RLU/OD_{600}), while all the others displayed signals below the detection limit (<$4x10^2$ RLU/OD_{600}).

Summarizing, our results show that we can distinguish two classes for the strong (class 1: st4, st5, st7, st8 st11; class 2: st3), and two classes for the weak (class1: wk6, wk7, wk5, wk11; class 2: wk2, wk4,). RBSs. In both cases, the members of each class displayed a similar dynamic response. Indeed, class 1-RBSs and class 2-RBSs confer a higher or lower expression level for mild arabinose inductions, respectively, while the expression at full induction is overall similar. In case of low (10^{-6}%) and no-induction, the RBSs within each class presents a similar pattern to the one described above, with class 1-RBSs displaying higher expression levels than class 2-RBSs (with the exception of class1-RBS wk5 and wk11 that displayed values below the detection limit for 0 and 10^{-6}% arabinose). We then conclude, that at least one RBS from each class represents an interesting choice to variate the gene translation efficiency in novel synthetic circuits.

3.3.3 ECF σ, *ecf* promoters, and anti-σ factors

In this project, we focus on developing synthetic circuits using ECF σ factors. As introduced in Section 1.4 and Section 1.5, V. Rhodius and collaborators screened different heterologus ECF σ factors as well as their cognate anti-σ factors for functionality in *E. coli*[63]. In their work, they found 20 ECF σs that were able to activate their target promoters showing limited cross-reactivity with non-target ECF promoters, as well as 12 AS factors that can regulate the cognate ECFs (Figure 1.8A and Figure 1.9). Thus, starting from the best 20 orthogonal ECF σ previously characterized, we excluded *E. coli* endogenous ECF σ (ECF02_2817), as well as ECF03_1198 and ECF33_423, due to the high toxic effect on cell growth showed previously[63]. Moreover, we excluded ECF42_4454 and ECF41_491 due to the possession of a c-terminal extension that modulates ECF activity and can lead to unexpected behavior[66]. Therefore, we selected the remaining set of 15 orthogonal ECF σs and their cognate promoters and included them in our library.

Anti-σ factors (AS) are transmembrane or cytosolic proteins that bind and block the cognate ECF σ factor keeping it inactive (see Section 1.5). To control ECF activity in our synthetic circuits we, therefore, included in the library the AS factors that regulate the ECFs we previously selected. Among them, ECF32 does not have a known AS factor, therefore, we included the remaining 14 cognates AS factors in our library[63]. Moreover, we generated and included in the library 21 truncated, soluble, AS factor variants that are described in Chapter 5. The ECFs and anti-σ factors present in our library will be deeply analyzed in Chapter 4 and Chapter 5.

3.3.4 Insulation of neighboring transcription units

Terminators are nucleic acid sequences that mark the end of a gene or an operon and enhance the dissociation of RNA polymerase, terminating the transcription. In synthetic biology, strong terminators are highly desirable since strong promoters are frequently used to generate circuits containing multiple transcription units encoded on a relatively short stretch of linear DNA. This leads to a high flux of RNA polymerase from the first promoter of the circuit, that can then interfere with the expression of the following transcription units. A strategy to efficiently terminate transcription consists of using multiple strong terminators in series. However, the limited number of available natural strong terminator lead to their reuse and therefore can generate homologous recombination[122]. Indeed, the presence of multiple DNA stretch with ~20 base pairs of complete

homology, is enough for significant recombination in *E. coli*, thus generating instability of the synthetic circuit[123]. In order to solve this problem, the laboratory of C. Voigt characterized 582 natural and synthetic terminators, finding 39 strong terminators (>50-fold reduction in downstream expression) that also have enough sequence diversity to reduce homologous recombination when used together in a circuit[112].

In order to mark the end of our transcription units and build insulator elements, that block the interaction between adjacent TUs, we arranged the 39 synthetic terminators according to strength and selected the 12 strongest for our library. Next, to assess the termination efficiency of these terminators in our circuits and to infer the best insulation strategy for our genetic circuits, we assembled, on medium copy plasmids, the circuits illustrated in Figure 3.10A.

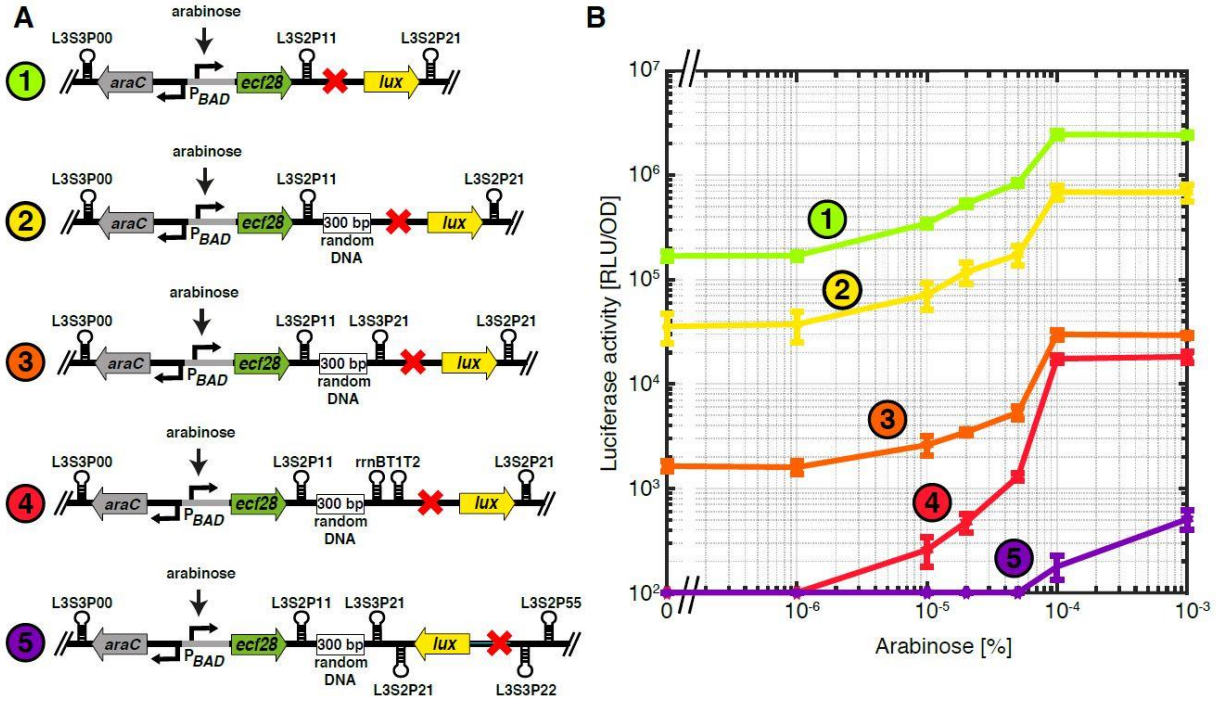

Figure 3.10. Insulation of neighboring transcription units from transcriptional read-through and other polar effects. (A) Different DNA constructs carrying a variable number of non-redundant transcriptional terminators described by Chen Y. *et al.*, [112], 300 base pairs of random-non-coding DNA[30], as well as alternating orientations between an upstream transcription unit and a downstream luciferase reporter gene cassette. (B) Downstream luciferase activity of the genetic circuits illustrated in (A) 4 h after the addition of indicated concentrations of arabinose. The luciferase activity is reported as relative luminescence units normalized by optical density measured at 600 nm. The results are averaged from at least two independent biological assays and error bars denote standard deviations. *This figure was taken from Paper III* (Pinto *et. al.*, 2018) by permission of Oxford University Press.

All the circuits (from 1 to 5) are composed of two transcription units. In the first transcription unit, the P_{BAD} promoter drives the expression of *ecf28*, an alternative ECF σ factor used as a dummy coding sequence, which is terminated by the strongest terminator (L3S2P11) in the previously mentioned collection[112]. In the second transcription unit, we placed a promoter-less dummy sequence of 15 random base pairs (indicated by the red cross), upstream the *lux* operon. We, therefore, measured the luciferase signal in the absence and in the presence of the inducer and plotted the results as dose-response curves (Figure 3.10B). In the case of the first circuit, we observed a basal signal of $2x10^5$ RLU/OD_{600} followed by ~10-fold increase to $2{,}5x10^6$ RLU/OD_{600}

upon full promoter induction (Figure 3.10A; 1). The basal signal seems to be caused by the combination of the basal activity of the P_{BAD} promoter that we observed previously (cfr. Figure 3.8A) together with the incomplete termination of the transcription by L3S2P11. We reasoned that the close proximity of the terminator to the following *lux*-containing transcription unit could lead to suboptimal termination efficiency. In this scenario, the presence of ribosomes translating the spurious mRNA containing also the second transcription unit could interfere with the formation of the secondary structure necessary for efficient termination. To further investigate this phenomenon we increased the distance of the two transcription units, placing between them a spacer of 300 random base pairs[30], that we analyzed with the software Bprom (http://www.softberry.com/berry.phtml?topic=bprom) to ensure that no promoter-like sequence was present (Figure 3.10A; 2). Strikingly the only augmentation of the distance between the two transcription units lowered both the basal signal ($5x10^4$ RLU/OD_{600}) and the full induced signal ($7x10^5$ RLU/OD_{600}). To further improve the insulation we added a single (L3S3P21[112]), Figure 3.10A; 3) or double (*rrnB*T1T2[21] Figure 3.10A; 4) terminator following the 300 base pairs element. This further lowered both the basal signal ($<10^2$ RLU/OD_{600} and $2x10^3$ RLU/OD_{600}) and the full induced signal ($2\text{-}3x10^4$ RLU/OD_{600}), yet, in both cases, we still observed high luciferase activity (~100-fold above background) at high arabinose concentrations. Only assembling the last circuit (Figure 3.10A; 5) with a convergent arrangement of the transcription units we finally obtained an output signal close to the background. In this construct we also added a new insulating element (composed by the two additional synthetic terminators L3S3P22, L3S2P55[112] and a different promoter-less 300bp random DNA sequence[30]) after the second transcription unit, to prevent any read through from the plasmid backbone.

Summarizing, to characterize the chosen synthetic terminators and decide for the best insulation strategy in our genetic circuits, we decided to use the highly sensitive *lux* reporter instead of the previously used fluorophores[112]. This allowed analyzing the termination efficiency with a higher resolution, demonstrating the limits of natural and synthetic terminators. This must be taken into account when generating genetic circuits that include more than one TU in close proximity. Only with the combination of insulating elements and the convergent arrangement we achieved complete insulation of the two TUs. Therefore, we conclude that the alternation of convergent and divergent arrangements of the TUs represents an optimal choice for encoding multiple TUs in a synthetic circuit.

3.4 Summary

In this chapter, we introduced our expansions to the MoClo system, represented by a new medium copy reporter vector (pSVM-mc) for the fast assembly of synthetic circuits from level 1 parts (Section 3.1). Moreover, to add more degrees of freedom to the possible configurations of a given synthetic circuit, we generated 32 CRIMoClo vectors. These vectors allow for an easy assembly and chromosomal integration of MoClo-compatible genetic circuits. Using CRIMoClo plasmids we characterized the expression levels from four different phage attachment (*att*) sites in the genome of *E. coli*. Our results showed that the four *att* sites are orthogonal and suitable for the simultaneous expression of different genetic constructs (Section 3.2).

Next, we introduced a novel MoClo-compatible library of genetic parts, giving an overview of the dynamic response of three distinct inducible promoters (Figure 3.8) and showing the translation efficiency of 12 different ribosome binding sequences (Figure 3.9). Moreover, we identified the best

insulation strategy to clone multiple transcription units in close proximity, avoiding any interference such as transcriptional-readthrough (Figure 3.10).

All the genetic parts presented above, together with the level 0 dummies, the new MoClo vector pSVM-mc, and the 32 CRIMoClo plasmids constitute the ECF toolbox (Table 9.2, Table 9.3, and Figure 3.11). We developed this toolbox with the aim of facilitating the generation of large synthetic ECF-based circuits in different genetic configuration, from a library of reusable parts. The design characteristics of the toolbox allow further expansions, e.g. to include more ECF σ factors and cognate promoters. Moreover, even if the toolbox is designed for *E. coli*, it allows, in principle, the generation of genetic constructs that can be sub-cloned into vectors suitable for the expression in a different model organism. We, therefore, consider the ECF toolbox as a valuable tool to generate ECF-based synthetic constructs and in order to prove it, we extensively used it for the generation of all the genetic circuits described in this study (Tables 9.3-9.6).

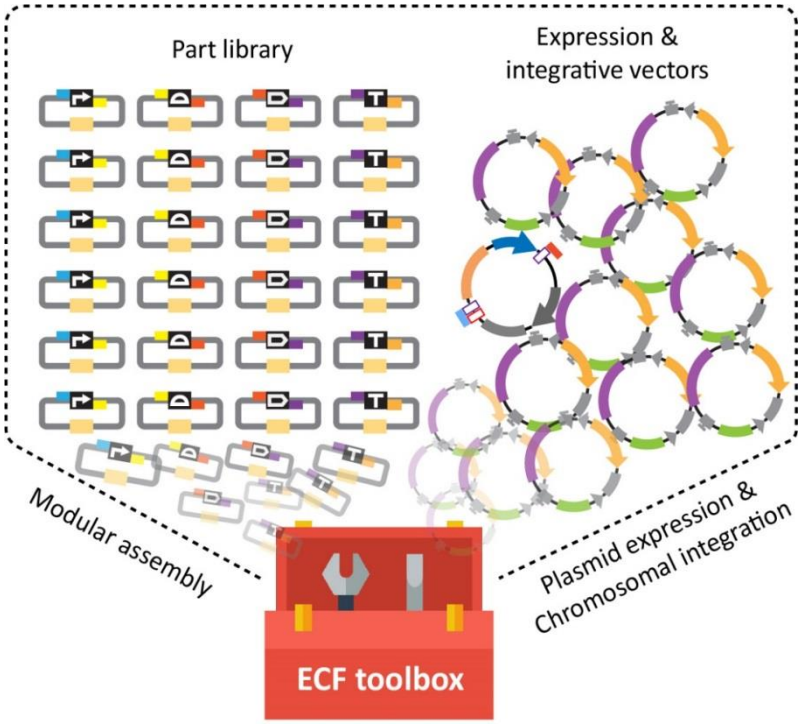

3.11. ECF Toolbox. A MoClo-based genetic toolbox for the fast and reliable assembly, expression and chromosomal integration of ECF-based synthetic circuits in *E. coli*.

4. ECF σ factors as the core of novel, orthogonal synthetic circuits

The previous chapters introduced the ECF toolbox and our typical experiment setup that were used for the construction and the evaluation of different genetic constructs, respectively. This chapter focus on using ECF σ factors to generate genetic circuits with increasing complexity. First, we characterize 15 distinct ECF/P_{ecf}-switches analyzing the dynamic of their target promoter activation among different ECF expression levels and in different genetic configurations (e.g. plasmid encoded and chromosomally integrated). Next, we combine different ECF-switches, designing ECF σ factor cascades, featuring the functionality of "genetic timers" – circuits that activate a series of ECF σ factor genes with increasing time delays. Moreover, we validate our experimental results, by using mathematical models that can describe and predict the behavior of the circuits. Finally, we show that the design of ECF-based "genetic timers" can be applied also in the phylogenetically distant organism *Bacillus subtilis*.

4.1 ECF σ factors characterization

In Section 3.3.3 we illustrated our selection of 15 out of 20 orthogonal ECFs previously screened by V. Rhodius and collaborators[63]. In order to rationally assemble these ECFs and their target promoters in genetic circuits with increasing complexity, we first analyzed their dose-response characteristics, as well as their effects on the growth of the bacterial cells, in our experimental conditions. To this end, we assembled 15 ECF-switches, in the medium copy plasmid pSVM-mc, in which an arabinose-inducible promoter (P_{BAD}) controls the expression of an ECF, that can then activate his target promoter fused with the *lux* operon (Table 9.5). These ECF-switches were then introduced into our reporter strain SV01, described in Section 2.1, generating the GFC strains reported in Table 9.1. We then used microplate experiments to monitor the growth of the bacterial strains in MOPS minimal media (Section 7.1), measuring the optical density at 600 nm (OD_{600}), as well as the reporter signal over time, upon ECF σs expression achieved using different inducer concentrations (Section 7.10). Using this experimental setup we generated time evolution plots (Figure 4.1). In these graphs, we display, for each ECF-switch, the OD_{600} in the function of time, as well as and the reporter signal, indicated as relative luminescent units (RLU), divided by OD_{600}.

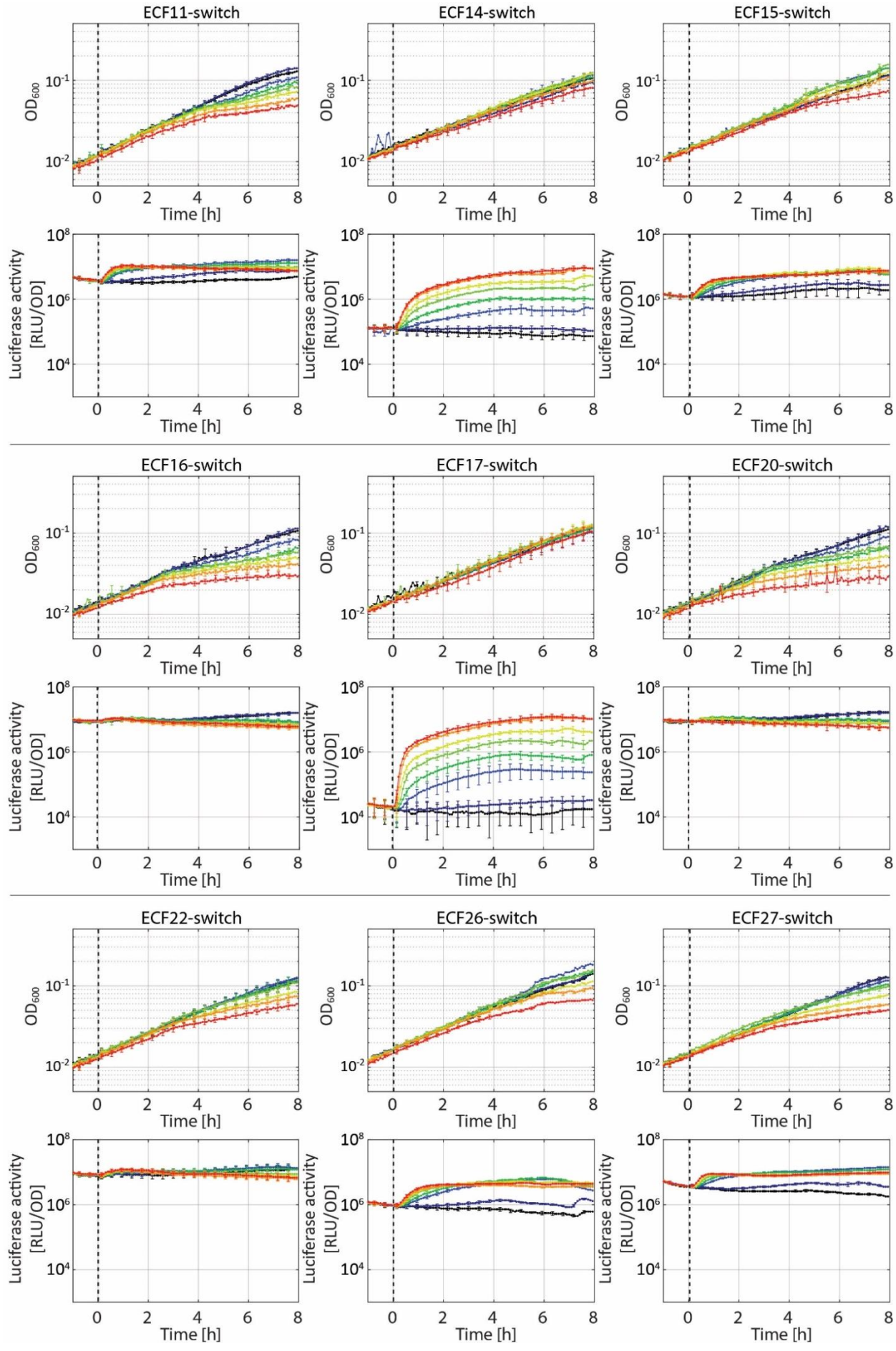
ECF11-switch
ECF14-switch
ECF15-switch
ECF16-switch
ECF17-switch
ECF20-switch
ECF22-switch
ECF26-switch
ECF27-switch
OD600
Luciferase activity [RLU/OD]
Time [h]

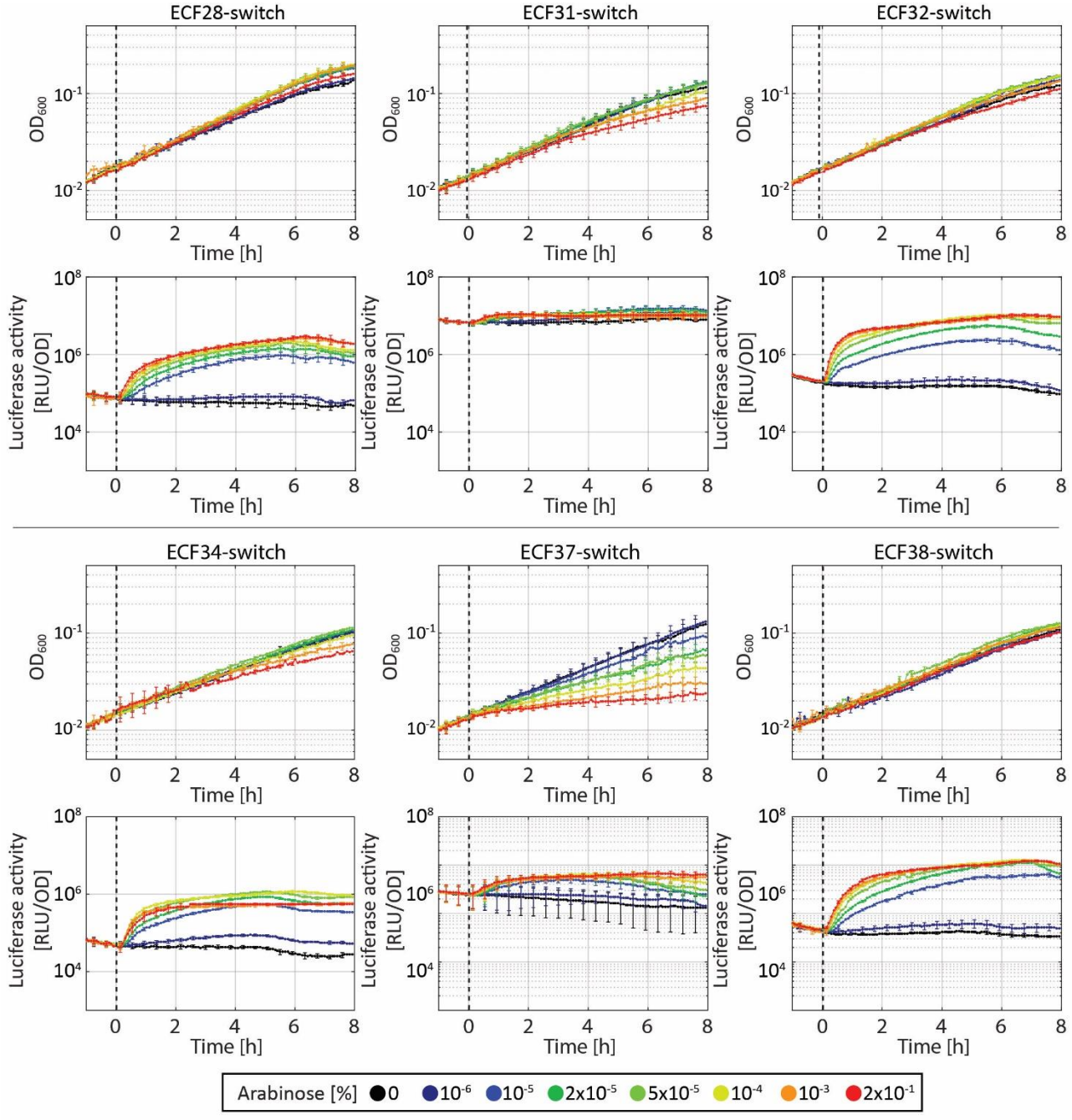

Figure 4.1. Time evolution of bacterial density and luciferase activity, obtained from 15 ECF-switches. The bacterial density is indicated as the optical density measured at 600 nm. The reporter activities are shown in relative luminescence units, normalized by the optical density measured at 600 nm. The black dashed line indicates the time point for the addition of the indicated concentrations of inducer (t=0 h). All ECF-switches were introduced in *E. coli* strain SV01 on medium copy plasmid pSVM-mc (Table 9.5) generating the GFC strains listed in Table 9.1. The genetic organization of the parts composing the switches is indicated in the main text and in Table 9.1 and Table 9.5. The results are averaged from at least two independent biological assays and error bars denote standard deviations.

Analyzing the OD_{600}, we observed that for the majority of the strains, the overexpression of the ECF σ factor does not interfere with the cell growth, in particular for mild induction levels (Figure 4.1; OD_{600} graphs). Indeed, in these conditions, the strains displayed, overall, an exponential growth (obtained as indicated in Section 7.10), with a doubling time ~175 min. In contrast, in the strains

harboring, ECF16, ECF20, and ECF37 even the induction intermediate arabinose concentrations (>10^{-5}%) seem to cause deleterious effect on the cell growth, when compared with the same strains induced with lower arabinose concentrations. To better compare the growth defects, caused by increasing ECF expression levels, in different ECF-switches, we plotted the OD_{600} (6 hours after ECF induction) in the function of the arabinose concentrations (Figure 4.2). The results confirm that ECF expression in ECF16, ECF20, and ECF37 switches, with arabinose induction superior to 10^{-5}% lead to >2-fold decrease in the 6-h OD_{600}, when compared with the uninduced switches. These growth defects can be caused by the burden to the cellular machinery due to protein overexpression, or by the cross-reaction between the overexpressed ECFs and stress-related pathways as it will be further discussed in Section 6.4.

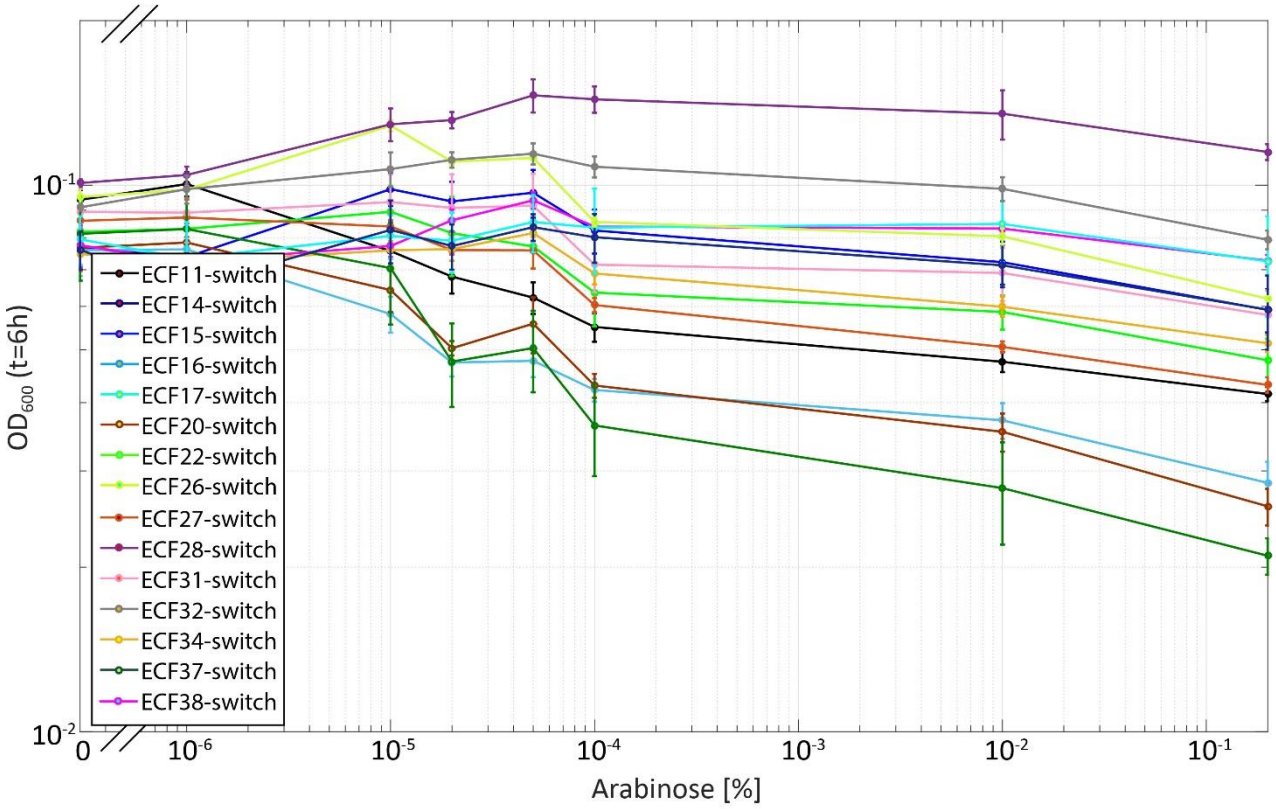

Figure 4.2. ECF σ factors toxicity evaluation. Bacterial density (indicated as the optical density measured at 600 nm) achieved by 15 *E. coli* strains, carrying the indicated ECF-switch circuits, 6 hours after the induction with the indicated arabinose concentrations. All ECF-switches were introduced in *E. coli* strain SV01 on medium copy plasmid pSVM-mc (Table 9.5) generating the GFC strains listed in Table 9.1. The genetic organization of the parts composing the switches is indicated in the main text. The results are averaged from at least two independent biological assays and error bars denote standard deviations.

Analyzing the luciferase signals of all the switches we observed, overall, the ability of ECFs of recognizing and activating their target promoters (Figure 4.1; RLU/OD_{600} graphs). Overall, we found that different ECF-switches display different basal activities, as well as different maximum signal output levels, that then lead to different dynamic ranges. To better compare the differences in the baseline signal and in the output dynamic range, we plotted the luciferase signal, registered 6h after induction from all ECF-switches, in the function of the inducer concentration, generating dose-response curves (Figure 4.3).

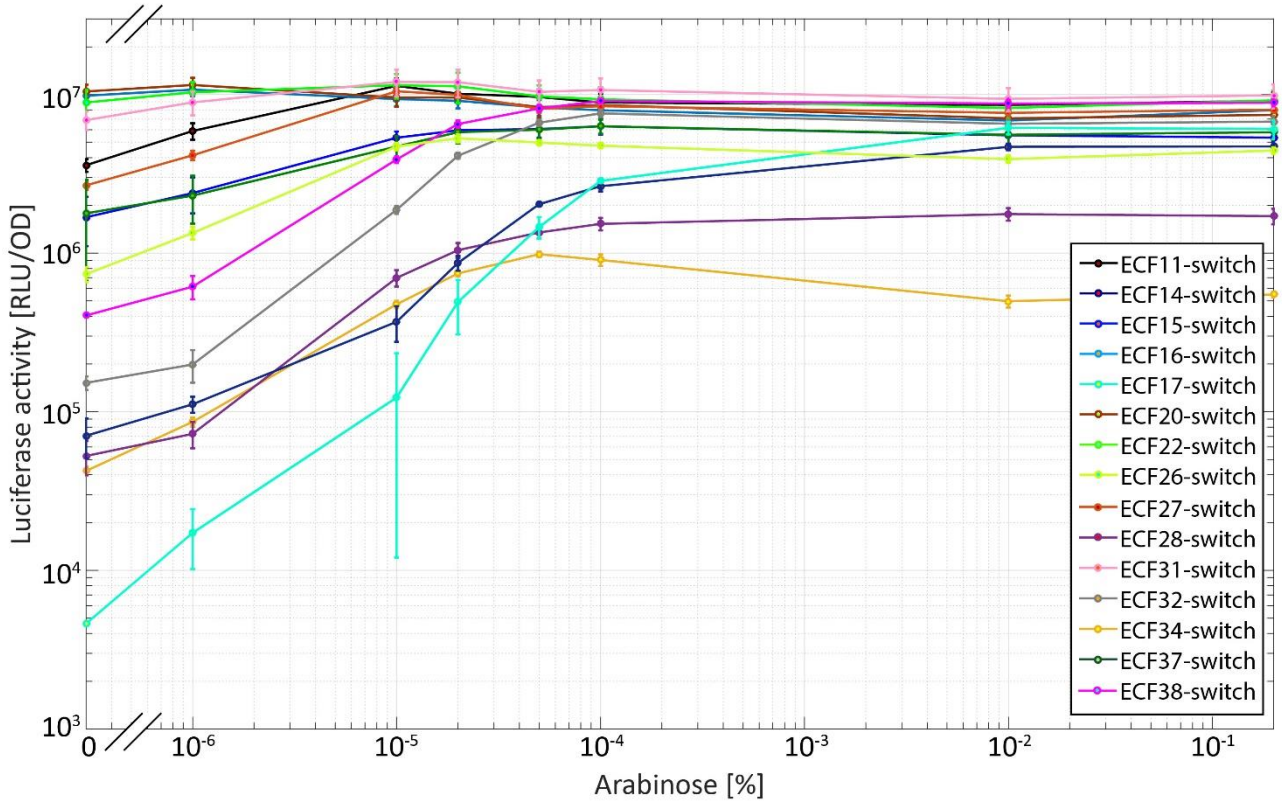

Figure 4.3. Dose-response characteristics of plasmid-borne ECF-switches. The dose-response characteristics of 15 ECF target promoter activities, were measured, in plasmid-encoded ECF-switch circuits, as a function of ECF σ expression levels, 6 hours after the induction with the indicated arabinose concentrations. All ECF-switches were introduced in *E. coli* strain SV01 on medium copy plasmid pSVM-mc (Table 9.5) generating the GFC strains listed in Table 9.1. The genetic organization of the parts composing the switches is indicated in the main text. The results are averaged from at least two independent biological assays and error bars denote standard deviations.

Comparing the dose-response curves of all the switches, we notice that four ECFs (ECF16, ECF20, ECF22, and ECF31) have a particularly strong basal signal level (~10^7 RLU/OD_{600}) with almost no fold-change between the OFF (uninduced) and ON (induced) state. However, overall, all the other ECF-switches appear to be inducible with a minimal and maximal dynamic range between 5-fold (ECF11) and 500-fold (ECF17), thus indicating their ability to tune gene expression levels. Analyzing the dose-response curves we observed a high variation in the basal activity level for different ECFs (>1000-fold comparing all the basal activities). We then reasoned that such differences could arise by the cross-reaction of endogenous σ factors, that activate a-specifically the ECF σ promoters, or by the basal expression of the ECFs in absence of the inducer. To further investigate these hypotheses we constructed a series of negative controls were the 15 *ecf* promoters were fused with the *lux* operon and measured the output signal in absence of the expression of the cognate ECF σ factor (Figure 4.4).

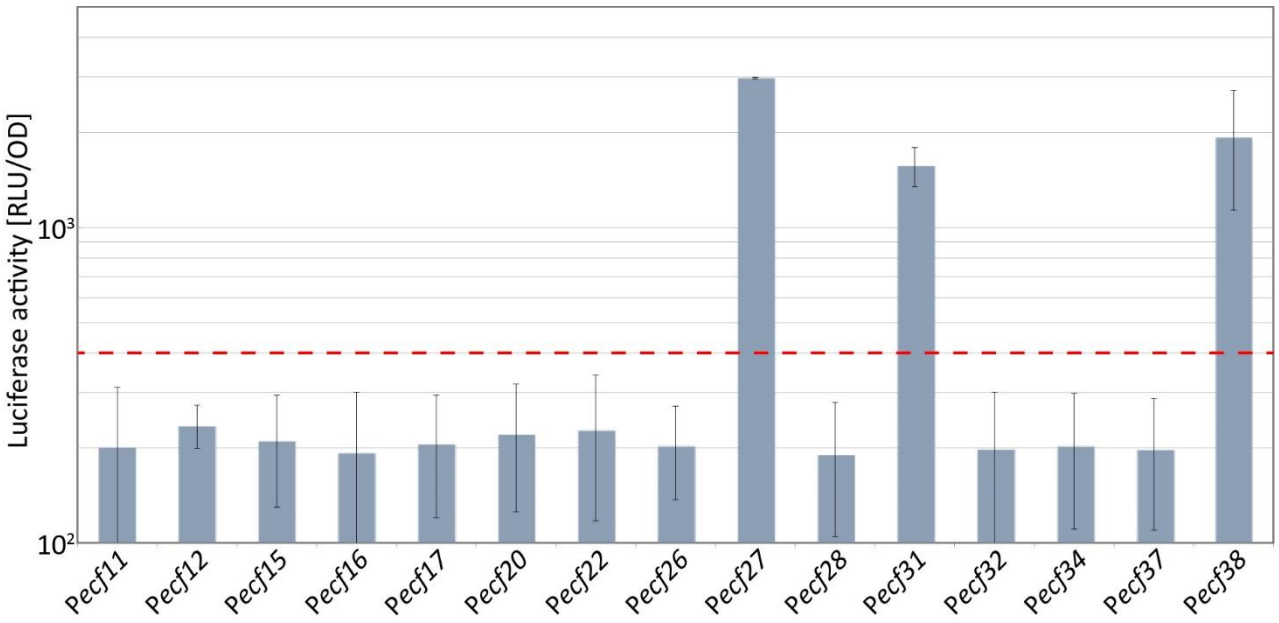

Figure 4.4. Comparison of 15 *ecf* promoters activity in the absence of cognate ECF σs. P_{ecf} promoters activity was measured in *E. coli* SV01 using plasmid-borne P_{ecf}-*lux* constructs. The red dashed line represents the plate reader low detection limit. All the construct were introduced in *E. coli* strain SV01 on medium copy plasmid pSVM-mc (Table 9.5) generating the GFC strains listed in Table 9.1. The results are averaged from at least two independent biological assays and error bars denote standard deviations.

The results show that 80% of the *ecf* promoters, in the absence of the cognate ECF, generate a luciferase signal $<4x10^2$ RLU/OD_{600} thus, within the low detection limit of the plate reader (Figure 4.4; red dashed line). When looking at the *ecf* promoters of the switches that were constitutively ON in the previous experiment (Figure 4.3; ECF16, ECF20, ECF22, ECF31), we did not observe, in the case of P_{ecf16}, P_{ecf20}, and P_{ecf22}, a detectable luciferase signal in absence of the cognate ECFs (Figure 4.4). This indicates that these promoters are not cross-activated by endogenous σs. In contrast, the promoter P_{ecf31} showed a basal activity $\sim 2x10^3$ RLU/OD_{600} even in the absence of the cognate ECFs, suggesting cross-reaction with other σ factors present in the cell (Figure 4.4). However, the basal activity registered in the ECF31-P_{ecf31}/switch is ~4500-fold higher when compared with the control lacking the ECF σ factor (Figure 4.3; pink curve $\sim 9x10^6$ RLU/OD_{600} and Figure 4.4; P_{ecf31} $\sim 2x10^3$ RLU/OD_{600}). We, therefore, concluded that also in the case of ECF31 the cross-reactivity with endogenous σs do not explain the high basal activities we registered in the relative ECF-switch.

In order to justify the constitutive activation of these ECF-switches, we then took into account the characteristics of the inducible P_{BAD} promoter. Our previous analysis revealed that even in the absence of inducer, the promoter has a certain basal activity when encoded on medium copy plasmid (Figure 3.8A). This suggests that when the promoter drives the expression of an ECF σ, a certain amount of σ factors is produced, even in the OFF state. Depending on the binding proprieties of the ECFs and considering that the ECF-switches are encoded on medium copy plasmids, the number of ECF produced by the basal P_{BAD} activity can reach the threshold of cognate promoter activation, thus generating the high basal activities (close to promoter saturation levels) that we observed in these ECF-switches (Figure 4.3).

To validate this hypothesis, we lowered the expression level of all the circuits by cloning them in CRIMoClo plasmids and integrating them into the chromosome of *E. coli* at the att_{HK022}. We,

therefore, measured the dynamic response of the circuits using time course experiments and plotted the results as dose-response curves 6 hours after the addition of the inducer (Figure 4.5).

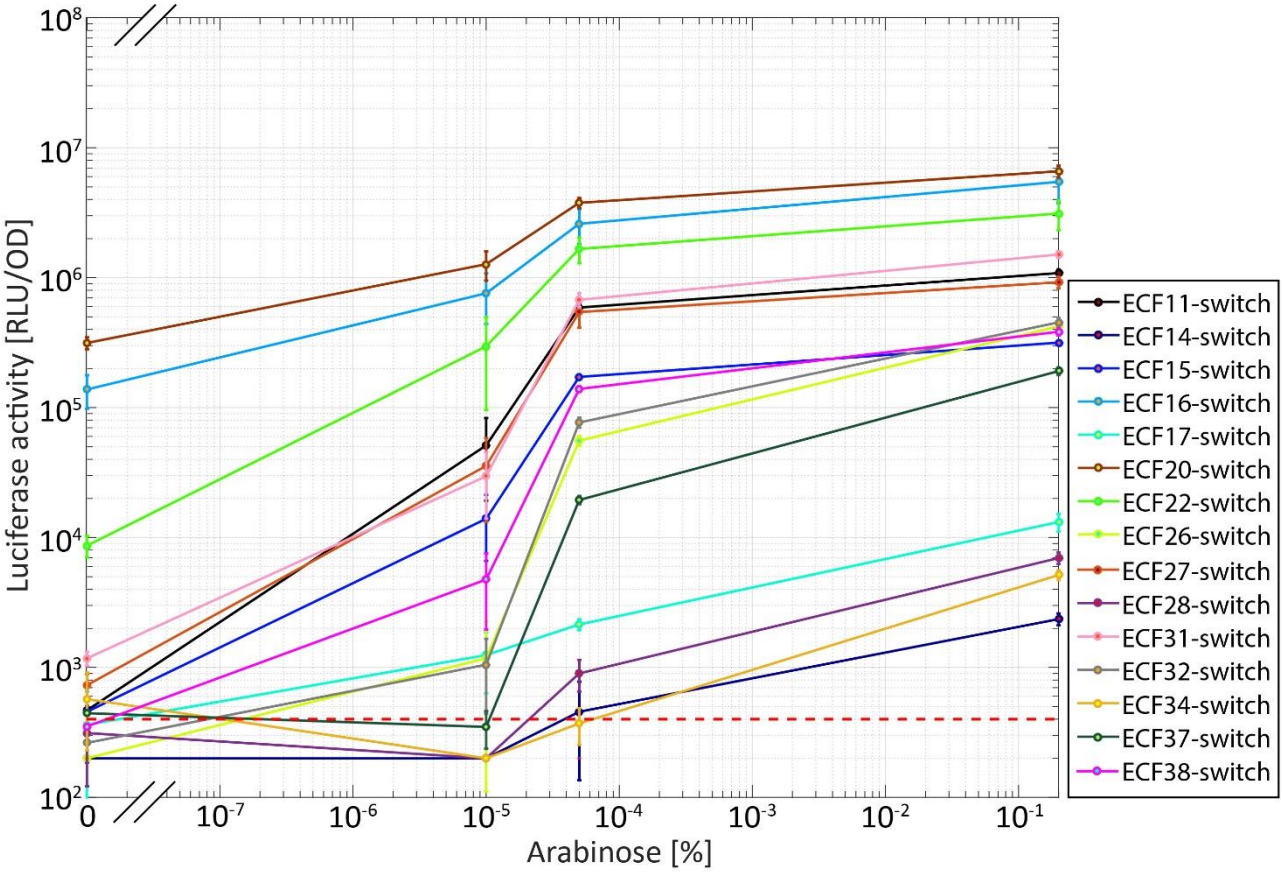

Figure 4.5. Dose-response characteristics of chromosomally integrated ECF-switches. The dose-response characteristics of 15 ECF target promoter activities, were measured in chromosomally integrated ECF-switch circuits, as a function of ECF σ expression levels, 6 hours after the induction with the indicated arabinose concentrations. All ECF-switch circuits were integrated into the chromosome of *E. coli* strain SV01 at the phage HK022 attachment site, using the pSV plasmid series (Table 9.6) and generating the GFC strains listed in Table 9.1. The red dashed line represents the plate reader low detection limit. The results are averaged from at least two independent biological assays and error bars denote standard deviations.

Interestingly, with this genetic configuration all the previously constitutively ON ECF-switches appear to be inducible (Figure 4.5; ECF16: 27.5-fold induction, ECF20: 24-fold induction, ECF22: 200-fold induction, ECF31: 800-fold induction, between the OFF and the ON state). This suggests that these ECFs possess a high affinity for their target promoters, that together with the basal activity of P_{BAD} leads to constitutive activation of the relative plasmid-encoded ECF-switches. The result of the experiments also shows that some ECFs (e.g. ECF14, ECF28, and ECF34) present a much lower dynamic range (10 to 20-fold) when compared with the same circuits encoded on medium copy plasmids (Figure 4.5 and Figure 4.3 respectively). This suggests a low affinity of these ECFs for their target promoters, that together with their expression from single-copy circuits, results in a basal promoter activity that falls below the lower detection limit, and a sub-optimal promoter activation, even in presence of maximum P_{BAD} induction levels.

The results obtained from these experiments (Figure 4.3 - Figure 4.5) support the hypothesis that different ECF σ factors have different binding affinities for the target promoters. Indeed, lowering

the copy number of the switches encoding for ECFs with a high promoter binding affinity allows for the reduction of their basal activity, while maintaining a strong activity in the presence of high level of inducer. Consequently, this leads to an increased output dynamic range. In contrast, lowering the copy number of ECF-switches where the ECFs display a low promoter binding affinity results in a severe reduction of their basal activity (below the detection limit) and in non-saturating levels of target promoter activation. This, in turn, leads to a reduction of the circuits output dynamic range.

Assuming that ECF σ factors can activate the target promoter with different strengths, we further characterized the dynamic range of all ECF-switches by tuning the input/output signal ratio. To this end, we integrated the P_{BAD}-*ecf* portion (input) of the circuit into the chromosome and placed the cognate P_{ecf}-*lux* reporter system (output) on medium copy plasmids. We then measured the luciferase signal of the circuits using time course experiments and plotted the results as dose-response curves 6 hours after the addition of the inducer (Figure 4.6).

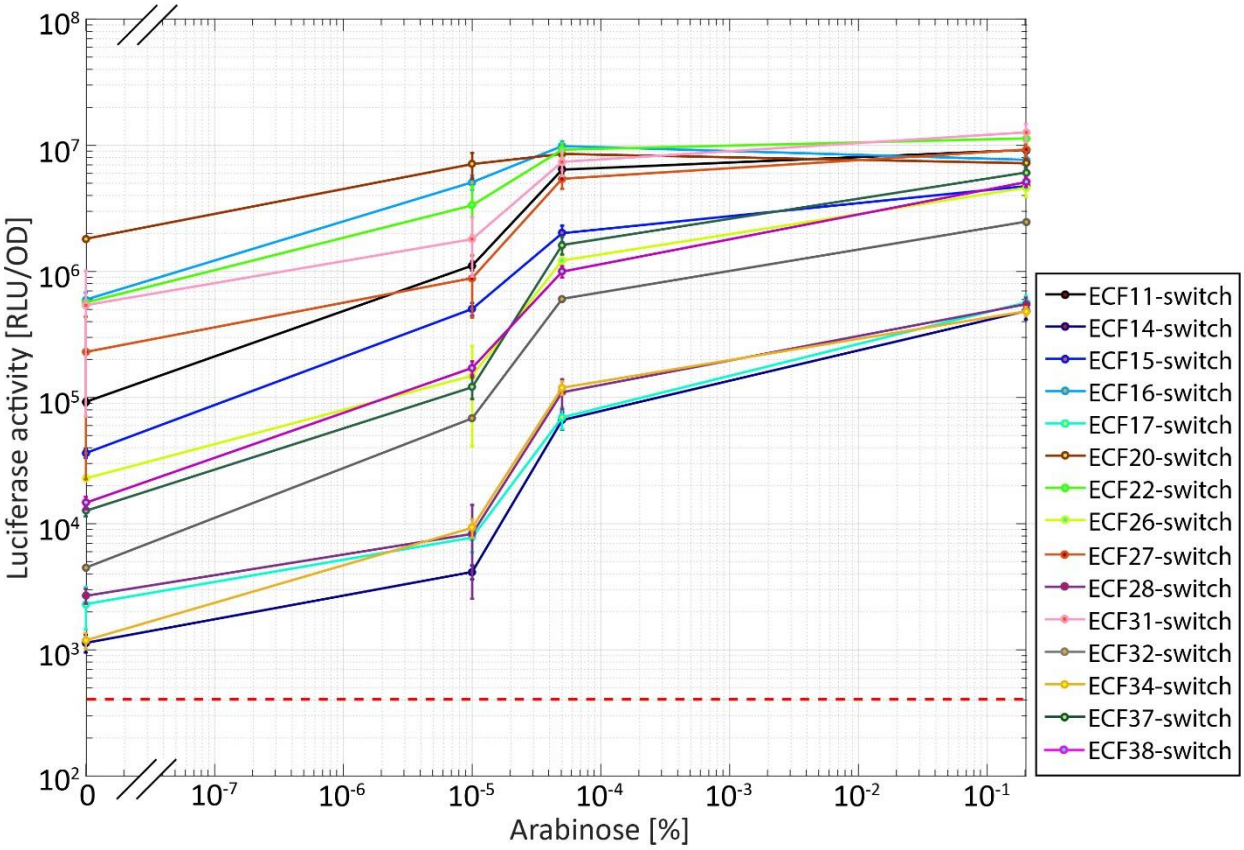

Figure 4.6. Dose-response characteristics of 15 ECF-switches encoded in mixed genetic configuration. The dose-response characteristics of ECF target promoter activities, in ECF-switch circuits encoded in mixed configuration (see main text), were measured as a function of ECF σ expression levels, 6 hours after the induction with the indicated arabinose concentrations. In all circuits the P_{BAD}-*ecf* genetic module was integrated into the chromosome of *E. coli* strain SV01 at the phage HK022 attachment site, using the pSV plasmid series (Table 9.5). Subsequently, the P_{ecf}-*lux* reporter constructs (encoded on pSVM-mc plasmids (Table 9.5) were introduced into the newly engineered strains, generating the GFC strains listed in Table 9.1. The red dashed line represents the plate reader low detection limit. The results are averaged from at least two independent biological assays and error bars denote standard deviations.

The results in Figure 4.6 show that in this configuration all ECF-switches are inducible, with a fold-change between the OFF and the ON state that ranges between 800-fold (ECF32) and 3,5-fold (ECF20). Compared with the single copy configuration (Figure 4.5), this arrangement of the two genetic modules (P_{BAD}-*ecf* and P_{ecf}-*lux*) guarantee the availability of a higher number of cognate promoters, while maintaining a low level of basal ECF expression from P_{BAD}. For the ECFs that present a low promoter binding affinity (e.g. ECF14, ECF28, ECF34) this results in an increased number of "free" ECF promoters that these ECFs can bind, thus improving the signal output level in these switches. At the same time, for the ECFs that present high promoter binding affinity (ECF16, ECF20, ECF22, ECF31), the lower levels of basal ECF expression (when compared with plasmid-encoded switches, Figure 4.3) avoids the saturation of the promoters prior to the induction, allowing a certain level of inducibility of the relative ECF-switches (Figure 4.6) with values that ranges from 3.5-fold (ECF20) to 8.5-fold (ECF31).

Taken together, the results show that our setup allows for highly sensitive monitoring of ECF target promoter activity. We confirmed that *ecf* promoters are orthogonal in respect of endogenous *E. coli* σ factors (Figure 4.4) and that ECFs have a broad range of binding affinities for their cognate promoters. Hence, changing the copy of the switches, we were able to tune their dynamic range (Figure 4.3, Figure 4.5, Figure 4.6). Interestingly, there is great variability in the dynamic range when the switches are encoded on plasmids or chromosomally integrated, that in some cases can not be explained simply by a reduction of the circuits copy number. For instance, ECF11-switch shows ~2-fold-induction in the plasmid configuration (Figure 4.3) and ~2000-fold-induction in the single-copy configuration (Figure 4.5). This is somehow similar to the effects we observed previously in the P_{BAD}-*lux* constructs compared in two genetic configurations (Figure 3.8A, B). Thus, in the case of the ECF-switches, this dynamic range variability between the two genetic configurations seems to arise by the different repression levels of the P_{BAD} promoter, together with the different binding affinities of the ECFs and the cognate promoters.

Finally, as we showed with the experiments presented in this section, the dynamic range of each ECF-switch can be tuned by varying the inducer concentration and the copy number of the components of the switch. Hence, using this strategy, it is possible to adjust the input/output signal ratio, to match the characteristics that are required to assemble ECF-switches in higher order circuits.

4.2 Engineering ECF σ factor-based genetic-timer circuits in *E. coli*

The results of this section are published in Paper II (Pinto *et al*., 2018)

In the previous section, we showed that the majority of ECFs that we selected for this study had zero or low toxic effect on cell growth (Figure 4.2). Moreover, we showed that, overall, ECFs displayed highly titratable induction of the target promoters, that, overall, can be tuned by varying the inducer concentrations and the copy number of the constructs (Figure 4.3, Figure 4.5, Figure 4.6). These features suggest that, theoretically, it is possible to combine multiple ECFs in a higher order circuit. Indeed, multiple ECF-switches can be in principle combined together, generating an ECF cascade where an inducible promoter drives the expression of the first ECF, which then activates expression of a second ECF, etc. until the final target gene is activated. We expect for such a circuit, upon induction, an overall increase in the time delay for the signal production that will scale with the increasing cascade length. The time delay is due to the finite time required for the

production and the accumulation of each ECF, that is necessary for inducing the expression of the following ECFs in the cascade. Such gene regulatory cascades would serve as proof of concept for using multiple ECF σ factors as orthogonal regulators and will help in understanding whether their characteristics are suitable for combining them into larger circuits.

To assess our hypothesis, we focused on using ECF28 and ECF32 to generate ECF σ factor cascades with increasing complexity. We chose to these ECFs because they had no detectable deleterious effects on cell growth (Figure 4.2) and they showed a high fold-inductions of the target promoter (30-fold and 100-fold, respectively), in the plasmid-borne configuration (Figure 4.3). Moreover, their promoters resulted to be inducible also in the chromosomally integrated configuration (Figure 4.5; ECF28 ∼20-fold induction, ECF32 ∼150-fold induction).

We first analyzed the timing behavior in the induction of ECF28 and ECF32 switches that we generated previously, in comparison with a control strain harboring a P_{BAD}-*lux* construct. To this end, we measured their kinetic response in luciferase activity after the addition of the inducer (arabinose) at different concentration. Moreover, to compare circuit dynamics between switches cascades of different length, we defined their response time as the time between the addition of the highest inducer concentration and the time at which luciferase activity first exceeds its pre-induction activity more than 2-fold (Figure 4.7).

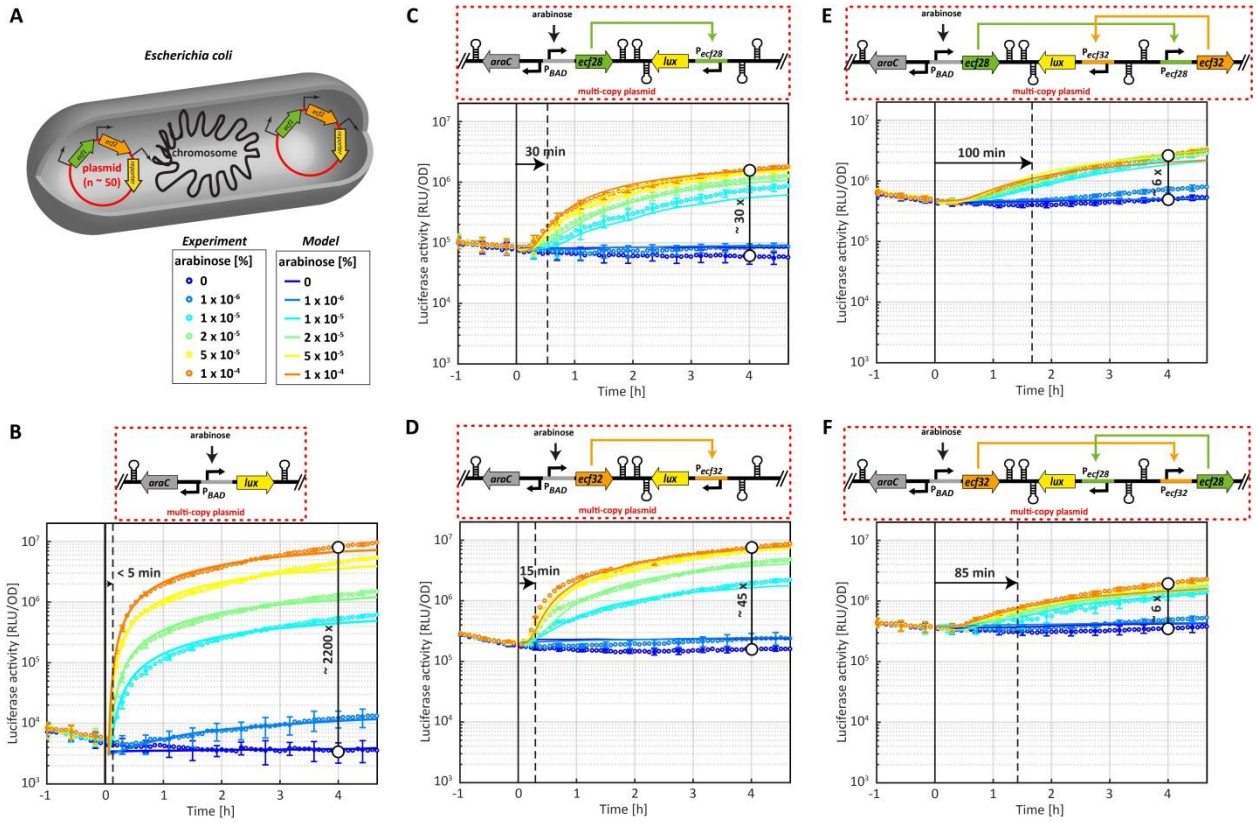

Figure 4.7. Time delayed response of synthetic ECF cascades in *E. coli*. (A) All circuits shown in the cartoons of (B-F) were introduced in *E. coli* strain SV01 on medium copy plasmid pSVM-mc (Table 9.5) generating the GFC strains listed in Table 9.1. Panels (B-F) show the dynamical response of luciferase activity (shown in relative luminescence units normalized by the optical density measured at 600 nm) in synthetic ECF cascades featuring no (B), one (C, D) and two (E, F) ECF σ factors, after the addition of various concentrations of arabinose at t=0 h (black solid line). The time delay of gene induction (black dashed line) is indicated for the highest arabinose concentration used (10^{-4}%) and was defined as the time when luciferase activity first exceeded the pre-induction value by 2-fold. Maximal fold induction is also indicated. The experimental response dynamics (circles) was recorded during exponential growth, as described in Section 7.10. The response dynamics of the computational model (solid colored lines) was obtained by a simultaneous fit of all experimental data in (B-F). *This figure was taken from Paper III* (Pinto *et. al.*, 2018) by permission of Oxford University Press.

The results show that the activation of the luciferase in the ECF28 and ECF32 switches was delayed by 15–30 minutes, when compared to the P_{BAD}-*lux* construct (Figure 4.7B, C, D). This suggests that upon induction, functional ECF σ factors have to gradually accumulate to the threshold required for the activation of the cognate ECF promoter fused with the luciferase reporter, generating a certain time delay. To test our hypothesis we assembled negative controls of the switches which lack the cognate *ecf* promoter or ECF σ factor (Figure 4.8).

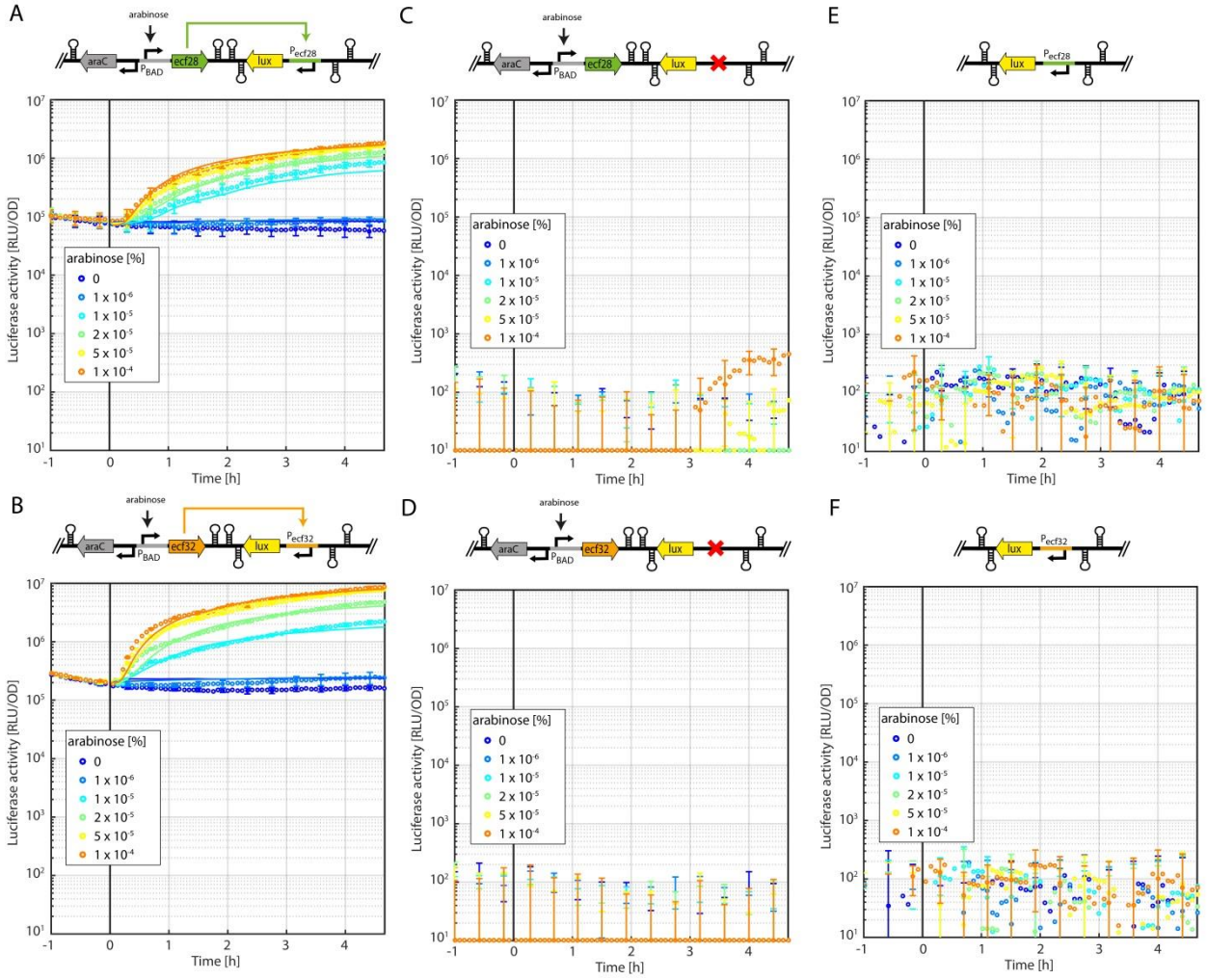

Figure 4.8 Dynamic response of 1-step timers in comparison with negative control circuits lacking the cognate *ecf* promoter, or the *ecf* gene. All circuits shown in the cartoons of (A-F) were introduced in *E. coli* strain SV01 on medium copy plasmid pSVM-mc (Table 9.5) generating the GFC strains listed in Table 9.1 The graphs show the dynamical response of luciferase activity (shown in relative luminescence units normalized by the optical density measured at 600 nm) after the addition of various concentrations of arabinose at t=0 h (black solid line). The response dynamics of the computational model is shown in solid, colored lines in panels A and B. *This figure was taken from Paper III* (Pinto *et. al.*, 2018) by permission of Oxford University Press.

The results show that there is no significant increase in luciferase activity upon induction of the P_{BAD} promoter when the cognate *ecf* promoter is missing (Figure 4.8 C, D). Moreover, the controls in Figure 4.8 E and F confirm that the *ecf* promoters alone are not recognized by endogenous σ factors. This suggests that the delayed response we observed (Figure 4.7C, D) is specific to the slow accumulation of ECF σ factors and consequent target promoters activation. Hence, based on the observed time delay and the fact that each circuit involves the expression of one *ecf* gene, we refer to these switches as 1-step timer circuits from now on.

After obtaining a 15-30 minutes time delay, using single ECFs in the 1-step timer circuits we measured the time delay in circuits were ECF28 and ECF32 were combined into 2-step timer cascades in different permutations (Figure 4.7E, F). Strikingly, we found that the activation of the luciferase, upon the induction of the first ECF, was delayed by 100 minutes (Figure 4.7E) and

85minutes (Figure 4.7F). The results confirm our assumption that the time delay for the reporter activation scales with the length of the ECF cascade. Moreover, we can observe that the variability of time delays measured in the independent biological replicates (Figure 4.7; horizontal error bars) is less than 5 minutes. Thus, indicating the robustness of the circuit performance within the cell population.

Despite the reproducible timing, however, the results also show a reduced output-dynamic range that scales with the length of the cascade. Indeed, the P_{BAD}-*lux* control strain (which we refer to as 0-step timer) showed the highest fold induction (2200-fold) upon arabinose addition, followed by the 1-step timers (30-fold for ECF28, 45-fold for ECF32) and the 2-step timers (6-fold for both). The loss of output dynamic range is mainly caused by the baseline activity of the circuits that increase for longer cascades. Indeed, the 0-step timer display a basal signal ~10^4 RLU/OD_{600} (Figure 4.7B; dark blue curve), while the 1-step timers and the 2-step timers ~$2x10^5$ RLU/OD_{600} and ~$6x10^5$ RLU/OD_{600} even in absence of the inducer (Figure 4.7C, D, E, F; dark blue curves). To investigate if the baseline activity increase, observed in the 2-step timers, was caused by off-target promoter activation of the ECFs, we build 2-step timers negative controls in which the second ECF of the cascade is not present (Figure 4.9).

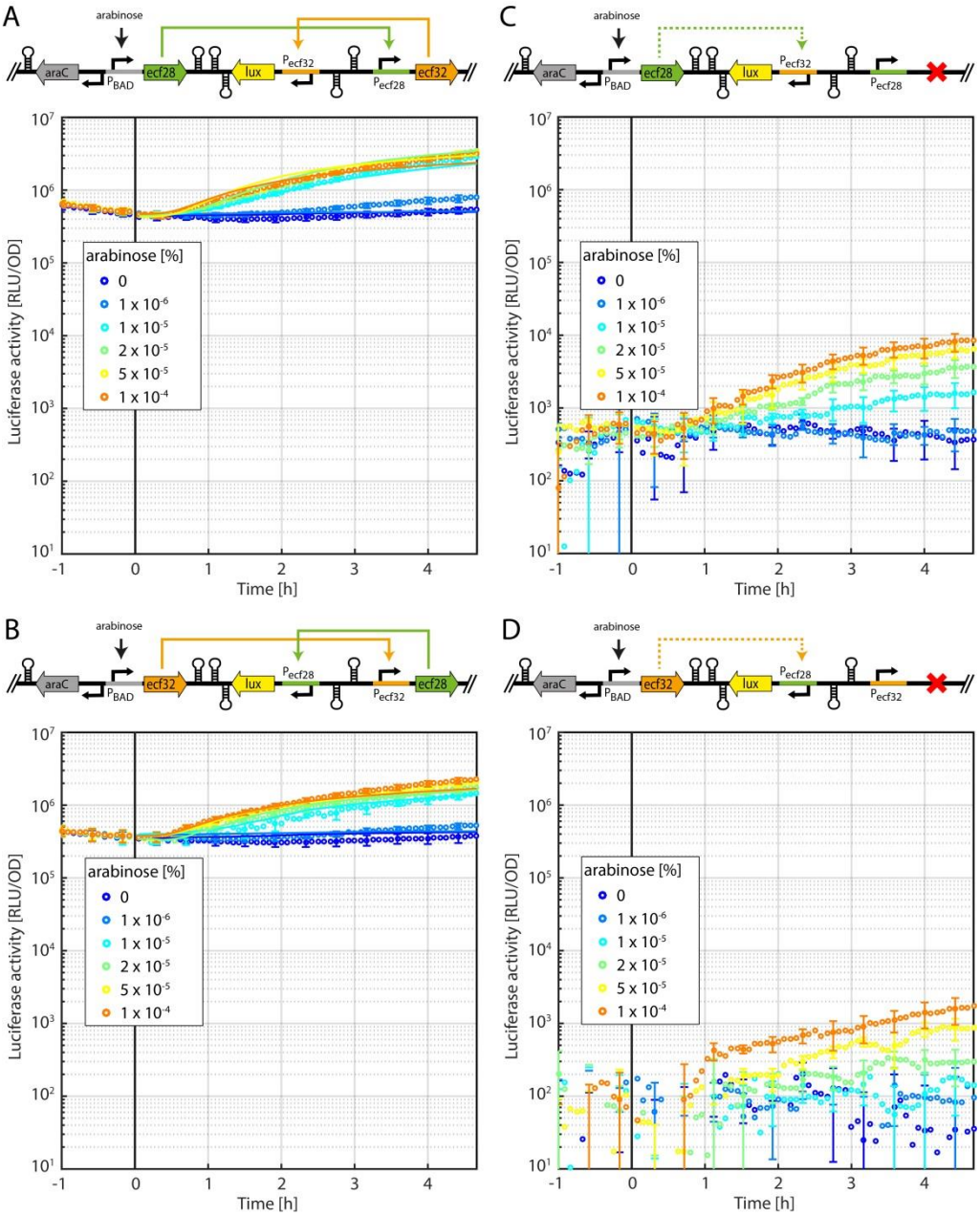

Figure 4.9. **Dynamic response of 2-step timers (A, B) compared with the corresponding negative control circuits lacking the second *ecf* gene in the cascade (C, D).** All circuits shown in the cartoons of (A-D) were introduced in *E. coli* strain SV01 on medium copy plasmid pSVM-mc (Table 9.5) generating the GFC strains listed in Table 9.1. The graphs show the dynamical response of luciferase activity (shown in relative luminescence units normalized by the optical density measured at 600 nm) after the addition of various concentrations of arabinose at t=0 h. The luciferase activity detected in the negative controls, indicate promoter activation by the non-cognate ECFs. However, this activity is 300-fold (C) and 1000-fold (D) lower than the activities obtained by the cognate ECFs in (A) and (B). *This figure was taken from Paper III* (Pinto *et. al.*, 2018) by permission of Oxford University Press.

The results show limited cross-reaction between ECF28-P_{ecf32} (30-fold between the uninduced and the induced strain; Figure 4.9C) and ECF32-P_{ecf28} (10-fold between the uninduced and the induced strain; Figure 4.9D). However, the overall non-cognate target promoter activity in the two controls is 300-fold and 1000-fold weaker than the regulation by the cognate ECF (Figure 4.8), indicating that the increasing baseline activity in the 2-step timers is not caused by non-specific ECF promoter activation.

To explain such increase baseline activity we took in account several factors such as the basal activity of the P_{BAD} promoter, the copy number of the genetic circuits and the binding affinity of the ECFs for their target promoters. First, we looked at the luciferase activity in the 0-step timer circuit. This circuit displayed a baseline signal of 10^4 RLU/OD_{600} even in the absence of induction (Figure 4.7B). This suggests the existence of a certain basal activity of the P_{BAD} promoter, observed also in previous experiments (Figure 3.8A) that, in this case, leads to the production of a certain number of ECFs even in the OFF state. Since the circuits are encoded on medium copy plasmids, the number of ECFs produced can then reach the threshold required for the activation of their target promoter, causing, in the 1-step timers, the production of the luciferase and therefore an increase in the signal baseline activity. The binding affinity of specific ECFs for their target promoter will then cause the specific differences in the baseline shift between the two different 1-step timers. For instance, in the case of ECF32 1-step timer, the baseline activity is higher than the one in the ECF28 1-step timer, suggesting a higher binding affinity of ECF32 for his target promoter. Hence, in the 2-step timers, the first ECF, produced in absence of the inducer by the basal activity of the P_{BAD} promoter, will bind to the cognate promoter producing the second ECF. The promoter binding affinity, together with the high copy number of the target promoters will then lead to the production of an even higher number of the second ECF, thus, causing a further upshift of the baseline signal. Finally, the fact that each ECF σ factor produces more ECF σ of the downstream step in the cascade, will inevitably lead, for longer ECF cascades, to an amplification of the baseline signal until full downstream promoter saturation. To test this hypothesis, we added another ECF to the cascades (ECF34) to build 3-step timer circuits with the ECFs in two different permutations (Figure 4.10A, B).

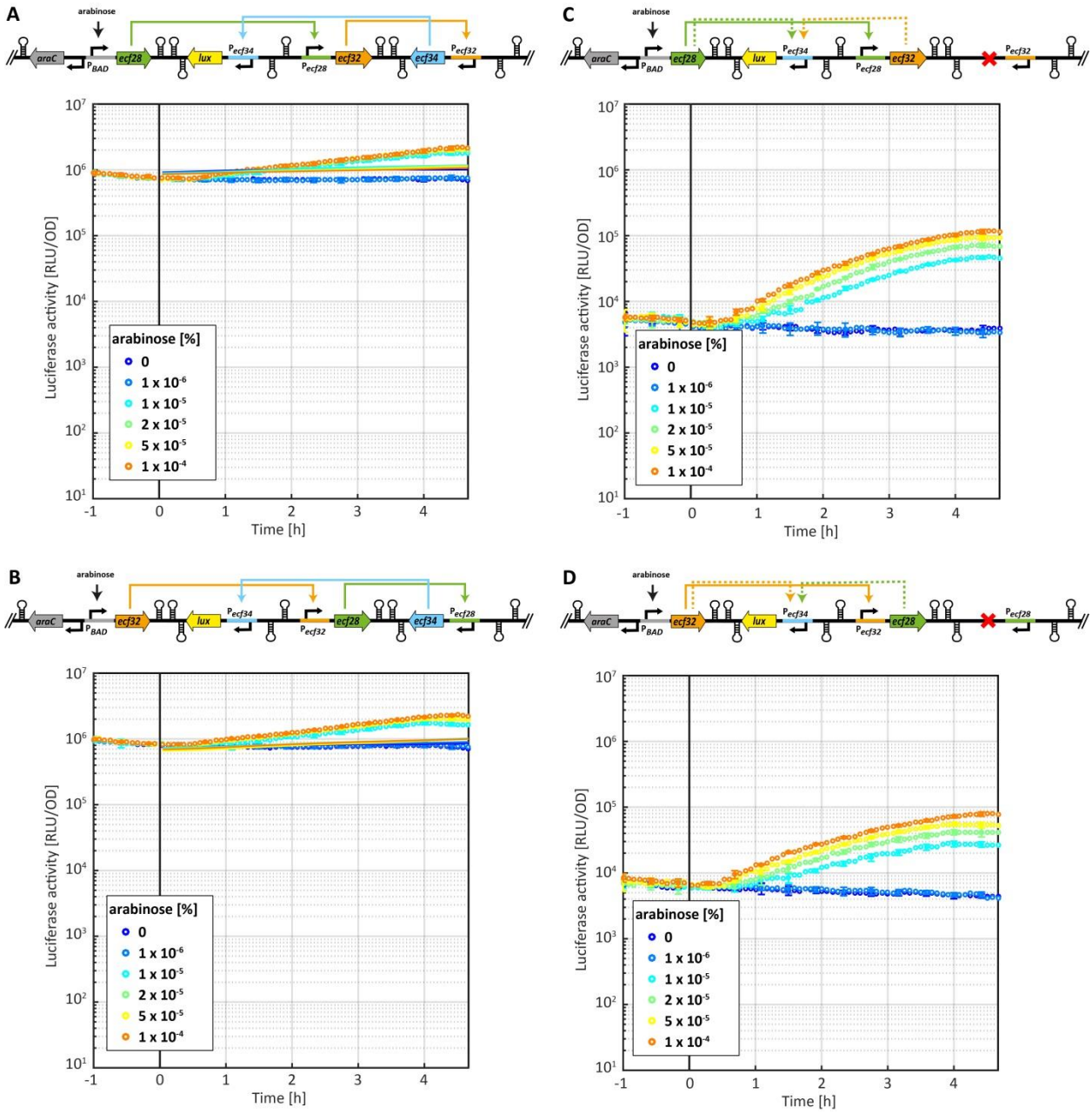

Figure 4.10. Dynamic response of 3-step timers in *E. coli* (A, B) compared with the corresponding negative control circuits lacking the second *ecf* gene in the cascade (C, D). All circuits shown in the cartoons of (A-D) were introduced in *E. coli* strain SV01 on medium copy plasmid pICH82094[26] (Table 9.6) generating the GFC strains listed in Table 9.1. The graphs show the dynamical response of luciferase activity (shown in relative luminescence units normalized by the optical density measured at 600 nm) after the addition of various concentrations of arabinose at t=0 h. The response dynamics of the computational model is shown in solid colored lines in panels A and B. *This figure was taken from Paper III* (Pinto *et. al.*, 2018) by permission of Oxford University Press.

Interestingly, both 3-step timers showed a baseline activity higher than the 2-step timers, that lead to an almost loss of their output dynamic range. Analyzing the negative controls, where ECF34 is not present (Figure 4.10C, D) we can also observe 500-fold induction between the induced and uninduced circuits that is probably caused by cross-reaction of ECF28 and ECF32 with the *ecf34* promoter. However, the signal generated by the cross-reactivity is not strong enough to justify alone the increased baseline activity of the 3-step timers. Thus, we confirmed that longer ECF cascades

encoded on medium copy plasmids lead to an amplification of the baseline signal and, as result, to a limited fold induction, due to the fact that the last promoter of the cascade is already close to saturating level.

Since the high copy number of the circuits was one of the factors determining the signal baseline amplification, and therefore the loss of signal transmission, we decided to use CRIMoClo plasmids to chromosomally integrate and test the 1- and 2-step timers (Figure 4.11).

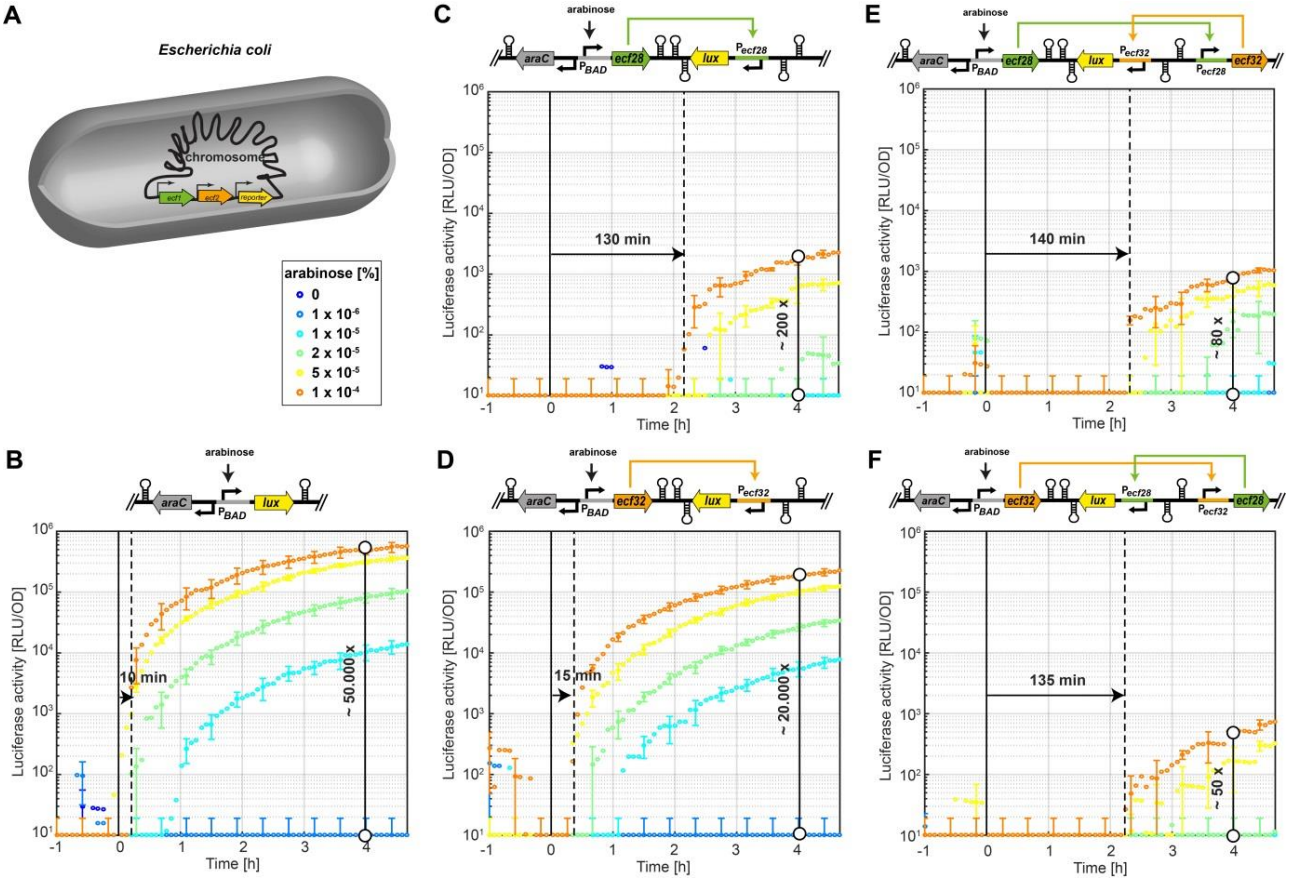

Figure 4.11. Single-copy autonomous timer circuits in *E. coli*. (A) All circuits shown in the cartoons of (B-F) were integrated into the chromosome of *E. coli* strain SV01 at the phage HK022 attachment site, using the pSV plasmid series (Table 9.5) and generating the GFC strains listed in Table 9.1. Panels (B-F) show the dynamical response of luciferase activity (shown in relative luminescence units normalized by the optical density measured at 600 nm) in synthetic ECF cascades featuring no (B), one (C, D) and two (E, F) ECF σ factors, after the addition of various concentrations of arabinose at t=0 h (black solid line). The time delay of gene induction (black dashed line) is indicated for the highest arabinose concentration (10^{-4}%) and was defined as the time when luciferase activity first exceeded the pre-induction value by 2-fold. Maximal fold induction is also indicated. *This figure was taken from Paper III* (Pinto *et. al.*, 2018) by permission of Oxford University Press.

The results show that in this configuration, even the full activation of the P_{BAD} promoter generates a reduction in the output signal in the 1-step timers when compared with the 0-step timer (250-fold-reduction for ECF28 1-step timer and 2.5-fold-reduction for ECF32 1-step timer; Figure 4.11B, C, D). The signal reduction can be explained by the number of ECFs produced, that is ~50-times lower when the circuits are encoded into the chromosome, together with the binding affinity of the ECF for their target promoters, that not allows full promoter saturation with the number of available ECFs. This hypothesis is confirmed when looking at the results of the 2-step timers

integrated into the chromosome, where we can observe an even lower final output signal (up to 500-fold-reduction) when compared to the 0-step timer (Figure 4.11B, E, F). This is due to the fact that the number of the first ECF produced is not enough to fully activate the target promoter, leading to the production of an even lower number of the second ECF and therefore causing a loss of output dynamic range that scales with the length of the cascade.

However, when looking at the timing of the circuit activation we can observe how integrated ECF28 1-step timers (Figure 4.11C) showed a time delay of 130 minutes (100 minutes more than the same circuit encoded on plasmid; Figure 4.7C), while the two 2-step timers (Figure 4.11E, F) displayed a time delay of 140 and 135 minutes (40 and 50 minutes more than the same circuit encoded on plasmid; Figure 4.7E, F). This general increase of the time delay, suggests that lowering the copy number of our timer circuits can effectively lower the baseline signal of the switches and consequently improve the signal transmission.

Even though we obtained convincing qualitative results that supported our hypothesis on the behavior of the timer circuits, we wanted to test whether the experimental data could be rationalized at a quantitative level. In particular, we asked if the dynamics and fold change of the 1- and 2-step timer were in quantitative agreement. To this end, we developed a set of computational models for all the ECF timer circuits. These models take into account the transcription and translation rates of the two ECF σ factors, as well as the *lux* reporter cassette, the degradation and/or dilution of the resulting mRNA and protein species, binding of the ECF σ factor to the RNA polymerase core, as well as binding of the resulting holoenzymes to their cognate promoters (Figure 4.12).

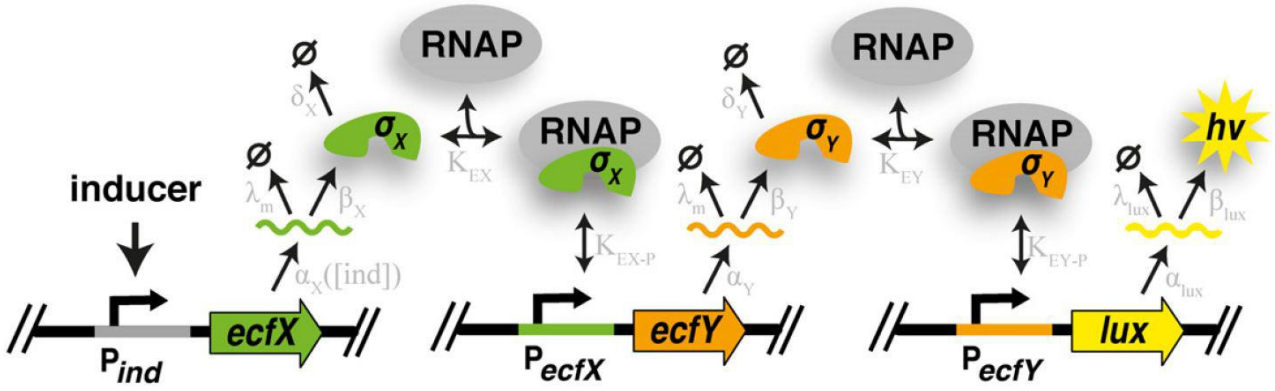

Figure 4.12. Graphic representation of the parameters included in the computational model for ECF cascades. In the model, we included transcription and translation of genes and mRNAs of *ecfX*, *ecfY* and the *lux* cassette, with transcription rates α_i and translation rates β_i (i = *X*, *Y*, *lux*). In addition, degradation and/or dilution of mRNA and protein species occur at rates λ_i and δ_i, respectively, ECF σ factors bind to core RNA polymerase with an equilibrium dissociation constant K_{Ei} and the resulting holoenzymes bind to their cognate promoters with a dissociation constant K_{Ei}-*P* (i = *X*, *Y*). All the details of the model are published in *Paper III* (Pinto *et al.*, 2018). *This figure was adapted from Paper III* (Pinto *et. al.*, 2018) by permission of Oxford University Press.

We then tested the reliability of the model by fitting our model to the data of the 0-step timer (Figure 4.7B; solid lines). Doing so, we derived the kinetic parameters that describe the P_{BAD} promoter as well as the luciferase reporter. Then we kept fixed those parameters and varied only the parameters specific to the individual ECF σ factors, thereby fitting the models of the 1- and 2-step timers simultaneously to the experimental data. Notably, all experimental data are well captured by models sharing a single set of parameters, indicating that ECF28 and ECF32 display the same

quantitative behavior in both 1- and 2-step timers (Figure 4.7 C, D, E, F; solid lines). Indeed, the fact that we were able to capture the dynamics of all circuits using a set of models that shares the same parameters for the same ECF σ factors, indicates that they display orthogonality when embedded in the different circuits. Finally, our models confirm the hypothesis that we made to explain the loss of output dynamic range in the timer circuits. Indeed, according to the model, the copy number of the circuits as well as the ECF promoters characteristics lead to an amplification of the baseline activity in ECF cascades encoded on plasmids (Figure 4.7; solid lines) and to a quick decay of circuits maximal output signal in ECF cascades integrated into the chromosome (Figure 4.11; not shown). Moreover, the model predicts that the optimal circuit copy number, to achieve maximal signal transmission, depends on the strength of the ECF promoters involved. Stronger ECF promoters require lower circuit copy number, while weaker ECF promoters require a higher circuit copy number.

Once we validated our experimental observations we tested how our timer circuits respond going from an ON state (full induction) to an OFF state (no induction). To do so we precultured the bacterial strain harboring the 0- 1- and 2- step timers in presence of the highest arabinose concentration used previously (10^{-4}%). Then, we removed the inducer, by washing the cells with inducer free media, and followed the dynamic of the luciferase signal in a microplate reader. The results (Figure 4.13) show that after inducer removal (t=0) the luciferase signal first increased ~2-fold within 0.5–2 hours and then decreased with different rates.

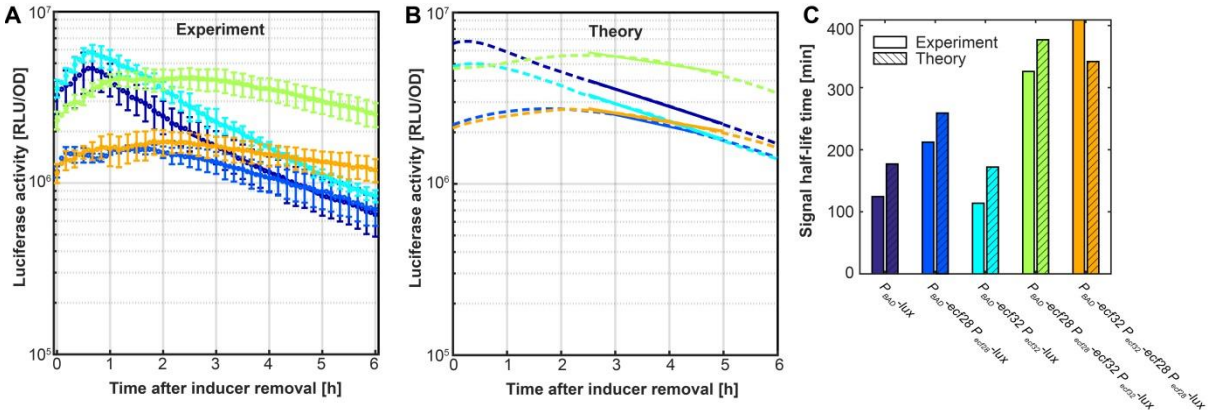

Figure 4.13. Switching synthetic ECF cascades from ON to OFF state. Decay of luciferase activity in (A) plasmid-encoded timer circuits, when cells are shifted from inducer-rich (10^{-4}% arabinose) to inducer-free medium at t = 0h. The strains used in (A) are the same described in Figure 4.7. Symbols and error bars indicate mean and standard deviation from three independent biological replicates. (B) show the computational prediction (dashed lines) for the switching kinetics from ON to OFF state in the models for the timer circuits, when the transcription rate of the inducible promoter is shifted to its basal value at t = 0 h. Solid lines in (A and B) correspond to fits of an exponentially decaying function, which was used to infer the experimental and theoretical signal half-life times reported in (C). Note that the time interval for these fits (2.5 - 5 h in A and B) was restricted to a period of constant exponential growth (not shown in the figure). *This figure was adapted from Paper III* (Pinto *et. al.*, 2018) by permission of Oxford University Press.

This somewhat unexpected increase in luciferase activity after inducer removal (Figure 4.13A) is presumably caused by a transient decrease in the growth rate after the washing step, which results in a decreased protein dilution rate and hence in increased accumulation of luciferase enzymes. However, overall, we observed that the decay of luciferase signal scales with the length of the ECF-

cascade (Figure 4.13C). Indeed, in the 0-step timer, we observed a decay of the signal (half-life 130 min) that is only slightly faster than the cell doubling time in these experiments (~175 min), suggesting that the luciferase enzymes are generally stable and gets diluted due to cell growth. In the ECF28 1-step timer we measured a luciferase half-life of ~200 min, suggesting that the ECFs present have first to be diluted and/or degraded in order to turn OFF the cognate promoter and consequently the luciferase production. Interestingly the luciferase in the ECF32 1-step timer showed a much shorter half-life (~130 min), suggesting a faster degradation rate i.e. less stable ECF σ factor. Finally, the two-step timers displayed a longer half-life of the luciferase (~320-400 min) leading to ~2–4 fold increase in signal half-life times when compared with the 0-step timer. These results confirm the qualitative expectation that more time is required in order to degrade and/or dilute the two ECFs in the 2-step timers and consequently switching OFF the downstream promoter. Strikingly when we simulated these experiments, using our mathematical model and the parameters inferred before, we were able to predict similar results to the experimental data, including the growth-rate induced peak in luciferase signal (Figure 4.13B, C). Although the signal half-life time predicted by the model is slightly higher than determined experimentally, the model captures the temporal hierarchy of switching kinetics across the different cascades very well – including also the rapid OFF-switching of the ECF32-containing 1-step timer. Taking together both the experimental and the model prediction results, we were able to validate the general behavior of the timer circuits, including the peculiar characteristics of the ECF σ factors involved.

4.2.1 ECF σ factor-based genetic-timer circuits in *B. subtilis*

In the previous section, we showed the orthogonal behavior of ECF σ factors in *E. coli* and the possibility of combining them in cascades of different length that resulted in the activation of a reporter gene with an increasing time delay. Since ECF σ factors are widespread among different bacterial phyla, it would be interesting to test if ECF-based circuit could be implemented in a different model organism. The gram-positive *Bacillus subtilis* is one of the most used model organism and it is phylogenetically distant from *E. coli*, thus represents an optimal candidate to test the implementation of ECF-based genetic circuits. Parallel to our project, our collaborators (T. Mascher and D. Pinto) used the P_{liaI} inducible promoter[124] and the luciferase reporter, to identify ECF σ factors that displayed to be functional in *B. subtilis*. Among 10 different ECF/promoter pairs analyzed, belonging to the *Proteobacteria*, *Actinobacteria* and *Firmicutes* they identified three ECFs (ECF41, ECFUN, and ECF105) that were non-toxic, did not show cross-regulation and were able to activate their target promoter. Indeed, the titration of ECF41, ECFUN, and ECF105 switches lead to a 100-, 30- and 15-fold induction from the OFF to the ON state, respectively, while the negative control strains not expressing the ECF σ factors showed target promoter activities close to the luminescence background (data not shown). Thus, they used ECF41 and ECFUN to assemble and characterize 0- 1- and 2-step timers in *B. subtilis* (Figure 4.14).

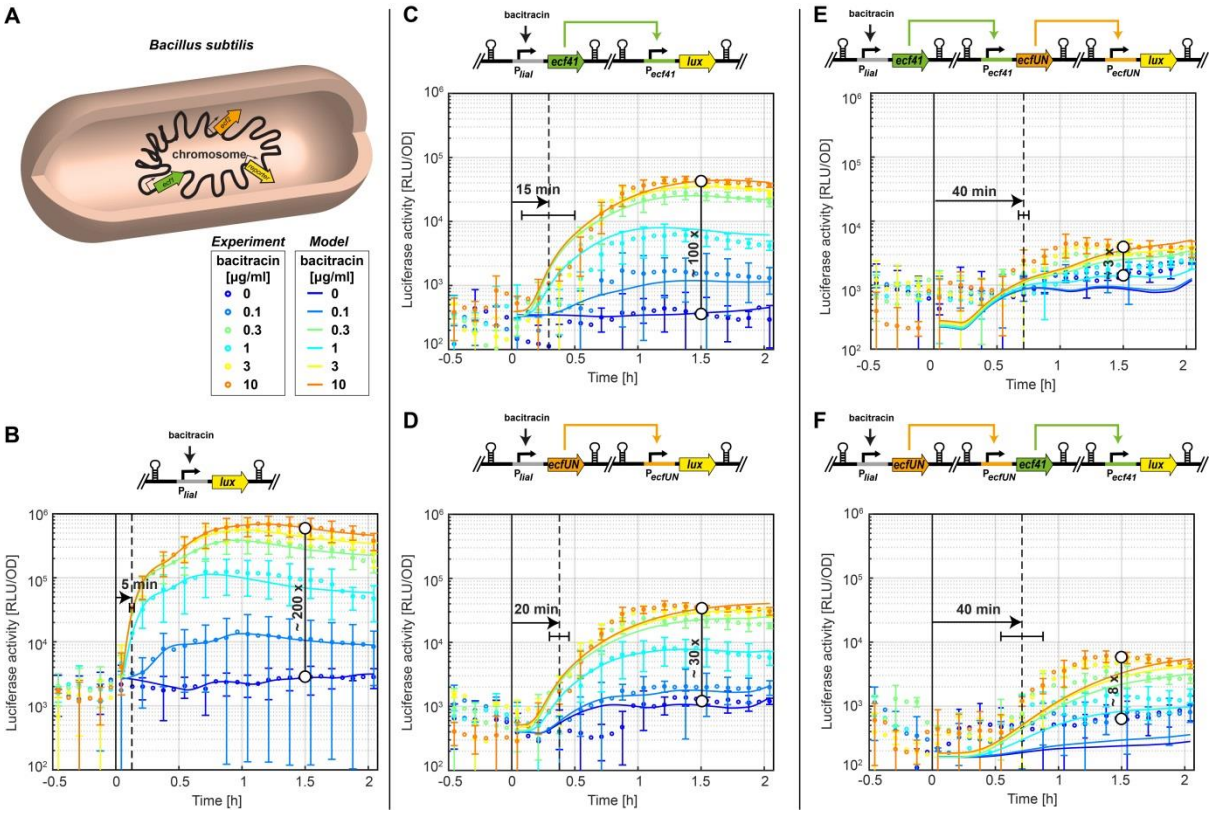

Figure 4.14. Time delayed response of synthetic ECF cascades in *B. subtilis* (measured by D. Pinto in the laboratory of Thorsten Mascher[125]). (A) All circuits shown in the cartoons of (B-F) were integrated into the chromosome of *B. subtilis* 168. Panels (B-F) show the dynamical response of luciferase activity (shown in relative luminescence units normalized by the optical density measured at 600 nm) in synthetic ECF cascades featuring no (B), one (C, D) and two (E, F) ECF σ factors, after the addition of various concentrations of bacitracin at t=0 h (black solid line). The time delay of gene induction (black dashed line) is indicated for the highest bacitracin concentration (10 µg/ml) and was defined as the time when luciferase activity first exceeded the pre-induction value by 2-fold. Maximal fold induction is also indicated. The experimental response dynamics (circles) was recorded throughout growth, as described in *Paper III* (Pinto *et. al.*, 2018). The response dynamics of the computational model (solid colored lines) was obtained by a simultaneous fit of all experimental data in (B-F), showing that the behavior of all 5 circuits can be explained with one self-consistent set of physiological parameters. The details of the computational model and the parameters are described in *Paper III* (Pinto *et. al.*, 2018). *This figure was adapted from Paper III* (Pinto *et. al.*, 2018) by permission of Oxford University Press.

Strikingly the timer circuits show, like in the case of *E. coli*, an increased time delay between the promoter induction and the luciferase signal production that scales with the length of the cascade. In particular, the 1-step timers built using ECF41 and ECFUN display a time delay of 15 minutes and 20 minutes respectively, while the 2-step timers with the ECFs in different permutations have a time delay of 40 minutes. The timer circuits were integrated into the genome and notably, we observed again a reduced output signal for longer ECFs cascades. In particular, the output-dynamic decreased from ~200-fold induction in the 0-step timer to ~15–100-fold induction in the 1-step timers. The reduced dynamic range is in agreement with the result obtained in *E. coli* and is also captured by our mathematical models. Finally, these results clearly demonstrate that more complex ECF circuits can also be functionally implemented in *B. subtilis*, where they display similar characteristics to ECF circuits tested in *E. coli*.

4.3 Summary

In order to generate ECF-based circuit with increasing level of complexity, in this chapter, we first characterized 15 distinct ECF-P_{ecf} switches in our reporter system. Overall we found that ECFs are non-toxic and functional, although they displayed different levels of promoter activation (Figure 4.1-4.6). This seems to be mainly caused by the different binding affinities of the ECFs for the cognate target promoters. By changing the copy number of the ECFs and tuning the input/output signal ratio we showed that it is possible, in principle, to optimize the output dynamic range of the ECF-switches. We, therefore, combined ECF-switches into more complex circuits, generating ECF σ factor cascades, that activate a series of ECF σ factor genes with characteristic time delays. We showed that optimizing the output dynamic range, varying the copy number of the components, can improve the signal transmission in ECF σ cascades. Moreover, the results show that the proof of concept of such "genetic-timer circuits" is also applicable in the phylogenetically distant organism *Bacillus subtilis* and that the dynamic characteristics of the circuits, in both organisms, can be captured by a set of mathematical models sharing a single set of parameters (Section 4.2).

Summarizing, all the ECF σ features illustrated in this chapter make ECFs great candidates to be used as orthogonal regulators in synthetic circuits. However, their characteristics, so far pose a challenge for assembling multiple ECF-switches into complex circuits. For instance, as we showed in Section 4.2, high basal activity of a switch can lead to the undesired the activation of the next switch in series and ultimately to the loss of output-dynamic range. Thus, the control of the basal activity of the ECF-switches embedded in a circuit represents a key feature to optimize the signal transmission in complex multi-ECF circuits. Previously, it was demonstrated that the addition of a sequestering molecule into a switch allows to control the activity of a transcriptional regulator and to lower the background signal[126]. ECF σ factors, in nature, are often regulated by anti-σ factors that can bind and block the ECFs, keeping it inactive. Hence, in order to add a new layer of control, we decided to introduce anti-σ factors in our ECF-based genetic circuits.

5. Implementation of anti-σ factors in ECF σ-based synthetic circuits

In the previous chapter, we implemented 15 ECF-switches and combined three of them in "genetic-timer circuits", where the induction of ECF cascades of different length, was activating a reporter gene with increasing time delay. However, we also observed a general decrease of signal output-dynamic range and, consequently loss of signal transmission that was scaling with the length of the ECF-cascade. This is due to the different binding characteristics of the ECFs for their target promoters, together with the different number of ECFs produced in each genetic configuration. Indeed, in plasmid-borne circuits, the decrease of output dynamic range was caused by the increasing level of baseline signals that was scaling with the number of ECFs in the cascade. In nature, signal transmission of σ factor cascades (e.g. the sporulation cascade of *Firmicutes bacteria*), heavily relies on the expression of anti-σ factors[127]. Anti-σ factors (AS) are transmembrane or cytosolic proteins and represent one of the mechanisms of signal transduction in bacteria[59]. Generally, an AS factor bind and block the cognate ECF σ factor keeping it inactive. Hence, AS factors represent one of the best options to control ECF activity and improve the dynamic response of ECF σ based synthetic circuits by reducing the *ecf* basal promoter activity. Moreover, using AS factors allows, in principle, to establish a time tunable time delay between ECF production and downstream promoter activation. Hence, in order to increase our control of ECF activity, and to establish a tunable time delay, we implemented anti-σ factors in our genetic circuits.

As illustrated in Section 1.5, AS factors can be toxic when expressed at a high level in *E. coli*. Moreover, the release of ECFs from membrane-anchored AS factors can be triggered by a variety of external stimuli. In this chapter, in order to use AS factors, we first analyze the effects of their overexpression on the growth of our reporter strain. Thus, we generate soluble, truncated, AS factor variants to alleviate the observed growth defects and isolate the AS factors activity from external stimuli. We then focus on using AS factors to generate ECF/AS threshold gate circuits. Using such circuits, we evaluate the ability of AS factors in establishing non-linear dynamic response and a tunable time delay in ECF-switches, for increasing ECF levels. Finally, we focus on a set of AS factors to design time-tunable suicide circuits in *E. coli*.

5.1 Toxicity evaluation of wild type anti-σ factors

In Chapter 4, we analyzed the dynamic range of 15 ECF σ factors by building ECF-switches (Figure 4.3, 4.5, 4.6). Among these ECFs, 14 have a known AS factor. In order to implement these AS factors in our circuits, we first evaluated their ability in sequestering the cognate ECFs into inactive complexes and, at the same time, the effects of their overexpression on cell growth. To do so, we designed 14 new circuits by adding the cognate AS factors to the previously generated ECF-switches (Figure 4.3). In each circuit, we maintained the inducible P_{BAD} promoter driving the expression of an *ecf* gene and added a second inducible promoter (P_{tet}) to control the expression of the cognate AS factor. Each circuit maintains the relative *ecf* promoter fused with the luciferase reporter, to measure the output signal of the circuit for increasing AS levels (Figure 5.1).

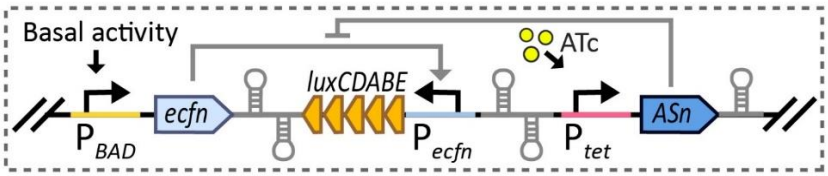

Figure 5.1. Genetic organization of the modules in ECF-AS-switch circuits. The basal activity of an arabinose-inducible P_{BAD} promoter drives the expression of an ECF σ factor. The expression of the cognate AS factor (that regulates the ECF activity) is controlled by an ATc inducible P_{tet} promoter. The light signal produced by the relative *ecf* promoter, fused with the luciferase operon, represent the output of the circuit.

Our previous results showed that all plasmid-borne ECF-switches possess certain basal activities, even in the absence of inducer, due to their binding characteristics for the cognate promoters and to the basal activity of the P_{BAD} promoter (Figure 4.3). Therefore, to evaluate AS activity, we relayed on this basal signal, assembling the AS-circuits on medium copy plasmids and measuring the changes in the baseline signal (RLU/OD_{600}), during time-course experiments, were we only induced the AS expression. During the experiments, we also measured the optical density at 600 nm (OD_{600}) of all strains, in order to evaluate growth defect among AS induction. Finally, to compare the toxicity and the activity of different AS factors we plotted, for each circuit, the OD_{600} and luminescence normalized by the OD_{600} (RLU/OD_{600}) values, in absence (ATc 0ng/mL) and in presence (ATc 100ng/mL) of AS, 6 h after the induction (Figure 5.2 A, B).

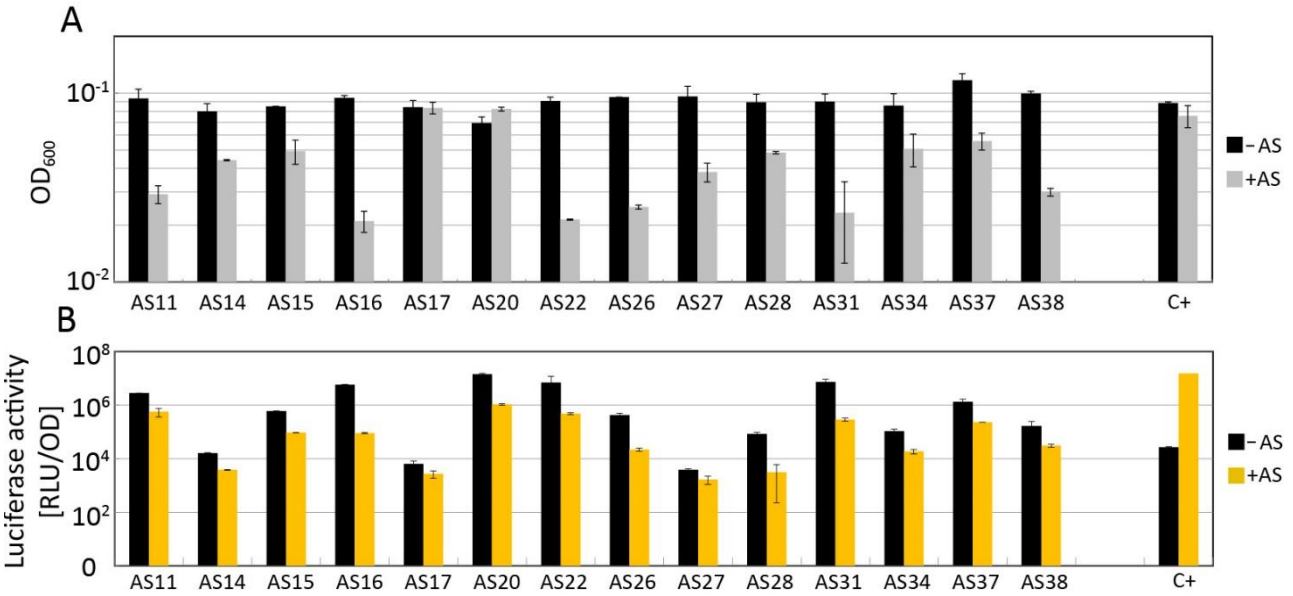

Figure 5.2. Characterization of wild type AS factors. All circuits were introduced in *E. coli* strain SV01 on medium copy plasmid pSVM-mc (Table 9.5) generating the GFC strains listed in Table 9.1. (A) bacterial density (indicated as the optical density measured at 600 nm) achieved by 14 *E. coli* strains carrying the indicated ECF/AS circuits (the circuit is named after the AS factor) and a positive control strain (C+), 6 hours after the induction with 0 (-AS) and 100 (+AS) ng/mL ATc. The positive control (C+) is an *E. coli* strains carrying a plasmid-borne P_{tet}-*lux* construct. (B) Luciferase activity (shown in relative luminescence units normalized by the optical density measured at 600 nm) of the strains described in (A), 6 hours after the induction with 0 (-AS) and 100 (+AS) ng/mL ATc. The results are averaged from at least two independent biological assays and error bars denote standard deviations.

Overall, our result shows that AS overexpression has a deleterious effect on cell growth. Indeed, most of the AS factors cause a reduction in the 6h-OD_{600} to 50% or higher of the uninduced strain (Figure 5.2A). There are, however, two exceptions represented by AS17 and AS20 that did not show any toxic effect. In contrast, AS16, AS22, and AS31 resulted to be particularly toxic, causing a >75% fold-reduction in the 6h-OD_{600} when compared with the uninduced strain (Figure 5.2A). Analyzing the luminescence signal in absence and presence of AS factors (Figure 5.2B) we noticed, overall, the ability of the AS factors of lowering the signal produced by the basal activity of the cognate ECFs (from ~2-fold; AS27 to ~64-fold; AS16, between uninduced and fully induced AS conditions). The non-toxic AS17 and AS20 are also able to lower the ECF activity (Figure 5.2B; ~2-fold and ~14-fold respectively), confirming that these AS factors are functional and at the same time non-toxic. However, especially for highly toxic AS factors (e.g. AS16), it is not possible to discriminate at which extent the baseline signal reduction is caused by AS activity, or by reduced viability of the strains.

With the results obtained from these experiments, we gained a general overview of AS toxicity and activity. Overall, AS appeared to be functional, but exhibited also a medium/high level of toxicity that, in some cases, could enhance the luciferase signal reduction. Thus, in order to use AS factors in synthetic circuits and to better characterize their activity, the toxicity of the AS factors have to be reduced. To do so, we decided to generate AS truncations.

5.2 Toxicity evaluation of truncated, soluble anti-σ factors

Anti-σ factors are often transmembrane proteins and since the space in the cell membrane is limited[128], we reasoned that purely the possession of a transmembrane domain of a strongly expressed protein could significantly reduce the viability of the host. As introduced in Section 1.5, the σ factor binding domain is encoded in the N-terminal portion of the AS factor. In transmembrane AS factors, the N-terminal domain is situated in the cytoplasm and it is followed by a transmembrane domain and a periplasmic C-terminus that is responsible for sensing extracellular stimuli[59]. Therefore, to generate AS truncations, we required to remove the transmembrane domain of the proteins, avoiding the deletion of any portion that is important for ECF-binding. To this end, the former master student in our laboratory Angelika Diehl predicted the secondary structure and the transmembrane domains of AS factors using Jared[129] and TOPCONS[130] respectively. Using this approach, she successfully identified transmembrane domains in 12 over the 14 selected AS factors. In particular, AS15 is known to be already soluble and therefore it was not possible to generate a truncated variant[68]. AS16, on the other hand, is predicted to have 6 transmembrane domains and an N-terminus portion of only 25 amino acids. Within this number of amino acid, it is possible to accommodate only 1.5 α-helices that seems to be not enough for the binding of the ECF σ factor[56]. Moreover, we found highly conserved residues in the otherwise variable transmembrane domains. These conserved residues face the cytoplasm, suggesting that they are important for ECF binding. For the reasons described above we then decided to not generate a truncated variant of this AS.

For all the other AS factors, after identifying a suitable site for cutting the transmembrane domain, we generated, by PCR amplification, and Golden gate assembly, AS truncations (Table 9.3). To ascertain at least one functional construct, we generated, if possible, two truncation variants of different length for each AS. Moreover, to prevent the exposition of degradation-tags at the C-terminus and to eventually allow protein purification, we added a C-terminal FLAG-tag to each AS

truncation[131]. Using this approach, we generated 21 FLAG-tagged soluble AS factors that possess only the N-terminal domain responsible for the ECF binding (Table 5.1).

	N-terminus		Trunc. 1	Trunc. 2
Name	**Length/Aa**	**TM**	**Length/Aa**	
AS11_987	72-109	0	109	80
AS14_1324	156	1	146	87
AS17_1691	114	1	94	-
AS20_992	86-75	1	86	75
AS22_4450	39	4	39	-
AS26_4464	98	1	93	80
AS27_4265	118	1	109	77
AS28_1088	77	1	71	67
AS31_34	45	2	45	22
AS34_1384	105	1	100	87
AS37_2513	80	1	74	48
AS38_1322	156	1	155	-

Table 5.1. Anti-σ factor truncations. The original names of the AS factors assigned by V. Rhodius *et al.*,[63] are indicated. TM: Number of transmembrane domains. Trunc: truncation.

To evaluate the effects of AS-truncations overexpression on cell growth, we assembled AS-circuits as illustrated previously (Figure 5.1). Briefly, the circuit, encoded on medium copy plasmid, contains two distinct inducible promoters (P_{BAD} and P_{tet}) that drive the expression of an ECF σ factor and the cognate AS factor truncation respectively. The relative P_{ecf} promoter, fused with the luciferase cassette, is used to assay AS activity. We evaluated the toxicity and the activity of the AS-truncations by measuring the OD_{600} and the changes in the luciferase signal (RLU/OD_{600}), produced by the basal ECF activity in absence (ATc 0ng/mL) and in the presence (ATc 100ng/mL) of AS, respectively (Figure 5.3).

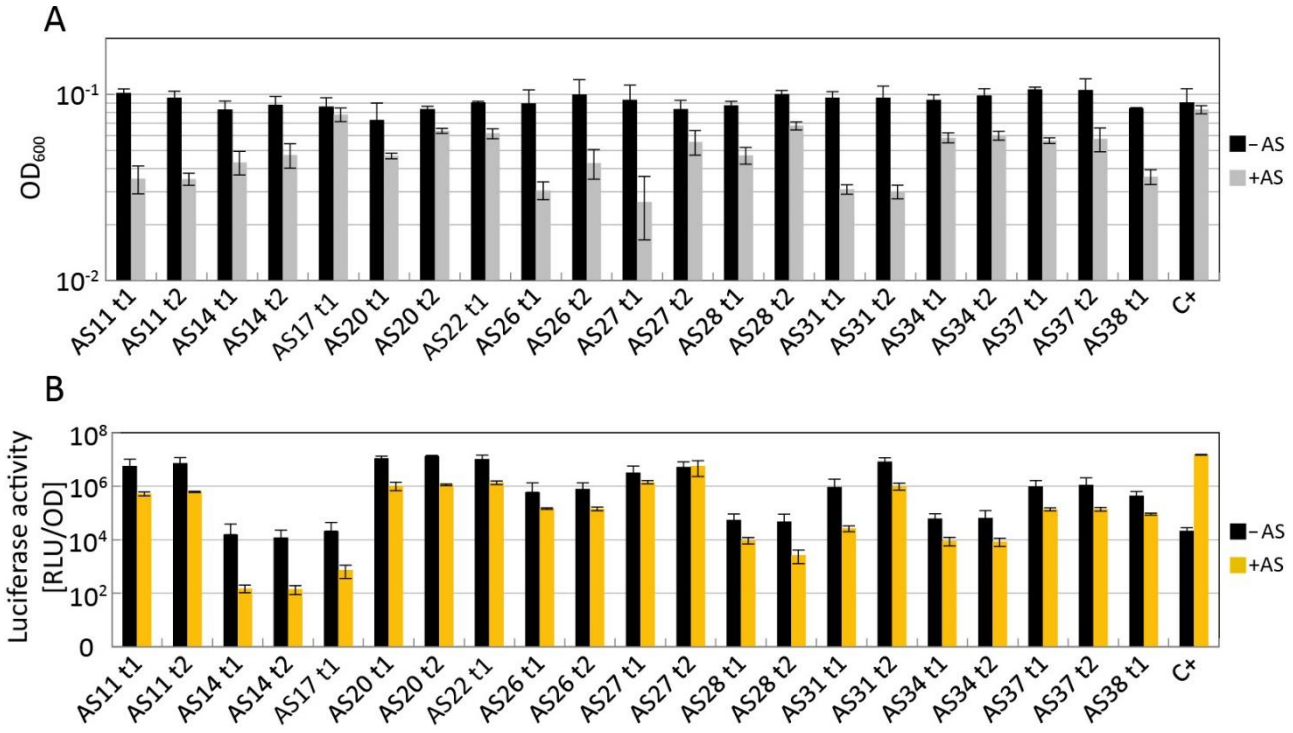

Figure 5.3. Characterization of truncated AS factor variants. All circuits were introduced in *E. coli* strain SV01 on medium copy plasmid pSVM-mc (Table 9.5) generating the GFC strains listed in Table 9.1. (A) bacterial density (indicated as the optical density measured at 600 nm) achieved by 21 *E. coli* strains carrying the indicated ECF/AS circuits (the circuit is named after the AS truncation variant) and a positive control (C+), carrying a plasmid-borne P_{tet}-*lux* construct, 6 hours after the induction with 0 (-AS) and 100 (+AS) ng/mL ATc. (B) Luciferase activity (shown in relative luminescence units normalized by the optical density measured at 600 nm) of the strains described in (A), 6 hours after the induction with 0 (-AS) and 100 (+AS) ng/mL ATc. The results are averaged from at least two independent biological assays and error bars denote standard deviations.

Figure 5.3 shows the OD_{600} and the luciferase signal (RLU/OD_{600}) of 21 AS-truncation and a P_{tet}-*lux* control at time 6 h from AS induction. Analyzing the growth of strains in which the AS expression was not induced, we observed, in all the strains, an OD_{600} ~0.1 (Figure 5.3A; black bars). This is similar to the result obtained for wild type AS (Figure 5.2A; black bars) and indicates an overall non-toxic effect on cell growth of uninduced AS circuits (wild type or truncated). After the induction of AS factor truncations, half of the strains presented overall growth defects, showing a reduction in the 6hr-OD_{600} to 50% or lower of the uninduced strain (Figure 5.3A; grey bars). An exception is represented by AS22 truncation, that alleviated enormously the toxicity, from ~76% 6h-OD_{600} reduction of the wild type AS, to ~30% 6h-OD_{600} reduction of the truncated variant (Figure 5.2A; AS22, Figure 5.3A; AS22 t1). Moreover, all other truncations resulted to be equally, or less toxic, than the relative wild type AS possessing equal or higher 6h-OD_{600} (Figure 5.2A and Figure 5.3A; grey bars). The results also show that, if available, the truncation 2 (shorter AS variant) exhibited, overall, less toxicity then truncation 1 (higher 6hr-OD_{600} when compared to truncation 1).

Analyzing the luciferase signal, (Figure 5.3B) we noticed, upon induction, a general ability of the AS truncations of lowering the luciferase signals (from ~2-fold, AS27 t1, to ~100-fold, AS14 t1, t2), indicating that AS truncations are still able to bind the cognate ECF σ factors. Overall, for a

given AS truncation, there is almost no difference in activity between the two truncations (Figure 5.3B; equal RLU/OD-fold reduction when comparing truncation 1 and truncation 2) with the exception of AS31 (~35 and ~8 RLU/OD-fold reduction for t1 and t2 respectively). Moreover, when comparing the fold reduction in luciferase signal between wild type (Figure 5.2B) and truncated AS (Figure 5.3B) we observed, overall, similar results, with the exception of AS14. Strikingly, the truncations of this particular AS factor showed an increased ability in binding the cognate ECF, enhancing the ~4-fold signal reduction of the wild type (Figure 5.2B; AS14) to ~100-fold for both the truncated variants (Figure 5.3B; AS14 t1, AS14 t2).

Summarizing, our results suggest that truncated AS are generally functional, being able to block the ECFs and lowering the activation of the *ecf* target promoters. Moreover, AS truncations are equally or less toxic than the wild type counterpart, indicating that the deletion of the transmembrane domains partially reduced the toxicity of the AS factors. The residual toxic effect in AS truncation could then be explained by cross-reaction between the soluble AS factors and endogenous sigma factors required for the basal cellular processes. Hence, the overexpression of AS factors encoded on medium copy plasmids, even in the soluble form, could lead to the growth defects we observed. Since toxic proteins expressed from medium and high copy plasmids can generate undesired effects on cellular physiology[34,35], lowering the copy number of the toxic construct, is often a solution. Hence, to ultimately alleviate the AS toxicity, we decided to analyze the AS truncation-circuits in single copy configuration.

5.3 Characterization of chromosomally integrated anti-σ factor circuits

As a test case study, we first chromosomally integrated and evaluated the wild type AS16-based circuit. We chose this wild type AS factor because previously resulted to be the most toxic and active AS (Figure 5.2). We, therefore, wanted to evaluate how the expression in single copy of this AS would affect its toxicity and activity. We then measured, using time-course experiments, the luciferase activity and the OD_{600} of strains harboring the AS16-based circuit on medium copy plasmid, or chromosomally integrated (Figure 5.4).

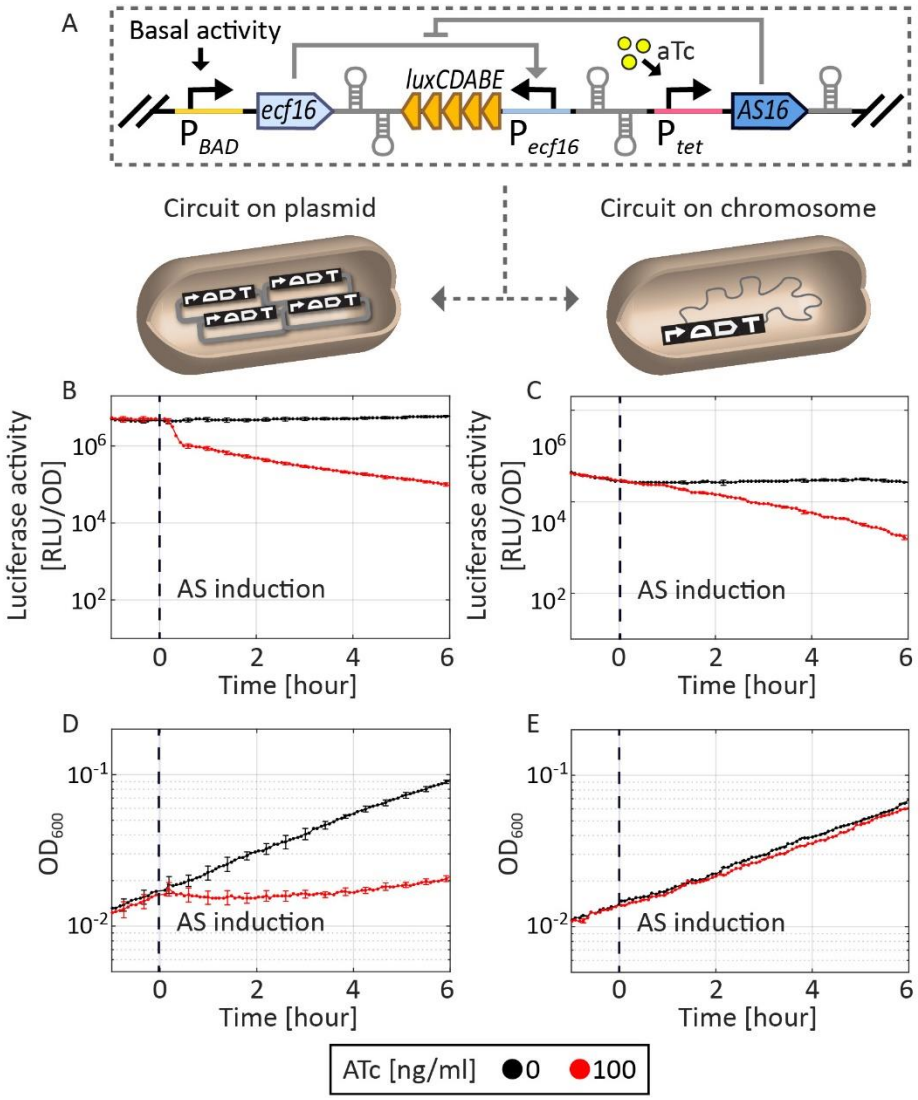

Figure 5.4. Toxicity and activity of plasmid-borne and chromosomally integrated ECF/AS16 circuit. Comparison of ECF/AS16 circuit (A) encoded on medium copy plasmid (B, D) and chromosomally integrated (C, E). Luciferase activity (shown in relative luminescence units normalized by the optical density measured at 600 nm) from an ECF16 σ-dependent promoter (B, C), and optical density measured at 600 nm (D, E) in absence (ATc 0 ng/mL), or presence (ATc 100 ng/mL) of cognate anti-σ. The growth defects observed when the circuit is encoded on medium copy number plasmids (D) are abolished when the circuit integrated into the genome (E), while the ability of the anti-σ of sequestering the cognate ECFσ is maintained (B, C). The data indicate averages from three independent biological assays and error bars denote standard deviations.

The results for the plasmid-borne circuit showed, 6 h after induction, a decrease of 5-fold in the OD_{600} values together with ~60-80-fold reduction of the luciferase signal (Figure 5.4B, D). As previously illustrated, in this case, it is not possible to discriminate if the reduction of luciferase signal is due to the inhibiting activity of the AS on the ECF σ factor, or to the AS overexpression that causes a growth defect in the strain analyzed. However, when examining the same ECF/AS circuit integrated into the chromosome, we also observed a significant decrease in the luciferase signal (~30-fold; Figure 5.4C), while the OD_{600} values of the AS-induced and uninduced conditions resulted almost identical (Figure 5.4E). These results indicate that in the chromosomally integrated

circuit, the AS factor retained the ability to sequester the cognate ECF σ factor, while the toxicity effects observed on medium copy plasmid were completely abolished.

After evaluating the behavior of the wild type AS16 and confirming that expressing the AS factor in single copy completely abolish the growth defects observed previously, we deiced to integrate all the truncated AS circuits (together with AS15 and AS16 which do not possess truncated variants) into the genome of *E. coli*. To do so, we used CRIMoClo vectors to sub-clone and subsequently chromosomally integrate the previously generated AS circuits (Figure 5.3). Strikingly, we found that all single copy AS circuits did not cause a toxic effect on cell growth. Indeed, all the strains displayed similar 6h-OD_{600} values in both uninduced and induced conditions (Figure 5.5A).

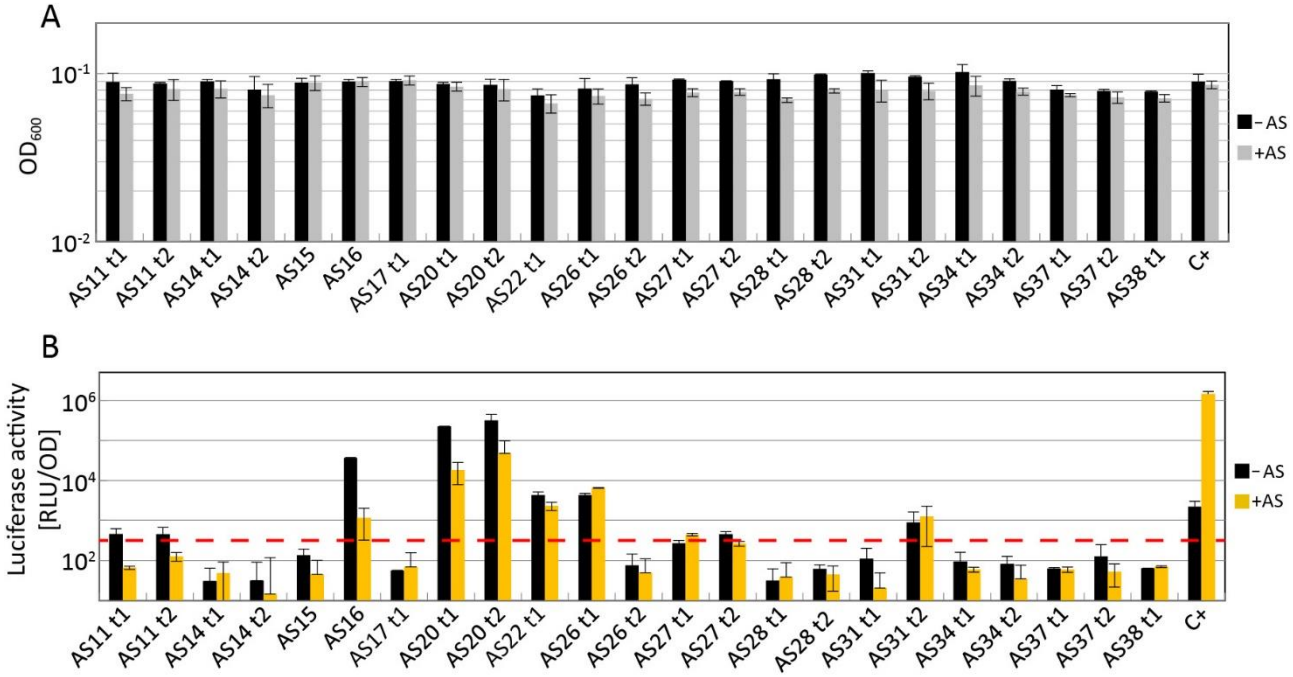

Figure 5.5. Characterization of chromosomally integrated truncated AS factor variants. All circuits were integrated into the chromosome of *E. coli* strain SV01 at the phage HK022 attachment site, using the pSV plasmid series (Table 9.5) and generating the GFC strains listed in Table 9.1. (A) bacterial density (indicated as the optical density measured at 600 nm) achieved by 23 *E. coli* strains carrying the indicated ECF/AS circuits (the circuit is named after the AS or the AS truncation variant) and a positive control (C+; P_{tet}-*lux*), 6 hours after the induction with 0 (-AS) and 100 (+AS) ng/mL ATc. (B) Luciferase activity (shown in relative luminescence units normalized by the optical density measured at 600 nm) of the strains described in (A), 6 hours after the induction with 0 (-AS) and 100 (+AS) ng/mL ATc. The red dashed line represents the plate reader low detection limit. The results are averaged from at least two independent biological assays and error bars denote standard deviations.

Analyzing the AS functionality (Figure 5.5B) we found that AS11 t1-t2, AS16, AS20 t1-t2, AS22 t1 presented a fold reduction on the luciferase signal, ranging from 2-fold (AS22 t1) to 30-fold (AS16). In contrast, AS26 t1, and AS31 t2 appear to have lost the ability to sequester the cognate ECF σ factors when compared to plasmid-borne circuits (cfr. Figure 5.3B). This suggests that the activity observed previously in the plasmid-configuration was mainly due to the growth defects caused by the AS overexpression (Figure 5.3A). In the case of AS27 t1-t2 variants (Figure 5.5B), we obtained similar luciferase values in the presence and the absence of expression of the AS

factor truncations (~4x10^2 RLU/OD$_{600}$). These values are close to the detection limit of the plate reader, however, overall, AS27 and its truncations did not show a significant ability in reducing the ECF activity, also in all other experiments (min. 0-fold reduction in Figure 5.3B; AS27t2, – max. 2-fold reduction in Figure 5.2B; AS27), thus, we assume that this AS does not bind efficiently to the cognate ECF σ. Finally, in the case of the other AS-circuits (Figure 5.5B; ECF14 t1-t2, AS15, AS17 t1, AS26 t2, AS28 t1-t2, AS31 t1, AS34 t1-t2, AS37 t1-t2, AS38 t1) the basal ECF activity generated a low luciferase signal that is below the detection limit of the plate reader (~4x10^2 RLU/OD$_{600}$). Therefore, for these circuits, it was not possible to evaluate AS activity accurately.

In order to recover the luciferase signal in these circuits, we repeated the experiment inducing full ECFs expression prior to and during the measurement, using 0.2% arabinose (saturating concentration of the P$_{BAD}$ promoter; cfr. Figure 3.8B). Then, we followed the dynamic of OD$_{600}$ and luciferase signal (RLU/OD$_{600}$) in the absence (ATc 0ng/mL) and in the presence (ATc 100ng/mL) of AS, respectively (Figure 5.6).

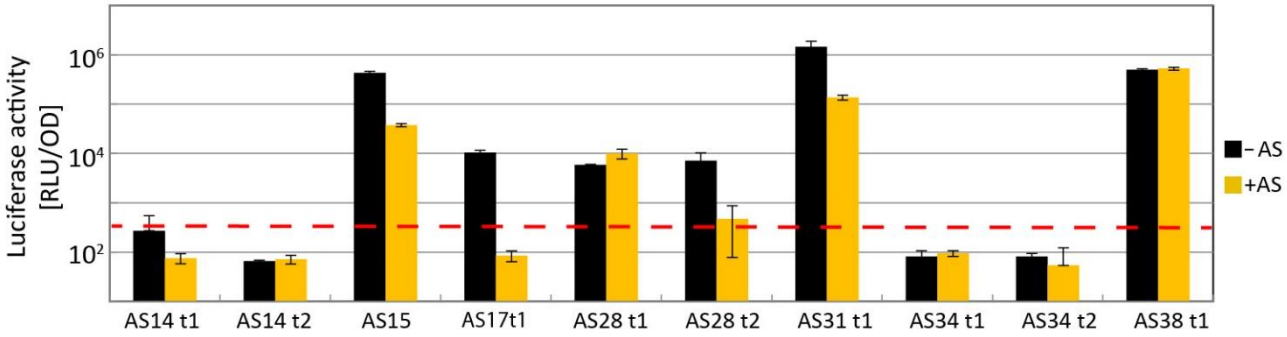

Figure 5.6. Characterization of chromosomally integrated truncated AS factor variants in the presence of high ECF σ levels. All circuits were integrated into the chromosome of *E. coli* strain SV01 at the phage HK022 attachment site, using the pSV plasmid series (Table 9.5) and generating the GFC strains listed in Table 9.1 Luciferase activity (shown in relative luminescence units normalized by the optical density measured at 600 nm) of 10 *E. coli* strains carrying the indicated ECF/AS circuits (the circuit is named after the AS or the AS truncation variant), 6 hours after the induction with 0 (-AS) and 100 (+AS) ng/mL ATc. The red dashed line represents the plate reader low detection limit. The results are averaged from at least two independent biological assays and error bars denote standard deviations.

Using this experimental setup, we were able to register a detectable the signal for ECF15, ECF17 ECF28, ECF31, and ECF38 showing at the same time AS activity for AS15, AS17, AS28t2, AS31t1 (Figure 5.6; from 10-fold: AS31 t1 to 120-fold: AS17 t1). In contrast, in the case of AS28t1 and AS38 t1, we did not observe any change in the luciferase level among AS induction, suggesting a poor ability of these AS factors in regulating the cognate ECFs. In the case of ECF14 and ECF34, the overnight induction did not produce a detectable luciferase signal (Figure 5.6; AS14 t1-t2, AS34 t1-t2, black bars), even in presence of high level of inducer (0.2% arabinose). This can be explained by looking at the dose-response curves generated for the corresponding chromosomally integrated ECF-switches (Figure 4.5). Indeed, among all the switches ECF14 and ECF34, exhibited the lowest activity at full arabinose induction when expressed in single copy (~2x10^3 RLU/OD$_{600}$). This combined with the presence of AS factors, produced by the basal activity of the P$_{tet}$ promoter (cfr. Figure 3.8D), can explain the low signal (below the plate reader detection limit) that we registered in this experiment (Figure 5.6).However, this observation also implies a certain ability of these AS truncation in binding the cognate ECFs. Finally, the strains carrying AS26 t2 and AS37 t1-t2

displayed severe slow growth during the experiment (in all the biological replicates), after full overnight induction of ECF sigma factors, therefore were excluded from this analysis. In case of AS37 t1 and t2, the reduced growth can be attributed to the toxic effect given by the overexpression of the relative ECF as shown in Figure 4.2, while the reasons for the slow growth observed in strain encoding the ECF/AS26 t2 circuit remain elusive. However, these AS factor truncations appeared to be active when assayed on medium copy plasmids (Figure 5.2B), even though they displayed, at the same time, toxic effects on cell growth (>50% fold-reduction in the 6h-OD600), therefore, we cannot exclude that they are at least partially functional.

5.4 Anti-σ factor threshold gate circuits

In the previous sections, we showed that AS factors are able to bind the ECFs sequestering them into transcriptionally unproductive ECF σ/anti-σ factor complexes. Thus, in this section, we show our experiments to determine if AS factors can be effectively used to lower the baseline signal of ECF-switches. We reasoned that if we set a certain expression level of AS factor, the pool of induced ECFs have to overcome the AS threshold in order to activate the target promoter. This will, in principle, generate a non-linear dynamic response of the *ecf* promoters and a sharper transition between the OFF and the ON state of the switches, for increasing levels of ECFs. Moreover, the introduction of different levels of AS factors in ECF/AS-switches could lead, in principle, to the generation different time delays between ECF expression and downstream promoter activation.

To test our hypothesis we designed an experiment selecting the AS truncations that in the previous experiments displayed reduced toxicity and high activity (Figure 5.3B and Figure 5.5B; AS11 t2, AS14 t2, AS20 t2, AS22 t1, AS26 t2, AS27 t1, AS28 t2, AS31 t1, AS34 t1, AS37 t1, AS38 t1). Moreover, to simplify the experimental procedure, we wanted to assay all the switches at the same time, using the same inducer concentrations. Thus, we decided to use a configuration of the different genetic modules that ensured low AS toxicity and high reporter activity. Therefore, we engineered the bacterial strains integrating the P_{BAD}-*ecf* and the P_{tet}-*anti-σ* modules into the genome and subsequently transformed them with medium copy plasmid encoding the luciferase reporter gene fused with the relative *ecf* promoter. In this way we are able, in principle, to express safely the AS factors even at inducer levels close to P_{tet} promoter saturation (Figure 3.8D; aTC >1 ng/mL), without incurring in toxic effects (as shown in Figure 5.5A). Moreover, as previously showed in Section 4.1, this configuration (chromosomally integrated P_{BAD}-*ecf* and plasmid-borne P_{ecf}-*lux*) guaranteed an overall high level of output luciferase signal, upon the different concentration of arabinose induction (Figure 4.6).

In order to set two different AS levels, and knowing the P_{tet} promoter have a certain basal activity (cfr. Figure 3.8D), we grew the strains during the entire experiment, in absence (ATc 0 ng/mL) and in presence (ATc 2.5 ng/mL) of inducer, in order to set a low and a high AS expression level (cfr. P_{tet} promoter induction in Figure 3.8D). We then measured the circuits dynamic behavior, among different level of ECF expression and grouped the results according to the ability of the AS of lowering the luciferase signal produced by the basal ECF activity (Figure 5.7 and Figure 5.8).

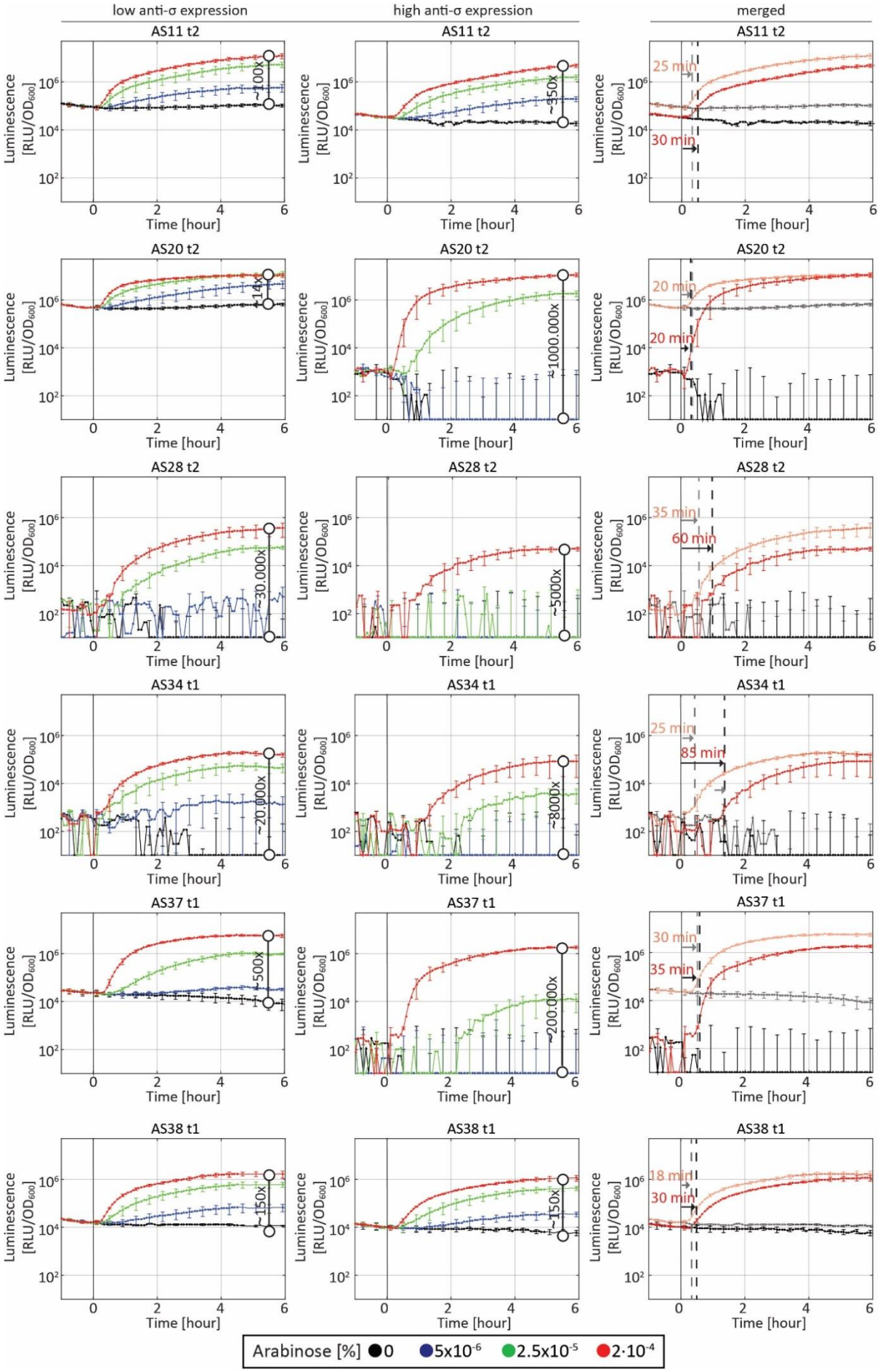
low anti-σ expression
high anti-σ expression
merged
AS11 t2
AS20 t2
AS28 t2
AS34 t1
AS37 t1
AS38 t1
Luminescence [RLU/OD600]
Time [hour]
~100x
~350x
25 min
30 min
~14x
~1000.000x
20 min
20 min
~30.000x
~5000x
35 min
60 min
~20.000x
~8000x
25 min
85 min
~500x
~200.000x
30 min
35 min
~150x
~150x
18 min
30 min
Arabinose [%] 0 5x10-6 2.5x10-5 2·10-4

Figure 5.7. Characterization of 6 threshold gate ECF/AS circuits. Dynamic response of threshold gated ECF/AS circuits. All P_{BAD}-*ecf* and P_{tet}-*anti-σ* TUs were integrated into the chromosome of *E. coli* strain SV01 at the phage HK022 attachment site, using the pSV plasmid series (Table 9.5). Subsequently, the P_{ecf}-*lux* reporter system (encoded on pSVM-mc plasmids, Table 9.5) were introduced into the newly engineered strains, generating the GFC strains listed in Table 9.1. The graphs show, for each circuit (named after the AS truncation variant), the dynamical response of luciferase activity (shown in relative luminescence units normalized by the optical density measured at 600 nm) after the addition of arabinose at the indicated concentrations at t=0 h (solid black lines), in presence of low (ATc 0 ng/mL) and high (ATc 2.5 ng/mL) AS threshold levels. The maximum fold induction is indicated. The merged panels show the signals obtained for low (faded curves) and high (solid curves) AS expression, in the uninduced (arabinose 0 %) and highly induced (arabinose $2x10^{-4}$%) strains. The time delay of *ecf* induction (dashed lines) is indicated for the highest arabinose concentration ($2x10^{-4}$%) and was defined as the time when luciferase activity first exceeded the pre-induction value by 2-fold. The experimental response dynamics were recorded during exponential growth, as described in Section 7.10 The results are averaged from at least two independent biological assays and error bars denote standard deviations.

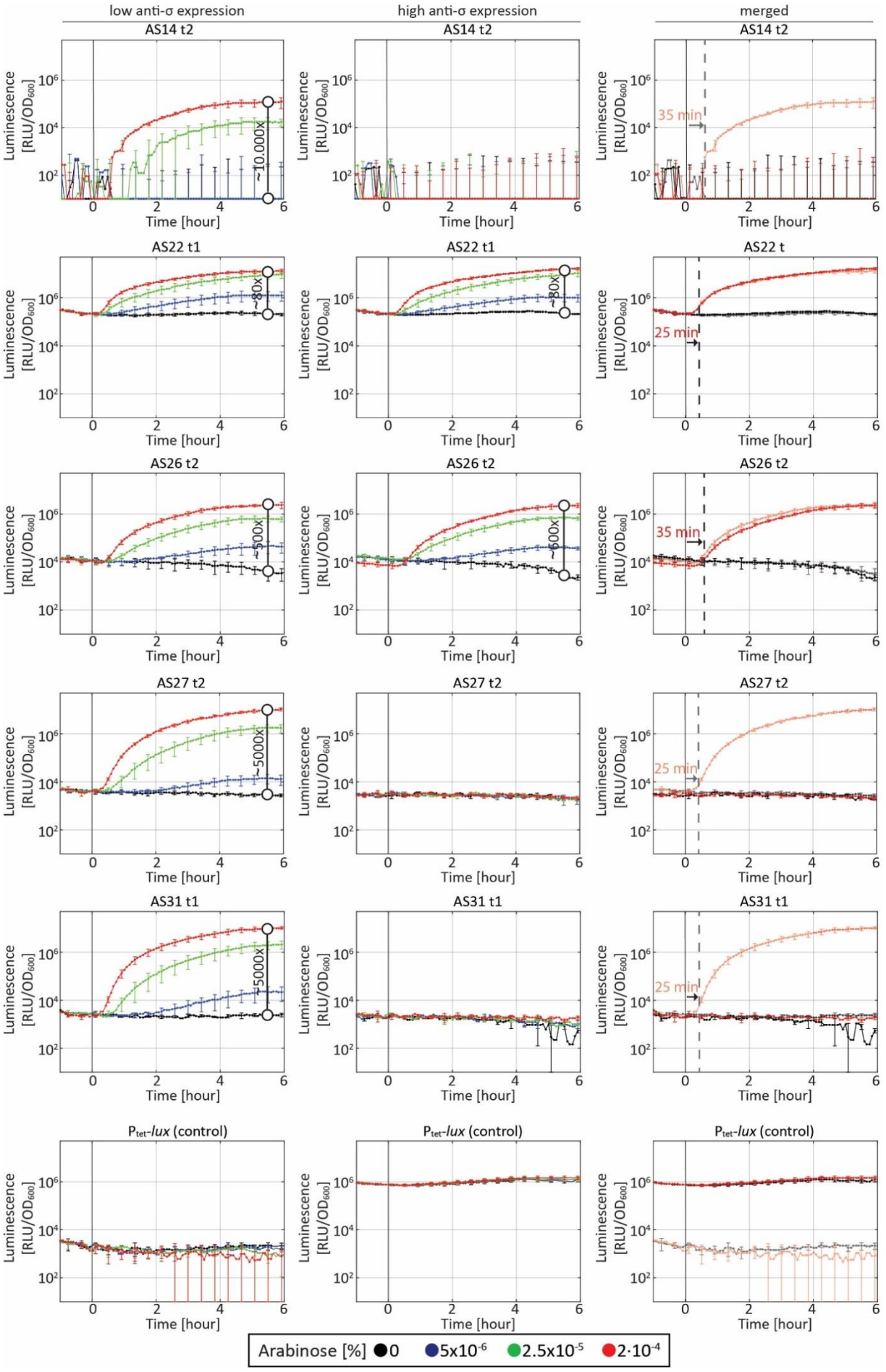
low anti-σ expression
high anti-σ expression
merged
AS14 t2
AS22 t1
AS22 t
AS26 t2
AS27 t2
AS31 t1
Ptet-lux (control)
Luminescence [RLU/OD600]
Time [hour]
~10.000x
~80x
~500x
~600x
~5000x
35 min
25 min
Arabinose [%] 0 5x10-6 2.5x10-5 2·10-4

Figure 5.8. Characterization of 5 threshold gate ECF/AS circuits (and positive control). Dynamic response of threshold gated ECF/AS circuits. All P_{BAD}-*ecf* and P_{tet}-*anti-σ* TUs were integrated into the chromosome of *E. coli* strain SV01 at the phage HK022 attachment site, using the pSV plasmid series (Table 9.5). Subsequently, the P_{ecf}-*lux* reporter system (encoded on pSVM-mc plasmids, Table 9.5) were introduced into the newly engineered strains, generating the GFC strains listed in Table 9.1. The positive control strain (GFC310; Table 9.1) possess a P_{tet}-*lux* construct integrated at the phage HK022 attachment site. The graphs show, for each circuit (named after the AS truncation variant), the dynamical response of luciferase activity (shown in relative luminescence units normalized by the optical density measured at 600 nm) after the addition of arabinose at the indicated concentrations at t=0 h (solid black lines), in presence of low (ATc 0 ng/mL) and high (ATc 2.5 ng/mL) AS threshold levels. The maximum fold induction is indicated. The merged panels show the signals obtained for low (faded curves) and high (solid curves) AS expression, in the uninduced (arabinose 0 %) and highly induced (arabinose $2x10^{-4}$%) strains. The time delay of *ecf* induction (dashed lines) is indicated for the highest arabinose concentration ($2x10^{-4}$%) and was defined as the time when luciferase activity first exceeded the pre-induction value by 2-fold. The experimental response dynamics were recorded during exponential growth, as described in Section 7.10. The results are averaged from at least two independent biological assays and error bars denote standard deviations.

The control strain (P_{tet}-*lux*) in Figure 5.8 shows the two levels of gene expression obtained from the chromosomally integrated P_{tet} promoter, using ATc at concentrations of 0 and 2.5 ng/mL. The basal signal (~10^3 RLU/OD_{600}) is consistent with the one registered previously (Figure 3.8D). Moreover, the induction with ATc at 2.5 ng/mL leads to a signal ~10^6 RLU/OD_{600} that is close to promoter saturation (cfr. Figure 3.8D). This confirms that using these levels of ATc inducer allows setting a low and a high expression level from the P_{tet} promoter, that in turn results in a low and high AS expression in our ECF/AS circuits.

In the low AS expression condition (Figure 5.7, Figure 5.8; left panels), we observed, overall, the ability of the different ECFs of activating the target promoters with different fold inductions (from ~14-fold in ECF/AS20 t2 to ~30000-fold ECF/AS28 t2). In the high AS expression condition (Figure 5.7 and Figure 5.8 middle panels) the results show that some circuits displayed a variance in the basal activity levels (circuits in Figure 5.7) and others were the baseline signal did not show significative differences (circuits Figure 5.8). In particular, in Figure 5.8, ECF/AS22 t1 and ECF/AS26 t2 circuits displayed almost identical basal activity in presence of low and high AS expression levels (~$2x10^5$ RLU/OD_{600} and ~$2x10^4$ RLU/OD_{600} respectively), suggesting a weak ECF/AS factor binding affinity. In contrast, even though ECF/AS14 t2, ECF/AS27 t2, and ECF/AS31 t1, showed identical baseline signal values for low and high AS induction, they were no more inducible, when growing the strain in the presence of a high AS expression level (Figure 5.8; AS14 t2, AS27 t2, AS31 t1 – left and middle panels). This suggests a strong AS factor binding affinity for the cognate ECFs that is then unable to activate the target promoter. In the case of ECF/AS14 t2 this can be confirmed by the fact that the baseline signal is below the detection limit of the plate reader (~$4x10^2$; Figure 5.8, not shown), thus, we cannot appreciate the baseline signal down-shift between low and high AS expression levels. In contrast, when looking at ECF27/AS27 t2 and ECF31/AS31 t1 we notice identical baseline signals for low and high AS expression levels (Figure 5.8; AS27 t2, AS31 t1, low AS expression and high AS expression panels ~3-$x10^3$ RLU/OD_{600}). This apparent lack of AS factor activity can be explained by looking at the promoter activity of these ECFs in the control experiment showed in Figure 4.4. Indeed, both P_{ecf27} and P_{ecf31} presented a baseline signal ~$3x10^3$ RLU/OD_{600} even in absence of the cognate ECF σ factor. This suggests that also in threshold gate experiment (Figure 5.8) AS27 t2 and AS31 t1 are highly

functional, binding the cognate ECFs in inactive complexes (also in case of high ECF expression levels) and that the baseline signal observed in the experiment is caused by cross-reaction between the *ecf* promoters and endogenous σ-factors.

All the other ECF/AS switches analyzed (Figure 5.7) showed, overall, lower baseline signal values and higher output dynamic ranges, when comparing low and high AS expression conditions (Figure 5.7 left and middle panels). In particular, setting a high AS expression level produced dynamic ranges of the circuits from ~150-fold-induction of ECF/AS38 t1 to ~1000000-fold-induction of ECF/AS20 t2 (Figure 5.7; middle panels). This suggests that the AS factors are sequestering the cognate ECFs, thus reducing the target promoter activity at low ECF levels. This, in some cases (e.g. ECF/AS20 t2 and ECF/AS37 t1), generates also a digital-like, sharper transition between the OFF and the ON state for increasing ECF levels (Figure 5.7; ECF/AS20 t2 and ECF/AS37 t1, middle panels).

In order to assay if AS factors are able to generate a threshold effect that delays the ECF σ target promoter activation, we merged the curves obtained for low and high AS expression, showing only the signals for uninduced and fully induced ECF expression (Figure 5.7 and Figure 5.8 merged panels). The result of the merged graph of Figure 5.7 and Figure 5.8 show, overall, similar time delays (measured as the time when luciferase activity first exceeded the pre-induction value by 2-fold, for maximum arabinose induction) among the different circuits (18-35 min) in the low AS expression condition (Figure 5.7 and Figure 5.8; faded curves). In contrast, the time delays of the circuits in the high AS condition showed more variability (from 20 to 85 minutes; Figure 5.7 and Figure 5.8; solid colored curves). Moreover, in the case of AS14 t2, AS27t2, and AS31 t1, we can only appreciate the time delays obtained in the low AS expression condition (Figure 5.8; faded curves). This is probably due to the fact that, in these switches, the induced ECFs did not exceed the threshold level set by a high AS expression level. In the other ECF/AS switches analyzed in Figure 5.8 (AS22, AS26) we obtained identical time delays, when comparing low and high AS expression conditions (Figure 5.8; faded curves, and solid colored curves, respectively). These results confirm the poor ability of these AS in binding the cognate ECFs. This was hypothesized previously by looking at the lack of baseline downshift (Figure 5.8) and it is further confirmed by the fact that setting a higher AS expression level did not lead to increased time delays in ECF σ target promoter activation (Figure 5.8; merged panels).

In contrast, comparing the time delays, set by the low and high AS expression levels, of the switches in Figure 5.7 (AS factors that are able to lower ECFs basal activity), we observed differences, in the time delays set by the low and high AS conditions, in 5 out of 6 ECF/AS circuits (Figure 5.7; merged panels). Indeed, with the exception of ECF/AS20, all the circuits presented increasing time delays, in ECF σ target promoter activation, for increasing expression levels of the AS. In particular, the longer time delays were obtained in ECF/AS28 t2 (35 and 60 min when comparing low and high AS levels) and ECF/AS34 t1 (25 and 85 min when comparing low and high AS levels). Interestingly, overall, the results show that the time delay does not scale with the efficiency of AS in lowering the baseline signal. For instance, upon high AS expression levels ECF/AS20 t2 (Figure 5.7; AS20 t2) showed the highest baseline down-shift (800-fold) but displayed the shortest time delay (~20 min). Moreover, despite the great baseline downshift, there is no difference in the time delay obtained for low and high AS expression. This suggests that together, the number of ECF and AS factors, the ECF promoter binding affinity and the AS factor binding affinity for the cognate ECF, all play a role in determining the circuit output dynamic and

time delay. To assay this hypothesis and further evaluate if the time delay can be tuned by using different levels of AS expression, we focused our analysis on a specific ECF/AS switch and encoded it in pSVM-mc medium copy plasmid.

We used ECF/AS14 t2 circuit, that in the previous configuration (were *ecf* and *anti-σ* factor genes were expressed in single copy and P_{ecf}-*lux* was encoded medium copy plasmid; Figure 5.8) did not show any fold change upon ECF expression, in presence of high AS induction. AS14 truncations previously appeared to be particularly active (Figure 5.3B and 5.5B). Moreover, by looking at the dose-response curves of the ECF14-switch circuits encoded in mixed configuration (Figure 4.6), we noticed that the switch has the smallest fold induction (~100-fold between the uninduced and full induction condition). Taken together, these results suggest that in the threshold gate experiment (Figure 5.8), the number of ECF14, produced by inducing the chromosomally integrated P_{BAD} promoter, was not enough to overcome the threshold level set by the AS factor, thus not allowing the activation of the target promoter. Therefore, by increasing the copy number of the circuit components we expect to increase the output signal. Finally, since AS14 t2 did not show high toxicity levels when expressed from medium copy plasmid, (displaying less than 50% reduction in 6h-OD_{600} when compared with the uninduced strain; Figure 5.3A) we hypothesized that this ECF/AS pair was an optimal candidate to perform the threshold gate experiment with the switch encoded medium copy plasmid.

To precisely characterize the dynamic behavior of all the components of the switch we followed the changes in both ECF and AS expression by using two different fluorescent proteins. Therefore, we assembled two distinct operons in which we placed a *gfp* a *mCherry* gene, present in our library, downstream the P_{BAD}-*ecf* and the P_{tet}-*anti-σ* constructs respectively. The circuit output was then evaluated by using the cognate P_{ecf} promoter fused with the luciferase reporter. In order to set different time delays among ECF expression and output signal production, we used different ATc concentrations (0, 1 and 2.5 ng/mL) that allowed different levels of AS expression. Finally, we followed the dynamic evolution of all the output signals, among different levels of ECF induction (Figure 5.9).

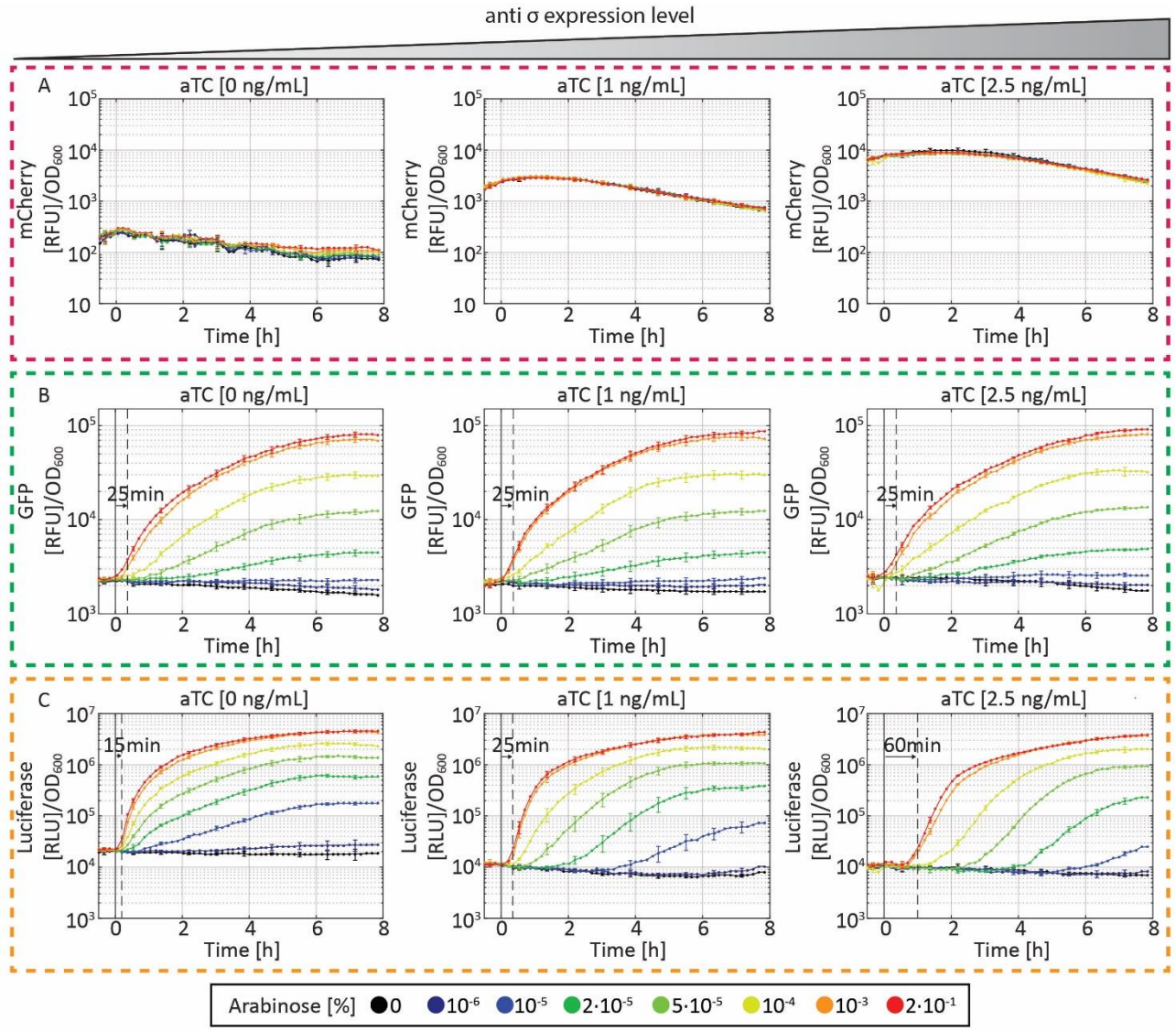

Figure 5.9. Dynamic response of plasmid-borne ECF14/AS14 t2 threshold gate circuit. The circuit was introduced in *E. coli* strain SV01 on medium copy plasmid pICH82094[26] (Table 9.6) generating the strain GFC0549 (Table 9.1). The graphs show the dynamical response of mCherry (A), GFP (B) and luciferase (C) activity (shown in relative fluorescence, or luminescence units normalized by the optical density measured at 600 nm) after the addition of various concentrations of arabinose at t=0 h in presence of low (ATc 0 ng/mL), medium (ATc 1 ng/mL) and high (ATc 2.5 ng/mL) AS expression levels. The mCherry (A) and GFP (B) signals monitor AS and ECF production respectively. The luciferase signal (C) indicates the *ecf* promoter activity. The time delay of gene induction (dashed lines) is indicated for the highest arabinose concentration (0.2%) and was defined as the time when GFP or luciferase activities first exceeded the pre-induction value by 2-fold. The experimental response dynamics were recorded during exponential growth, as described in Section 7.10. The results are averaged from at least two independent biological assays and error bars denote standard deviations.

Looking at the mCherry channel it is possible to appreciate the different levels of P_{tet} promoter activity that in turn set different thresholds of AS (Figure 5.9A). The *mCherry* signal (Figure 5.9A) shows some variation, even in absence of AS inducer, during the time course-experiment (a sharp increase ~2-fold, followed by a decrease ~3-fold). A change in P_{tet} promoter activation was also observed previously, as discussed in Section 3.3.1. However, in case of the results of the experiment

in Figure 5.9A, the deactivation of the ATc due to light production could only explain the results obtained for the signals where the P_{tet} promoter was induced (Figure 5.9A; ATc 1 ng/mL and ATc 2.5 ng/mL). Thus the exact reasons behind the changes in the activation dynamics of the P_{tet} promoter, during the experimental procedure, remain elusive. Following the dynamic changes in the GFP channel (Figure 5.9B), it is possible to notice that the ECF expression appear to be robust upon different inducer levels, being almost identical among the different levels of AS expression. Moreover, we calculated identical time delays (25 min) among the maximum induction of the P_{BAD} promoter and ECF/GFP production in all three AS condition (Figure 5.9B). Thus, the ECF gene expression from the P_{BAD} promoter is consistent in all the assayed conditions. The results obtained in the luciferase channel (Figure 5.9C) show that ECF/AS14 t2 circuit, encoded on medium copy plasmid, is able to produce a detectable luciferase signal among all level of ECF induction, confirming that increasing the copy number of the circuit allowed the recovery of the output signal. Moreover, by increasing the level of AS expression we were, overall, able to lower the baseline signal (Figure 5.9; 2-fold luciferase baseline reduction comparing ATc 0ng/mL and ATc 2.5ng/mL). This confirms our previous hypothesis on the baseline downshift being masked by the low detection limit, in the ECF/AS14 t2 circuit tested in mixed configuration (Figure 5.8; low and high AS expression). Finally, despite the small changes observed in the basal luciferase signal down-shift, the three AS levels lead to distinct time delays between the ECF induction and target promoter activation. In particular, we calculated, for the highest ECF expression level, ~15min, ~25min, and ~60min for low, medium and high AS thresholds respectively (measured as the time when luciferase activity, induced with 0.2% arabinose, first exceeded the pre-induction value by 2-fold). Moreover, since for a given induction of the P_{BAD} promoter, the time delay for ECF production remains constant (Figure 5.9B; 25 min), while the delay for P_{ecf} activation scales with the threshold set by AS, we can ultimately confirm that the observed time delay is caused by the formation of ECF/AS complexes.

Summarizing, the results confirmed that is possible to use an AS factor to set different threshold levels that will, in turn, delay the time between *ecf* induction and target promoter activation. For fixed *ecf* expression levels, the delay can be set varying the inducer concentrations of the AS factor. However, since the inducible P_{tet} promoter showed some variance even in the absence of inducer, we further tested the circuit, using two different constitutive promoters to drive the expression of the AS factors. We used a weak (P_{J23117}) and strong (P_{J23108}) *E. coli* constitutive promoters (present in our library; Table 9.3) to drive the expression of the AS factor, thus establishing two fixed AS threshold levels (Figure 5.10).

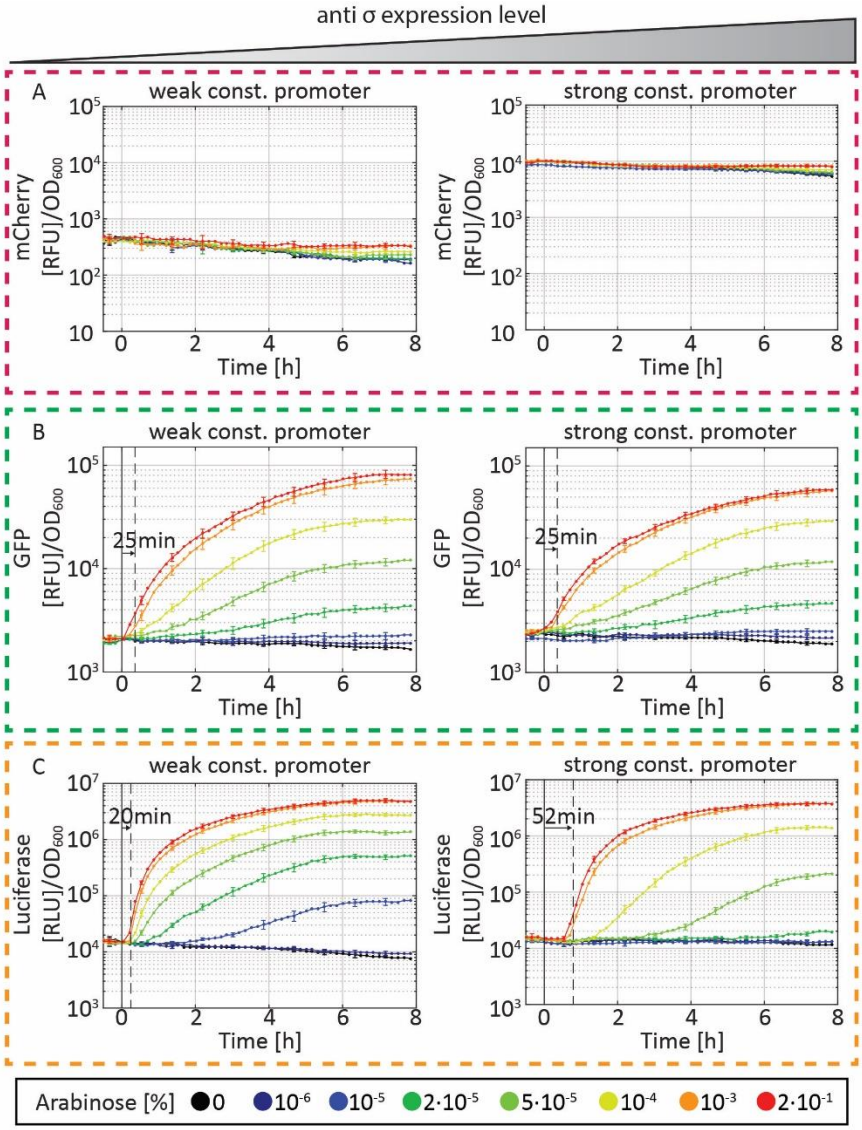

Figure 5.10. Dynamic response of plasmid-borne ECF14/AS14 t2 threshold gate circuit with AS factor expression controlled by constitutive promoters. The circuit was introduced in *E. coli* strain SV01 on medium copy plasmid pICH82094[26] (Table 9.6) generating the strains GFC0550, GFC551 (Table 9.1). The graphs show the dynamical response of mCherry (A), GFP (B) and luciferase (C) activity (shown in relative fluorescence, or luminescence units normalized by the optical density measured at 600 nm) after the addition of various concentrations of arabinose at t=0 h in presence of low (weak constitutive promoter, P_{J23117}), and high (strong constitutive promoter, P_{J23108}) AS expression levels. The mCherry (A) and GFP (B) signals monitor AS and ECF production respectively. The luciferase signal (C) indicates the *ecf* promoter activity. The time delay of gene induction (dashed lines) is indicated for the highest arabinose concentration (0.2%) and was defined as the time when GFP or luciferase activities first exceeded the pre-induction value by 2-fold. The experimental response dynamics were recorded during exponential growth, as described in Section 7.10. The results are averaged from at least two independent biological assays and error bars denote standard deviations.

Interestingly the results show more stable expression of the AS operon when it is fused with the weak and the strong constitutive promoters (Figure 5.10A; ~$2x10^3$ RLU/OD_{600} and ~10^4 RLU/OD_{600} respectively). This suggests that the changes observed previously in the P_{tet} promoter activation (Figure 5.9A) were related to changes in the regulation of the promoter activity.

Comparing the mCherry signals obtained with the inducible and constitutive promoters we observe that the signal relative to the weak constitutive promoter (~$2x10^2$ RLU/OD_{600}) is ~1.5x higher than the one obtained previously, using ATc at 0 ng/mL (Figure 5.10A and Figure 5.9A). Moreover, the mCherry signal relative to the strong constitutive promoter (~10^4 RLU/OD_{600}) is close to the one obtained in the strain induced with 2.5 ng/mL ATc (Figure 5.8A; ~10^4 RLU/OD_{600} before signal decay). When comparing the time delays observed in the GFP channel (Figure 5.10B; 25 min) we observe perfect agreement with the results obtained previously (Figure 5.9B; 25 min) confirming that different levels of AS expression do not influence the expression of the ECFs from the P_{BAD} promoter. Finally also in the experiment in Figure 5.10 we were able to set distinct time delays between ECF production and downstream promoter activation (Figure 5.10C). Indeed for maximum ECF induction, we calculated time delays of 20 and 45 min in low and high AS expression conditions. Moreover, by comparing the two experiments in Figure 5.9 and Figure 5.10 we can qualitatively correlate the time delays necessary for the activation of the *ecf* promoter with the mCherry signals and thus with the AS expression level. Indeed, the time delay generated by AS expression from the weak constitutive promoter in Figure 5.10C (20 min) is higher to the one generated by AS expression using ATc at 0 ng/mL (15 min), like in the case of the mCherry signals of the two constructs (Figure 5.9A and Figure 5.10A). The same applies, to the time delay generated by AS expression from the strong constitutive promoter (Figure 5.9C; 55 min) that is close and the one obtained using ATc at 2.5 ng/mL (Figure 5.9C; 60 min). Indeed we obtained, for these constructs, also similar mCherry signals, as discussed above (Figure 5.9A and Figure 5.10A).

Summarizing, the results presented in this section confirmed the hypothesis that using AS factors can effectively reduce the ECF target promoter activity, generating a non-linear dose-response behavior for increasing ECF levels. Using threshold gate circuits, we were able to further characterize the differences in the interaction dynamic between the selected ECFs and their cognate AS factors (Figure 5.7 and Figure 5.8). Overall, we found AS factors (e.g. AS22 t1 and 26 t2) that did not generate a reduction in the basal promoter activity (Figure 5.8), and AS factors (AS20 t1 and AS34 t1) that showed a high impact on the basal promoter activity (Figure 5.7; 800-fold and 100-fold reduction respectively). In our experimental conditions, we were also able to generate a sharp transition between the OFF and the ON state of the switches in the presence of high AS expression levels (Figure 5.7; AS20 t2, AS37 t1). Moreover, the results presented in the merged panels in Figure 5.7 suggest that, in most cases, setting different AS expression levels allows for the establishment of distinct time delays between ECF production and downstream promoter activation. However, the time delay does not seem to depend only by the ability of the AS factors in lowering the signal produced by the basal activity of the ECFs, but also by the binding proprieties of the ECFs for the target promoters and by the amount of ECFs and AS factors produced.

Finally, the results of the experiments illustrated in Figure 5.9 and Figure 5.10 confirms that the time delays observed in the ECF/AS switches are due to the time required for the production and maturation of ECF σ factors, that have to accumulate and overcome the threshold level set by the AS factors, in order to activate their target promoters. Moreover, our experiments demonstrate that is possible to tune the time delay by variating the level of ECF and AS expression. This can be achieved, for instance, using different inducer concentrations for both ECF and AS factor or varying the copy number of the genes. Moreover, we also demonstrated that is possible to simplify the experimental procedure by setting different AS expression levels using constitutive promoters with different transcriptional strengths.

5.5 ECF/anti-σ factor suicide circuits

After evaluating the toxicity of AS factors and characterizing their dynamics in binding the cognate ECF σ factors in our experimental conditions, we used them to generate novel time tunable ECF/AS factors circuits. We aimed to generate a prototype of a self-destruction circuit in *E. coli.* Synthetic circuits that allow the programmed lysis of the bacterial cells represent a valuable tool in synthetic biology. Indeed, such circuits would allow for the recovery of intracellularly expressed proteins avoiding using mechanical and chemical cell disruption techniques that can cause protein denaturation and require the purchase of expensive reagents, respectively[132]. Moreover, such circuits would allow for the production and the release of recombinant proteins which secretion is difficult to achieve[133].

In the previous section, we demonstrated that is possible to establish a tunable time delay between ECF expression and target promoter activation. Therefore, we reasoned that using the previously generated ECF/AS switches and fusing the *ecf* promoter with a bacterial toxin, it is possible, in principle, to generate circuits that kill the cells with a tunable time delay. Such suicide circuits will serve as proof of concept for a future design of a time tunable self-destruction circuit in *E. coli* using ECF and AS factors. In order to generate a suicide circuit, we decided to use the CcdB toxin that poisons the gyrase-DNA complex, blocking the passage of polymerases, leading to double-strand breakage of the DNA and death of the bacterial cells[134]. In order to clone the *ccdB* gene in our library, we used the *E. coli* strain DB3.1 that has a mutation in the DNA gyrase that does not allow the interaction with CcdB, therefore abolishing its toxic effects[135]. The strategy we choose was to use the CcdB-resistant strain DB3.1 to assemble plasmid-borne P_{ecf}-*ccdB* constructs (Table 9.5). We then transformed these plasmids into previously generated bacterial strain possessing P_{BAD}-*ecf* and the P_{tet}-*anti-σ* constructs integrated into the genome, generating the GFC strains in Table 9.1. To avoid basal *ccdB* expression that would lead to premature cell death, or adaptive mutations, we choose the ECF/AS pairs that in the previous experiments did not showed basal activity in the low AS expression condition (Figure 5.7, Figure 5.8), i.e. ECF/AS14 t2, ECF/AS 28t2, ECF/AS34 t1, ECF/AS37 t2. By further expressing the AS factors in these strains, when they were carrying the P_{ecf}-*ccdB* plasmids, we then ensured virtually zero basal activity from the *ecf* promoters, preserving the cellular viability. We assayed the strains in plate reader experiments, monitoring the optical density at 600 nm, among different ECF induction levels (Figure 5.11). By pre-culturing the strains in the presence of two different ATc concentrations, we introduced two different AS threshold levels that the ECFs have to overcome before they can activate their target promoter expressing the toxin. Moreover, for each strain, we washed the cells with inducer-free media, prior to starting the measurement (Section 7.10). In this way, the AS factors produced overnight dilutes during the plate reader experiment, due to cell replication, generating a third, lower AS threshold level (Figure 5.11).

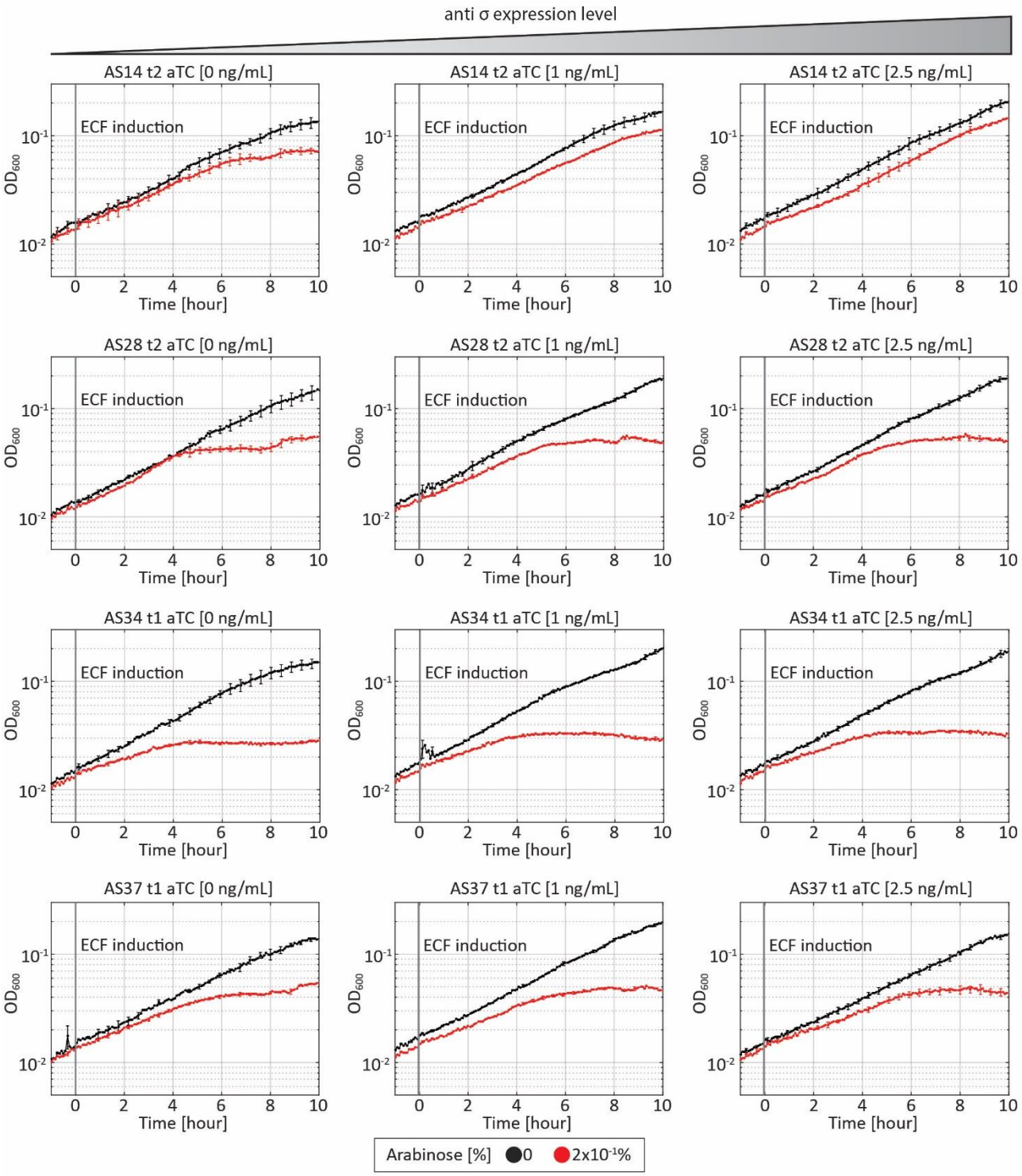

Figure 5.11. Characterization of ECF/AS suicide circuits in *E. coli* (bacterial density). Time evolution of bacterial density (indicated as the optical density measured at 600 nm) of 4 suicide circuits, for no- (0%, black lines) and full (0.2%, red lines) arabinose induction, in presence of low (ATc=0 ng/mL), medium (ATc=1 ng/mL) and high (ATc=2.5 ng/mL) AS threshold levels. In all circuits (named after the AS factor truncation) the P_{BAD}-*ecf* and P_{tet}-*anti-σ* modules were integrated into the chromosome of *E. coli* strain SV01 at the phage HK022 attachment site, using the pSV plasmid series (Table 9.5). Subsequently, the gene encoding toxin *ccdB*, fused with one of the different *ecf* promoters (encoded on pSVM-mc plasmids, Table 9.5) was introduced into the newly engineered strains, generating the GFC strains listed in Table 9.1. The results are averaged from at least two independent biological assays and error bars denote standard deviations.

Overall, the results show a severe change in the OD_{600} values (Figure 5.11, red curves) ~4 h after ECF σ factor induction (t=0), while the uninduced strains grow exponentially with the typical doubling time in our experimental setup ~175 min (Figure 5.11, black curves). The toxic effect is more evident for the lowest AS threshold level (Figure 5.11; aTC 0 ng/mL panels) and it seems to reduce for increasing AS expression levels (Figure 5.11; aTC 1 ng/mL and aTC 2.5 ng/mL panels). To better estimate the effect of ECF, and thus of *ccdB*, expression, on cellular growth among different AS levels and to compare the time required to generate the growth defects in the different conditions, we plotted the results shown in Figure 5.11 as growth rates of the bacterial strains in the function of time (Figure 5.12)

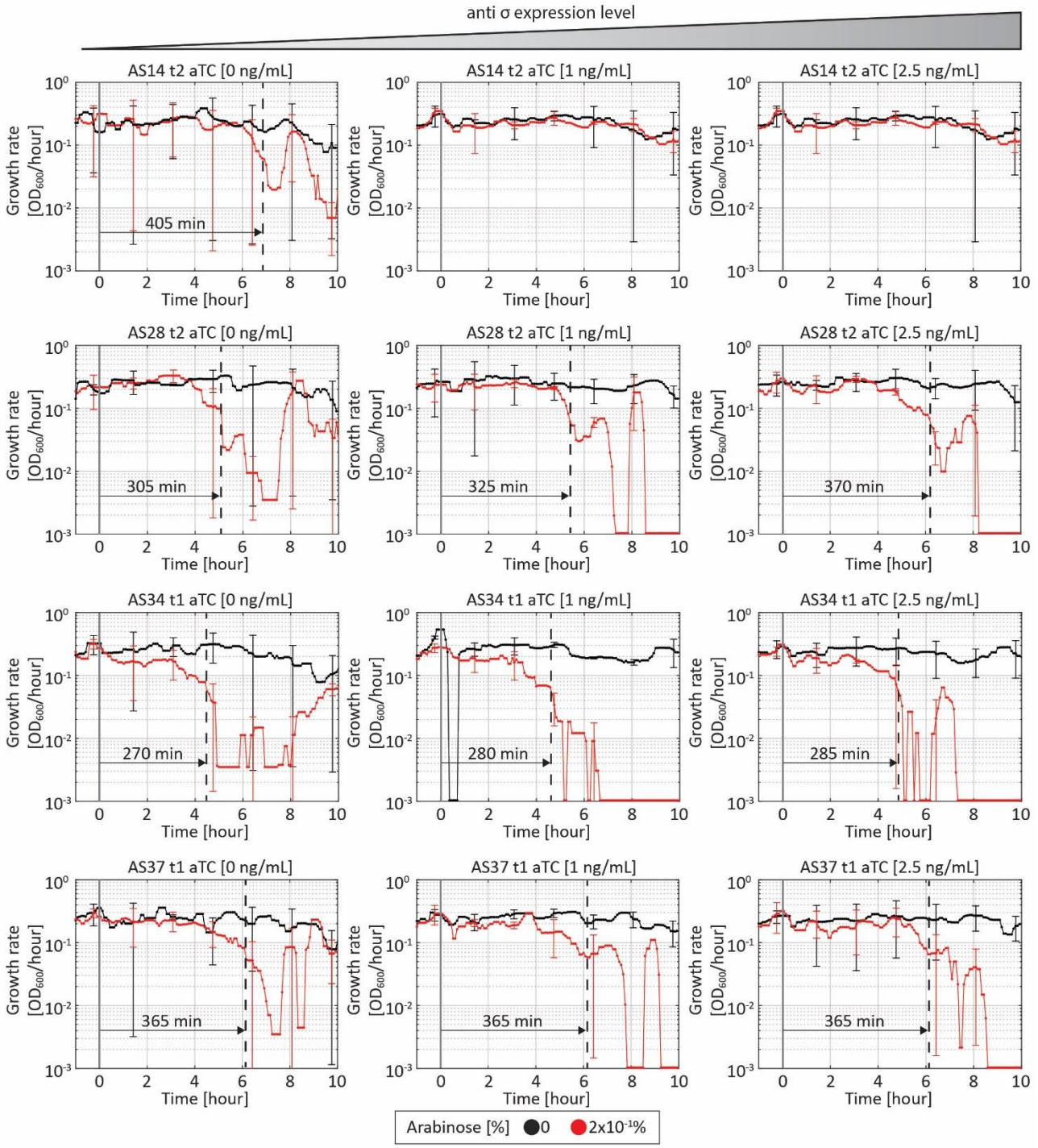

Figure 5.12. Characterization of ECF/AS suicide circuits in *E. coli* (growth rates). Time evolution of growth rate (indicated as the optical density measured at 600 nm in the function of time expressed in hour) of 4 suicide circuits illustrated in Figure 5.11. The time delay of *ccdB* expression is indicated for the highest arabinose concentration (0.2%) and was defined as the time were Growth rate (OD_{600}/h), first show a 70% reduction of the pre-induction value (dashed lines). The results are averaged from at least two independent biological assays and error bars denote standard deviations.

The results confirm that the induction of the ECF, in all strain, leads to growth defects (defined as a 70% reduction of the growth rate of the uninduced strain), especially in case of a low AS expression level. Analyzing the time delay of the circuits (defined as the time where the growth rate (OD_{600}/h), first show a 70% reduction of the pre-induction value; black dashed lines) in the washed

strains (Figure 5.12; left panels) we observed that AS14 t2 was able to generate the longest delay (405 min) between ECF expression and growth rate reduction. Moreover, in the same strain, increasing level of AS expression lead to zero growth defects (Figure 5.12; middle and right panels). This is a further confirmation of the results obtained previously (Figure 5.3B, Figure 5.6B, Figure 5.8) that showed how the proprieties of this ECF and relative AS truncation allow for a strong reduction of ECF activity. The results in Figure 5.12 also show that in three circuits, increasing concentrations of AS generate increasing time delays, between ECF expression and 70%-growth rate reduction.

In order to ensure that the growth defect we observed were due to the CcdB toxin and not due to ECF toxicity, we also analyzed the OD_{600} values of the corresponding ECF-switches (not harboring the *ccdB* gene) expressed in single copy (Figure 5.13).

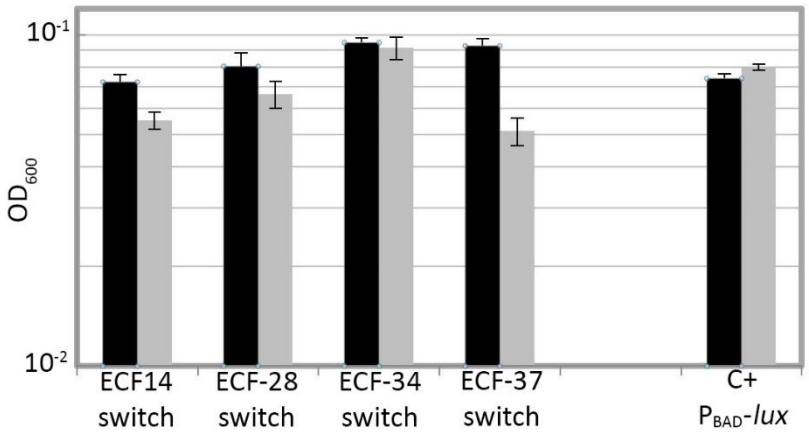

Figure 5.13. Effects on the bacterial density of ECF expression from chromosomally integrated ECF-switches. Bacterial density (indicated as the optical density measured at 600 nm) achieved by 4 previously characterized (Figure 4.5) *E. coli* strains carrying the indicated ECF-switches circuits and a positive control (C+), 6 hours after the induction with 0 (black bars) and 0.2% (grey bars) of arabinose. The positive control (C+) represents *E. coli* strains carrying a plasmid-borne P_{BAD}-*lux* construct. The results are averaged from at least two independent biological assays and error bars denote standard deviations.

The result shows how the expression of ECF14, ECF28, and ECF34 do not result in a toxic phenotype (6h-OD_{600} fold reduction <20% of the uninduced strain). In contrast, we noticed that the expression of ECF37 caused a 44% fold-reduction in the 6h-OD_{600} of the uninduced strain. This result is coherent with the high toxic effect displayed by ECF37 when encoded on medium copy plasmid (Figure 4.2). Since ECF/AS37 t1 suicide circuit did not display increasing time delays in the generation of the growth defects, among different AS expression levels, we wanted to further assay if in this circuit the growth defects are due to the *ccdB* expression. Thus we repeated the experiment by using an ECF/AS37 t1 control strain, were the P_{ecf} promoter drives the expression of the luciferase reporter. The results, in Figure 5.14, shows that even if there are some growth defects in the induced strains, especially in the washed condition (4% growth rate reduction of the pre-induction value, Figure 5.14 left panels), the toxic effects are lighter than the one observed in the strain carrying the CcdB toxin (70% growth rate reduction of the pre-induction value, Figure 5.12 left panel). We then conclude that the growth defects of the strain carrying the ECF/AS37 t1 suicide circuit, observed in Figure 5.12 are caused by ECF driven *ccdB* expression, even though it was not possible to generate a time delay by increasing the level of AS factor.

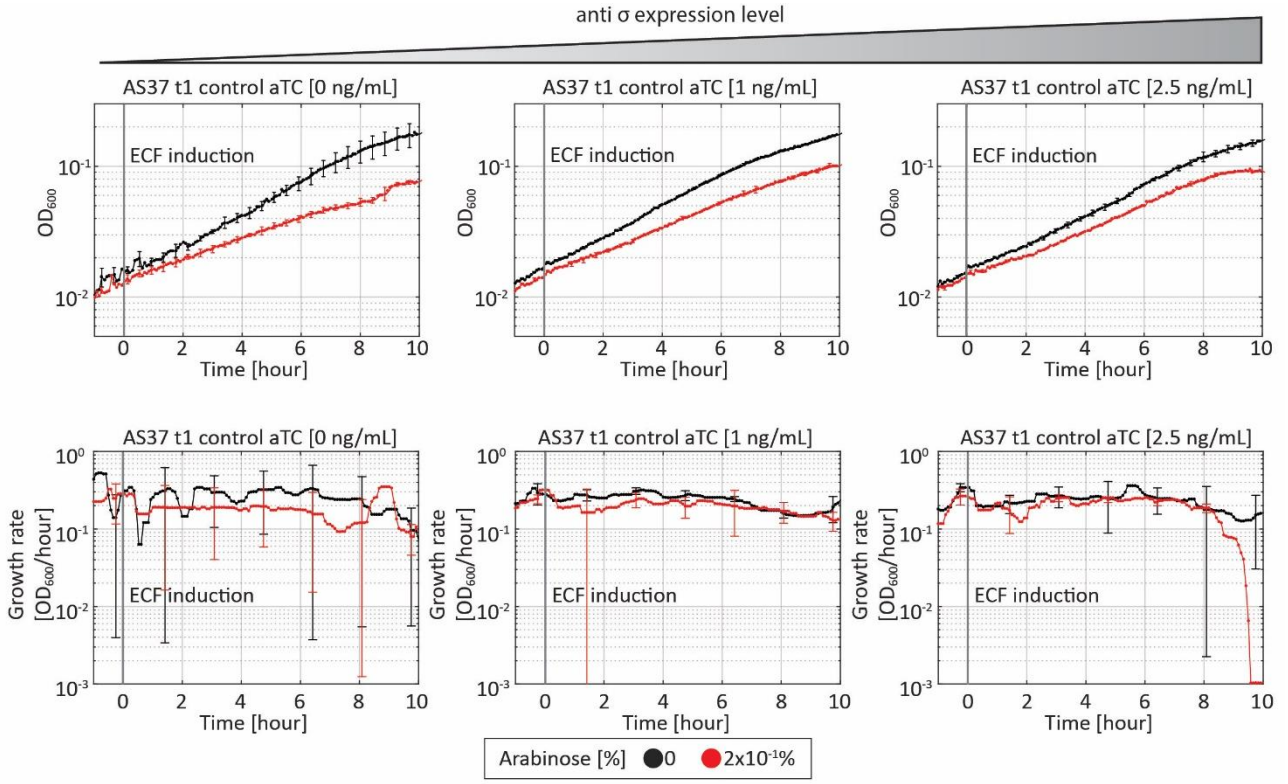

Figure 5.14. Time evolution of bacterial density and growth rate of ECF/AS37 control circuit. The ECF/AS37 t1 control circuit, do not encode for the CcdB toxin. The bacterial density is indicated as the optical density measured at 600 nm. The growth rate is indicated as the optical density measured at 600 nm in the function of time (h). The results are averaged from at least two independent biological assays and error bars denote standard deviations.

Summarizing, the experiments presented in this section demonstrated that AS factors can lower the ECF activity also in suicide circuits, allowing the establishment of a time delay between gene expression and cellular death. However, comparing the result obtained in Figure 5.12 and Figure 5.7 we observed qualitative agreements and discrepancies. For instance, in Figure 5.7 ECF/AS28 t2 shows, for low AS expression, a longer time delay when compared with ECF/AS34 t2 (35 min and 25 min respectively; Figure 5.7, faded curves). This is in agreement with the result obtained for the corresponding suicide circuits in Figure 5.12 (AS28 t2 time delay=305 min, AS34 t1 time delay=270 min). However, when looking at the time delays of the two strains in presence of a high AS expression level in the threshold experiment (Figure 5.7; merged panels, solid curves) we observed a smaller time delay in ECF/AS28 t2 circuit (60 min), than the one obtained for ECF/AS34 t2 circuit (85 min). This contrasts with the result obtained in the corresponding suicide circuits (Figure 5.12; right panels), where these switches showed the opposite behavior (AS28 t2 time delay=370 min, AS34 t1 time delay=285 min). The discrepancies can be explained by the fact that in the suicide circuit experiments (Figure 5.12) we used a higher maximal arabinose concentration than the one used in the threshold gate experiment in Figure 5.7 (0.2% and $2x10^{-4}$% respectively). This is due to the fact that we did not observe significative growth defects, by inducing the suicide circuits with $2x10^{-4}$% arabinose (data not shown). However, these discrepancies in the results confirm that the differences in the dynamical reduction of ECF activity, obtained in the threshold gate experiments (Figure 5.7, Figure 5.8) cannot be completely explained simply by the affinity between a given AS truncation and cognate ECF σ factor. However, our

threshold gate experiments (Figure 5.7, Figure 5.8), still serve as a good qualitative indicator for the discrimination of the ECF/AS factor pairs that show interesting characteristics, such as time-delayed activation or digital-like activation of the *ecf* promoter.

5.6 Summary

The experiments presented in this chapter, prove that it is possible to successfully implement AS factors into ECF-switches, in order to reduce ECF basal activity and set time tunable delays for *ecf* promoter activation. The analysis presented in Sections 5.1-5.3 gives a general overview of the toxicity and activity of the AS factors that we chose to design synthetic circuits. Overall, the results of the analysis on AS toxicity confirmed that most of AS factors we chose can cause severe growth defects upon their overexpression (Figure 5.2A). In order to solve this issue, we generated soluble, truncated AS factors. Using the truncated version of AS factors we partially alleviated the toxicity (Figure 5.3A), generating soluble AS variants that are equally or less toxic than wild type AS factors, when encoded on medium copy plasmids. Thus, our results confirm that the toxic effect can partially arise from the overexpression of transmembrane proteins. However, only expressing AS truncations from chromosomally integrated circuits, we were able to fully recover cell viability in all strains (Figure 5.5). Using different experimental approaches we also showed that both wild type and truncated AS are able to bind cognate σ factors (Figure 5.2-5.6). The effects of AS factors expression generate different levels of output signal reduction. This can be due to different binding affinities of the AS factors for the cognate ECFs, combined with the different binding affinities of the ECFs for the target promoters. Finally, even though we did not perform any experiment to validate this hypothesis, the AS truncations could allow a more robust ECF-binding that is not influenced by external stimuli, since these AS factors do not possess any transmembrane domain.

After showing the different degree of AS toxicity and activity, we evaluated if AS factors can be used to introduce a non-linear dynamic response and a tunable time delay in our synthetic circuits. Thus, we selected, for each AS truncation, the best performing variant (i.e. less toxic and more active) and further characterized the dynamic of interaction between ECF σ and AS factors, by tuning their expression levels. We proved the hypothesis that using AS factors allow to decrease the baseline expression in ECF-switches, thus implementing a digital-like OFF/ON switching behavior and ultimately increasing the output dynamic range (Figure 5.7-5.8). Moreover, we were also able to generate 8 functional ECF/AS threshold gate circuits, where increasing AS expression levels generate increasing time delays among ECF expression and target promoter activation (Figure 5.7, Figure 5.8). However, we also observed that the effects of AS expression on the dynamic of ECF σ activity is susceptible to changes that depend on the affinity of the AS for the cognate ECF, the promoter binding affinity of the ECF and from the number of ECF and AS produced. This must be taken into account in the design of ECF/AS based synthetic circuits, and indicates that a broader characterization of the ECF/AS circuits that infers a higher number of possible conditions is needed, in order to rational design ECF/AS based circuits. Nonetheless, simply by utilizing the qualitative results of our experiments (Figure 5.7-5.8), we were able to select 4 AS factors truncations to successfully implement 4 prototype ECF/AS self-destruction circuits. Even though the behaviour of our suicide circuits can be largely improved, we proved that the dynamic interaction between ECF and AS factor can be used to generate different type of circuits featuring a time-tunable delay.

6. Discussion and conclusions

The synthetic biology field aims to use a forward-engineering approach, to modify existing biological systems and create new biological parts or networks[1]. Within this approach, the creation of synthetic circuits follows a bottom-up strategy, in which each DNA-encoded component is considered as an isolated part and their combination allows for the generation of higher order circuits that feature increasing complexity[9]. Hence, in the rational design of synthetic circuits, a robust characterization of the individual parts is fundamental to reveal their features and limitations and better understand how to interconnect them in increasingly complex circuits.

As introduced in Chapter 1, a robust characterization of the genetic parts under certain conditions is only one of the challenges in synthetic biology. Indeed, the performance of the synthetic circuits, embedded in living organisms, are often affected by the interconnection of all the compounds within the cell that generate context-dependence. Thus, another challenge in the synthetic biology field is the development of strategies that minimize the context-dependence and increase the orthogonality of the synthetic circuits.

In this chapter will first discuss our effort to establish a high throughput experimental setup that allows for a precise quantitative characterization of the genetic circuits. Next, we will examine the ECF toolbox, our optimized framework for the generation of different genetic parts and synthetic circuits, analyzing the results of our characterization of the genetic building blocks. Finally, we will discuss our findings on the possibility of implementing ECF σ factors as orthogonal regulators in novel synthetic circuits.

6.1 A robust experimental setup for synthetic circuit evaluation

In this study, we aim to establish ECF σ factors as transcriptional regulators for novel synthetic circuits, thus we first had to characterize them thoroughly in the context of synthetic circuit design. This required the establishment of a robust experimental setup that allows for a precise quantitative characterization of the genetic circuits that we generate and for a comparison of their features. To this end, we developed the experimental setup described in Chapter 2. We first selected an *E. coli* strain the allows for the utilization of the commonly used transcriptional regulators (TetR[50], LacI[48] and AraC[49]). This was necessary since ECF σ factor regulation, in nature, occurs mainly through anti-σ factors that respond to a broad range of stimuli that in most cases are unknown, or difficult to reproduce experimentally (Section 1.5). Thus, in order to create ECF transcriptional circuits, we have to use an inducible promoter to initiate ECF expression. To this end, we selected the *E. coli* strain MK01 that like the majority of *E. coli* strains is suitable for utilizing genetic constructs regulated by the TetR, due to the exogenous nature this regulator. Additionally, MK01 is not able to metabolize the arabinose and abolished the all or none response of *E. coli* to this inducer, allowing for networks embedding the AraC regulator. Finally, the strain has the endogenous *lacI* copy knocked out, thus increasing the context independency of networks featuring this regulator[80]. With simple recombination using the Cre-Lox system (Section 2.1 and Section 7.3), we removed the chloramphenicol cassette present in MK01, generating the *E. coli* strain SV01 that maintains all the above-mentioned features and allows for the utilization of the chloramphenicol selection marker (Table 2.1). This allowed, for instance, to assay the quadruple integration using CRIMoClo plasmids (Section 3.2.3). Moreover, the strain resulted to be suitable for reliable induction using different inducers simultaneously (see Chapter 5) and a valuable choice, especially for AraC regulated networks. Indeed, we obtained a highly reproducible response to the induction using

different arabinose concentrations, when comparing the different experiments in this study. Moreover, the bacterial population showed a homogeneous response to the inducer, as showed in the ECF-cascade experiment (Figure 4.7). For these reasons, SV01 represents an optimal *E. coli* strain for the development of complex circuits, embedding multiple classical transcriptional regulators, as well as ECF and anti-σ factors.

The quantitative characterization of synthetic circuits benefits from methodologies that allow for the simultaneous high throughput analysis of different genetic constructs with a high resolution. To this end, in Section 2.2 we introduced our standard experimental setup. This consists of the usage of plate reader experiments together with a highly sensitive reporter. We showed that the luciferase cassette from *Photorhabdus luminescens*[97] allows the increase of resolution, dynamic range, and temporal response, of the circuit output signal when compared with the commonly used GFP fluorescent reporter. This confirms that luciferase reporters represent a valid system to measure gene expression dynamics in *E. coli*[92,94]. To date, the characterization of the basic genetic parts such as promoters and terminators is often performed using fluorophores[27,28,64,112,136], while we encourage the use of luminescent reporters, with their exquisite signal-to-background ratio. To this end, we developed an algorithm that fixes one of the major limitations in using luciferase reporters in high throughput analysis, such as plate reader experiments. This limitation arises from the constant emission of light from the luminescent reporters that can generate bleed-through (i.e. light-scattering) in neighboring wells of the microplate. Indeed, a light emitting strain placed in a single well can illuminate more than 50% the other empty wells (Figure 2.2A), biasing the measurement of luminescent signals. In Section 2.3 we extensively demonstrated how our bleed-through correcting algorithm can reveal the "true" luminescence intensities in all wells of a fully filled microplate (black and transparent). Moreover, in *Paper I* (Mauri *et al.*, 2019) we show that the method can be also applied to a different plate reader. Thus, the robustness of the results we presented suggests that the approach could also be applicable to other experimental setups (e.g. cell-free expression experiments measured in 384-well or 1536-well format), ultimately encouraging the usage of luminescent reporters in high throughput analysis.

6.2 ECF toolbox: MoClo expansion

The general idea within the circuit design in the synthetic biology field is to treat the basic biological components of the synthetic circuits (such as promoters, ribosome binding sequences, coding sequences, and terminators) like building blocks, that can be assembled in different combinations, generating genetic circuits with increasing order of complexity. To this end, the Synbio field benefits from every methodology that allows for hierarchical combinatorial assembly, sharing of the parts, and generation of standardized part libraries.

In Section 1.2 we illustrated the different available methodologies for the manipulation of the DNA and the design of genetic constructs highlighting how the MoClo represents, to date, one of the best frameworks for the generation of the synthetic circuit from reusable parts. Indeed, the presence of small (4bp) scars in between the assembled parts and the necessity of curing the DNA sequences for two Type IIs restriction sites is a small price to pay, in order to use a framework that allows for the generation of libraries of parts and their combinatorial assembly in circuits with increasing levels of complexity. For these reasons, we decided to adopt extensively the MoClo system as a base for the generation of the ECF toolbox, presented in this study.

Chapter 3 introduces our expansions to the MoClo system that are part of the ECF toolbox. These include the new expression vector pSVM-mc that allows for a faster assembly of reporter constructs from MoClo level 1 parts (Section 3.1), together with 32 CRIMoClo vectors that can be used for the generation and the chromosomal integration of the genetic circuits from MoClo compatible parts (Section 3.2). The latter are particularly interesting because even though the expression of plasmid-encoded circuits present certain advantages (e.g. higher protein expression yield and higher signal output over single copy constructs), lowering the copy number of a construct allows to solve problems such as cellular metabolic burden that can arise from the expression of plasmid-borne genetic constructs[32,33,36]. Thus, in Section 3.2 we presented our efforts in fusing the MoClo features with the ones of the CRIM plasmids that allow for chromosomal integration by site-specific recombination[39]. In particular, we showed how our system allows for the generation of genetic circuits from reusable, MoClo-compatible parts and their easy integration into four *att* sites into the genome of *E. coli*. Moreover, we achieved another fundamental goal for the expression of synthetic circuits, i.e. the context-independence of the integration *loci*. The results presented in Figure 3.4-3.6 demonstrate how the utilization of CRIMoClo plasmids allow for easy sequential multiple integrations, of the genetic constructs, in four *E. coli* phage attachment sites. Strikingly our results show that the gene expression from the four *loci* is robust and well isolated from the genetic context. This represents a major innovation since, to date, there is a lack of orthogonal and well-characterized *loci* for the chromosomal integration in *E. coli*[137]. Finally, as further improvement, the CRIMoClo vectors could be modified by adding the gene encoding for the integrase protein, following the strategy presented by St-Pierre and collaborators[40]. This would avoid the necessity of co-transforming the host with the helper plasmid (that carries the integrase gene) and will open the possibility of performing a simultaneous integration of different constructs in different loci.

Concluding, the CRIMoClo framework allows for filling the gap between easy circuit generation and chromosomal integration, facilitating the assay of the constructs in different genetic configurations. Indeed, it was recently demonstrated that the copy number of a circuit can also affect the behavior and the performances of a synthetic circuit[138]. Thus, CRIMoClo and similar systems[30], represents a fundamental innovation in the synthetic biology field, since they allow for a flawless transition between plasmid-encoded and chromosomally integrated genetic circuits, adding another degree of freedom to the possible configurations of a given synthetic circuit.

6.3 ECF toolbox: part library

Aside from our additions to the MoClo system, the ECF toolbox includes a set of well-characterized genetic parts that are described in Chapter 3, Chapter 4 and Chapter 5. It is important to notice that the ECF toolbox is the first framework that features a library for use in bacterial systems that is fully compatible with the original MoClo vectors. Indeed the only other available library, which parts are encoded in MoClo vectors, was developed for plant transformation[139]. On the other hand, the other known bacterial DNA part libraries such as CIDAR[27] and EcoFlex[28] apply the same combinatorial assembly principles of the MoClo, but they are not compatible with the original MoClo system. This is because they also aim to define two new assembly standards since the genetic parts are assembled on a set of custom destination vectors. In particular, the CIDAR focuses more on an automated workflow for the combinatorial assembly[27], while the EcoFlex aims to provide a combinatorial library toolbox for different biological applications in *E. coli*[28]. However,

both systems, compared with the MoClo present some limitations. For instance, they feature an overall smaller number of cloning vectors, that limits the flexibility of the circuit design (e.g. lack of the possibility of cloning the TUs in reverse orientation from a set of genetic parts). Moreover, in both systems, the genetic circuits are ultimately cloned into a level M or level P equivalent destination vectors, without the possibility of further circuit expansion. For these reasons, in this study, we decided to use the original MoClo system to encode the level 0 library of parts and expand it by creating the CRIMoClo system.

In Section 3.3.1 we illustrated the selection and the characterization of the three inducible promoters (P_{BAD}, P_{tet}, $P_{Llac0\text{-}1}$) included in our library. The analysis performed using a highly sensitive luciferase reporter revealed a broad induction range of the promoters (Table 3.2). Interestingly both, P_{BAD} and $P_{LlacO\text{-}1}$ promoters displayed dynamic ranges that are in good agreement with the results obtained previously. In particular, Kogenaru and Tans measured up to 898-fold induction for the P_{BAD} promoter in the SV01 parental strain MK01, while we were able to achieve 3000-fold induction (Figure 3.8A). Moreover, Lutz and collaborators measured a dynamic range of 620-fold for $P_{Llac0\text{-}1}$ promoter, that is a result similar to the one that we obtained (Figure 3.8D; 500-fold induction). The discrepancies we observed between the promoter fold-inductions arise probably from the different reporter proteins and plasmids backbones used in the analysis. Indeed, the P_{BAD} construct measured by Kogenaru and Tans was encoded on a plasmid possessing the p15A origin of replication (like in the case of our genetic constructs), in contrast, their reporter system was represented by the fluorescent protein mCherry. Thus, our 3-fold higher dynamic range can be explained with the higher sensitivity of the luciferase cassette, illustrated in Section 2.2. In case of $P_{LlacO\text{-}1}$, Lutz, and collaborators, in their original work, measured the promoter by fusing it with a luciferase reporter (like in our construct), but encoding the resulting construct on plasmids possessing the high copy number origin of replication ColE1 (50-70 copies per bacterial cell). Thus, the lower copy number of our reporter plasmid pSVM-mc (20-50 copies per bacterial cell) could explain the 1.2-fold lower dynamic range that we obtained. These striking correlations between similar constructs, but different experimental conditions (such as media, and detection methods) confirm that these two promoters display a high orthogonal behavior.

In case of $P_{tet,}$ we obtained a high fold-induction (1000-fold) in both plasmid-borne and chromosomally integrated circuit (Figure 3.8C, D), by using the original P_{tet} promoter of the transposon Tn10, which sequence was described by Chalmers and collaborators[109]. However, this result cannot be directly compared to the original measurement of the promoter activity since it was performed using a *tetA–lacZ* translational fusion as reporter system[140]. An alternative choice, for an ATc inducible promoter, could be represented by a different version of the phage λ promoter developed by Lutz and collaborators ($P_{Ltet0\text{-}1}$) that displayed a dynamic range of 3670-fold induction. However, due to time limitations and since the main goal of this study resides in the development of ECF-based circuits, we did not include this promoter in the library. Nonetheless, the design characteristics of our library facilitate and encourage the integration of a newly improved version of each part. For instance, further implementations could include the above-mentioned ATc inducible promoter, as well as different P_{tet} synthetic promoter variants[141] and novel synthetic inducible promoters that respond to the induction with different aptamers, and commonly used inducers[142].

Section 3.3.2 shows our experiment on 11 ribosome binding sequences possessing different translational strength. We included these RBSs in the library, with the aim of tune the protein

production in ECF-based synthetic circuits. The results (Figure 3.9) find good agreement with the RBSs strength classification performed previously[111] and allowed to appreciate differences in the dynamic response of different RBS, especially in response to mild inducer concentrations that were not described before[111]. According to these findings, we classified the RBSs into two classes, which possess different characteristics. We concluded that at least one RBS from each class represents a valuable choice to variate the gene translation efficiency in novel synthetic circuits. However, in the ECF-based circuits that we generated, we always used the strong (st8) RBS that guarantees, overall, optimal translation efficiency over a broad range of inducer concentrations (Figure 3.9). This is due to the fact that designing each ECF-based circuit, testing also different RBSs, would have led to an extremely high labor-intensive and time-consuming process. Finally, if necessary, our library of RBSs can be easily expanded e.g. by including the RBSs described by Chris Anderson (https://parts.igem.org/Ribosome_Binding_Sites/Prokaryotic/Constitutive/Anderson).

In Section 3.3.4 we introduced the terminator sequences that are included in our library, represented by the 12 strongest recombination-resistant, synthetic terminators developed by Chen Y. and collaborators[112]. Even though we did not re-measured the strength of all terminator sequences, the results of our experiments, performed using the luciferase reporter, display the limits of the termination strength of both natural and synthetic terminators (Figure 3.10). However, even if we observed a certain degree of transcriptional read through, we registered a similar termination strength when comparing the strong natural terminators *rrnB*T1T2[21] and the strong synthetic terminator L3S3P21[112] (Figure 3.10; construct 3 and construct 4). This suggests that, at least in one case, the synthetic terminators represent a comparable alternative, in terms of termination strength, to the natural *E. coli* terminators. In the same section, we also investigated on the best strategy to insulate two neighboring TUs of a synthetic circuit. The aim was to acquire knowledge on the best strategy for the insulation of multiple genetic modules placed in close proximity. Our findings indicate that even though the termination efficiency can be improved by spacing the two transcription units with random DNA sequences (~300 base pairs), only the convergent orientation of the TUs guarantee complete insulation. Even though we do not think that our results represent universal design rules, they point out to the necessity of testing different organization of the genetic modules in multipart synthetic circuits, in order to find the configuration that offers the maximum insulation.

6.4 ECF toolbox: ECF σ and anti-σ factors

In Section 4.1 and Section 5.1-5.3 we characterized the ECF σ anti-σ and anti-σ truncation variants, included in the ECF toolbox library. To date, our study and the pioneering work of Rhodius and collaborators[63] represent the first efforts in characterizing a large pool of heterologous ECF σ in *E. coli*. Thus, we only have one term of comparison for the results that we obtained in the characterization of ECF- and ECF/AS-switches. Overall, we found that our results are consistent with the ones obtained previously, an indication of the robust and reproducible behavior of ECFs and anti-σ factors in different experimental conditions. In this section, we will compare the results obtained in the two characterizations, explaining the possible reasons behind the similarities and the differences that we observed.

In Figure 4.2 we show the effects of ECF overexpression on cellular growth, measured as bacterial density. Overall, we found that only the overexpression of ECF16, ECF20, and ECF37

lead to >2-fold decrease in the 6-h OD_{600} for low arabinose induction (10^{-5}%) when compared with the uninduced strain. Interestingly none of these ECFs were considered toxic (<75% 8-h OD_{600} when compared with a wild type strain) in the previous characterization[63]. Moreover, in the previous publication, ECF20 was, surprisingly, the less toxic σ factor among all 86 tested ECFs[63]. To explain these discrepancies in the results, we took into account the different media used in the experiments. Indeed, Rhodius and collaborators performed their assays in LB media, while our experiments were performed using the MOPS minimal medium (see Section 7.1). We chose to use this minimal medium because we found that it allows the establishment of a long (10-13h) continuous exponential growth of the SV01-based strains and represents an optimal time window to assay the dynamic performances of complex genetic circuits (see Section 7.10). However, the use of such a minimal medium could lead to the observed growth defects due to the nutrients reduced condition, when compared with the nutrient-rich LB media. Thus, since the ECF-switches embedding ECF16, ECF20, and ECF37 also displayed a high level of luciferase signal (~10^7 RLU/OD_{600}; Figure 4.3). the growth defects could be caused by the metabolic burden to the cellular machinery due to protein overexpression in these strains grown in nutrients reduced condition. However, when looking at the luciferase signals, generated by of all other ECF-switches (Figure 4.3), we found that some ECF-switches (e.g. ECF31-switch) led to a luciferase signal that is identical to the one obtained for the toxic ECFs, while, at the same time, they did not cause the same growth defects (Figure 4.2). This suggests that the growth defects, observed in our experimental conditions when overexpressing ECF16, ECF20 and ECF37, are likely related to cross-reactions with *E. coli* stress-pathways. To test this hypothesis, we reserve to test these ECFs in LB media. However, the results obtained for all other ECF-switches (Figure 4.2) confirmed that 80% of the ECFs included in our library did not cause relevant growth defects, even when grown in minimal media and in presence of high concentrations of the inducer.

Analyzing the output signal of the ECF-switches we found that ECFs display different fold-inductions when comparing the uninduced and the induced conditions (Figure 4.3). This is mainly caused by the different basal activities of the *ecf* promoters in the presence of uninduced ECF. Indeed, the majority of the ECFs displayed similar luciferase signals, comprised between $4x10^6$ RLU/OD_{600} and 10^7 RLU/OD_{600}, when fully induced (Figure 4.3). The highly variable baseline signals were also observed by Rhodius and collaborators, that measured an overall variability of 100-fold in the basal OFF state in the presence of uninduced ECF[63]. In our experimental setup, we were able to show a higher difference (1000-fold), among all the basal activities of the uninduced switches, probably due to the higher resolution offered by the luciferase reporter (Figure 4.3). Moreover, our further experiments on the ECF-switches and controls, (Figure 4.4 to Figure 4.6) overall, confirmed that *E. coli* σ factors do not interact with heterologous *ecf* promoters and that the different basal activities of the ECF-switches are caused by a broad range of ECFs binding affinities for the target promoters. In addition, we showed that the dynamic range of the ECF-switches can be controlled, in principle, by varying the number of ECFs and target promoters. This can be achieved by using different genetic configurations (e.g. multi copy, single copy), as well as by using different inducer concentrations, as shown in Figure 4.3, Figure 4.5 and Figure 4.6. However, the variability of the ECF-switches dynamic response poses a challenge in combining them in higher order circuits, as it will be discussed in Section 6.5.

An alternative way to tune the response of ECF-switches relies on controlling ECF activity through AS factors. Previously Rhodius and collaborators found that in most cases the

overexpression of AS factors lead to growth defect in *E. coli*[63]. Thus, in order to implement AS factors in our library and in our circuit design, we assayed the effects of their overexpression on SV01 growth, in our experimental conditions. Overall, we found that 7 out of 14 tested AS factors caused a reduction in the 6h-OD_{600} to 50% of the relative uninduced strain (Figure 5.2A). Moreover, we found that AS16, AS22, and AS31 resulted to be highly toxic, causing a >75% OD_{600} reduction 6h after the induction, when compared with the uninduced strains. In their original work, Rhodius and collaborators also indicated that AS16 and AS31 caused a 75% reduction in the OD_{600} values (8 h after induction), but they found AS22 to be non-toxic. Moreover, in their analysis AS14, ECF28 were highly toxic (>75% 8h-OD_{600} when compared with a wild type *E. coli* strain), while in our experiments they reduced the 6h-OD_{600} of 45% and 46% respectively. These small discrepancies are probably due to the different experimental conditions, as discussed above in the case of the ECF toxicity. However, both experiments, overall, confirmed that AS overexpression can generate an adverse effect on the viability of the host cell. Finally, the previous analysis was only showing which AS factors were causing (or not causing) a >75% reduction in the 8h-OD_{600}[63], while our results highlight, for each AS factor, the differences between the uninduced and the induced AS condition. This allowed to better compare the level of toxicity of the different AS factors, showing, for instance, that the overexpression of AS17 and AS20 results in an identical OD_{600} phenotype when comparing the uninduced and the induced conditions (Figure 5.2A).

Analyzing AS factors activity (Figure 5.2B) we found that all AS factors we tested are able to repress their target ECF activity, from 2- to 63-fold (AS17 and AS16 respectively). This is in perfect agreement with the results obtained in the previous study, were the AS factors that we chose for our library were also able to repress the ECF activity >2-fold[63]. We also found, overall, good correlations with the extent of ECF activity reduction by the AS. For instance, among the tested AS factors, in both analysis AS17 resulted to be the weakest AS (~2-fold reduction) while AS16 appeared to be strongest AS (>10-fold reduction).

Since the overexpression of transmembrane proteins leads to growth defects in *E. coli*[128], in order to diminish the adverse effects caused by AS factors overexpression, we additionally generated 21 truncated, soluble AS variants (Table 5.1). Analyzing the effects of the overexpression of truncated AS factors, we found that all truncated variants resulted to be equally or less toxic than the wild type AS factors. In particular, we found that AS11 truncation 1 was the most toxic truncation variant displaying the same 6h-OD_{600} reduction (65%) of the wild type AS. In contrast, AS22 truncation resulted to be the less toxic AS when compared with the un-truncated variant. Indeed, AS22 truncation showed 46% less toxicity when compared to the wild type AS. This striking result seems to be related to the fact that this AS has 4 predicted TM domains, thus their deletion allowed for a higher alleviation of the toxicity, when compared to other AS factors possessing 1 or 2 predicted TM domains.

When looking at the activity of the AS truncations we found that all the truncations, except AS27 t2, were functional, with the highest activity showed by AS14 t1 and t2 (Figure 5.3B; 100-fold reduction of basal luciferase activity). Analyzing the AS27 we found that the overexpression of the wild type AS27 showed the smallest activity (2-fold ECF repression) together with a 60% reduction in the OD_{600} (Figure 5.2). On the other end, the truncation 1 exhibited similar values in both activity and toxicity when compared with the wild type, while the truncation 2 resulted less toxic (30% reduction in the OD_{600}) but not active (Figure 5.3). Thus, we conclude that the limited reduction in ECF27 activity by the wild type AS27 and AS27 t1 is probably caused by the observed growth

defects and that this AS factor and the truncated variants possess overall a poor ability to reduce the activity of the cognate ECF.

The striking performances of AS14 truncations, that resulted to be ~23-fold more active than the wild type AS (Figure 5.3B), seems to be related to a higher affinity of the truncations for the cognate ECF σ factor, together with the low promoter binding affinity showed by ECF14 (Figure 4.3). A similar result was not observed for the truncations of other AS factors that in the wild type form showed similar signal fold reduction to the one produced by AS14 and have, at the same time, cognate ECFs with similar promoter binding affinity to the one showed by ECF14 (Figure 5.3B; AS28, AS34). Indeed, even though ECF28 and ECF34 showed weaker promoter binding affinity then ECF14 (Figure 4.3), the relative AS factor truncations resulted similarly active to the corresponding wild type AS factors. We then conclude that the AS14 truncations particularly enhanced the ability of the AS in sequestering the cognate ECF, even when compared with other AS truncations. The reason for such enhanced activity is not clear. We speculate that the higher affinity of the AS14 truncations for the cognate ECF could be due to higher accessibility of the ECF-binding interface in the soluble AS factors. However, this hypothesis does not explain why this effect, that should be an overall feature of the AS truncations, applied only to this particular AS. A more fascinating explanation takes into account the fact that the truncations of AS14 could be less sensitive to the stimulus that triggers the ECF release in the corresponding wild type AS. Thus, being uncoupled by the sensing domain, AS14 truncations will keep the ECFs into the inactive form in a more stable way than the wild type AS. However, this hypothesis can still not be confirmed, since the details of the mechanism of activation of AS14-like factors has not been studied yet[68].

Concluding, our extensive AS analysis found good agreement with the previous results[63]. In particular, all AS factors resulted to be able to reduce ECF activity more >2-fold. Moreover, we found good agreement with AS17 and AS16 that resulted to be in both analyses the less and most active AS respectively. By showing that AS17 possess a non-toxic phenotype we confirmed that the 2-fold signal reduction observed in the strain carrying this AS was caused by AS activity. We were also able to confirm the result obtained for AS16. Indeed, by expressing this AS together with the target ECF σ factor in single copy (Figure 5.4), we showed that, even in perfectly viable cells, the AS is still able to repress the cognate ECF by 30-fold (the highest fold-reduction also in chromosomally integrated AS circuits). Moreover, both analysis, also showed that in the majority of the cases, the overexpression of the AS factors in *E. coli* can lead to a toxic phenotype. We showed that the toxic effect can be partially alleviated by generating soluble variants of the AS factors, that also maintains their activity, and it is completely abolished by expressing the AS factors in single copy.

The toxic effect showed even by the overexpression of the truncated AS variants is probably due to cross-reactions with endogenous σ factors of *E. coli.* Interestingly, 9 out of 14 tested AS factors belong to the same phylum of *E. coli* (Proteobacteria), thus there is a higher chance that they recognize the endogenous σ factors. Moreover, a closer look at the results revealed that among the 5 AS factors (AS14, AS17, AS22, AS27, AS34) that belong to different phyla (Actinobacteria and Cyanobacteria[59]), AS14, AS17, and AS34 showed respectively 41%, 0%, and 44% reduction in the 6h-OD_{600} of the uninduced strain (Figure 5.2A). These values are generally lower than the one observed for other AS factors and even though this is not a general rule, it suggests that AS factors of a phylogenetically different organism, may act in a more orthogonal way, in respect to endogenous σ factors. Finally, since the Proteobacteria are currently one of the overrepresented

phyla in the ECF group classification, a further availability of sequences from organisms belonging to underrepresented phyla, and their inclusion in the ECF classification, will lead to the expansion of the available ECF and AS sequences.

6.5 ECF σ synthetic regulatory circuits

After discussing our experimental setup and about the ECF toolbox, in this section, we want finally discuss our findings on the implementation of ECF σ factors, as orthogonal core regulators and anti-σ factors, as ECF activity modulators, in novel synthetic circuits. After the work of Virgil and collaborators[63] and prior to this study, ECF σ factors were only used to generate insulated switches[64], or regulatory circuits[65] featuring one ECF. Thus, in this study we aimed to generate the first synthetic circuits harboring multiple ECFs, verifying at the same time if multi-ECF circuits feature orthogonality and predictability. To this end in Section 4.2, we introduced our ECF σ factor-based genetic-timer circuits, as proof of concept of multi-ECF-circuits.

The genetic-timer circuits harbor an increasing number of ECF-switches that are connected in series, such as that the output of a switch is the input of the next switch in the cascade, with the last switch producing an output signal. We refer to these circuit as 0-, 1-, 2- and 3-step timers, depending on the number of ECFs included. We expected, for such circuits, an increasing time delay between induction of the first ECF and signal production that scales with the length of the cascade. The time delay is due to the time required for ECF production, maturation, and accumulation until the activation threshold of the target promoter is reached. Strikingly the results we obtained confirmed our expectations. Indeed, all timer circuits, encoded in two genetic configurations (plasmid-borne and chromosomally integrated), displayed an increasing time delay among ECF induction and output signal production, that scales with the number of ECFs embedded in the cascade (Figure 4.7 and Figure 4.11). Our results then demonstrate that it is possible to create synthetic regulatory circuits using heterologous ECFs in *E. coli*. Moreover, the results obtained by our collaborators (Figure 4.14) show that similar ECF-based regulatory circuits can also be implemented a different bacterial species. Finally, our mathematical model confirmed that ECFs display an orthogonal behavior. This due to the fact that the quantitative parameters that describe the single ECF-switches in the model are constant, even when these switches are embedded in higher order circuits. These striking results also suggest that in principle we can predict the behavior of different ECF-switches cascades, by starting from the characterization of the single genetic components. Thus, we could find new combinations of the ECF-switches that lead to better results, in terms of time delay or signal transmission within the ECF-cascade. Aside from being a proof-of-concept for the implementation of multi-ECF circuits in *E. coli* and *B. subtilis*, our ECF-based regulatory cascades could also serve for biotechnological applications that rely on enzyme pathways. For instance, they could increase the yield of a product by tuning the expression timing of the enzymes in a pathway. This has been previously achieved by connecting the expression of all the pathway components to the bacterial growth phase[143]. In contrast, by using our ECF-based timer circuits, we could establish a precise time hierarchy between the expression of the individual pathway components. This would allow, for instance, to delay the expression of the last enzyme that catalyzes the formation of a toxic compound, until sufficient intermediates have accumulated[144].

Aside from the positive findings, our experiments on the timer circuits unveiled also a general negative feature of our ECF-based regulatory circuits, represented by an overall loss of output

dynamic range and thus of signal transmission, that scales with the length of the cascade. This is the results of the general promoter binding characteristics of the ECFs, together with the genetic organization of the ECF-switches. Indeed, it is important to notice that ECFs bind to the RNA polymerase as monomers, so they activate the target promoters in a non-cooperative manner following Michaelis-Menten kinetics (Hill coefficient=1). Previous theoretical studies predicted that in non-cooperative regulatory cascades, without feedback, the signal propagation critically depends on a precise fine-tuning of input and output-dynamic ranges[145]. These observations were confirmed by our experimental results. Indeed, we showed that the copy number of the circuits and the binding affinities of the different ECFs for their target promoters are the key features to tune and improve the signal propagation. The effects of the different ECF binding affinities, together with the effects of the ECF and *ecf* promoters copy number variation are shown in Figure 4.7 and Figure 4.11. For instance, looking at the 1-step timers encoded on plasmids we can observe how ECF32 has a higher binding affinity for the cognate promoter when compared with ECF28 (Figure 4.7). This lead to the behavior observed in the 2-step timer. Indeed, when ECF28 drives the production of ECF32, its lower affinity for the promoter is counterbalanced by the high affinity of ECF32 for the cognate promoter, that generates a certain baseline *lux* signal (Figure 4.7E; $6x10^5$ RLU/OD_{600}). On the other end, when ECF32 drives the production of the ECF28, the high affinity for the cognate promoter is counterbalanced by a weaker affinity of ECF28 for the target promoter that ultimately results in a weaker baseline signal (Figure 4.7F $4x10^5$ RLU/OD_{600}). This general correlation between promoter affinity and copy number is confirmed by the results obtained by chromosomally integrated timer circuits (Figure 4.11). Indeed, ECF32 shows again a higher binding affinity for the target promoter than ECF28. Thus, when the two ECFs are combined in a 2-step timer, even though ECF28 produces a very low amount of ECF32, these ECFs can still generate a detectable signal, since they have a high affinity for the target promoters (Figure 4.11E). On the other end, in the second 2-step timer permutation (Figure 4.11F), the strong P_{ecf32} leads to the production of a high number of ECF28 σ factors, that consequently can still produce a detectable signal, despite the lower binding affinity for its cognate target promoter.

A different factor that could affect the response of the different *ecf* promoters is related to the stability of the ECFs. Figure 4.13 display the different half-lives of the luciferase signal produced by the ECFs in the two 1-step timers. The results show a faster luciferase signal decay for ECF32 1-step timer (luciferase half-life ~130 min), suggesting a higher instability of ECF32 when compared to ECF28 (luciferase half-life in ECF28 1-step timer ~200 min). The higher instability of ECF32 can also be correlated to the faster response of the circuits where P_{ecf32} drives the output signal production. Indeed, faster protein degradation leads to faster attainment of the protein steady state and therefore faster promoter activation. Hence, the ability of ECF32 of turning on the target promoter in a faster way than ECF28 could raise by a combination of a higher promoter binding affinity together with a faster degradation of the ECF σ factor.

Overall, these results confirm that varying the copy number and by choosing ECFs with different promoter binding affinities (and eventually by tuning the protein stability) we can modulate the input/output signals of the switches and improve the signal transmission. Moreover, our mathematical model, described in detail in *Paper II* (Pinto *et al.*, 2018), predicts that the optimal signal transmission can only be achieved when the output of a switch match the input of the next switch of the cascade. Thus, by fitting the model to the data obtained from different ECF-switches in the different genetic configuration we could discover, in principle, the best conditions (ECF to

use, circuit copy number, inducer level) that guarantee an optimized signal propagation in ECF-based timer circuits.

6.6 ECF σ/anti-σ synthetic circuits

A different approach to improve signal transmission in transcriptional circuits consists of introducing cooperativity in promoter activation of the genetic switches. Indeed, cooperativity that generates a more digital OFF/ON switching behavior, allows for decreasing the required input range from an upstream circuit, matching more easily the induction threshold of the next switch in the cascade[146]. One way to increase the cooperativity in transcriptional circuits ìs represented by the introduction of a sequestering molecule that binds a circuit component[146]. Sequestration can be achieved by using sRNAs that bind to mRNA inhibiting its translation, or decreasing its stability[147,148], or by using proteins that bind to the transcription factors and form inactive complexes[126,149]. In the case of ECFs, their activity and the temporal expression can be controlled by AS factors[63,65]. In Section 6.4 we discussed the characterization of the AS factors and their truncated variants present in our library. Here, we will discuss their application in ECF-based synthetic circuits. With the experiments performed using 11 AS truncations (Figure 5.7 and Figure 5.8) we aimed to assay if the overexpression of these AS factors can lower the ECF-switches baseline. Moreover, we tested if AS factors can be used to set a time delay between ECF expression and downstream promoter activation. The results showed that 7 out of 11 highly expressed AS factor truncations, were able to lower the baseline activity in corresponding ECF-switches, from minimum 2-fold (AS37 t1) to maximum of 800-fold (AS20 t1). In the case of these two particular AS factors, we also observed a sharper transition between the OFF and the ON state of the circuit, under high AS concentration condition (Figure 5.7). This is an interesting feature since in gene regulation it is desirable to switch between two extreme expression values while only using a relatively small change in the concentration of the controlling protein[150]. Thus, the achievement of such “ultrasensitive” response in ECF/AS circuits is a valuable feature of the ECF regulators, in the context of synthetic biology. Indeed, it has been shown that ultrasensitivity allows to improve the robustness and to reduce the noise propagation in circuits built using different regulators than ECFs[151,152].

When looking at the dynamical activation of *ecf* promoters in ECF/AS circuits, we found that in the experimental conditions we used, most of AS factors were able to establish distinguishable time delays between ECF production and target promoter activation among different AS expression levels (Figure 5.7 and Figure 5.8 merged panels). However, we also found that the time delay does not depend only by the ability of the AS in lowering the baseline signal produced by the ECFs. Indeed, ECF/AS20 t1 and ECF/AS37 t1 circuits, that exhibited the highest fold-reduction in the baseline signal (800-fold, and 100-fold upon maximum induction, respectively) also showed one of the smallest difference in the time delay, when comparing low and high AS expression levels (Figure 5.7, merged panels). In contrast, the ECF/AS38 t1 circuit that showed only a 2-fold reduction of the uninduced ECF baseline signal, still achieved a time delay of 12 minutes in the promoter activation, when comparing low and high AS expression levels (Figure 5.8, merged panels). Thus the results suggest that aside from the capacity of the AS in sequestering the ECF and reduce the baseline signal, the time delay is also determined by the binding proprieties of the ECFs for the target promoters and by the amount of ECF and AS factors produced. This was confirmed by

the experiments presented in Figure 5.9 and Figure 5.10 where we were able to recover the signal in the circuit ECF14/AS14 t2, that was absent for high AS expression (Figure 5.8), tuning, at the same time, the time delay, by increasing the copy number of the circuit. Finally, the results show that the ECF/AS circuits, having highly active AS (>10-fold reduction of ECF basal activity) and ECFs with a weak binding affinity for their promoters, feature an analog increase of the output signal, together with the longest time delays (Figure 5.8; AS14 t2 N/D; Figure 5.7; AS28 t1 60 min, Figure 5.7; AS34 t1 85 min – for high AS expression levels). Interestingly, in case of ECF/AS14 t2, increasing the copy number of circuit allowed to maintain long time delays (60 min for the highest AS expression level) while generating at the same time a sharper sigmoidal curve in the output signal between the OFF and the ON state (Figure 5.9). However, a similar result was not reproducible for ECF/AS28 t1 and ECF/AS34 t1 (data not shown). This is an indication that simply changing the copy number of the ECF and AS modules in the genetic circuit does not always result in a different ECF/AS circuit behavior.

Concluding, the results discussed in this section suggest that AS factors can successfully be implemented in order to control and tune ECF-based circuits. However, they also demonstrate that it is necessary to screen the ECF/AS circuits at a higher resolution, by using more genetic configurations to variate the proportions between ECF and AS factors, together with the conditions that allow fine-tuning ECF and AS production. Nonetheless, our coarse grain characterization allows to insight some of the ECF/AS interaction features that will help in the development of ECF/AS circuits. To demonstrate it we selected 4 ECF/AS factors pairs to design novel synthetic circuits in *E. coli*, featuring a tunable time-delay

Our aim is to apply the ECF regulators together with the AS factors to design circuits that allow the time-programmable lysis of the bacterial cell. As illustrated in Section 5.5 synthetic self-destruction circuits allow for the generation of a product of interest and its release in the extracellular medium, avoiding the usage of natural secretion systems, or invasive cell disruption techniques. Indeed, besides the several advantageous characteristics of *E. coli* (e.g. fast growth and high protein yields), its inability to easily secrete recombinant proteins into the extracellular medium remains a drawback for industrial production processes[153]. Moreover, the usage of mechanical and chemical cell disruption techniques can cause protein denaturation, may require the purchase of expensive reagents, and sometimes it is not applicable at an industrial scale[132]. To date, we know different self-destruction circuits that allow the release of recombinant proteins produced in *E. coli* and they have been developed by using classical transcriptional regulators[132,154,155]. In this study, we aimed to build a time tunable suicide circuits in *E. coli*, by using ECF and AS factors. Such circuits will serve as prototypes for the future implementation of autonomous ECF/AS self-destruction circuits. The development of such circuits, featuring ECF and anti σ factors, would allow for the increase of the orthogonality of the self-destruction circuits and for the establishment of a tunable time delay between the generation of the product of interest and the cell disruption. Indeed, in the previous iterations of the self-destruction circuits, the time delay between the generation of the product of interest and the cell disruption was only depended by the time necessary for the accumulation of the different functional proteins after the induction of the lysis genes. Moreover, even though the cell lysis was triggered by different mechanisms (e.g. different inducer levels, heat-shock or glucose availability) the generation of the product of interest and the activation of the cell disruption were generally controlled by two separate mechanisms[132,154,155]. In contrast, by using ECFs and AS factors as regulators of the circuits it is possible, in principle, to set

different time delays for the cell disruption and, at the same time, automatize the generation of the product and the cell lysis upon the addition of only one inducer.

As illustrated in Section 5.5 we built a prototype of such circuit by using 4 different ECF/AS pairs, together with the CcdB toxin generating 4 *E. coli* suicide circuits. The results demonstrated that the time delay for the activation of the *ecf* promoters by the ECFs, that in turn causes the growth defect in the host (70% reduction of the growth rate when compared with the uninduced strain), can be effectively tuned by using different levels of AS factors (Figure 5.12). Indeed, we observed distinct time delays for 3 out of 4 ECF/AS circuits. Moreover, even though the experimental conditions were different, ECFAS28 t1 and ECF/AS34 t2 circuits showed a good qualitative agreement, in the time delays, with the circuits harboring the same ECF/AS pairs, assayed in the threshold gate experiments (Figure 5.7 and Figure 5.8). Indeed, in both experiments, ECF/AS28 t1 pair produced a luminescent signal and caused growth defects at a faster rate than ECF/AS34 t2, in the low AS expression condition. This confirms that our ECF/AS characterization can give good qualitative indications on the promising ECF/AS pairs in terms of generation of time delay in gene expression. However, even though our suicide circuits confirmed that we can in principle generate a time-programmable adverse effect on the host, they still need to be deeply improved. Indeed, the CcdB toxin primarily poisons the gyrase-DNA complex, leading to double-strand breakage of the DNA and death of the bacterial cells[134], but does not directly induce their lysis. Hence, the usage of a different kind of genes, such as a lytic gene[156], is necessary to achieve the cellular disruption. Moreover, our prototype does still not produce any product of interest, before the time-delayed production of the toxin. Indeed, as illustrated in Section 5.5, we used the same genetic configuration of the threshold gate circuits (P_{BAD}-*ecf* and P_{tet}-*anti-* σ integrated into the genome) and replaced the luciferase reporter construct with a P_{ecf}-*ccdB* construct. However, the gene(s) encoding for a product of interest, could be in principle controlled by the same promoter that drives the *ecf* expression (P_{BAD}) by creating an *ecf* operon. For instance, we could include the gene *dspB*, encoding for the enzyme responsible for biofilm degradation[157]. This enzyme represents a valuable product since it can detach and disperse the biofilm cells of *A. actinomycetemcomitans*, that colonizes the human oral cavity causing juvenile periodontitis[158]. Additionally, the MoClo framework would allow for the easy generation of an operon encoding for different enzymes that overall target bacterial biofilm, such as glycoside hydrolases[159], as well as protease, amylase, and pectinase[160].

In the experiments presented in Figure 5.9 and Figure 5.10, we showed that in ECF/AS circuits the accumulation of a protein encoded by a gene embedded in an *ecf* operon is a feasible possibility. Indeed, in these experiments, we produced a GFP protein from an *ecf* operon that reached a maximum value ~$8x10^3$ RFU/OD_{600} for the largest time-delay in the luciferase expression (Figure 5.9B, C; right panels, time delay=60 min). Consequently, the time delay set by using one AS factor would allow a certain product generation, before cell lysis. Alternatively, a more complex scenario involves the usage of two ECFs and relative target promoters, together with two cognate AS factors, as illustrated in Figure 6.1.

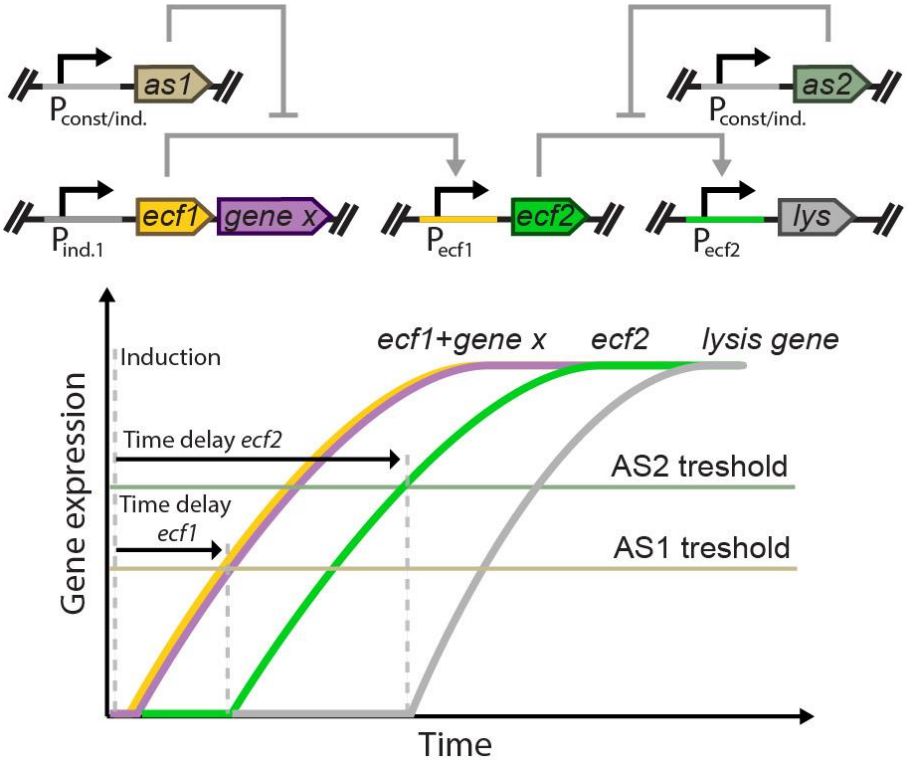

Figure 6.1. Autonomous ECF/AS self-destruction circuit. Blueprint of a self-destruction circuit featuring two ECF/AS pairs. Two different AS factors allow setting different AS threshold levels that, in turn, will allow the accumulation of a product of interest before cellular lysis.

In this case, the expression of the AS factors, using constitutive or inducible promoters, will establish two AS thresholds. AS1 will mainly be responsible for lowering the basal activity of the first ECF in the cascade, avoiding signal propagation prior to the induction. AS2, on the other end, will set the time delay for the activation of the *ecf2* promoters and the cell lysis. Thus, the induction of the *ecf1* operon will lead to the immediate generation of the product (encoded by *gene x*) that will start to accumulate, while ECF1 σ will bind to the target promoter only after exceeding the threshold set by AS1. Thus, after a certain time delay set by AS1, *ecf2* will be produced, but its target promoter will only be activated when ECF2 will overwhelm the threshold set by AS2, ultimately leading to the lysis of the cells. This kind of circuit will then possess two distinct time delays: the first set by AS1, for the activation of the *ecf1* promoter and the second, set by AS2, for the activation of the *ecf2* promoter. In this scenario, the time delay among the generation of a product of interest and cell lysis will be longer than the one generated by using only one AS factor. Additionally, the time delay can be tuned at a greater level, for instance by varying the concentration of the two AS factors. Strikingly, the generation of such a circuit, composed of 5 genetic modules, is already feasible using the tools included in the ECF toolbox. However, the dose-response characteristics of ECF σ and AS factors described in this study, together with the number of possible permutations and genetic configurations of the different modules embedded in the circuit, pose a challenge in terms of conditions that have to be tested, in order to achieve the desired circuit behavior. Nonetheless, the results obtained for the ECF-based timer circuits presented in this work (Section 4.2), suggest that mathematical modeling could assist the generation of the self-destruction circuit. For instance, in the experiments presented in Figure 5.9 and Figure 5.10, we demonstrated that the AS expression can be monitored and correlated with a certain time

delay between ECF induction and gene expression. Thus, it should be possible to generate for each ECF/AS module a mathematical model that describes its behavior (such as baseline reduction and time delay duration) in different conditions (such as genetic configuration and inducers levels). Finally, like in the ECF-based timer circuit, the orthogonality of the ECF-based modules should allow for the prediction of the optimal experimental conditions to achieve the best performances when the modules are combined in more complex circuits.

6.7 Conclusions

In this study, we aimed to establish ECF σ factors as alternative building blocks for the generation of synthetic circuits. In order to achieve our goal and to provide more tools for the synthetic biology community, we developed the ECF toolbox. The toolbox contains vectors for the expression and the chromosomal integration of the synthetic circuits, together with a MoClo-encoded library of parts which include, commonly used genetic building blocks, as well as, ECF, *ecf* promoters and anti σ factors. We showed that our toolbox, relying on the well established MoClo framework, allows a bottom-up, fast and modular assembly of multiple, reusable, genetic parts, in different genetic configurations. Next, using a high throughput experimental setup we characterized different genetic parts encoded in the part library, determining the best strategy for a rational design of ECF-based synthetic circuits. This led to the characterization of 15 ECF σ switches that we used to assemble higher order circuits. Indeed, by combining multiple ECF-switches into ECF-cascades we created the first synthetic ECF regulatory circuit harboring more than one ECF. We showed that the ECFs embedded in our timer circuits exhibit a robust, quantitative behavior that can be also predicted by a series of mathematical models. Next, we explored the possibility of implementing anti-σ factors in ECF-based circuits. By doing so we generated 21 soluble truncated variants of the AS factors. Overall, the truncations appeared to be functional and equally or less toxic than the wild type AS. Additionally, we showed that the chromosomal integration of the AS factors and truncated variants, abolish completely their toxicity, allowing at the same time to control ECF activity. Finally, by combining ECF and anti-σ factors in different genetic configurations, we proved that AS factors can be used to design threshold gate circuits, allowing for a time-tunable control of ECF σ factors activity and, in turn, time-delayed downstream protein expression.

Overall, this study revealed the multiple advantages of applying ECF σ factors in the context of synthetic biology such as predictability and orthogonality of the ECF-based circuits. However, we also encountered one of the biggest limitations in synthetic circuit design using ECF σ factors and the cognate AS factors. Indeed, the numerous experimental conditions that have to be tested in order to achieve the desired result, pose a serious challenge in the development of ECF-based synthetic circuits. Nevertheless, the characteristics of the ECF toolbox enhances the possibility of performing a high throughput combinatorial circuit assembly, for instance by using the highly automated Drop-on-Demand Technology[161]. Moreover, the numerous generated circuits could be screened for functionality in highly automated frameworks, by using robotic platforms[162]. Finally, as demonstrated in this study, a quantitative analysis of the results and the generation of mathematical models allows for the characterization and the prediction of the behaviour of the circuits. Thus, the combination of precise and robust high throughput analysis, together with a rational model-driven design, will ultimately assist and ease the generation of ECF-based synthetic circuits.

7. Materials and methods

7.1. Bacterial Strains and growth conditions.

E. coli strains used in this study are listed in Table 9.1. The strains were cultivated in LB (LB Broth Miller, Sigma Aldrich Cat.No. L3522) medium or MOPS minimal medium (TEKNOVA Cat.No. M2106; 0.5% glycerol as carbon source) at 37 °C shaking at 250rpm. To maintain plasmids, the following antibiotics were used: chloramphenicol at 25μg/ml, kanamycin at 50 μg/ml, spectinomycin at 100μg/ml, gentamicin at 10μg/ml. For the selection of single-copy integrants antibiotics were added as follows: chloramphenicol at 6μg/ml, kanamycin at 10μg/mL, spectinomycin at 35μg/ml, gentamicin at 5μg/ml. For the blue-white screening, LB plates containing isopropyl β-D-1-thiogalactopyranoside (IPTG) at 0.1mM and 5-Bromo-4-chloro-3-indolyl-β-D-galactoside (X-Gal) at 40μg/ml were used.

7.2. Molecular biology techniques.

Oligonucleotides were provided by Sigma-Aldrich (Germany). PCR reactions were performed using Q5 High-Fidelity DNA Polymerase (New England Biolabs) or Taq DNA Polymerase (New England Biolabs). PCR mixtures were purified using the E.Z.N.A. Cycle-Pure Kit (Omega Bio-Tek). For gel extraction, Zymoclean Gel DNA Recovery Kit (Zymo Research, Germany) was used. Phosphorylation of the 5'OH of linear DNA fragments was performed using T4 Polynucleotide Kinase (T4 PNK) provided by New England Biolabs. Type IIs restriction enzymes (BpI and BsaI) and T4 DNA ligase were purchased from Thermo Scientific (Germany). DNA sequence verification was performed by Eurofins Genomics (Germany). Transformation of different chemically competent *E. coli* strains was performed according to the Inoue method[163] or using the transformation and storage solution (TSS) methodology[106].

7.3. Recombination of the chloramphenicol cassette from *E. coli* strain SV01

E. coli strain MK01 carries a chloramphenicol selection marker, flanked by two loxP sites. In order to remove the chloramphenicol cassette we used the Cre-lox system as follows. The plasmid pCM157, (tetracycline resistant)[164] encoding an IPTG inducible *cre* recombinase gene, was transformed in chemically competent MK01 cells. The cells were incubated for 30 min on ice and transformed by heat shock. 950μL of liquid LB was then added to the transformation mix, and the cells were recovered for 45 min at 37 °C. 40μL of the transformation mix was plated on LB plates containing IPTG at a final concentration of 1 mM (inducing the expression of the Cre recombinase) and incubated overnight at 37°C. 20 emerging colonies were re-streaked twice on LB plates without antibiotic selection for loss of plasmid pCM157. 10 single colonies were then streaked on LB plates without antibiotic selection, LB plates containing chloramphenicol selection and LB plates containing tetracycline. 2 colonies that displayed loss of pCM157 (not being able to grow on tetracycline agar plates) and at the same time displayed successful recombination events (no being able to growth on chloramphenicol agar plates) were tested by colony PCR for loss of the chloramphenicol cassette and grown overnight at 37°C in LB media without antibiotic selection. The pre-cultures were then used for the creation of bacterial glycerol stocks.

7.4. pSVM-mc MoClo vector construction.

The pSVM-mc vector generated in this study was created via Gibson assembly[19]. The plasmid backbone of the MoClo vector pICH82094[26] was PCR-amplified, using the primers GF0078-GF0079 (Table 9.7). The multiple cloning site of pICH82094, was PCR-amplified using the primers GF0080-GF0081 (Table 9.7) that provide the homology region necessary for the Gibson assembly and at the same time allowed the exchange of the MoClo fusion sites from level P to level M. Each PCR product was digested (37 °C 1 h) using DpnI endonuclease, to destroy the methylated template used in the PCR reaction. Subsequently, the PCR products were purified via gel extraction and fused by Gibson assembly[19]. The reaction was set as follows: 50ng of backbone DNA (0.03pmol) were mixed with 0.09pmol of insert and Gibson Reaction Mix (New England Biolabs) in a final volume of 20μL. Gibson reaction was performed for 1 h at 50 °C. 2μL of the reaction mix were transformed in 50μL of chemically competent DH5α cells as described by[163], plated on selective agar plates and incubated overnight at 37 °C. 10 different emerging colonies were assayed by colony PCR using the primers GF070-GF071 (Table 9.7). The plasmids were isolated from the positive clones and further verified by restriction digest using BsaI and BpiI. Two correctly digested plasmids were finally sequenced to determine the correctness of the nucleotide sequence in the insert region.

7.5. CRIMoClo vectors construction.

CRIMoClo vectors generated in this study (Table 9.2) were assembled using Ligase Cycling Reaction (LCR)[20] and Gibson Assembly[19]. For the construction of the first 8 CRIMoClo vectors (level M and P with chloramphenicol resistance and 4 att sites), DNA fragments were PCR amplified using Q5 High-Fidelity DNA Polymerase (New England Biolabs) and the primers reported in Table 9.7. In particular, the *tL3* terminator together with one of four different phages attachment sites (att_{HK022}, att_{P21}, $att_{\phi 80}$, att_{λ}) was amplified using the universal forward primer GF0524 in combination with the reverse primers GFC0525-GFC0526-GFC0530, using CRIM plasmids pAH68, pAH81, pAH153[39] as templates. The amplification of att_{λ} from pAH120[39] was performed in two-step using the primers GFC0524-GFC0527 and GFC0528-0529 to remove an undesired BpiI restriction site. The γ conditional origin of replication of R6K was amplified from pAH68[39] using the primers GFC0531 and GFC0532, while the chloramphenicol resistance cassette was amplified from pKD3[42] using the primers GFC0533-GFC0534. The *rgnB* terminator was amplified from pAH68[39] using the primers GFC0535-GFC0536. Finally, the MoClo multicloning region was amplified with the primers GFC0537-GFC0538 using pSVM-mc (created in this study) and pICH82094[26] as Level M and Level P templates respectively. The generated fragments (blunt-end and 5′ phosphorylated) were fused via ligase cycling reaction (LCR) according to de Kok *et al.*,[20]. In particular 0.3 U Taq ligase (New England Biolabs), 3 nM DNA parts, 30 nM bridging oligonucleotides (Table 9.7), and 8% (v/v) DMSO were applied. The following conditions were used: 2 min at 94 °C and then 50 cycles of 10 seconds at 94°C, 30 seconds at 60°C, and 60 seconds at 65°C, followed by incubation at 4°C. The newly generated set of plasmids (Table 9.2) were used as template for the assembly of the next 8 CRIMoClo plasmids having the kanamycin resistance cassette, using Gibson assembly[19]. In particular, the backbones from pSV004, pSV006, pSV008, pSV077, pSV016, pSV018, pSV080, pSV079 and the kanamycin cassette from pSVM-mc were

PCR amplified using Q5 High-Fidelity DNA Polymerase (New England Biolabs) using the primers GF0807-GF0532 and GF0805-GF0808. The generated fragments were fused via Gibson assembly[19], setting a reaction were 50ng of backbone DNA (0.03pmol) were mixed with 0.09pmol of insert (represented by the resistance cassette) and Gibson Reaction Mix (New England Biolabs) in a final volume of 20μL. Gibson reaction was performed for 1 h at 50 °C. The resulting plasmids were then used as template to generate 8 gentamicin and 8 spectinomycin resistant CRIMoClo plasmids, using Gibson assembly[19]. In particular, the backbones (pSV125, pSV126, pSV127, pSV128, pSV219, pSV220, pSV221, pSV222) were PCR amplified using Q5 High-Fidelity DNA and the primers GF0945-GF0532 in order to maintain the promoter of the kanamycin cassette. These fragments were then fused with the spectinomycin and gentamicin coding sequences (amplified from pMA333[30] and pABC2[21] using the primers GF0858-GF0947 and GF0856-GF0949 respectively) via Gibson assembly, following the protocol described above.

7.6. CRIMoClo plasmid integration using competent cells pre-transformed with the helper plasmid.

The chromosomal integration of the CRIMoClo plasmids was performed similarly as described by Haldimann and Wanner[39]. In particular, 2μL of purified plasmid was added to 50μL chemically competent *E. coli* SV01 cells, carrying one of the CRIM helper plasmids (pAH69, pAH121, pINT ts, pAH123[39]). The cells were incubated for 30 min on ice and transformed by heat shock. 950μL of liquid LB was then added to the transformation, and the cells were incubated at 37°C for 1 h and at 42°C for 30 min (to induce the phage-derived integrase (*int*) gene and simultaneously cure the helper plasmid). 80μL of the transformation were spread onto selective agar plates and incubated at 37°C overnight. The emerging colonies were tested by colony PCR using the primers P1–P2–P3–P4. The nucleotide sequences of P1 and P4 primers (specific for each attB site) are reported in Table 9.7 (GF0512 to GF0521), together with the nucleotide sequences of P2 and P3 (Table 9.7; GF0971-GF0521). The positive colonies were purified once non-selectively and then tested for antibiotic resistance for stable integration and loss of the helper plasmid.

7.7. CRIMoClo plasmid integration using TSS competent cells.

As an alternative way to achieve integration (e.g. in the multi-integration experiment described in Section 3.2.3) we prepared competent cells using the TSS method[106]. A single clone of *E. coli* SV01 was picked from LB agar plates and pre-cultured in 3ml of LB media at 37°C, shaking 250rpm. When OD600 reached 0.5-0.8, the cells were chilled in ice for 10 minutes and then 500μL of cell culture were mixed with 500μL of TSS 2x and left in ice for 45 minutes. Subsequently, 50μg of purified CRIMoClo-based plasmid and 50μg of the cognate helper plasmid were added to the cell mixture and left in ice for 45 minutes, followed by 1 hour at 30°C and 30 minutes at 42°C shaking at 250rpm. 200μL of the cell culture was then plated on selective plates and grown overnight at 37°C. In the case of strains possessing multiple resistance cassettes, we selected only for the resistance of the latest integrated construct. The emerging colonies were tested by colony PCR using the primers P1–P2–P3–P4 (see Section 7.6), purified once non-selectively and then tested for antibiotic resistance for stable integration and loss of the helper plasmid.

7.8. Generation of the Level 0 part library.

The complete part library used in this study, encoded on MoClo level 0 plasmids, is listed in Table 9.3 that indicates also the primers and the templates utilized to generate the part inserts (by PCR-amplification or oligonucleotides annealing), together with the MoClo destination vectors used for each part. The constructs that required to be cured for BpiI and BsaI restriction sites are also indicated. The cure of undesired BpiI and BsaI sites was performed according to Wanner *et al.*, as described in Section 3.3. To generate the genetic parts present in the library we used PCR-amplification or annealing of DNA oligonucleotides. In the case of PCR-amplification, the PCR products were verified by electrophoresis with 1, or 2% agarose gels and purified by gel extraction or column purification, following the protocols of the manufactures. The purified product was used to clone the insert into the appropriate MoClo destination vector, following the procedure described in Section 7.9. In case of annealing of DNA oligonucleotides, the reaction of annealing and the phosphorylation of the 5'OH was performed as follow: 2 µL of 100 µM oligonucleotides stock were mixed with 2 µL 10X T4 DNA ligase buffer, 1 µL of T4 Polynucleotide Kinase and 15 µL of sterile water. The reaction mixture was incubated at 37 °C for 1 hour and at 65 °C for 20 minutes to heat inactivate the T4 PNK. An aliquot of reaction mix was then used to clone the insert into the appropriate MoClo destination vector, following the procedure described in Section 7.9.

In the generation of the part pSV0-1_002, encoding the P_{BAD} promoter and the repressor AraC, we added the synthetic terminator L3S3P00[112] at the end of the *araC* gene. To do so, we first generated the terminator L3S3P00 by oligonucleotides annealing using the primers GF0046-GF0047 (Table 9.7). Subsequently we PCR-amplified *araC*, together with the P_{BAD} promoter, from pAraC-pBAD-mCherry-v2[80] using the primers GFC0034-GFC0010 (Table 9.7). The parts were then fused by Golden gate assembly, into the MoClo destination vector pICH41233, using the procedure described in Section 7.9.

In the generation of the part pSV0-1_004, encoding the $P_{LlacO-1}$ promoter and the repressor LacI, the two parts were generated independently and fused by Golden gate assembly. In particular, the promoter $P_{LlacO-1}$[110] was generated by oligonucleotides annealing using the primers GF0050-GF0051 (Table 9.7). The LacI repressor together with the *rrnbT1* terminator was PCR-amplified by pLacI-Ptrc-eYFP-v2 donated by Kogenaru M. & Tans S.[80], using the primers GF0035-GF0032, GF0033-GF0006, GF0007-GF0037 (Table 9.7) that were designed to remove, at the same time, 2 undesired BpiI sites. The different parts were then fused by Golden gate assembly, into the MoClo destination vector pICH41233, using the procedure described in Section 7.9.

In the generation of pSV0-1_005 encoding the P_{tet} promoter and the repressor TetR we added the synthetic terminator L3S1P13[112] at the end of the *tetR* gene. To do so, we first generated the terminator L3S1P13 by oligonucleotides annealing using the primers GF0048-GF0049 (Table 9.7). Subsequently we PCR- amplified *tetR*, together with the P_{tet} promoter[50], from pCATTRE18 donated by the laboratory of Torsten Waldminghaus using the primers GFC0038-GFC0039 (Table 9.7). The parts were then fused by Golden gate assembly, into the MoClo destination vector pICH41233, using the procedure described in Section 7.9.

7.9 Modular Cloning (MoClo) reactions (Golden gate assembly).

The MoClo-encoded parts and synthetic circuits, as well as the integrative CRIMoClo-based plasmids generated in this study, are listed in Tables 9.3-9.6. All constructs were assembled on MoClo[24,26] and CRIMoClo vectors (generated in this study), using linear DNA fragments (PCR-amplificated products, or phosphorylated annealed oligonucleotides) or the MoClo-encoded parts listed in Table 9.3 (level 0 parts), Table 9.4 (level 1 parts), Table 9.5 (level M parts). Each table indicates the list of the parts used to generate the constructs and a brief description of the constructs.

All MoClo reactions were set up using 15 fmol of each DNA part (PCR product or plasmid), 1μL of the required restriction enzyme (BsaI or BpiI), 1 μL of T4DNA ligase (5 U/μL) and 2 μL of Thermo ligase buffer (10x), in a final reaction volume of 20 μL. The reaction was incubated in a thermocycler for 5 h at 37 °C, 10 min at 50 °C and 10 min at 80 °C. 2 μL of the reaction mixture was then added to 50 μL chemically competent *E. coli* DH5α cells (*E. coli* DH5α λ*pir* cells in case of CRIMoClo constructs), incubated for 30 min on ice and transformed by heat shock. 950μL of liquid LB was then added to the transformation, and the cells were recovered for 45 min at 37 °C. 40 μL of the transformation mix was plated on selective LB-IPTG-X-Gal plates and incubated overnight at 37 °C. The emerging colonies were tested by colony PCR and restriction digestion.

7.10. Microplate reader assays.

Microplate reader assays were performed in a Tecan Infinite F200 pro machine using the black and transparent 96-well plates from GREINER (catalog No.: 655097 and 655101). For each *E. coli* strain, a single bacterial colony was picked from selective plates and grown in liquid LB medium, supplemented with appropriate antibiotics, until stationary phase (37 °C shaking at 250 rpm; 7-8 hours). The day-cultures were diluted 1:6000 into MOPS minimal medium (Section 7.1), supplemented with appropriate antibiotics and grown overnight (37 °C shaking at 250 rpm) until they reached an optical density at 600 nm (OD_{600}) of 0.5–0.6. The cultures were then diluted to an OD_{600} of 0.05 in fresh MOPS minimal medium (Section 7.1), without antibiotic selection. This allows for the synchronization of the cell cultures and the collection of population-wide data. 100 μL of the culture dilutions were loaded in the wells of a 96-well plate. The plate was incubated for a minimum of 8 h to a maximum of 12 h (37 °C with shaking) and OD_{600}, as well as luminescence, were measured every 5 minutes (10 minutes in case of sequential fluorescence/luminescence measurements). In all experiments, for inducing gene expression, cells were induced, after two hours of incubation, with the final concentrations of inducer described in each section of this study, and incubation was resumed. The entire procedure described above, allows obtaining a continuous exponential growth of *E. coli* SV01 (Section 7.3), with and a doubling time ~175min. This represents an optimal time window for assaying the dynamical response of the genetic circuits.

In the experiment described in Section 4.2 (switching ECF-cascades from the ON to the OFF state), all cultures were grown in the conditions described above, supplementing the MOPS minimal medium (Section 7.1) with 10^{-4} % arabinose (to induce gene expression prior to the measurement). The cultures were grown overnight (37 °C shaking at 250 rpm) until they reached an optical density at 600 nm (OD_{600}) of 0.5–0.6. The cultures were then washed twice using fresh arabinose-free MOPS minimal medium, then diluted to an OD_{600} of 0.05 in fresh arabinose-free MOPS minimal medium, and incubated in a microplate reader as described above.

In the experiments described in Section 5.4 (ECF/AS threshold gate circuits), for each *E. coli* strain, a single bacterial colony was picked from selective plates and grown in liquid LB medium, supplemented with appropriate antibiotics, until stationary phase (37 °C shaking at 250 rpm; 7-8 hours). The day-cultures were diluted 1:6000 into MOPS minimal medium (Section 7.1), supplemented with appropriate antibiotics and the indicated concentrations of ATc, in order to set different thresholds of AS expression. The diluted cultures were grown overnight (37 °C shaking at 250 rpm) until they reached OD_{600} of 0.5–0.6. The cultures were then diluted to an OD_{600} of 0.05 in fresh MOPS minimal medium, supplemented with the indicated concentrations of ATc, without antibiotic selection and assayed in a plate reader experiment as described above.

In the experiment described in Section 5.5 (ECF/AS suicide circuits), all *E. coli* strain, following the introduction of plasmids encoding the *ccdB* toxin, were grown (in both solid and liquid phases) in presence of ATc at a final concentration of 1 ng/mL and 2.5 ng/mL. For each strain, a single bacterial colony was picked from selective plates and grown in liquid LB medium, supplemented with ATc (at the concentrations indicated above) and appropriate antibiotics, until stationary phase (37 °C shaking at 250 rpm; 7-8 hours). The day-cultures were diluted 1:6000 into MOPS minimal medium (Section 7.1), supplemented with appropriate antibiotics and ATc at the above-mentioned concentrations. The cultures were grown overnight (37 °C shaking at 250 rpm) until they reached an optical density OD_{600} of 0.5–0.6. An aliquot of the bacterial cultures grown in the presence of ATc [1 ng/mL] was then washed twice using fresh ATc-free MOPS medium and diluted to an OD_{600} of 0.05 in fresh MOPS minimal medium. The remaining cultures (grown in presence of ATc [1 ng/mL] and [2.5 ng/mL]), were also diluted to an OD_{600} of 0.05 in fresh MOPS minimal medium supplemented ATc at the above-mentioned concentrations. 100 µL of all culture dilutions were loaded in the wells of a 96-well plate. The plate was incubated for 12 h (37 °C with shaking) and OD_{600} was measured every 5 minutes. After two hours of incubation, cells were induced with 0 and 0.2% arabinose and incubation was resumed.

7.11. Analysis of plate reader measurements and luciferase bleed-through correction.

All the data generated with plate reader experiments were obtained using a Tecan Infinite F200 pro machine. The data were evaluated using Microsoft Excel and MathWorks Matlab software to produce all the graphs and the analysis presented in this study.

The raw optical density (measured at 600nm – OD_{600}) data obtained from microplate reader measurements were background-corrected by subtracting OD_{600} values obtained from a control well containing the growth medium alone. The resulting values were used for generating the graphs and perform the analysis as described in each section of this study.

The raw fluorescence data obtained from microplate reader measurements were background-corrected by subtracting fluorescence values obtained from a control well containing the growth medium alone. The resulting values were used for generating the graphs and perform the analysis as described in each section of this study.

The raw luminescence data obtained from microplate reader measurements were background-corrected by subtracting luminescence values obtained from a control well containing the growth medium alone. The data were then corrected for luminescence bleed through (i.e. light-scattering) from neighboring wells on the microplate, by using the de-convolution algorithm introduced in Section 2.3 and published in *Paper I* (Mauri *et al.,* 2019). The resulting values were used for

generating the graphs and perform the analysis as described in each section of this study. The computational model mentioned in Section 4.2 was developed by Hao Wu and it is described in detail in *Paper III* (Pinto *et al.*, 2018).

8. Bibliography

1. Andrianantoandro, E., Basu, S., Karig, D. K. & Weiss, R. Synthetic biology: new engineering rules for an emerging discipline. *Mol. Syst. Biol.* **2**, 1–14 (2006).

2. Bond-Watts, B. B., Bellerose, R. J. & Chang, M. C. Y. Enzyme mechanism as a kinetic control element for designing synthetic biofuel pathways. *Nat. Chem. Biol.* **7**, 222–227 (2011).

3. Zhang, F., Carothers, J. M. & Keasling, J. D. Design of a dynamic sensor-regulator system for production of chemicals and fuels derived from fatty acids. *Nat. Biotechnol.* **30**, 354–359 (2012).

4. Gibson, D. G. *et al.* Creation of a Bacterial Cell Controlled by a Chemically Synthesized Genome. *Science (80-.).* **329**, 52–56 (2010).

5. Cardinale, S. & Arkin, A. P. Contextualizing context for synthetic biology - identifying causes of failure of synthetic biological systems. *Biotechnol. J.* **7**, 856–866 (2012).

6. Morey, K. J. *et al.* Crosstalk between endogenous and synthetic components - synthetic signaling meets endogenous components. *Biotechnol. J.* **7**, 846–855 (2012).

7. Hartwell, L. H., Hopfield, J. J., Leibler, S. & Murray, A. W. From molecular to modular cell biology. *Nature* (1999). doi:10.1038/35011540

8. Qian, Y., Huang, H.-H., Jiménez, J. I. & Del Vecchio, D. Resource Competition Shapes the Response of Genetic Circuits. *ACS Synth. Biol.* **6**, 1263–1272 (2017).

9. Ellis, T., Adie, T. & Baldwin, G. S. DNA assembly for synthetic biology: from parts to pathways and beyond. *Integr. Biol.* **3**, 109–118 (2011).

10. Arkin, A. Setting the standard in synthetic biology. *Nat. Biotechnol.* **26**, 771–774 (2008).

11. Knight, T. Idempotent Vector Design for Standard Assembly of Biobricks. in *MIT Synthetic Biology Working Group* (2003).

12. Shetty, R. P., Endy, D. & Knight, T. F. Engineering BioBrick vectors from BioBrick parts. *J. Biol. Eng.* **2**, 5 (2008).

13. Casini, A., Storch, M., Baldwin, G. S. & Ellis, T. Bricks and blueprints: methods and standards for DNA assembly. *Nat. Rev. Mol. Cell Biol.* **16**, 568–576 (2015).

14. Anderson, J. C. *et al.* BglBricks: A flexible standard for biological part assembly. *J. Biol. Eng.* **4**, 1 (2010).

15. Liu, J.-K., Chen, W.-H., Ren, S.-X., Zhao, G.-P. & Wang, J. iBrick: A New Standard for Iterative Assembly of Biological Parts with Homing Endonucleases. *PLoS One* **9**, e110852 (2014).

16. Horton, R. M., Hunt, H. D., Ho, S. N., Pullen, J. K. & Pease, L. R. Engineering hybrid genes without the use of restriction enzymes: gene splicing by overlap extension. *Gene* **77**, 61–68 (1989).

17. Quan, J. & Tian, J. Circular Polymerase Extension Cloning of Complex Gene Libraries and Pathways. *PLoS One* **4**, e6441 (2009).

18. Eckert, K. A. & Kunkel, T. A. DNA polymerase fidelity and the polymerase chain reaction. *Genome Res.* **1**, 17–24 (1991).

19. Gibson, D. G. *et al.* Enzymatic assembly of DNA molecules up to several hundred kilobases. *Nat. Methods* **6**, 343–345 (2009).

20. de Kok, S. *et al.* Rapid and reliable DNA assembly via ligase cycling reaction. *ACS Synth. Biol.* **3**, 97–106 (2014).

21. Döhlemann, J. *et al.* A Family of Single Copy repABC -Type Shuttle Vectors Stably Maintained in the Alpha-Proteobacterium *Sinorhizobium meliloti*. *ACS Synth. Biol.* **6**, 968–984 (2017).

22. Szybalski, W., Kim, S. C., Hasan, N. & Podhajska, A. J. Class-IIS restriction enzymes — a review. *Gene* **100**, 13–26 (1991).

23. Lippow, S. M. *et al.* Creation of a type IIS restriction endonuclease with a long recognition sequence. *Nucleic Acids Res.* **37**, 3061–3073 (2009).

24. Weber, E., Engler, C., Gruetzner, R., Werner, S. & Marillonnet, S. A Modular Cloning System for Standardized Assembly of Multigene Constructs. *PLoS One* **6**, e16765 (2011).

25. Guet, C. C., Elowitz, M. B., Hsing, W. & Leibler, S. Combinatorial synthesis of genetic networks. *Science* **296**, 1466–1470 (2002).

26. Werner, S., Engler, C., Weber, E., Gruetzner, R. & Marillonnet, S. Fast track assembly of multigene constructs using Golden Gate cloning and the MoClo system. *Bioengineered* **3**, 38–43 (2012).

27. Iverson, S. V, Haddock, T. L., Beal, J. & Densmore, D. M. CIDAR MoClo: Improved MoClo Assembly Standard and New *E. coli* Part Library Enable Rapid Combinatorial Design for Synthetic and Traditional Biology. *ACS Synth. Biol.* **5**, 99–103 (2016).

28. Moore, S. J. *et al.* EcoFlex: A Multifunctional MoClo Kit for *E. coli* Synthetic Biology. *ACS Synth. Biol.* **5**, 1059–1069 (2016).

29. Andreou, A. I. & Nakayama, N. Mobius Assembly: A versatile Golden-Gate framework towards universal DNA assembly. *PLoS One* **13**, e0189892 (2018).

30. Schindler, D., Milbredt, S., Sperlea, T. & Waldminghaus, T. Design and Assembly of DNA Sequence Libraries for Chromosomal Insertion in Bacteria Based on a Set of Modified MoClo Vectors. *ACS Synth. Biol.* **5**, 1362–1368 (2016).

31. Engler, C., Gruetzner, R., Kandzia, R. & Marillonnet, S. Golden Gate Shuffling: A One-Pot DNA Shuffling Method Based on Type IIs Restriction Enzymes. *PLoS One* **4**, e5553 (2009).

32. Gorochowski, T. E. *et al.* Absolute quantification of translational regulation and burden using combined sequencing approaches. *Mol. Syst. Biol.* **15**, e8719 (2019).

33. Ceroni, F. *et al.* Burden-driven feedback control of gene expression. *Nat. Methods* **15**, 387–393 (2018).

34. Cunningham, D. S., Koepsel, R. R., Ataai, M. M. & Domach, M. M. Factors affecting plasmid production in *Escherichia coli* from a resource allocation standpoint. *Microb. Cell Fact.* **8**, 27 (2009).

35. Paulsson, J. & Ehrenberg, M. Trade-off between segregational stability and metabolic burden: A mathematical model of plasmid ColE1 replication control. *J. Mol. Biol.* **279**, 73–88 (1998).

36. Diaz Ricci, J. C. & Hernández, M. E. Plasmid Effects on *Escherichia coli* Metabolism. *Crit. Rev. Biotechnol.* **20**, 79–108 (2000).

37. Sabri, S., Steen, J. A., Bongers, M., Nielsen, L. K. & Vickers, C. E. Knock-in/Knock-out (KIKO) vectors for rapid integration of large DNA sequences, including whole metabolic pathways, onto the *Escherichia coli* chromosome at well-characterised loci. *Microb. Cell Fact.* **12**, 60 (2013).

38. Juhas, M. & Ajioka, J. W. Lambda Red recombinase-mediated integration of the high molecular weight DNA into the *Escherichia coli* chromosome. *Microb. Cell Fact.* **15**, 172 (2016).

39. Haldimann, A. & Wanner, B. L. Conditional-replication, integration, excision, and retrieval plasmid-host systems for gene structure-function studies of bacteria. *J. Bacteriol.* **183**, 6384–93 (2001).

40. St-Pierre, F. *et al.* One-Step Cloning and Chromosomal Integration of DNA. *ACS Synth. Biol.* **2**, 537–541 (2013).

41. Wei, X.-X. *et al.* A mini-Mu transposon-based method for multiple DNA fragment integration into bacterial genomes. *Appl. Microbiol. Biotechnol.* **87**, 1533–1541 (2010).

42. Datsenko, K. A. & Wanner, B. L. One-step inactivation of chromosomal genes in *Escherichia coli* K-12 using PCR products. *Proc. Natl. Acad. Sci. U. S. A.* **97**, 6640–5 (2000).

43. Sharan, S. K., Thomason, L. C., Kuznetsov, S. G. & Court, D. L. Recombineering: a homologous recombination-based method of genetic engineering. *Nat. Protoc.* **4**, 206–223 (2009).

44. Englaender, J. A. *et al.* Effect of Genomic Integration Location on Heterologous Protein Expression and Metabolic Engineering in *E. coli*. *ACS Synth. Biol.* **6**, 710–720 (2017).

45. Juhas, M. *et al. Escherichia coli* Flagellar Genes as Target Sites for Integration and Expression of Genetic Circuits. *PLoS One* **9**, e111451 (2014).

46. Grindley, N. D. F., Whiteson, K. L. & Rice, P. A. Mechanisms of Site-Specific Recombination. *Annu. Rev. Biochem.* **75**, 567–605 (2006).

47. Del Vecchio, D. Modularity, context-dependence, and insulation in engineered biological circuits. *Trends Biotechnol.* **33**, 111–119 (2015).

48. Müller-Hill, B. *The lac operon: A short history of a genetic paradigm*. (DE GRUYTER, 2011). doi:10.1515/9783110879476

49. Schleif, R. AraC protein, regulation of the l-arabinose operon in *Escherichia coli*, and the light switch mechanism of AraC action. *FEMS Microbiology Reviews* **34**, 779–796 (2010).

50. Bertram, R. & Hillen, W. The application of Tet repressor in prokaryotic gene regulation and expression. *Microb. Biotechnol.* **1**, 2–16 (2008).

51. Slusarczyk, A. L., Lin, A. & Weiss, R. Foundations for the design and implementation of synthetic genetic circuits. *Nature Reviews Genetics* **13**, 406–420 (2012).

52. Gao, Y. *et al.* Complex transcriptional modulation with orthogonal and inducible dCas9 regulators. *Nat. Methods* **13**, 1043–1049 (2016).

53. Chappell, J., Takahashi, M. K. & Lucks, J. B. Creating small transcription activating RNAs. *Nat. Chem. Biol.* **11**, 214–220 (2015).

54. Westbrook, A. M. & Lucks, J. B. Achieving large dynamic range control of gene expression with a compact RNA transcription–translation regulator. *Nucleic Acids Res.* **45**, 5614–5624 (2017).

55. Lonetto, M. A., Brown, K. L., Rudd, K. E. & Buttner, M. J. Analysis of the *Streptomyces coelicolor* sigE gene reveals the existence of a subfamily of eubacterial RNA polymerase sigma factors involved in the regulation of extracytoplasmic functions. *Proc. Natl. Acad. Sci. U. S. A.* **91**, 7573–7 (1994).

56. Sineva, E., Savkina, M. & Ades, S. E. Themes and variations in gene regulation by extracytoplasmic function (ECF) sigma factors. *Curr. Opin. Microbiol.* **36**, 128–137 (2017).

57. Feklístov, A., Sharon, B. D., Darst, S. A. & Gross, C. A. Bacterial Sigma Factors: A Historical, Structural, and Genomic Perspective. *Annu. Rev. Microbiol.* **68**, 357–376 (2014).

58. Campagne, S., Marsh, M. E., Capitani, G., Vorholt, J. A. & Allain, F. H.-T. Structural basis for −10 promoter element melting by environmentally induced sigma factors. *Nat. Struct. Mol. Biol.* **21**, 269–276 (2014).

59. Staroń, A. *et al.* The third pillar of bacterial signal transduction: classification of the extracytoplasmic function (ECF) σ factor protein family. *Mol. Microbiol.* **74**, 557–581 (2009).

60. Jogler, C. *et al.* Identification of Proteins Likely To Be Involved in Morphogenesis, Cell Division, and Signal Transduction in Planctomycetes by Comparative Genomics. *J. Bacteriol.* **194**, 6419–6430 (2012).

61. Huang, X., Pinto, D., Fritz, G. & Mascher, T. Environmental Sensing in Actinobacteria: a Comprehensive Survey on the Signaling Capacity of This Phylum. *J. Bacteriol.* **197**, 2517–2535 (2015).

62. Pinto, D. & Mascher, T. The ECF Classification: A Phylogenetic Reflection of the Regulatory Diversity in the Extracytoplasmic Function σ Factor Protein Family. in *Stress and Environmental Regulation of Gene Expression and Adaptation in Bacteria* 64–96 (John Wiley & Sons, Inc., 2016). doi:10.1002/9781119004813.ch7

63. Rhodius, V. A. *et al.* Design of orthogonal genetic switches based on a crosstalk map of σ, anti-σ, and promoters. *Mol. Syst. Biol.* **9**, 702–702 (2013).

64. Zong, Y. *et al.* Insulated transcriptional elements enable precise design of genetic circuits. *Nat. Commun.* **8**, 52 (2017).

65. Chen, D. & Arkin, A. P. Sequestration-based bistability enables tuning of the switching boundaries and design of a latch. *Mol. Syst. Biol.* **8**, 620 (2012).

66. Wu, H. *et al.* The role of C-terminal extensions in controlling ECF σ factor activity in the widely conserved groups ECF41 and ECF42. *Mol. Microbiol.* (2019). doi:10.1111/mmi.14261

67. Campbell, E. A. *et al.* A conserved structural module regulates transcriptional responses to diverse stress signals in bacteria. *Mol. Cell* **27**, 793–805 (2007).

68. Mascher, T. Signaling diversity and evolution of extracytoplasmic function (ECF) σ factors. *Curr. Opin. Microbiol.* **16**, 148–155 (2013).

69. Ho, T. D. & Ellermeier, C. D. Extra cytoplasmic function σ factor activation. *Curr. Opin. Microbiol.* **15**, 182–188 (2012).

70. Chaba, R., Grigorova, I. L., Flynn, J. M., Baker, T. A. & Gross, C. A. Design principles of the proteolytic cascade governing the E-mediated envelope stress response in *Escherichia coli*: keys to graded, buffered, and rapid signal transduction. *Genes Dev.* **21**, 124–136 (2007).

71. Heinrich, J. & Wiegert, T. Regulated intramembrane proteolysis in the control of extracytoplasmic function sigma factors. *Res. Microbiol.* **160**, 696–703 (2009).

72. Braun, V. & Mahren, S. Transmembrane transcriptional control (surface signalling) of the *Escherichia coli* Fec type. *FEMS Microbiol. Rev.* **29**, 673–684 (2005).

73. Mettrick, K. A. & Lamont, I. L. Different roles for anti-sigma factors in siderophore signalling pathways of *Pseudomonas aeruginosa*. *Mol. Microbiol.* **74**, 1257–1271 (2009).

74. Trepreau, J. *et al.* Spectroscopic Characterization of the Metal-Binding Sites in the Periplasmic Metal-Sensor Domain of CnrX from *Cupriavidus metallidurans* CH34. *Biochemistry* **50**, 9036–9045 (2011).

75. Li, W. *et al.* Identification and Structure of the Anti-sigma Factor-binding Domain of the Disulphide-stress Regulated Sigma Factor σR from *Streptomyces coelicolor*. *J. Mol. Biol.* **323**, 225–236 (2002).

76. Greenwell, R., Nam, T.-W. & Donohue, T. J. Features of *Rhodobacter sphaeroides* ChrR Required for Stimuli to Promote the Dissociation of σE/ChrR Complexes. *J. Mol. Biol.* **407**, 477–491 (2011).

77. Francez-Charlot, A. *et al.* Sigma factor mimicry involved in regulation of general stress response. *Proc. Natl. Acad. Sci.* **106**, 3467–3472 (2009).

78. Herrou, J., Foreman, R., Fiebig, A. & Crosson, S. A structural model of anti-anti-σ inhibition by a two-component receiver domain: the PhyR stress response regulator. *Mol. Microbiol.* **78**, 290–304 (2010).

79. Gruber, T. M. & Gross, C. A. Multiple sigma subunits and the partitioning of bacterial transcription space. *Annu. Rev. Microbiol.* **57**, 441–66 (2003).

80. Kogenaru, M. & Tans, S. J. An improved *Escherichia coli* strain to host gene regulatory networks involving both the AraC and LacI inducible transcription factors. *J. Biol. Eng.* **8**, 2 (2014).

81. Siegele, D. A. & Hu, J. C. Gene expression from plasmids containing the *araBAD* promoter at subsaturating inducer concentrations represents mixed populations. *Proc. Natl. Acad. Sci. U. S. A.* **94**, 8168–72 (1997).

82. Fritz, G. *et al.* Single Cell Kinetics of Phenotypic Switching in the Arabinose Utilization System of *E. coli*. *PLoS One* **9**, e89532 (2014).

83. Khlebnikov, A., Datsenko, K. A., Skaug, T., Wanner, B. L. & Keasling, J. D. Homogeneous expression of the PBAD promoter in *Escherichia coli* by constitutive expression of the low-affinity high-capacity araE transporter. *Microbiology* **147**, 3241–3247 (2001).

84. Sternberg, N. & Hamilton, D. Bacteriophage P1 site-specific recombination. I. Recombination between *loxP* sites. *J. Mol. Biol.* **150**, 467–486 (1981).

85. Chavez, M., Ho, J. & Tan, C. Reproducibility of High-Throughput Plate-Reader Experiments in Synthetic Biology. *ACS Synth. Biol.* **6**, 375–380 (2017).

86. Mihalcescu, I., Van-Melle Gateau, M., Chelli, B., Pinel, C. & Ravanat, J.-L. Green autofluorescence, a double edged monitoring tool for bacterial growth and activity in micro-plates. *Phys. Biol.* **12**, 066016 (2015).

87. Surre, J. *et al.* Strong increase in the autofluorescence of cells signals struggle for survival. *Sci. Rep.* **8**, 12088 (2018).

88. Meighen, E. A. Bacterial bioluminescence: organization, regulation, and application of the *lux* genes. *FASEB J.* **7**, 1016–22 (1993).

89. Meighen, E. A. Molecular biology of bacterial bioluminescence. *Microbiol. Rev.* **55**, 123–42 (1991).

90. Craney, A. *et al.* A synthetic *luxCDABE* gene cluster optimized for expression in high-GC bacteria. *Nucleic Acids Res.* **35**, e46 (2007).

91. Uliczka, F. *et al.* Monitoring of Gene Expression in Bacteria during Infections Using an Adaptable Set of Bioluminescent, Fluorescent and Colorigenic Fusion Vectors. *PLoS One* **6**, e20425 (2011).

92. Sunya, S., Gorret, N., Delvigne, F., Uribelarrea, J.-L. & Molina-Jouve, C. Real-time monitoring of metabolic shift and transcriptional induction of *yciG::luxCDABE E. coli* reporter strain to a glucose pulse of different concentrations. *J. Biotechnol.* **157**, 379–390 (2012).

93. Close, D. *et al.* The Evolution of the Bacterial Luciferase Gene Cassette (*lux*) as a Real-Time Bioreporter. *Sensors* **12**, 732–752 (2012).

94. Benedetti, I. M., de Lorenzo, V. & Silva-Rocha, R. Quantitative, Non-Disruptive Monitoring of Transcription in Single Cells with a Broad-Host Range GFP-luxCDABE Dual Reporter System. *PLoS One* **7**, e52000 (2012).

95. Bozcal, E., Dagdeviren, M., Uzel, A. & Skurnik, M. *luxCDE-luxAB*-based promoter reporter system to monitor the *Yersinia enterocolitica O:3* gene expression in vivo. *PLoS One* **12**, e0172877 (2017).

96. Bisicchia, P., Botella, E. & Devine, K. M. Suite of novel vectors for ectopic insertion of GFP, CFP and IYFP transcriptional fusions in single copy at the *amyE* and *bglS* loci in *Bacillus subtilis*. *Plasmid* **64**, 143–149 (2010).

97. Gödeke, J., Heun, M., Bubendorfer, S., Paul, K. & Thormann, K. M. Roles of Two *Shewanella oneidensis* MR-1 Extracellular Endonucleases. *Appl. Environ. Microbiol.* **77**, 5342–5351 (2011).

98. Mazo-Vargas, A., Park, H., Aydin, M. & Buchler, N. E. Measuring fast gene dynamics in single cells with time-lapse luminescence microscopy. *Mol. Biol. Cell* **25**, 3699–3708 (2014).

99. Abelson, J. N., Simon, M. I., Ziegler, M. M., and Baldwin, T. O. *Bioluminescence and chemiluminescence*. (Elsevier Ltd, 2000).

100. Kishony, R. & Leibler, S. Environmental stresses can alleviate the average deleterious effect of mutations. *J. Biol.* **2**, 14 (2003).

101. Aspelmeier, T., Egner, A. & Munk, A. Modern Statistical Challenges in High-Resolution Fluorescence Microscopy. *Annu. Rev. Stat. Its Appl.* **2**, 163–202 (2015).

102. Smith, S. W. *The Scientist and Engineer's Guide to Digital Signal Processing* (California Technical Publishing San Diego, CA, USA 1999). doi:10.1007/BF02834636

103. Wang, Z., Xiang, L., Shao, J., Wegrzyn, A. & Wegrzyn, G. Effects of the presence of ColE1 plasmid DNA in *Escherichia coli* on the host cell metabolism. *Microb. Cell Fact.* **5**, 34 (2006).

104. Boyd, D., Weiss, D. S., Chen, J. C. & Beckwith, J. Towards Single-Copy Gene Expression Systems Making Gene Cloning Physiologically Relevant: Lambda InCh, a Simple *Escherichia coli* Plasmid-Chromosome Shuttle System. *J. Bacteriol.* **182**, 842–847 (2000).

105. Metcalf, W. W., Jiang, W. & Wanner, B. L. Use of the rep technique for allele replacement to construct new *Escherichia coli* hosts for maintenance of R6K gamma origin plasmids at different copy numbers. *Gene* **138**, 1–7 (1994).

106. Chung, C. T., Niemela, S. L. & Miller, R. H. One-step preparation of competent *Escherichia coli*: transformation and storage of bacterial cells in the same solution. *Proc. Natl. Acad. Sci. U. S. A.* **86**, 2172–5 (1989).

107. Sobetzko, P. Transcription-coupled DNA supercoiling dictates the chromosomal arrangement of bacterial genes. *Nucleic Acids Res.* **44**, 1514–1524 (2016).

108. Guzman, L. M., Belin, D., Carson, M. J. & Beckwith, J. Tight regulation, modulation, and high-level expression by vectors containing the arabinose PBAD promoter. *J. Bacteriol.* **177**, 4121–30 (1995).

109. Chalmers, R., Sewitz, S., Lipkow, K. & Crellin, P. Complete nucleotide sequence of Tn10. *J. Bacteriol.* **182**, 2970–2972 (2000).

110. Lutz, R. & Bujard, H. Independent and tight regulation of transcriptional units in *Escherichia coli* via the LacR/O, the TetR/O and AraC/I1-I2 regulatory elements. *Nucleic Acids Res.* **25**, 1203–10 (1997).

111. Luis Vellanoweth, R. & Rabinowitz, J. C. The influence of ribosome-binding-site elements on translational efficiency in *Bacillus subtilis* and *Escherichia coli in vivo*. *Molecular Microbiology* **6**, (1992).

112. Chen, Y. *et al.* Characterization of 582 natural and synthetic terminators and quantification of their design constraints. *Nat. Methods* **10**, 659–664 (2013).

113. Kuchina, A., Espinar, L., Garcia-Ojalvo, J. & Süel, G. M. Reversible and noisy progression towards a commitment point enables adaptable and reliable cellular Decision-Making. *PLoS Comput. Biol.* **7**, (2011).

114. Goedhart, J. *et al.* Structure-guided evolution of cyan fluorescent proteins towards a quantum yield of 93%. *Nat. Commun.* **3**, 751 (2012).

115. Nguyen, T. N., Phan, Q. G., Duong, L. P., Bertrand, K. P. & Lenski, R. E. Effects of carriage and expression of the Tn10 tetracycline-resistance operon on the fitness of *Escherichia coli* K12. *Mol. Biol. Evol.* **6**, 213–25 (1989).

116. Berens, C. & Hillen, W. Gene regulation by tetracyclines. Constraints of resistance regulation in bacteria shape TetR for application in eukaryotes. *Eur. J. Biochem.* **270**, 3109–3121 (2003).

117. Muthukrishnan, A.-B. B. *et al.* Dynamics of transcription driven by the *tetA* promoter, one event at a time, in live *Escherichia coli* cells. *Nucleic Acids Res.* **40**, 8472–8483 (2012).

118. Schleif, R. Regulation of the *L-arabinose* operon of *Escherichia coli*. *Trends in Genetics* **16**, 559–565 (2000).

119. Chen, D. & Lilley, D. M. J. Transcription-induced hypersupercoiling of plasmid DNA. *J. Mol. Biol.* **285**, 443–448 (1999).

120. Samul, R. & Leng, F. Transcription-coupled Hypernegative Supercoiling of Plasmid DNA by T7 RNA Polymerase in *Escherichia coli* Topoisomerase I-Deficient Strains. *J. Mol. Biol.* **374**, 925–935 (2007).

121. Miller, J. *Experiments in Molecular Genetics*. (Cold Spring Harbor protocols, 1972).

122. Sleight, S. C., Bartley, B. A., Lieviant, J. A. & Sauro, H. M. Designing and engineering evolutionary robust genetic circuits. *J. Biol. Eng.* **4**, 12 (2010).

123. Watt, V. M., Ingles, C. J., Urdea, M. S. & Rutter, W. J. Homology requirements for recombination in *Escherichia coli*. *Proc. Natl. Acad. Sci.* **82**, 4768–4772 (1985).

124. Toymentseva, A. A., Schrecke, K., Sharipova, M. R. & Mascher, T. The LIKE system, a novel protein expression toolbox for *Bacillus subtilis* based on the *liaI* promoter. *Microb. Cell Fact.* (2012). doi:10.1186/1475-2859-11-143

125. Pinto, D. *et al.* Engineering orthogonal synthetic timer circuits based on extracytoplasmic function σ factors. *Nucleic Acids Res.* **46**, 7450–7464 (2018).

126. Buchler, N. E. & Cross, F. R. Protein sequestration generates a flexible ultrasensitive response in a genetic network. *Mol. Syst. Biol.* **5**, 272 (2009).

127. Fimlaid, K. A. & Shen, A. Diverse mechanisms regulate sporulation sigma factor activity in the Firmicutes. *Current Opinion in Microbiology* **24**, 88–95 (2015).

128. Drew, D., Fröderberg, L., Baars, L. & De Gier, J. W. L. Assembly and overexpression of membrane proteins in *Escherichia coli*. *Biochimica et Biophysica Acta - Biomembranes* **1610**, 3–10 (2003).

129. Drozdetskiy, A., Cole, C., Procter, J. & Barton, G. J. JPred4: A protein secondary structure prediction server. *Nucleic Acids Res.* **43**, W389–W394 (2015).

130. Tsirigos, K. D., Peters, C., Shu, N., Käll, L. & Elofsson, A. The TOPCONS web server for consensus prediction of membrane protein topology and signal peptides. *Nucleic Acids Res.* **43**, W401–W407 (2015).

131. Hopp, T. P. *et al.* A Short Polypeptide Marker Sequence Useful for Recombinant Protein Identification and Purification. *Bio/Technology* **6**, 1204–1210 (1988).

132. Pasotti, L., Zucca, S., Lupotto, M., Cusella De Angelis, M. G. & Magni, P. Characterization of a synthetic bacterial self-destruction device for programmed cell death and for recombinant proteins release. *J. Biol. Eng.* **5**, 8 (2011).

133. Lin, Z. & Cai, Z. Cell lysis methods for high-throughput screening or miniaturized assays. *Biotechnology Journal* **4**, 210–215 (2009).

134. Bahassi, E. M. *et al.* Interactions of CcdB with DNA: Gyrase in activation of GyrA, poisoning of the gyrase-DNA complex, and the antidote action of CdcA. *J. Biol. Chem.* **274**, 10936–10944 (1999).

135. Bernard, P. *et al.* The F plasmid CcdB protein induces efficient ATP-dependent DNA cleavage by gyrase. *J. Mol. Biol.* **234**, 534–541 (1993).

136. Rudge, T. J. *et al.* Characterization of Intrinsic Properties of Promoters. *ACS Synth. Biol.* **5**, 89–98 (2016).

137. Juhas, M. & Ajioka, J. W. Identification and Validation of Novel Chromosomal Integration and Expression Loci in *Escherichia coli* Flagellar Region 1. *PLoS One* **10**, e0123007 (2015).

138. Liu, Q., Schumacher, J., Wan, X., Lou, C. & Wang, B. Orthogonality and Burdens of Heterologous and Gate Gene Circuits in *E. coli*. *ACS Synth. Biol.* **7**, 553–564 (2018).

139. Engler, C. *et al.* A Golden Gate modular cloning toolbox for plants. *ACS Synth. Biol.* **3**, 839–843 (2014).

140. de la Torre, J. C. *et al.* Plasmid vectors based on Tn10 DNA: Gene expression regulated by tetracycline. *Plasmid* **12**, 103–110 (1984).

141. Stanton, B. C. *et al.* Genomic mining of prokaryotic repressors for orthogonal logic gates. *Nat. Chem. Biol.* **10**, 99–105 (2014).

142. Chen, Y. *et al.* Tuning the dynamic range of bacterial promoters regulated by ligand-inducible transcription factors. *Nat. Commun.* **9**, (2018).

143. Gupta, A., Reizman, I. M. B., Reisch, C. R. & Prather, K. L. J. Dynamic regulation of metabolic flux in engineered bacteria using a pathway-independent quorum-sensing circuit. *Nat. Biotechnol.* **35**, 273–279 (2017).

144. Weber, W. *et al.* A synthetic time-delay circuit in mammalian cells and mice. *Proc. Natl. Acad. Sci.* **104**, 2643–2648 (2007).

145. Ferrell, J. E. & Ha, S. H. Ultrasensitivity part III: Cascades, bistable switches, and oscillators. *Trends in Biochemical Sciences* **39**, 612–618 (2014).

146. Brophy, J. A. N. & Voigt, C. A. Principles of genetic circuit design. *Nature Methods* **11**, 508–520 (2014).

147. Legewie, S., Dienst, D., Wilde, A., Herzel, H. & Axmann, I. M. Small RNAs establish delays and temporal thresholds in gene expression. *Biophys. J.* **95**, 3232–8 (2008).

148. Levine, E., Zhang, Z., Kuhlman, T. & Hwa, T. Quantitative characteristics of gene regulation by small RNA. *PLoS Biol.* **5**, 1998–2010 (2007).

149. Lu, M. S., Mauser, J. F. & Prehoda, K. E. Ultrasensitive synthetic protein regulatory networks using mixed decoys. *ACS Synth. Biol.* **1**, 65–72 (2012).

150. Sneppen, K. *Models of Life*. (Cambridge University Press, 2014). doi:10.1017/CBO9781107449442

151. Shopera, T., Henson, W. R. & Moon, T. S. Dynamics of sequestration-based gene regulatory cascades. *Nucleic Acids Res.* **45**, 7515–7526 (2017).

152. Hooshangi, S., Thiberge, S. & Weiss, R. Ultrasensitivity and noise propagation in a synthetic transcriptional cascade. *Proc. Natl. Acad. Sci.* **102**, 3581–3586 (2005).

153. Kleiner-Grote, G. R. M., Risse, J. M. & Friehs, K. Secretion of recombinant proteins from *E. coli*. *Engineering in Life Sciences* **18**, 532–550 (2018).

154. Yun, J., Park, J., Park, N., Kang, S. & Ryu, S. Development of a novel vector system for programmed cell lysis in *Escherichia coli*. *J. Microbiol. Biotechnol.* **17**, 1162–1168 (2007).

155. Morita, M., Asami, K., Tanji, Y. & Unno, H. Programmed *Escherichia coli* cell lysis by expression of cloned T4 phage lysis genes. *Biotechnol. Prog.* **17**, 573–576 (2001).

156. Coleman, J., Inouye, M. & Atkins, J. Bacteriophage MS2 lysis protein does not require coat protein to mediate cell lysis. *J. Bacteriol.* **153**, 1098–1100 (1983).

157. Kaplan, J. B., Ragunath, C., Ramasubbu, N. & Fine, D. H. Detachment of *Actinobacillus actinomycetemcomitans* biofilm cells by an endogenous β-hexosaminidase activity. *J. Bacteriol.* **185**, 4693–4698 (2003).

158. Zambon, J. J. *Actinobacillus actinomycetemcomitans* in human periodontal disease. *Journal of Clinical Periodontology* **12**, 1–20 (1985).

159. Baker, P. *et al.* Exopolysaccharide biosynthetic glycoside hydrolases can be utilized to disrupt and prevent *Pseudomonas aeruginosa* biofilms. *Sci. Adv.* **2**, e1501632 (2016).

160. Singh, V. *et al.* Enzymatic degradation of bacterial biofilms using *Aspergillus clavatus* MTCC 1323. *Microbiology* **84**, 59–64 (2015).

161. Schober, L. *et al.* Cell Dispensing in Low-Volume Range with the Immediate Drop-on-Demand Technology (I-DOT). *J. Lab. Autom.* **20**, 154–163 (2015).

162. Jessop-Fabre, M. M. & Sonnenschein, N. Improving Reproducibility in Synthetic Biology. *Front. Bioeng. Biotechnol.* **7**, (2019).

163. Im, H. The Inoue Method for Preparation and Transformation of Competent *E. coli*: 'Ultra Competent' Cells. *BIO-PROTOCOL* **1**, 1–7 (2011).

164. Marx, C. J. & Lidstrom, M. E. Broad-Host-Range cre-lox System for Antibiotic Marker Recycling in Gram-Negative Bacteria. *Biotechniques* **33**, 1062–1067 (2002).

9. Appendix

9.1 Bacterial strains and plasmids used in this study

***E. coli* strains**				
Name	Genotype	Resistance	Reference	Description
DH5α	F- Φ80*lacZ*ΔM15 Δ(*lacZYA-argF*) U169 *recA1 endA1 hsdR17* (rK-, mK+) *phoA supE44 thi-1 gyrA96 relA1* λ-	Nal^R	Grant et al., 1990	cloning strain
DH5α λpir	*cf.* DH5α, λ+	Nal^R	Miller and Mekalanos, 1988	cloning strain
MK01	MG1655 *rph-1*, λ-, Δ(*araD-araB*)*567*, Δ*lacZ4787*(::rrnB-3), Δ(*araH-araF*)570(::FRT), Δ*araEp*-532(::FRT), φP_{cp8}*araE535*, Δ(*rhaD-rhaB*)568, *hsdR514*, Δ*lacI*(::*cat*)	Cm^R	Kogenaru and Tans, 2014	reporter strain
SV01	MG1655 *rph-1*, λ-, Δ(*araD-araB*)*567*, Δ*lacZ4787*(::rrnB-3), Δ(*araH-araF*)570(::FRT), Δ*araEp*-532(::FRT), φP_{cp8}*araE535*, Δ(*rhaD-rhaB*)568, *hsdR514*, Δ*lacI*(::Lox)	-	This study	reporter strain
DB3.1	F- *gyrA462 endA1* Δ(*sr1-recA*) *mcrB mrr hsdS20*(rB-, mB-) *supE44 ara-14 galK2 lacY1 proA2 rpsL20*(SmR) *xyl-5* λ- *leu mtl1*	Str^R	Bernard *et al*., 1993	cloning strain
GFC0089	*cf.*SV01 + pSVM-mc_074	Km^R	This study	Insulator test construct
GFC0117	*cf.*SV01 + pSVM-mc_095	Km^R	This study	Insulator test construct
GFC0119	*cf.*SV01 + pSVM-mc_097	Km^R	This study	Insulator test construct
GFC0132	*cf.*SV01 + pSVM-mc_111	Km^R	This study	ECF 28-switch/1-step timer
GFC0133	*cf.*SV01 + pSVM-mc_112	Km^R	This study	ECF 32-switch/1-step timer
GFC0134	*cf.*SV01 + pSVM-mc_113	Km^R	This study	Insulator test construct
GFC0136	*cf.*SV01 + pSVM-mc_115	Km^R	This study	ECF switch neg. control
GFC0137	*cf.*SV01 + pSVM-mc_116	Km^R	This study	ECF switch neg. control
GFC0138	*cf.*SV01 + pSVM-mc_117	Km^R	This study	2-step timer *ecf28* P*ecf32*
GFC0139	*cf.*SV01 + pSVM-mc_118	Km^R	This study	2-step timer *ecf32* P*ecf28*
GFC0141	*cf.*SV01 + pSVM-mc_120	Km^R	This study	2-step timer *ecf28* neg. control
GFC0143	*cf.*SV01 + pSVM-mc_122	Km^R	This study	2-step timer *ecf32* neg. control
GFC0153	*cf.*SV01 + pSVM-mc_038	Km^R	This study	P*BAD-lux* reporter construct
GFC0155	*cf.*SV01 + pSVM-mc_133	Km^R	This study	ECF/AS14 circuit
GFC0156	*cf.*SV01 + pSVM-mc_134	Km^R	This study	ECF/AS15 circuit
GFC0157	*cf.*SV01 + pSVM-mc_135	Km^R	This study	ECF/AS16 circuit
GFC0158	*cf.*SV01 + pSVM-mc_136	Km^R	This study	ECF/AS17 circuit
GFC0159	*cf.*SV01 + pSVM-mc_137	Km^R	This study	ECF/AS20 circuit

GFC0160	*cf.*SV01 + pSVM-mc_138	Km^R	This study	ECF/AS22 circuit
GFC0161	*cf.*SV01 + pSVM-mc_139	Km^R	This study	ECF/AS26 circuit
GFC0162	*cf.*SV01 + pSVM-mc_140	Km^R	This study	ECF/AS27 circuit
GFC0163	*cf.*SV01 + pSVM-mc_141	Km^R	This study	ECF/AS28 circuit
GFC0164	*cf.*SV01 + pSVM-mc_142	Km^R	This study	ECF/AS31 circuit
GFC0165	*cf.*SV01 + pSVM-mc_143	Km^R	This study	ECF/AS34 circuit
GFC0166	*cf.*SV01 + pSVM-mc_144	Km^R	This study	ECF/AS37 circuit
GFC0167	*cf.*SV01 + pSVM-mc_145	Km^R	This study	ECF/AS38 circuit
GFC0168	*cf.*SV01 + pSVM-mc_146	Km^R	This study	ECF 14-switch
GFC0169	*cf.*SV01 + pSVM-mc_147	Km^R	This study	ECF 15-switch
GFC0170	*cf.*SV01 + pSVM-mc_148	Km^R	This study	ECF 16-switch
GFC0171	*cf.*SV01 + pSVM-mc_149	Km^R	This study	ECF 17-switch
GFC0172	*cf.*SV01 + pSVM-mc_150	Km^R	This study	ECF 20-switch
GFC0172	*cf.*SV01 + pSVM-mc_151	Km^R	This study	ECF 22-switch
GFC0173	*cf.*SV01 + pSVM-mc_152	Km^R	This study	ECF 26-switch
GFC0175	*cf.*SV01 + pSVM-mc_153	Km^R	This study	ECF 27-switch
GFC0176	*cf.*SV01 + pSVM-mc_154	Km^R	This study	ECF 31-switch
GFC0177	*cf.*SV01 + pSVM-mc_155	Km^R	This study	ECF 34-switch
GFC0178	*cf.*SV01 + pSVM-mc_156	Km^R	This study	ECF 37-switch
GFC0180	*cf.*SV01 + pADM-mc_160	Km^R	This study	ECF14/AS14 t1-switch
GFC0181	*cf.*SV01 + pADM-mc_161	Km^R	This study	ECF14/AS14 t2-switch
GFC0182	*cf.*SV01 + pADM-mc_162	Km^R	This study	ECF17/AS17 t-switch
GFC0183	*cf.*SV01 + pADM-mc_163	Km^R	This study	ECF20/AS20 t1-switch
GFC0184	*cf.*SV01 + pADM-mc_164	Km^R	This study	ECF20/AS20 t2-switch
GFC0185	*cf.*SV01 + pADM-mc_165	Km^R	This study	ECF22/AS22 t-switch
GFC0186	*cf.*SV01 + pADM-mc_166	Km^R	This study	ECF26/AS26 t1-switch
GFC0187	*cf.*SV01 + pADM-mc_167	Km^R	This study	ECF26/AS26 t2-switch
GFC0188	*cf.*SV01 + pADM-mc_171	Km^R	This study	ECF28/AS28 t1-switch
GFC0189	*cf.*SV01 + pADM-mc_172	Km^R	This study	ECF28/AS28 t2-switch
GFC0191	*cf.*SV01 + pADM-mc_169	Km^R	This study	ECF27/AS27 t1-switch
GFC0192	*cf.*SV01 + pADM-mc_170	Km^R	This study	ECF27/AS27 t2-switch
GFC0193	*cf.*SV01 + pADM-mc_173	Km^R	This study	ECF31/AS31 t1-switch
GFC0194	*cf.*SV01 + pADM-mc_174	Km^R	This study	ECF34/AS34 t1-switch
GFC0195	*cf.*SV01 + pADM-mc_175	Km^R	This study	ECF34/AS34 t2-switch
GFC0196	*cf.*SV01 + pADM-mc_176	Km^R	This study	ECF37/AS37 t1-switch
GFC0197	*cf.*SV01 + pADM-mc_177	Km^R	This study	ECF37/AS37 t2-switch
GFC0198	*cf.*SV01 + pADM-mc_178	Km^R	This study	ECF38/AS38 t1-switch

GFC0199	*cf.*SV01 + pADM-mc_179	Km^R	This study	ECF31/AS31 t2-switch
GFC0200	*cf.*SV01 + pSVM-mc_180	Km^R	This study	P*tet-lux* reporter construct
GFC0202	*cf.*SV01 + pSVM-mc_157	Km^R	This study	ECF 38-switch
GFC0214	*cf.*SV01, P_{BAD}*lux*::HK022	Cm^R	This study	Reporter construct (ch int.)
GFC0216	*cf.*SV01, P_{BAD}*lux*::P21	Cm^R	This study	Reporter construct (ch int.)
GFC0218	*cf.*SV01, P_{BAD}*lux*::φ80	Cm^R	This study	Reporter construct (ch int.)
GFC0219	*cf.*SV01 + pSVM-mc_182	Km^R	This study	ECF 11-switch
GFC0220	*cf.*SV01 + pSVM-mc_183	Km^R	This study	ECF/AS11 circuit
GFC0221	*cf.*SV01 + pSVM-mc_184	Km^R	This study	ECF11/AS11 t1-switch
GFC0222	*cf.*SV01 + pSVM-mc_185	Km^R	This study	ECF11/AS11 t2-switch
GFC0235	*cf.*SV01, P_{BAD}-*ecf11* P_{ecf11}-*lux* P_{tet}-*as11 t1*::HK022	Cm^R	This study	ECF11/AS11 t1-switch (ch. int.)
GFC0236	*cf.*SV01, P_{BAD}-*ecf11* P_{ecf11}-*lux* P_{tet}-*as11 t2*::HK022	Cm^R	This study	ECF11/AS11 t2-switch (ch. int.)
GFC0237	*cf.*SV01, P_{BAD}-*ecf14* P_{ecf12}-*lux* P_{tet}-*as14 t1*::HK022	Cm^R	This study	ECF14/AS14 t1-switch (ch. int.)
GFC0238	*cf.*SV01, P_{BAD}-*ecf14* P_{ecf12}-*lux* P_{tet}-*as14 t2*::HK022	Cm^R	This study	ECF14/AS14 t2-switch (ch. int.)
GFC0239	*cf.*SV01, P_{BAD}-*ecf15* P_{ecf15}-*lux* P_{tet}-*as15*::HK022	Cm^R	This study	ECF15/AS15-switch (ch. int.)
GFC0240	*cf.*SV01, P_{BAD}-*ecf16* P_{ecf16}-*lux* P_{tet}-*as16*::HK022	Cm^R	This study	ECF16/AS16-switch (ch. int.)
GFC0241	*cf.*SV01, P_{BAD}-*ecf17* P_{ecf17}-*lux* P_{tet}-*as17 t*::HK022	Cm^R	This study	ECF17/AS17 t1-switch (ch. int.)
GFC0243	*cf.*SV01, P_{BAD}-*ecf20* P_{ecf20}-*lux* P_{tet}-*as20 t1*::HK022	Cm^R	This study	ECF20/AS20 t1-switch (ch. int.)
GFC0244	*cf.*SV01, P_{BAD}-*ecf20* P_{ecf20}-*lux* P_{tet}-*as20 t2*::HK022	Cm^R	This study	ECF20/AS20 t2-switch (ch. int.)
GFC0245	*cf.*SV01, P_{BAD}-*ecf22* P_{ecf22}-*lux* P_{tet}-*as22 t*::HK022	Cm^R	This study	ECF22/AS22 t1-switch (ch. int.)
GFC0246	*cf.*SV01, P_{BAD}-*ecf26* P_{ecf26}-*lux* P_{tet}-*as26 t1*::HK022	Cm^R	This study	ECF26/AS26 t1-switch (ch. int.)
GFC0247	*cf.*SV01, P_{BAD}-*ecf26* P_{ecf26}-*lux* P_{tet}-*as26 t2*::HK022	Cm^R	This study	ECF26/AS26 t2-switch (ch. int.)
GFC0248	*cf.*SV01, P_{BAD}-*ecf27* P_{ecf25}-*lux* P_{tet}-*as27 t1*::HK022	Cm^R	This study	ECF27/AS27 t1-switch (ch. int.)
GFC0249	*cf.*SV01, P_{BAD}-*ecf27* P_{ecf25}-*lux* P_{tet}-*as27 t2*::HK022	Cm^R	This study	ECF27/AS27 t2-switch (ch. int.)
GFC0250	*cf.*SV01, P_{BAD}-*ecf28* P_{ecf19}-*lux* P_{tet}-*as28 t1*::HK022	Cm^R	This study	ECF28/AS28 t1-switch (ch. int.)
GFC0251	*cf.*SV01, P_{BAD}-*ecf28* P_{ecf19}-*lux* P_{tet}-*as28 t2*::HK022	Cm^R	This study	ECF28/AS28 t2-switch (ch. int.)
GFC0252	*cf.*SV01, P_{BAD}-*ecf31* P_{ecf31}-*lux* P_{tet}-*as31 t1*::HK022	Cm^R	This study	ECF31/AS31 t1-switch (ch. int.)
GFC0253	*cf.*SV01, P_{BAD}-*ecf31* P_{ecf31}-*lux* P_{tet}-*as31 t2*::HK022	Cm^R	This study	ECF31/AS31 t2-switch (ch. int.)
GFC0254	*cf.*SV01, P_{BAD}-*ecf34* P_{ecf18}-*lux* P_{tet}-*as34 t1*::HK022	Cm^R	This study	ECF34/AS34 t1-switch (ch. int.)
GFC0255	*cf.*SV01, P_{BAD}-*ecf34* P_{ecf18}-*lux* P_{tet}-*as34 t2*::HK022	Cm^R	This study	ECF34/AS34 t2-switch (ch. int.)
GFC0256	*cf.*SV01, P_{BAD}-*ecf37* P_{ecf39}-*lux* P_{tet}-*as37 t1*::HK022	Cm^R	This study	ECF37/AS37 t1-switch (ch. int.)
GFC0257	*cf.*SV01, P_{BAD}-*ecf37* P_{ecf39}-*lux* P_{tet}-*as37 t2*::HK022	Cm^R	This study	ECF37/AS37 t2-switch (ch. int.)
GFC0258	*cf.*SV01, P_{BAD}-*ecf38* P_{ecf38}-*lux* P_{tet}-*as38 t*::HK022	Cm^R	This study	ECF38/AS38 t1-switch (ch. int.)

GFC0295	*cf.*SV01, P_{BAD}-*ecf11* P_{ecf11}-*lux*::HK022	Cm^R	This study	ECF switch (ch. int.)
GFC0296	*cf.*SV01, P_{BAD}-*ecf14* P_{ecf12}-*lux*::HK022	Cm^R	This study	ECF switch (ch. int.)
GFC0297	*cf.*SV01, P_{BAD}-*ecf15* P_{ecf15}-*lux*::HK022	Cm^R	This study	ECF switch (ch. int.)
GFC0298	*cf.*SV01, P_{BAD}-*ecf16* P_{ecf16}-*lux*::HK022	Cm^R	This study	ECF switch (ch. int.)
GFC0299	*cf.*SV01, P_{BAD}-*ecf17* P_{ecf17}-*lux*::HK022	Cm^R	This study	ECF switch (ch. int.)
GFC0300	*cf.*SV01, P_{BAD}-*ecf20* P_{ecf20}-*lux*::HK022	Cm^R	This study	ECF switch (ch. int.)
GFC0301	*cf.*SV01, P_{BAD}-*ecf22* P_{ecf22}-*lux*::HK022	Cm^R	This study	ECF switch (ch. int.)
GFC0302	*cf.*SV01, P_{BAD}-*ecf26* P_{ecf26}-*lux*::HK022	Cm^R	This study	ECF switch (ch. int.)
GFC0303	*cf.*SV01, P_{BAD}-*ecf27* P_{ecf25}-*lux*::HK022	Cm^R	This study	ECF switch (ch. int.)
GFC0304	*cf.*SV01, P_{BAD}-*ecf28* P_{ecf19}-*lux*::HK022	Cm^R	This study	ECF switch/1-step timer (ch. int.)
GFC0305	*cf.*SV01, P_{BAD}-*ecf31* P_{ecf31}-*lux*::HK022	Cm^R	This study	ECF switch (ch. int.)
GFC0306	*cf.*SV01, P_{BAD}-*ecf32* P_{ecf32}-*lux*::HK022	Cm^R	This study	ECF switch/1-step timer (ch. int.)
GFC0307	*cf.*SV01, P_{BAD}-*ecf34* P_{ecf18}-*lux*::HK022	Cm^R	This study	ECF switch (ch. int.)
GFC0308	*cf.*SV01, P_{BAD}-*ecf37* P_{ecf39}-*lux*::HK022	Cm^R	This study	ECF switch (ch. int.)
GFC0309	*cf.*SV01, P_{BAD}-*ecf38* P_{ecf38}-*lux*::HK022	Cm^R	This study	ECF switch (ch. int.)
GFC0310	*cf.*SV01, P_{tet}*lux*::HK022	Cm^R	This study	Reporter construct (Ch int.)
GFC0311	*cf.*SV01, P_{BAD}-*ecf32* P_{ecf19}-*lux* P_{ecf32}-*ecf28*::HK022	Cm^R	This study	2-step timer (ch. Int)
GFC0325	*cf.*SV01 + pSVM-mc_205	Km^R	This study	Insulator test construct
GFC0335	*cf.*SV01 + pSVP-mc_009	Km^R	This study	3-step timer *ecf28 ecf32* P*ecf34*
GFC0336	*cf.*SV01 + pSVP-mc_010	Km^R	This study	3-step timer *ecf28 ecf32* neg. control
GFC0337	*cf.*SV01 + pSVP-mc_011	Km^R	This study	3-step timer *ecf32 ecf28* P*ecf34*
GFC0338	*cf.*SV01 + pSVP-mc_012	Km^R	This study	3-step timer *ecf32 ecf28* neg. control
GFC0339	*cf.*SV01, P_{BAD}-*ecf28* P_{ecf32}-*lux* P_{ecf19}-*ecf32*::HK022	Cm^R	This study	2-step timer (ch. Int)
GFC0360	*cf.*SV01, P_{BAD}-*ecf11* P_{tet}-*as11 t2*::HK022 + pSVM-mc_216	Cm^R + Km^R	This study	ECF11/AS11 t1 (ch. int.+reporter plasmid)
GFC0361	*cf.*SV01, P_{BAD}-*ecf14* P_{tet}-*as14 t2*::HK022 + pSVM-mc_217	Cm^R + Km^R	This study	ECF14/AS14 t2 (ch. int.+reporter plasmid)
GFC0365	*cf.*SV01, P_{BAD}-*ecf20* P_{tet}-*as20 t2*::HK022 + pSVM-mc_221	Cm^R + Km^R	This study	ECF20/AS20 t2 (ch. int.+reporter plasmid)
GFC0366	*cf.*SV01, P_{BAD}-*ecf22* P_{tet}-*as22 t1*::HK022 + pSVM-mc_222	Cm^R + Km^R	This study	ECF22/AS22 t1 (ch. int.+reporter plasmid)
GFC0367	*cf.*SV01, P_{BAD}-*ecf26* P_{tet}-*as26 t2*::HK022 + pSVM-mc_223	Cm^R + Km^R	This study	ECF26/AS26 t2 (ch. int.+reporter plasmid)
GFC0368	*cf.*SV01, P_{BAD}-*ecf27* P_{tet}-*as27 t2*::HK022 + pSVM-mc_224	Cm^R + Km^R	This study	ECF27/AS27 t2 (ch. int.+reporter plasmid)
GFC0369	*cf.*SV01, P_{BAD}-*ecf28* P_{tet}-*as28 t2*::HK022 + pSVM-mc_225	Cm^R + Km^R	This study	ECF28/AS28 t2 (ch. int.+reporter plasmid)
GFC0370	*cf.*SV01, P_{BAD}-*ecf31* P_{tet}-*as31 t1*::HK022 + pSVM-mc_226	Cm^R + Km^R	This study	ECF31/AS31 t1 (ch. int.+reporter plasmid)
GFC0371	*cf.*SV01, P_{BAD}-*ecf34* P_{tet}-*as34 t1*::HK022 + pSVM-mc_227	Cm^R + Km^R	This study	ECF34/AS34 t1 (ch. int.+reporter plasmid)
GFC0372	*cf.*SV01, P_{BAD}-*ecf37* P_{tet}-*as37 t1*::HK022 + pSVM-mc_228	Cm^R + Km^R	This study	ECF37/AS37 t1 (ch. int.+reporter plasmid)

GFC0373	*cf.*SV01, P_{BAD}-*ecf38* P_{tet}-*as38 t*::HK022 + pSVM-mc_229	Cm^R + Km^R	This study	ECF38/AS38 t1 (ch. int.+reporter plasmid)
GFC0389	*cf.*SV01, P_{BAD}-*ecf11*::HK022 + pSVM-mc_216	Cm^R + Km^R	This study	ECF switch (ch. int.+reporter plasmid)
GFC0390	*cf.*SV01, P_{BAD}-*ecf14*::HK022 + pSVM-mc_217	Cm^R + Km^R	This study	ECF switch (ch. int.+reporter plasmid)
GFC0391	*cf.*SV01, P_{BAD}-*ecf15*::HK022 + pSVM-mc_218	Cm^R + Km^R	This study	ECF switch (ch. int.+reporter plasmid)
GFC0392	*cf.*SV01, P_{BAD}-*ecf16*::HK022 + pSVM-mc_219	Cm^R + Km^R	This study	ECF switch (ch. int.+reporter plasmid)
GFC0393	*cf.*SV01, P_{BAD}-*ecf17*::HK022 + pSVM-mc_220	Cm^R + Km^R	This study	ECF switch (ch. int.+reporter plasmid)
GFC0394	*cf.*SV01, P_{BAD}-*ecf20*::HK022 + pSVM-mc_221	Cm^R + Km^R	This study	ECF switch (ch. int.+reporter plasmid)
GFC0395	*cf.*SV01, P_{BAD}-*ecf22*::HK022 + pSVM-mc_222	Cm^R + Km^R	This study	ECF switch (ch. int.+reporter plasmid)
GFC0396	*cf.*SV01, P_{BAD}-*ecf26*::HK022 + pSVM-mc_223	Cm^R + Km^R	This study	ECF switch (ch. int.+reporter plasmid)
GFC0397	*cf.*SV01, P_{BAD}-*ecf27*::HK022 + pSVM-mc_224	Cm^R + Km^R	This study	ECF switch (ch. int.+reporter plasmid)
GFC0398	*cf.*SV01, P_{BAD}-*ecf28*::HK022 + pSVM-mc_225	Cm^R + Km^R	This study	ECF switch (ch. int.+reporter plasmid)
GFC0399	*cf.*SV01, P_{BAD}-*ecf31*::HK022 + pSVM-mc_226	Cm^R + Km^R	This study	ECF switch (ch. int.+reporter plasmid)
GFC0400	*cf.*SV01, P_{BAD}-*ecf32*::HK022 + pSVM-mc_209	Cm^R + Km^R	This study	ECF switch (ch. int.+reporter plasmid)
GFC0401	*cf.*SV01, P_{BAD}-*ecf34*::HK022 + pSVM-mc_227	Cm^R + Km^R	This study	ECF switch (ch. int.+reporter plasmid)
GFC0402	*cf.*SV01, P_{BAD}-*ecf37*::HK022 + pSVM-mc_228	Cm^R + Km^R	This study	ECF switch (ch. int.+reporter plasmid)
GFC0403	*cf.*SV01, P_{BAD}-*ecf38*::HK022 + pSVM-mc_229	Cm^R + Km^R	This study	ECF switch (ch. int.+reporter plasmid)
GFC0404	*cf.*SV01, $PL_{lac0\text{-}1}$*lux*::HK022	Cm^R	This study	Reporter construct (Ch int.)
GFC0432	*cf.*SV01 + pSVM-mc_263	Km^R	This study	Reporter construct (RBS test)
GFC0433	*cf.*SV01 + pSVM-mc_264	Km^R	This study	Reporter construct (RBS test)
GFC0434	*cf.*SV01 + pSVM-mc_265	Km^R	This study	Reporter construct (RBS test)
GFC0435	*cf.*SV01 + pSVM-mc_266	Km^R	This study	Reporter construct (RBS test)
GFC0436	*cf.*SV01 + pSVM-mc_267	Km^R	This study	Reporter construct (RBS test)
GFC0437	*cf.*SV01 + pSVM-mc_268	Km^R	This study	Reporter construct (RBS test)
GFC0438	*cf.*SV01 + pSVM-mc_269	Km^R	This study	Reporter construct (RBS test)
GFC0439	*cf.*SV01 + pSVM-mc_270	Km^R	This study	Reporter construct (RBS test)
GFC0440	*cf.*SV01 + pSVM-mc_271	Km^R	This study	Reporter construct (RBS test)
GFC0441	*cf.*SV01 + pSVM-mc_272	Km^R	This study	Reporter construct (RBS test)
GFC0442	*cf.*SV01 + pSVM-mc_274	Km^R	This study	Reporter construct (RBS test)
GFC0484	*cf.*SV01, P_{BAD}*lux*::HK022	Km^R	This study	Reporter construct (ch int.)
GFC0485	*cf.*SV01, P_{BAD}*lux*::P21	Km^R	This study	Reporter construct (ch int.)
GFC0486	*cf.*SV01, P_{BAD}*lux*::φ80	Km^R	This study	Reporter construct (ch int.)
GFC0487	*cf.*SV01, P_{BAD}*lux*::λ	Km^R	This study	Reporter construct (ch int.)
GFC0500	*cf.*SV01, P_{BAD}*lux*::λ	Cm^R	This study	Reporter construct (ch int.)
GFC0505	*cf.*SV01, P_{BAD}*lux*::HK022, P_{BAD}*gfp*::P21	Cm^R + Km^R	This study	Reporter construct (ch int.)

GFC0509	*cf.*SV01, P_{BAD}*lux*::HK022	Cm^R	This study	Reporter construct (ch int.)
GFC0510	*cf.*SV01, P_{BAD}*lux*::P21	Cm^R	This study	Reporter construct (ch int.)
GFC0511	*cf.*SV01, P_{BAD}*lux*::φ80	Cm^R	This study	Reporter construct (ch int.)
GFC0512	*cf.*SV01, P_{BAD}*lux*::λ	Cm^R	This study	Reporter construct (ch int.)
GFC0514	*cf.*SV01, P_{BAD}*gfp*::P21	Km^R	This study	Reporter construct (ch int.)
GFC0518	*cf.*SV01, P_{BAD} *ecf22* P_{ecf22}-*lux* P_{tet}-*as22*::HK022	Cm^R	This study	ECF22/AS22-switch (ch. int)
GFC0521	*cf.*SV01, P_{BAD}*lux*::HK022	Gm^R	This study	Reporter construct (ch int.)
GFC0522	*cf.*SV01, P_{BAD}*lux*::P21	Gm^R	This study	Reporter construct (ch int.)
GFC0523	*cf.*SV01, P_{BAD}*lux*::φ80	Gm^R	This study	Reporter construct (ch int.)
GFC0524	*cf.*SV01, P_{BAD}*lux*::λ	Gm^R	This study	Reporter construct (ch int.)
GFC0525	*cf.*SV01, P_{BAD}*lux*::HK022	Spc^R	This study	Reporter construct (ch int.)
GFC0526	*cf.*SV01, P_{BAD}*lux*::P21	Spc^R	This study	Reporter construct (ch int.)
GFC0527	*cf.*SV01, P_{BAD}*lux*::φ80	Spc^R	This study	Reporter construct (ch int.)
GFC0528	*cf.*SV01, P_{BAD}*lux*::λ	Spc^R	This study	Reporter construct (ch int.)
GFC0531	*cf.*SV01, P_{BAD}*mCherry*::φ80	Spc^R	This study	Reporter construct (ch int.)
GFC0533	*cf.*SV01, P_{BAD}*lux*::HK022, P_{BAD}*gfp*::P21, P_{BAD}*mCherry*::φ80	Cm^R + Km^R + Spc^R	This study	Reporter construct (ch int.)
GFC0544	*cf.*SV01, P_{BAD}*mTurquoise*::λ	Gm^R	This study	Reporter construct (ch int.)
GFC0547	*cf.*SV01, P_{BAD}*lux*::HK022, P_{BAD}*gfp*::P21, P_{BAD}*mCherry*::φ80, P_{BAD}*mTurquoise*::λ	Cm^R + Km^R + Spc^R + GM^R	This study	Reporter construct (ch int.)
GFC0549	*cf.*SV01 + pSVP-mc_025	Km^R	This study	ECF/AS circuit (ch. int.)
GFC0550	*cf.*SV01 + pSVP-mc_026	Km^R	This study	ECF/AS circuit (ch. int.)
GFC0551	*cf.*SV01 + pSVP-mc_027	Km^R	This study	ECF/AS circuit (ch. int.)
GFC0558	*cf.*SV01, P_{BAD}-*ecf14* P_{tet}-*as14 t2*::HK022 + pSVM-mc_294	Cm^R + Km^R	This study	ECF14/AS14 t2 suicide circuit (ch. int.+reporter plasmid)
GFC0561	*cf.*SV01, P_{BAD}-*ecf28* P_{tet}-*as28 t2*::HK022 + pSVM-mc_297	Cm^R + Km^R	This study	ECF28/AS28 t2 suicide circuit (ch. int.+reporter plasmid)
GFC0562	*cf.*SV01, P_{BAD}-*ecf34* P_{tet}-*as34 t1*::HK022 + pSVM-mc_298	Cm^R + Km^R	This study	ECF34/AS34 t1 suicide circuit (ch. int.+reporter plasmid)
GFC0563	*cf.*SV01, P_{BAD}-*ecf37* P_{tet}-*as37 t1*::HK022 + pSVM-mc_299	Cm^R + Km^R	This study	ECF37/AS37 t1 suicide circuit (ch. int.+reporter plasmid)
GFC0564	*cf.*SV01 + pSVM-mc_216	Km^R	This study	ECF switch neg. control
GFC0565	*cf.*SV01 + pSVM-mc_217	Km^R	This study	ECF switch neg. control
GFC0566	*cf.*SV01 + pSVM-mc_218	Km^R	This study	ECF switch neg. control
GFC0567	*cf.*SV01 + pSVM-mc_219	Km^R	This study	ECF switch neg. control
GFC0568	*cf.*SV01 + pSVM-mc_220	Km^R	This study	ECF switch neg. control
GFC0569	*cf.*SV01 + pSVM-mc_221	Km^R	This study	ECF switch neg. control
GFC0570	*cf.*SV01 + pSVM-mc_222	Km^R	This study	ECF switch neg. control
GFC0571	*cf.*SV01 + pSVM-mc_223	Km^R	This study	ECF switch neg. control
GFC0572	*cf.*SV01 + pSVM-mc_224	Km^R	This study	ECF switch neg. control

GFC0573	*cf.*SV01 + pSVM-mc_225	Km^R	This study	ECF switch neg. control
GFC0575	*cf.*SV01 + pSVM-mc_227	Km^R	This study	ECF switch neg. control
GFC0576	*cf.*SV01 + pSVM-mc_228	Km^R	This study	ECF switch neg. control
GFC0577	*cf.*SV01 + pSVM-mc_229	Km^R	This study	ECF switch neg. control
GFC0578	*cf.*SV01, + pSVP-mc_028	Km^R	This study	PLlac0-1-*lux* reporter construct

Table 9.1. *E. coli* strains utilized in this study. The name, the genotype, the antibiotic resistance and a description of the strains are reported. The strains are listed in alphabetical order. Cm^R: chloramphenicol resistance, Gm^R: gentamicin resistance, Km^R: kanamycin resistance, Nal^R: nalidixic acid resistance, Spc^R: spectinomycin resistance, Str^R: streptomycin resistance. Ch. int: chromosomal integration.

CRIMoClo vectors				
Name	***att* site**	**Resistance**	**Parental MoClo vector**	**Helper plasmid**
pSV004	HK022	Cm^R	pSVM-mc (Level M)	pAH69
pSV006	P21	Cm^R	pSVM-mc (Level M)	pAH121
pSV008	φ80	Cm^R	pSVM-mc (Level M)	pAH123
pSV077	λ	Cm^R	pSVM-mc (Level M)	pINT ts
pSV125	HK022	Km^R	pSVM-mc (Level M)	pAH69
pSV126	P21	Km^R	pSVM-mc (Level M)	pAH121
pSV127	φ80	Km^R	pSVM-mc (Level M)	pAH123
pSV128	λ	Km^R	pSVM-mc (Level M)	pINT ts
pSV183	HK022	Spc^R	pSVM-mc (Level M)	pAH69
pSV184	P21	Spc^R	pSVM-mc (Level M)	pAH121
pSV185	φ80	Spc^R	pSVM-mc (Level M)	pAH123
pSV186	λ	Spc^R	pSVM-mc (Level M)	pINT ts
pSV187	HK022	Gm^R	pSVM-mc (Level M)	pAH69
pSV188	P21	Gm^R	pSVM-mc (Level M)	pAH121
pSV189	φ80	Gm^R	pSVM-mc (Level M)	pAH123
pSV190	λ	Gm^R	pSVM-mc (Level M)	pINT ts
pSV016	HK022	Cm^R	pICH82094 (Level P)	pAH69
pSV018	P21	Cm^R	pICH82094 (Level P)	pAH121
pSV080	φ80	Cm^R	pICH82094 (Level P)	pAH123
pSV079	λ	Cm^R	pICH82094 (Level P)	pINT ts
pSV219	HK022	Km^R	pICH82094 (Level P)	pAH69
pSV220	P21	Km^R	pICH82094 (Level P)	pAH121
pSV221	φ80	Km^R	pICH82094 (Level P)	pAH123
pSV222	λ	Km^R	pICH82094 (Level P)	pINT ts
pSV239	HK022	Spc^R	pICH82094 (Level P)	pAH69

pSV240	P21	Spc^R	pICH82094 (Level P)	pAH121
pSV241	φ80	Spc^R	pICH82094 (Level P)	pAH123
pSV242	λ	Spc^R	pICH82094 (Level P)	pINT ts
pSV243	HK022	Gm^R	pICH82094 (Level P)	pAH69
pSV244	P21	Gm^R	pICH82094 (Level P)	pAH121
pSV245	φ80	Gm^R	pICH82094 (Level P)	pAH123
pSV246	λ	Gm^R	pICH82094 (Level P)	pINT ts

Table 9.2. CRIMoClo vectors. The table reports the name of the plasmids, the *att* site used for the chromosomal integration, the antibiotic resistance, the MoClo parental vector (with which CRIMoClo vectors share the position of the Type IIs restriction sites and the fusion sites) and the original CRIM helper plasmid necessary for the expression of the integrase gene. Cm^R: chloramphenicol resistance, Gm^R: gentamicin resistance, Km^R: kanamycin resistance, Spc^R: Spectinomycin resistance.

Level 0 library						
Name	**Genetic part: Promoter**	**Destination vector**	**Donor**	**Primer forward**	**Primer reverse**	**Reference**
pSV0-1_002	P_{BAD} promoter + *araC* + L3S3P00	pICH41233	pAraC-pBAD-mCherry-v2 + synthetic DNA	GF0034 GF0046	GF0010 GF0047	[Kogenaru M, Tans S J, 2014] [Chen Y et al., 2013]
pSV0-1_004	$P_{llacO-1}$ promoter + *lacI* (corrected 2 BpiI sites)	pICH41233	pLacI-Ptrc-eYFP-v2-1 + synthetic DNA	GF0007 GF0033 GF0035	GF0006 GF0032 GF0037	[Kogenaru M, Tans S J, 2014] [Lutz R, Bujard H, 1997]
pSV0-1_005	P_{tet} promoter + *tetR* + L3S1P13	pICH41233	CATTRE18 + synthetic DNA	GF0038 GF0048	GF0039 GF0049	[Bertram R, Hillen W, 2007] [Chen Y et al., 2013]
pSV0-1_007	BBa_J23108	pICH41233	Synthetic DNA	GF0054	GF00055	http://parts.igem.org/Promoters/Catalog/Anderson
pSV0-1_008	BBa_J23117	pICH41233	Synthetic DNA	GF0056	GF0057	http://parts.igem.org/Promoters/Catalog/Anderson
pSV0-1_041	Pecf11_3726	pICH41233	pVRb11_3726	GF0133	GF0087	Rhodius V A *et al*., 2013
pSV0-1_010	Pecf12_up807	pICH41233	pVRb12_up807	GF0086	GF0087	Rhodius V A *et al*., 2013
pSV0-1_020	Pecf15_up436	pICH41233	pVRb15_up436	GF0086	GF0087	Rhodius V A *et al*., 2013
pSV0-1_011	Pecf16_3622	pICH41233	pVRb16_3622	GF0086	GF0087	Rhodius V A *et al*., 2013
pSV0-1_021	Pecf17_up1691	pICH41233	pVRb17_up1691	GF0086	GF0087	Rhodius V A *et al*., 2013
pSV0-1_012	Pecf20_992	pICH41233	pVRb20_992	GF0086	GF0087	Rhodius V A *et al*., 2013
pSV0-1_022	Pecf22_up1147	pICH41233	pVRb22_up1147	GF0086	GF0087	Rhodius V A *et al*., 2013
pSV0-1_013	Pecf26_up601	pICH41233	pVRb26_up601	GF0086	GF0087	Rhodius V A *et al*., 2013
pSV0-1_023	Pecf25_up4311	pICH41233	pVRb25_up4311	GF0086	GF0087	Rhodius V A *et al*., 2013
pSV0-1_014	Pecf19_up1315	pICH41233	pVRb19_up1315	GF0086	GF0087	Rhodius V A *et al*., 2013
pSV0-1_015	Pecf31_34	pICH41233	pVRb31_34	GF0086	GF0087	Rhodius V A *et al*., 2013
pSV0-1_016	Pecf32_1122	pICH41233	pVRb32_1122	GF0086	GF0087	Rhodius V A *et al*., 2013
pSV0-1_017	Pecf18_up1700	pICH41233	pVRb18_up1700	GF0086	GF0087	Rhodius V A *et al*., 2013
pSV0-1_024	Pecf39_up1413	pICH41233	pVRb39_up1413	GF0086	GF0087	Rhodius V A *et al*., 2013
pSV0-1_025	Pecf38_up1322	pICH41233	pVRb38_up1322	GF0086	GF0087	Rhodius V A *et al*., 2013

Name	Genetic part: RBS	Destination vector	Donor	Primer forward	Primer reverse	Reference
pSV0-9_001	RBS st8	pICH41246	Synthetic DNA	GF0058	GF0059	Vellanoweth R L, Rabinowitz J C, 1992
pSV0-9_002	RBS wk2	pICH41246	Synthetic DNA	GF0017	GF0018	Vellanoweth R L, Rabinowitz J C, 1992
pJM0-9_006	RBS st3	pICH41246	Synthetic DNA	GF0448	GF0449	Vellanoweth R L, Rabinowitz J C, 1992
pJM0-9_007	RBS st4	pICH41246	Synthetic DNA	GF0450	GF0451	Vellanoweth R L, Rabinowitz J C, 1992
pJM0-9_008	RBS st5	pICH41246	Synthetic DNA	GF0452	GF0453	Vellanoweth R L, Rabinowitz J C, 1992
pJM0-9_009	RBS st7	pICH41246	Synthetic DNA	GF0454	GF0455	Vellanoweth R L, Rabinowitz J C, 1992
pJM0-9_010	RBS st11	pICH41246	Synthetic DNA	GF0456	GF0457	Vellanoweth R L, Rabinowitz J C, 1992
pJM0-9_011	RBS wk2	pICH41246	Synthetic DNA	GF0458	GF0459	Vellanoweth R L, Rabinowitz J C, 1992
pJM0-9_012	RBS wk4	pICH41246	Synthetic DNA	GF0460	GF0461	Vellanoweth R L, Rabinowitz J C, 1992
pJM0-9_013	RBS wk5	pICH41246	Synthetic DNA	GF0462	GF0463	Vellanoweth R L, Rabinowitz J C, 1992
pJM0-9_014	RBS wk6	pICH41246	Synthetic DNA	GF0464	GF0465	Vellanoweth R L, Rabinowitz J C, 1992
pJM0-9_015	RBS wk7	pICH41246	Synthetic DNA	GF0466	GF0467	Vellanoweth R L, Rabinowitz J C, 1992
pJM0-9_017	RBS wk11	pICH41246	Synthetic DNA	GF0470	GF0471	Vellanoweth R L, Rabinowitz J C, 1992
Name	**Genetic part: CDS**	**Destination vector**	**Donor**	**Primer forward**	**Primer reverse**	**Reference**
pSV0-15_001	*gfp*-mut3-1 (BsaI site corrected)	pICH41308	pGFPamyE	GF0011, GF0013	GF0012, GF0014	Bisicchia P, *et. al.*, 2010
pSV0-15_002	*YFP*	pICH41308	pSac-Cm-YFP	GF0042	GF0043	Kuchina A, *et al.*,2011
pSV0-15_003	*mCherry*	pICH41308	pAraC-pBAD-mCherry-v2	GF0040	GF0041	Kogenaru M, Tans S J, 2014
pMC0-4_010	*mTurquoise*	pICH41308	Gene synthesis	-	-	Goedhart, J. et al., 2012
pSV0-15_024	*luxCDABE*	pICH41308	pBBR-MCS5	GF0134, GF0136, GFC0138	GF0135, GFC0137, GFC0139	Gödeke J et al., 2011
pSV0-15_005	*ecf11_987*	pICH41308	pVRa11_987	GF0088	GF0132	Rhodius V A *et al*., 2013
pSV0-15_006	*ecf14_1324*	pICH41308	pVRa14_1324	GF0090	GF0091	Rhodius V A *et al*., 2013
pSV0-15_016	*ecf15_436*	pICH41308	pVRa15_436	GF0092	GF0093	Rhodius V A *et al*., 2013
pSV0-15_007	*ecf16_3622*	pICH41308	pVRa16_3622	GF0094	GF0095	Rhodius V A *et al*., 2013
pSV0-15_020	*ecf17_1691*	pICH41308	pVRa17_1691	GF0096	GF0097	Rhodius V A *et al*., 2013
pSV0-15_008	*ecf20_992*	pICH41308	pVRa20_992	GF0098	GF0099	Rhodius V A *et al*., 2013
pSV0-15_017	*ecf22_4450*	pICH41308	pVRa22_4450	GF0100	GF0101	Rhodius V A *et al*., 2013
pSV0-15_009	*ecf26_4464*	pICH41308	pVRa26_4464	GF0102	GF0103	Rhodius V A *et al*., 2013
pSV0-15_018	*ecf27_4265*	pICH41308	pVRa27_4265	GF0104	GF0105	Rhodius V A *et al*., 2013
pSV0-15_010	*ecf28_1088*	pICH41308	pVRa28_1088	GF0106	GF0107	Rhodius V A *et al*., 2013
pSV0-15_011	*ecfF31_34*	pICH41308	pVRa31_34	GF0108	GF0110	Rhodius V A *et al*., 2013
pSV0-15_012	*ecf32_1122*	pICH41308	pVRa32_1122	GF0110	GF0111	Rhodius V A *et al*., 2013
pSV0-15_013	*ecf34_1384*	pICH41308	pVRa34_1384	GF0112	GF0113	Rhodius V A *et al*., 2013
pSV0-15_019	*ecf37_2513*	pICH41308	pVRa37_2513	GF0114	GF0115	Rhodius V A *et al*., 2013
pSV0-15_021	*ecf38_1322*	pICH41308	pVRa38_1322	GF0116	GF0117	Rhodius V A *et al*., 2013

pSV0-15_025	*as11_987*	pICH41308	pVRc11_987	GF0244	GF0245	Rhodius V A *et al*., 2013
pSV0-15_026	*as14_1324*	pICH41308	pVRc14_1324	GF0246	GF0247	Rhodius V A *et al*., 2013
pSV0-15_027	*as15_436*	pICH41308	pVRc15_436	GF0248	GF0249	Rhodius V A *et al*., 2013
pSV0-15_028	*as16_3622*	pICH41308	pVRc16_3622	GF0250	GF0251	Rhodius V A *et al*., 2013
pSV0-15_039	*as17_1691*	pICH41308	pVRc17_1691	GF0363	GF0364	Rhodius V A *et al*., 2013
pSV0-15_029	*as20_992*	pICH41308	pVRc20_992	GF0252	GF0253	Rhodius V A *et al*., 2013
pSV0-15_030	*as22_4450*	pICH41308	pVRc22_4450	GF0254	GF0255	Rhodius V A *et al*., 2013
pSV0-15_040	*as26_4464*	pICH41308	pVRc26_4464	GF0365	GF0366	Rhodius V A *et al*., 2013
pSV0-15_031	*as27_4265*	pICH41308	pVRc27_4265	GF0256	GF0257	Rhodius V A *et al*., 2013
pSV0-15_041	*as28_1088*	pICH41308	pVRc28_1088	GF0367	GF0368	Rhodius V A *et al*., 2013
pSV0-15_032	*as31_34*	pICH41308	pVRc31_34	GF0258	GF0259	Rhodius V A *et al*., 2013
pSV0-15_042	*as34_1384*	pICH41308	pVRc34_1384	GF0369	GF0370	Rhodius V A *et al*., 2013
pSV0-15_033	*as37_2513*	pICH41308	pVRc37_2513	GF0260	GF0261	Rhodius V A *et al*., 2013
pSV0-15_034	*as38_1322*	pICH41308	pVRc38_1322	GF0262	GF0263	Rhodius V A *et al*., 2013
pSV0-15_068	*ccdB*	pICH41308	pMA333	GF0998	GF0999	Schindler D *et al.*, 2016
pAD0-13_001	*as11_987 t1*	pAGM1287	pVRc11_987	GF0244	GF0406	Rhodius V A *et al*., 2013
pAD0-13_011	*as11_987 t2*	pAGM1287	pVRc11_987	GF0244	GF0407	Rhodius V A *et al*., 2013
pAD0-13_012	*as14_1324 t1*	pAGM1287	pVRc14_1324	GF0246	GF0408	Rhodius V A *et al*., 2013
pAD0-13_002	*as14_1324 t2*	pAGM1287	pVRc14_1324	GF0246	GF0409	Rhodius V A *et al*., 2013
pAD0-13_003	*as17_1691 t1*	pAGM1287	pVRc17_1691	GF0363	GF0410	Rhodius V A *et al*., 2013
pAD0-13_005	*as20_992 t1*	pAGM1287	pVRc20_992	GF0252	GF0412	Rhodius V A *et al*., 2013
pAD0-13_006	*as20_992 t2*	pAGM1287	pVRc20_992	GF0252	GF0413	Rhodius V A *et al*., 2013
pAD0-13_007	*as22_4450 t*	pAGM1287	pVRc22_4450	GF0254	GF0414	Rhodius V A *et al*., 2013
pAD0-13_008	*as26_4464 t1*	pAGM1287	pVRc26_4464	GF0365	GF0415	Rhodius V A *et al*., 2013
pAD0-13_009	*as26_4464 t2*	pAGM1287	pVRc26_4464	GF0365	GF0416	Rhodius V A *et al*., 2013
pAD0-13_013	*as27_4265 t1*	pAGM1287	pVRc27_4265	GF0256	GF0417	Rhodius V A *et al*., 2013
pAD0-13_014	*as27_4265 t2*	pAGM1287	pVRc27_4265	GF0256	GF0418	Rhodius V A *et al*., 2013
pAD0-13_015	*as28_1088 t1*	pAGM1287	pVRc28_1088	GF0367	GF0419	Rhodius V A *et al*., 2013
pAD0-13_016	*as28_1088 t2*	pAGM1287	pVRc28_1088	GF0367	GF0420	Rhodius V A *et al*., 2013
pAD0-13_017	*as31_34 t1*	pAGM1287	pVRc31_34	GF0258	GF0421	Rhodius V A *et al*., 2013
pAD0-13_018	*as31_34 t2*	pAGM1287	pVRc31_34	GF0258	GF0422	Rhodius V A *et al*., 2013
pAD0-13_019	*as34_1384 t1*	pAGM1287	pVRc34_1384	GF0369	GF0423	Rhodius V A *et al*., 2013
pAD0-13_020	*as34_1384 t2*	pAGM1287	pVRc34_1384	GF0369	GF0424	Rhodius V A *et al*., 2013
pAD0-13_021	*as37_2513 t1*	pAGM1287	pVRc37_2513	GF0260	GF0425	Rhodius V A *et al*., 2013
pAD0-13_022	*as37_2513 t2*	pAGM1287	pVRc37_2513	GF0260	GF0426	Rhodius V A *et al*., 2013
pAD0-13_010	*as38_1322 t1*	pAGM1287	pVRc38_1322	GF0262	GF0427	Rhodius V A *et al*., 2013
Name	**Genetic part: Terminator**	**Destination vector**	**Donor**	**Primer forward**	**Primer reverse**	**Reference**
pSV0-11_001	L3S2P21	pICH41276	Synthetic DNA	GF0019	GF0020	Chen Y *et al.*, 2013
pSV0-11_002	L3S2P11	pICH41276	Synthetic DNA	GF0021	GF0022	Chen Y *et al.*, 2013
pSV0-11_003	L3S3P21	pICH41276	Synthetic DNA	GF0060	GF0061	Chen Y *et al.*, 2013
pSV0-11_004	L3S3P22	pICH41276	Synthetic DNA	GF0062	GF0063	Chen Y *et al.*, 2013
pSV0-11_005	L3S2P55	pICH41276	Synthetic DNA	GF0064	GF0065	Chen Y *et al.*, 2013
pSV0-11_009	L3S3P11	pICH41276	Synthetic DNA	GF0264	GF0265	Chen Y *et al.*, 2013

pSV0-11_010	L3S3P23	pICH41276	Synthetic DNA	GF0266	GF0267	Chen Y *et al.*, 2013
pSV0-11_011	L3S2P24	pICH41276	Synthetic DNA	GF0268	GF0269	Chen Y *et al.*, 2013
pSV0-11_012	L3S1P22	pICH41276	Synthetic DNA	GF0270	GF0271	Chen Y *et al.*, 2013
pSV0-11_013	L3S1P47	pICH41276	Synthetic DNA	GF0272	GF0273	Chen Y *et al.*, 2013
pSV0-11_014	L3S3P45	pICH41276	Synthetic DNA	GF0274	GF0275	Chen Y *et al.*, 2013
pSV0-11_015	L3S2P44	pICH41276	Synthetic DNA	GF0276	GF0277	Chen Y *et al.*, 2013
pJM0-1_033	L3S3P22 RC	pICH41233	Synthetic DNA	GF0349	GF0350	Chen Y *et al.*, 2013
pSV0-1_052	*rrnb* T2 RC	pICH41233	Synthetic DNA	GF0677	GF0678	Chen Y *et al.*, 2013
pYE-11_003	*rrnB* T1-T2	pICH41276	Synthetic DNA	-	-	Döhlemann J et al., 2017
Name	**Genetic part: Dummy sequence**	**Destination vector**	**Donor**	**Primer forward**	**Primer reverse**	**Reference**
pSV0-1_028	Dummy 15bp	pICH41233	Synthetic DNA	GF0158	GF0159	this study
pSV0-2_002	Dummy 15bp	pAGM1263	Synthetic DNA	GF0196	GF0197	this study
pSV0-3_002	Dummy 15bp	pAGM1276	Synthetic DNA	GF0198	GF0199	this study
pSV0-4_002	Dummy 15bp	pICH41258	Synthetic DNA	GF0200	GF0201	this study
pSV0-5_002	Dummy 15bp	pAGM1299	Synthetic DNA	GF0202	GF0203	this study
pSV0-6_002	Dummy 15bp	pAGM1301	Synthetic DNA	GF0204	GF0205	this study
pSV0-7_002	Dummy 15bp	pICH53388	Synthetic DNA	GF0206	GF0207	this study
pSV0-8_001	Dummy 15bp	pICH53399	Synthetic DNA	GF0208	GF0209	this study
pJM0-9_005	Dummy 15bp	pICH41246	Synthetic DNA	GF0353	GF0354	this study
pSV0-11_008	Dummy 15bp	pICH41276	Synthetic DNA	GF0278	GF0279	this study
pSV0-12_001	Dummy 15bp	pAGM1251	Synthetic DNA	GF0671	GF0672	this study
pSV0-13_028	Dummy 15bp	pAGM1287	Synthetic DNA	GF0673	GF0674	this study
pSV0-14_003	Dummy 15bp	pICH41295	Synthetic DNA	GF0210	GF0211	this study
pSV0-15_022	Dummy 15bp	pICH41308	Synthetic DNA	GF0212	GF0213	this study
pSV0-16_001	Dummy 15bp	pICH41331	Synthetic DNA	GF0675	GF0676	this study
pSV0-1_027	Dummy 300bp	pICH41233	Synthetic DNA	GF0174	GF0175	Schindler D *et al.*, 2016
pSV0-2_001	Dummy 300bp	pAGM1263	Synthetic DNA	GF0176	GF0177	Schindler D *et al.*, 2016
pSV0-3_001	Dummy 300bp	pAGM1276	Synthetic DNA	GF0178	GF0179	Schindler D *et al.*, 2016
pSV0-4_001	Dummy 300bp	pICH41258	Synthetic DNA	GF0180	GF0181	Schindler D *et al.*, 2016
pSV0-5_001	Dummy 300bp	pAGM1299	Synthetic DNA	GF0182	GF0183	Schindler D *et al.*, 2016
pSV0-6_001	Dummy 300bp	pAGM1301	Synthetic DNA	GF0184	GF0185	Schindler D *et al.*, 2016
pSV0-7_001	Dummy 300bp	pICH53388	Synthetic DNA	GF0186	GF0187	Schindler D *et al.*, 2016
Name	**Genetic part: FLAG tag**	**Destination vector**	**Donor**	**Primer forward**	**Primer reverse**	**Reference**
pAD0-6_003	FLAG Tag	pAGM1301	Synthetic DNA	GF0431	GF0432	Hopp T et *al.*, 1988

Table 9.3. ECF toolbox level 0 library. MoClo-encoded level 0 parts generated in this study and composing the ECF toolbox library. The parts are listed according to type. Internal name abbreviations: (pSV) generated by Stefano Vecchione; (pAD) generated by Angelika Diehl, (pJM) generated by Julia Manning. The original name of MoClo destination vectors, in which the parts are encoded, as well as the original names of the donor plasmids and the primers used for the PCR-amplification, or oligonucleotides annealing are indicated.

Level 1 transcription units and insulator elements			
Internal name	Donor	Destination vector	Description
pAD1-5L_0034	pSV0-1_005 + pSV0-9_001 + pAD0-13_001 + pAD0-6_003 + pSV0-11_011	pICH47772	P_{tet} *as11* t1 + FLAG tag
pAD1-5L_0035	pSV0-1_005 + pSV0-9_001 + pAD0-13_011 + pAD0-6_003 + pSV0-11_011	pICH47772	P_{tet} *as11* t2 + FLAG tag
pAD1-5L_0036	pSV0-1_005 + pSV0-9_001 + pAD0-13_012 + pAD0-6_003 + pSV0-11_011	pICH47772	P_{tet} *as14* t1 + FLAG tag
pAD1-5L_0037	pSV0-1_005 + pSV0-9_001 + pAD0-13_002 + pAD0-6_003 + pSV0-11_011	pICH47772	P_{tet} *as14* t2 + FLAG tag
pAD1-5L_0038	pSV0-1_005 + pSV0-9_001 + pAD0-13_003 + pAD0-6_003 + pSV0-11_011	pICH47772	P_{tet} *as17* t + FLAG tag
pAD1-5L_0040	pSV0-1_005 + pSV0-9_001 + pAD0-13_005 + pAD0-6_003 + pSV0-11_011	pICH47772	P_{tet} *as20* t1 + FLAG tag
pAD1-5L_0041	pSV0-1_005 + pSV0-9_001 + pAD0-13_006 + pAD0-6_003 + pSV0-11_011	pICH47772	P_{tet} *as20* t2 + FLAG tag
pAD1-5L_0042	pSV0-1_005 + pSV0-9_001 + pAD0-13_007 + pAD0-6_003 + pSV0-11_011	pICH47772	P_{tet} *as22* t + FLAG tag
pAD1-5L_0043	pSV0-1_005 + pSV0-9_001 + pAD0-13_008 + pAD0-6_003 + pSV0-11_011	pICH47772	P_{tet} *as26* t1 + FLAG tag
pAD1-5L_0044	pSV0-1_005 + pSV0-9_001 + pAD0-13_009 + pAD0-6_003 + pSV0-11_011	pICH47772	P_{tet} *as26* t2 + FLAG tag
pAD1-5L_0045	pSV0-1_005 + pSV0-9_001 + pAD0-13_013 + pAD0-6_003 + pSV0-11_011	pICH47772	P_{tet} *as27* t1 + FLAG tag
pAD1-5L_0046	pSV0-1_005 + pSV0-9_001 + pAD0-13_014 + pAD0-6_003 + pSV0-11_011	pICH47772	P_{tet} *as27* t2 + FLAG tag
pAD1-5L_0047	pSV0-1_005 + pSV0-9_001 + pAD0-13_015 + pAD0-6_003 + pSV0-11_011	pICH47772	P_{tet} *as28* t1 + FLAG tag
pAD1-5L_0048	pSV0-1_005 + pSV0-9_001 + pAD0-13_016 + pAD0-6_003 + pSV0-11_011	pICH47772	P_{tet} *as28* t2 + FLAG tag
pAD1-5L_0049	pSV0-1_005 + pSV0-9_001 + pAD0-13_017 + pAD0-6_003 + pSV0-11_011	pICH47772	P_{tet} *as31* t1 + FLAG tag
pAD1-5L_0050	pSV0-1_005 + pSV0-9_001 + pAD0-13_018 + pAD0-6_003 + pSV0-11_011	pICH47772	P_{tet} *as31* t2 + FLAG tag
pAD1-5L_0051	pSV0-1_005 + pSV0-9_001 + pAD0-13_019 + pAD0-6_003 + pSV0-11_011	pICH47772	P_{tet} *as34* t1 + FLAG tag
pAD1-5L_0052	pSV0-1_005 + pSV0-9_001 + pAD0-13_020 + pAD0-6_003 + pSV0-11_011	pICH47772	P_{tet} *as34* t2 + FLAG tag
pAD1-5L_0053	pSV0-1_005 + pSV0-9_001 + pAD0-13_021 + pAD0-6_003 + pSV0-11_011	pICH47772	P_{tet} *as37* t1 + FLAG tag
pAD1-5L_0054	pSV0-1_005 + pSV0-9_001 + pAD0-13_022 + pAD0-6_003 + pSV0-11_011	pICH47772	P_{tet} *as37* t2 + FLAG tag
pAD1-5L_0055	pSV0-1_005 + pSV0-9_001 + pAD0-13_010 + pAD0-6_003 + pSV0-11_011	pICH47772	P_{tet} *as38* t + FLAG tag
pJM1-2L_0014	pSV0-14_003 + pSV0-4_001 + pSV0-5_002 + pSV0-6_002 + pYE-11_003	pICH47742	Insulator 300bp + double term.
pJM1-3R_002	pSV0-1_014 + pSV0-9_001 + pSV0-15_024 + pSV0-11_001	pICH47822	Pecf19 *luxCDABE*
pJM1-3R_003	pSV0-1_015 + pSV0-9_001 + pSV0-15_024 + pSV0-11_001	pICH47822	Pecf32 *luxCDABE*
pJM1-3R_004	pSV0-1_016 + pSV0-9_001 + pSV0-15_024 + pSV0-11_001	pICH47822	Pecf18 *luxCDABE*

pSV1-1L_0003	pSV0-1_002 + pSV0-9_001 + pSV0-15_004 + pSV0-11_001	pICH47732	P_{BAD} *mCherry*
pSV1-1L_0005	pSV0-1_002 + pSV0-9_001 + pSV0-15_001 + pSV0-11_001	pICH47732	P_{BAD} *gfp*
pSV1-1L_0006	pSV0-1_005 + pSV0-9_003 + pSV15_001 + pSV0-11_001	pICH47732	P_{tet} *lux*
pSV1-1L_0007	pSV0-1_004 + pSV0-9_003 + pSV15_001 + pSV0-11_001	pICH47732	P_{O-1} *lux*
pSV1-1L_0011	pSV0-1_002 + pSV0-9_001 + pSV0-15_005 + pSV0-11_002	pICH47732	P_{BAD} *ecf11*
pSV1-1L_0012	pSV0-1_002 + pSV0-9_001 + pSV0-15_006 + pSV0-11_002	pICH47732	P_{BAD} *ecf14*
pSV1-1L_0013	pSV0-1_002 + pSV0-9_001 + pSV0-15_007 + pSV0-11_002	pICH47732	P_{BAD} *ecf16*
pSV1-1L_0014	pSV0-1_002 + pSV0-9_001 + pSV0-15_008 + pSV0-11_002	pICH47732	P_{BAD} *ecf20*
pSV1-1L_0015	pSV0-1_002 + pSV0-9_001 + pSV0-15_009 + pSV0-11_002	pICH47732	P_{BAD} *ecf26*
pSV1-1L_0016	pSV0-1_002 + pSV0-9_001 + pSV0-15_010 + pSV0-11_002	pICH47732	P_{BAD} *ecf28*
pSV1-1L_0017	pSV0-1_002 + pSV0-9_001 + pSV0-15_011 + pSV0-11_002	pICH47732	P_{BAD} *ecf31*
pSV1-1L_0018	pSV0-1_002 + pSV0-9_001 + pSV0-15_012 + pSV0-11_002	pICH47732	P_{BAD} *ecf32*
pSV1-1L_0019	pSV0-1_002 + pSV0-9_001 + pSV0-15_013 + pSV0-11_002	pICH47732	P_{BAD} *ecf34*
pSV1-1L_0028	pSV0-1_002 + pSV0-9_001 + pSV0-15_024 + pSV0-11_001	pICH47732	P_{BAD} *lux*
pSV1-1L_0029	pSV0-1_002 + pSV0-9_001 + pSV0-15_016 + pSV0-11_002	pICH47732	P_{BAD} *ecf15*
pSV1-1L_0030	pSV0-1_002 + pSV0-9_001 + pSV0-15_020 + pSV0-11_002	pICH47732	P_{BAD} *ecf17*
pSV1-1L_0031	pSV0-1_002 + pSV0-9_001 + pSV0-15_017 + pSV0-11_002	pICH47732	P_{BAD} *ecf22*
pSV1-1L_0032	pSV0-1_002 + pSV0-9_001 + pSV0-15_018 + pSV0-11_002	pICH47732	P_{BAD} *ecf27*
pSV1-1L_0033	pSV0-1_002 + pSV0-9_001 + pSV0-15_019 + pSV0-11_002	pICH47732	P_{BAD} *ecf37*
pSV1-1L_0034	pSV0-1_002 + pSV0-9_001 + pSV0-15_021 + pSV0-11_002	pICH47732	P_{BAD} *ecf38*
pSV1-1L_0088	pSV0-1_052 + pJM0-9_005 + pSV0-13_028 + pSV0-11_013	pICH47732	Insulator term.+300bp+term.
pSV1-1L_0140	pSV0-1_002 + pSV0-9_001 + pSV0-15_024 + pSV0-11_001	pICH47732	P_{BAD} *lux* (RBS st3)
pSV1-1L_0141	pSV0-1_002 + pJM0-9_007 + pSV0-15_024 + pSV0-11_001	pICH47732	P_{BAD} *lux* (RBS st4)
pSV1-1L_0142	pSV0-1_002 + pJM0-9_008 + pSV0-15_024 + pSV0-11_001	pICH47732	P_{BAD} *lux* (RBS st5)
pSV1-1L_0143	pSV0-1_002 + pJM0-9_009 + pSV0-15_024 + pSV0-11_001	pICH47732	P_{BAD} *lux* (RBS st7)
pSV1-1L_0144	pSV0-1_002 + pJM0-9_010 + pSV0-15_024 + pSV0-11_001	pICH47732	P_{BAD} *lux* (RBS st11)
pSV1-1L_0145	pSV0-1_002 + pJM0-9_011 + pSV0-15_024 + pSV0-11_001	pICH47732	P_{BAD} *lux* (RBS wk2)

pSV1-1L_0146	pSV0-1_002 + pJM0-9_012 + pSV0-15_024 + pSV0-11_001	pICH47732	P_{BAD} *lux* (RBS wk4)
pSV1-1L_0147	pSV0-1_002 + pJM0-9_013 + pSV0-15_024 + pSV0-11_001	pICH47732	P_{BAD} *lux* (RBS wk5)
pSV1-1L_0148	pSV0-1_002 + pJM0-9_014 + pSV0-15_024 + pSV0-11_001	pICH47732	P_{BAD} *lux* (RBS wk6)
pSV1-1L_0149	pSV0-1_002 + pJM0-9_015 + pSV0-15_024 + pSV0-11_001	pICH47732	P_{BAD} *lux* (RBS wk7)
pSV1-1L_0151	pSV0-1_002 + pJM0-9_017 + pSV0-15_024 + pSV0-11_001	pICH47732	P_{BAD} *lux* (RBS wk11)
pSV1-1L_0162	pSV0-1_002 + pSV0-9_001 + pMC0-4_010 + pSV0-11_001	pICH47732	P_{BAD} *mTurquoise*
pSV1-1L_0163	pSV0-1_002 + pSV0-9_001 + pSV0-15_006 + pSV0-11_008	pICH47732	P_{BAD} *ecf14* no terminator
pSV1-1R_0003	pSV0-1_028 + pSV0-9_001 + pSV0-15_024 + pSV0-11_001	pICH47822	Du15 *luxCDABE*
pSV1-1R_0006	pSV0-1_002 + pSV0-9_001 + pSV0-15_024 + pSV0-11_001	pICH47802	P_{BAD} *lux* reverse orientation
pSV1-2L_0007	pSV0-14_003 + pSV0-4_001 + pSV0-5_002 + pSV0-6_002 + pSV0-11_003	pICH47742	Insulator 300bp + terminator
pSV1-2L_0008	pSV0-14_003 + pSV0-4_001 + pSV0-5_002 + pSV0-6_002 + pSV0-11_008	pICH47742	Insulator 300bp
pSV1-2L_0122	pSV0-1_028 + pSV0-9_001 + pSV0-15_001 + pSV0-11_001	pICH47742	du15 0-1 *gfp*
pSV1-3L_0034	pSV0-1_028 + pSV0-9_001 + pSV0-15_024 + pSV0-11_001	pICH47751	Du15 *luxCDABE*
pSV1-3L_0111	cfr. 1-2L_0007	pICH47751	Insulator 300bp + terminator
pSV1-3R_0011	pSV0-1_041 + pSV0-9_001 + pSV0-15_024 + pSV0-11_001	pICH47822	Pecf11 *luxCDABE*
pSV1-3R_0012	pSV0-1_010 + pSV0-9_001 + pSV0-15_024 + pSV0-11_001	pICH47822	Pecf12 *luxCDABE*
pSV1-3R_0013	pSV0-1_020 + pSV0-9_001 + pSV0-15_024 + pSV0-11_001	pICH47822	Pecf15 *luxCDABE*
pSV1-3R_0014	pSV0-1_011 + pSV0-9_001 + pSV0-15_024 + pSV0-11_001	pICH47822	Pecf16 *luxCDABE*
pSV1-3R_0015	pSV0-1_021 + pSV0-9_001 + pSV0-15_024 + pSV0-11_001	pICH47822	Pecf17 *luxCDABE*
pSV1-3R_0016	pSV0-1_012 + pSV0-9_001 + pSV0-15_024 + pSV0-11_001	pICH47822	Pecf20 *luxCDABE*
pSV1-3R_0017	pSV0-1_022 + pSV0-9_001 + pSV0-15_024 + pSV0-11_001	pICH47822	Pecf22 *luxCDABE*
pSV1-3R_0018	pSV0-1_013 + pSV0-9_001 + pSV0-15_024 + pSV0-11_001	pICH47822	Pecf26 *luxCDABE*
pSV1-3R_0019	pSV0-1_023 + pSV0-9_001 + pSV0-15_024 + pSV0-11_001	pICH47822	Pecf27 *luxCDABE*
pSV1-3R_0020	pSV0-1_017 + pSV0-9_001 + pSV0-15_024 + pSV0-11_001	pICH47822	Pecf31 *luxCDABE*
pSV1-3R_0021	pSV0-1_024 + pSV0-9_001 + pSV0-15_024 + pSV0-11_001	pICH47822	Pecf39 *luxCDABE*
pSV1-3R_0022	pSV0-1_025 + pSV0-9_001 + pSV0-15_024 + pSV0-11_001	pICH47822	Pecf38 *luxCDABE*
pSV1-3R_0045	pSV0-1_010 + pSV0-9_001 + pSV0-15_068 + pSV0-11_001	pICH47822	Pecf12 *ccdB*
pSV1-3R_0048	pSV0-1_014 + pSV0-9_001 + pSV0-15_068 + pSV0-11_001	pICH47822	Pecf19 *ccdB*

pSV1-3R_0049	pSV0-1_016 + pSV0-9_001 + pSV0-15_068 + pSV0-11_001	pICH47822	Pecf18 *ccdB*
pSV1-3R_0050	pSV0-1_024 + pSV0-9_001 + pSV0-15_068 + pSV0-11_001	pICH47822	Pecf39 *ccdB*
pSV1-4L_0004	pJM0-1_033 + pJM0-9_005 + pSV0-4_002 + pSV0-5_001 + pSV0-6_002 + pSV0-11_005	pICH47761	Insulator term.+300bp+term.
pSV1-4R_0003	pSV0-1_010 + pSV0-9_001 + pSV0-15_024 + pSV0-11_001	pICH47831	Pecf12 *luxCDABE*
pSV1-5L_0014	pSV0-1_014 + pSV0-9_001 + pSV0-15_012 + pSV0-11_010	pICH47772	Pecf19 *ecf32*
pSV1-5L_0015	pSV0-1_016 + pSV0-9_001 + pSV0-15_010 + pSV0-11_010	pICH47772	Pecf32 *ecf28*
pSV1-5L_0016	pSV0-1_014 + pSV0-9_001 + pSV0-15_022 + pSV0-11_010	pICH47772	Pecf19 Du15
pSV1-5L_0017	pSV0-1_016 + pSV0-9_001 + pSV0-15_022 + pSV0-11_010	pICH47772	Pecf32 Du15
pSV1-5L_0020	pSV0-1_005 + pSV0-9_001 + pSV0-15_025 + pSV0-11_011	pICH47772	P_{tet} *as11*
pSV1-5L_0021	pSV0-1_005 + pSV0-9_001 + pSV0-15_026 + pSV0-11_011	pICH47772	P_{tet} *as14*
pSV1-5L_0022	pSV0-1_005 + pSV0-9_001 + pSV0-15_027 + pSV0-11_011	pICH47772	P_{tet} *as15*
pSV1-5L_0023	pSV0-1_005 + pSV0-9_001 + pSV0-15_028 + pSV0-11_011	pICH47772	P_{tet} *as16*
pSV1-5L_0024	pSV0-1_005 + pSV0-9_001 + pSV0-15_039 + pSV0-11_011	pICH47772	P_{tet} *as17*
pSV1-5L_0025	pSV0-1_005 + pSV0-9_001 + pSV0-15_029 + pSV0-11_011	pICH47772	P_{tet} *as20*
pSV1-5L_0026	pSV0-1_005 + pSV0-9_001 + pSV0-15_030 + pSV0-11_011	pICH47772	P_{tet} *as22*
pSV1-5L_0027	pSV0-1_005 + pSV0-9_001 + pSV0-15_040 + pSV0-11_011	pICH47772	P_{tet} *as26*
pSV1-5L_0028	pSV0-1_005 + pSV0-9_001 + pSV0-15_031 + pSV0-11_011	pICH47772	P_{tet} *as27*
pSV1-5L_0029	pSV0-1_005 + pSV0-9_001 + pSV0-15_041 + pSV0-11_011	pICH47772	P_{tet} *as28*
pSV1-5L_0030	pSV0-1_005 + pSV0-9_001 + pSV0-15_032 + pSV0-11_011	pICH47772	P_{tet} *as31*
pSV1-5L_0031	pSV0-1_005 + pSV0-9_001 + pSV0-15_042 + pSV0-11_011	pICH47772	P_{tet} *as34*
pSV1-5L_0032	pSV0-1_005 + pSV0-9_001 + pSV0-15_033 + pSV0-11_011	pICH47772	P_{tet} *as37*
pSV1-5L_0033	pSV0-1_005 + pSV0-9_001 + pSV0-15_034 + pSV0-11_011	pICH47772	P_{tet} *as38*
pSV1-5L_0092	cfr. 1-4L_0004	pICH47772	Insulator term.+300bp+term.
pSV1-6L_0006	pSV0-6_001 + pJM0-9_005 + pSV0-15_022 + pSV0-11_012	pICH47781	Insulator 300bp + terminator
pSV1-6L_0007	pSV0-1_005 + pSV0-9_001 + pAD0-13_002 + pAD0-6_003 + pSV0-11_008	pICH47781	Ptet *as14 t2* no terminator
pSV1-6L_0008	pSV0-1_007 + pSV0-9_001 + pAD0-13_002 + pAD0-6_003 + pSV0-11_008	pICH47781	P108 *as14 t2* no terminator
pSV1-6L_0009	pSV0-1_008 + pSV0-9_001 + pAD0-13_002 + pAD0-6_003 + pSV0-11_008	pICH47781	P117 *as14 t2* no terminator
pSV1-7L_0008	pSV0-1_028 + pSV0-9_001 + pSV0-15_004 + pSV0-11_001	pICH47791	du15 0-1 *mCherry*

pSV1-7R_0002	pSV0-1_016 + pSV0-9_001 + pSV0-15_010 + pSV0-11_009	pICH47791	Pecf32 *ecf34*
pSV1-7R_0003	pSV0-1_014 + pSV0-9_001 + pSV0-15_012 + pSV0-11_009	pICH47791	Pecf19 *ecf34*
pSV1-7R_0004	pSV0-1_016 + pSV0-9_001 + pSV0-15_022 + pSV0-11_009	pICH47791	Pecf32 Du15
pSV1-7R_0005	pSV0-1_014 + pSV0-9_001 + pSV0-15_022 + pSV0-11_009	pICH47791	Pecf19 Du15

Table 9.4. Level 1 transcription units and insulator elements. The genetic constructs are listed in alphabetical order. Internal name abbreviations: (pSV) generated by Stefano Vecchione; (pAD) generated by Angelika Diehl, (pJM) generated by Julia Manning. The internal names of the level 0 parts used as well as the original names of the MoClo destination vectors, in which the parts are encoded, and a description of the constructs is indicated.

Level M parts and synthetic circuits			
Internal name	Donor	Destination vector	Description
pADM-mc_160	pSV1-1L_0012 + pSV1-2L_0007 + pSV1-3R_0012 + pSV1-4L_0004 + pAD1-5L_0036	pSVM-mc	ECF14/AS14 t1-switch
pADM-mc_161	pSV1-1L_0012 + pSV1-2L_0007 + pSV1-3R_0012 + pSV1-4L_0004 + pAD1-5L_0037	pSVM-mc	ECF14/AS14 t2-switch
pADM-mc_162	pSV1-1L_0030 + pSV1-2L_0007 + pSV1-3R_0015 + pSV1-4L_0004 + pAD1-5L_0038	pSVM-mc	ECF17/AS17 t-switch
pADM-mc_163	pSV1-1L_0014 + pSV1-2L_0007 + pSV1-3R_0016 + pSV1-4L_0004 + pAD1-5L_0040	pSVM-mc	ECF20/AS20 t1-switch
pADM-mc_164	pSV1-1L_0014 + pSV1-2L_0007 + pSV1-3R_0016 + pSV1-4L_0004 + pAD1-5L_0041	pSVM-mc	ECF20/AS20 t2-switch
pADM-mc_165	pSV1-1L_0031 + pSV1-2L_0007 + pSV1-3R_0017 + pSV1-4L_0004 + pAD1-5L_0042	pSVM-mc	ECF22/AS22 t-switch
pADM-mc_166	pSV1-1L_0015 + pSV1-2L_0007 + pSV1-3R_0018 + pSV1-4L_0004 + pAD1-5L_0043	pSVM-mc	ECF26/AS26 t1-switch
pADM-mc_167	pSV1-1L_0015 + pSV1-2L_0007 + pSV1-3R_0018 + pSV1-4L_0004 + pAD1-5L_0044	pSVM-mc	ECF26/AS26 t2-switch
pADM-mc_169	pSV1-1L_0032 + pSV1-2L_0007 + pSV1-3R_0019 + pSV1-4L_0004 + pAD1-5L_0045	pSVM-mc	ECF27/AS27 t1-switch
pADM-mc_170	pSV1-1L_0032 + pSV1-2L_0007 + pSV1-3R_0019 + pSV1-4L_0004 + pAD1-5L_0046	pSVM-mc	ECF27/AS27 t2-switch
pADM-mc_171	pSV1-1L_0016 + pSV1-2L_0007 + pJM1-3R_002 + pSV1-4L_0004 + pAD1-5L_0047	pSVM-mc	ECF28/AS28 t1-switch
pADM-mc_172	pSV1-1L_0016 + pSV1-2L_0007 + pJM1-3R_002 + pSV1-4L_0004 + pAD1-5L_0048	pSVM-mc	ECF28/AS28 t2-switch

pADM-mc_173	pSV1-1L_0017 + pSV1-2L_0007 + pSV1-3R_020 + pSV1-4L_0004 + pAD1-5L_0049	pSVM-mc	ECF31/AS31 t1-switch
pADM-mc_174	pSV1-1L_0019 + pSV1-2L_0007 + pJM1-3R_004 + pSV1-4L_0004 + pAD1-5L_0051	pSVM-mc	ECF34/AS34 t1-switch
pADM-mc_175	pSV1-1L_0019 + pSV1-2L_0007 + pJM1-3R_004 + pSV1-4L_0004 + pAD1-5L_0052	pSVM-mc	ECF34/AS34 t2-switch
pADM-mc_176	pSV1-1L_0033 + pSV1-2L_0007 + pSV1-3R_0021 + pSV1-4L_0004 + pAD1-5L_0053	pSVM-mc	ECF37/AS37 t1-switch
pADM-mc_177	pSV1-1L_0033 + pSV1-2L_0007 + pSV1-3R_0021 + pSV1-4L_0004 + pAD1-5L_0054	pSVM-mc	ECF37/AS37 t2-switch
pADM-mc_178	pSV1-1L_0034 + pSV1-2L_0007 + pSV1-3R_0022 + pSV1-4L_0004 + pAD1-5L_0055	pSVM-mc	ECF38/AS38 t1-switch
pADM-mc_179	pSV1-1L_0017 + pSV1-2L_0007 + pSV1-3R_020 + pSV1-4L_0004 + pAD1-5L_0050	pSVM-mc	ECF31/AS31 t2-switch
pJMM-mc_095	pSV1-1L_0016 + pSV1-2L_0008 + pSV1-3L_0034	pSVM-mc	P_{BAD} *ecf28* du300 du15 *lux*
pJMM-mc_097	pSV1-1L_0016 + pSV1-2L_0007 + pSV1-3L_0034	pSVM-mc	P_{BAD} *ecf28* du300 term. du15 *lux*
pSV012	pSV1-1L_0028	pSV004	P_{BAD} *lux att* HK022 cm^R
pSV013	pSV1-1L_0028	pSV006	P_{BAD} *lux att* P21 cm^R
pSV014	pSV1-1L_0028	pSV008	P_{BAD} *lux att* φ80 cm^R
pSV020	cfr. pSVM-mc_184	pSV0004	ECF11/AS11 t1-switch (for chromosomal int.)
pSV021	cfr. pSVM-mc_185	pSV0004	ECF11/AS11 t2-switch (for chromosomal int.)
pSV022	cfr. pADM-mc_160	pSV0004	ECF14/AS14 t1-switch (for chromosomal int.)
pSV023	cfr. pADM-mc_161	pSV0004	ECF14/AS14 t2-switch (for chromosomal int.)
pSV024	cfr. pSVM-mc_134	pSV0004	ECF15/AS15-switch (for chromosomal int.)
pSV025	cfr. pSVM-mc_135	pSV0004	ECF16/AS16-switch (for chromosomal int.)
pSV026	cfr. pADM-mc_162	pSV0004	ECF17/AS17 t-switch (for chromosomal int.)
pSV028	cfr. pADM-mc_163	pSV0004	ECF20/AS20 t1-switch (for chromosomal int.)
pSV029	cfr. pADM-mc_164	pSV0004	ECF20/AS20 t2-switch (for chromosomal int.)
pSV030	cfr. pADM-mc_165	pSV0004	ECF22/AS22 t-switch (for chromosomal int.)
pSV031	cfr. pADM-mc_166	pSV0004	ECF26/AS26 t1-switch (for chromosomal int.)
pSV032	cfr. pADM-mc_167	pSV0004	ECF26/AS26 t2-switch (for chromosomal int.)
pSV033	cfr. pADM-mc_169	pSV0004	ECF27/AS27 t1-switch (for chromosomal int.)
pSV034	cfr. pADM-mc_170	pSV0004	ECF27/AS27 t2-switch (for chromosomal int.)

pSV035	cfr. pADM-mc_171	pSV0004	ECF28/AS28 t1-switch (for chromosomal int.)
pSV036	cfr. pADM-mc_172	pSV0004	ECF28/AS28 t2-switch (for chromosomal int.)
pSV037	cfr. pADM-mc_173	pSV0004	ECF31/AS31 t1-switch (for chromosomal int.)
pSV038	cfr. pADM-mc_179	pSV0004	ECF31/AS31 t2-switch (for chromosomal int.)
pSV039	cfr. pADM-mc_174	pSV0004	ECF34/AS34 t1-switch (for chromosomal int.)
pSV040	cfr. pADM-mc_175	pSV0004	ECF34/AS34 t2-switch (for chromosomal int.)
pSV041	cfr. pADM-mc_176	pSV0004	ECF37/AS37 t1-switch (for chromosomal int.)
pSV042	cfr. pADM-mc_177	pSV0004	ECF37/AS37 t2-switch (for chromosomal int.)
pSV043	cfr. pADM-mc_178	pSV0004	ECF38/AS38 t1-switch (for chromosomal int.)
pSV073	pSV1-1L_0018 + pSV1-2L_0007 + pJM1-3R_002 + pSV1-4L_0004 + pSV1-5L_0015	pSV004	2-step timer *ecf32* Pecf28 (for chromosomal int.)
pSV074	pSV1-1L_0016 + pSV1-2L_0007 + pJM1-3R_003 + pSV1-4L_0004 + pSV1-5L_0014	pSV004	2-step timer *ecf28* Pecf32 (for chromosomal int.)
pSV080	pSV1-1L_0028	pSV077	P_{BAD} *att* λ cm^R
pSV089	pSV1-1L_0011 + pICH54033 + pSV1-3R_0011 + pSV1-4L_0004 + pAD1-5L_0035	pSV0004	ECF11/AS11 t2-switch, no rep. (for chromosomal int.)
pSV090	pSV1-1L_0012 + pICH54033 + pSV1-3R_0012 + pSV1-4L_0004 + pAD1-5L_0037	pSV0004	ECF14/AS14 t2-switch, no rep. (for chromosomal int.)
pSV093	pSV1-1L_0030 + pICH54033 + pSV1-3R_0015 + pSV1-4L_0004 + pAD1-5L_0038	pSV0004	ECF17/AS17 t-switch, no rep. (for chromosomal int.)
pSV094	pSV1-1L_0014 + pICH54033 + pSV1-3R_0016 + pSV1-4L_0004 + pAD1-5L_0041	pSV0004	ECF20/AS20 t2-switch, no rep. (for chromosomal int.)
pSV095	pSV1-1L_0031 + pICH54033 + pSV1-3R_0017 + pSV1-4L_0004 + pAD1-5L_0042	pSV0004	ECF22/AS22 t-switch, no rep. (for chromosomal int.)
pSV096	pSV1-1L_0015 + pICH54033 + pSV1-3R_0018 + pSV1-4L_0004 + pAD1-5L_0044	pSV0004	ECF26/AS26 t2-switch, no rep. (for chromosomal int.)
pSV097	pSV1-1L_0032 + pICH54033 + pSV1-3R_0019 + pSV1-4L_0004 + pAD1-5L_0045	pSV0004	ECF27/AS27 t1-switch, no rep. (for chromosomal int.)
pSV098	pSV1-1L_0016 + pICH54033 + pJM1-3R_002 + pSV1-4L_0004 + pAD1-5L_0048	pSV0004	ECF28/AS28 t2-switch, no rep. (for chromosomal int.)
pSV099	pSV1-1L_0017 + pICH54033 + pSV1-3R_020 + pSV1-4L_0004 + pAD1-5L_0049	pSV0004	ECF31/AS31 t1-switch, no rep. (for chromosomal int.)
pSV100	pSV1-1L_0019 + pICH54033 + pJM1-3R_004 + pSV1-4L_0004 + pAD1-5L_0051	pSV0004	ECF34/AS34 t1-switch, no rep. (for chromosomal int.)

pSV101	pSV1-1L_0033 + pICH54033 + pSV1-3R_0021 + pSV1-4L_0004 + pAD1-5L_0053	pSV0004	ECF37/AS37 t1-switch, no rep. (for chromosomal int.)
pSV102	pSV1-1L_0034 + pICH54033 + pSV1-3R_0022 + pSV1-4L_0004 + pAD1-5L_0055	pSV0004	ECF38/AS38 t1-switch, no rep. (for chromosomal int.)
pSV103	pSV0-1_002 + pSV0-9_001 + pSV0-15_005 + pSV0-11_002	pSV0004	P_{BAD} *ecf11* (for chromosomal int.)
pSV104	pSV0-1_002 + pSV0-9_001 + pSV0-15_006 + pSV0-11_002	pSV0004	P_{BAD} *ecf14* (for chromosomal int.)
pSV105	pSV0-1_002 + pSV0-9_001 + pSV0-15_016 + pSV0-11_002	pSV0004	P_{BAD} *ecf15* (for chromosomal int.)
pSV106	pSV0-1_002 + pSV0-9_001 + pSV0-15_007 + pSV0-11_002	pSV0004	P_{BAD} *ecf16* (for chromosomal int.)
pSV107	pSV0-1_002 + pSV0-9_001 + pSV0-15_020 + pSV0-11_002	pSV0004	P_{BAD} *ecf17* (for chromosomal int.)
pSV108	pSV0-1_002 + pSV0-9_001 + pSV0-15_008 + pSV0-11_002	pSV0004	P_{BAD} *ecf20* (for chromosomal int.)
pSV109	pSV0-1_002 + pSV0-9_001 + pSV0-15_017 + pSV0-11_002	pSV0004	P_{BAD} *ecf22* (for chromosomal int.)
pSV110	pSV0-1_002 + pSV0-9_001 + pSV0-15_009 + pSV0-11_002	pSV0004	P_{BAD} *ecf26* (for chromosomal int.)
pSV111	pSV0-1_002 + pSV0-9_001 + pSV0-15_018 + pSV0-11_002	pSV0004	P_{BAD} *ecf27* (for chromosomal int.)
pSV112	pSV0-1_002 + pSV0-9_001 + pSV0-15_010 + pSV0-11_002	pSV0004	P_{BAD} *ecf28* (for chromosomal int.)
pSV113	pSV0-1_002 + pSV0-9_001 + pSV0-15_011 + pSV0-11_002	pSV0004	P_{BAD} *ecf31* (for chromosomal int.)
pSV114	pSV0-1_002 + pSV0-9_001 + pSV0-15_012 + pSV0-11_002	pSV0004	P_{BAD} *ecf32* (for chromosomal int.)
pSV115	pSV0-1_002 + pSV0-9_001 + pSV0-15_013 + pSV0-11_002	pSV0004	P_{BAD} *ecf34* (for chromosomal int.)
pSV116	pSV0-1_002 + pSV0-9_001 + pSV0-15_019 + pSV0-11_002	pSV0004	P_{BAD} *ecf37* (for chromosomal int.)
pSV117	pSV0-1_002 + pSV0-9_001 + pSV0-15_021 + pSV0-11_002	pSV0004	P_{BAD} *ecf38* (for chromosomal int.)
pSV118	pSV1-1L_0007	pSV004	PL_{lacO-1} *lux att* HK022
pSV137	pSV1-1L_0028	pSV125	P_{BAD} *lux att* HK022 km^R
pSV138	pSV1-1L_0028	pSV126	P_{BAD} *lux att* P21 km^R
pSV139	pSV1-1L_0028	pSV127	P_{BAD} *lux att* φ80 km^R
pSV140	pSV1-1L_0028	pSV128	P_{BAD} *att* λ km^R
pSV172	pSV1-1L_0005	pSV126	P_{BAD} *gfp att P21*
pSV175	pSV1-1L_0028	pSV004	P_{BAD} *lux* rev. orientation *att* HK022
pSV176	pSV1-1L_0028	pSV006	P_{BAD} *lux* rev. orientation *att* P21
pSV177	pSV1-1L_0028	pSV008	P_{BAD} *lux* rev. orientation *att* φ80
pSV178	pSV1-1L_0028	pSV077	P_{BAD} *lux* rev. orientation *att* λ
pSV199	pSV1-1L_0028	pSV187	P_{BAD} *lux att* HK022 gm^R
pSV200	pSV1-1L_0028	pSV188	P_{BAD} *lux att* P21 gm^R
pSV201	pSV1-1L_0028	pSV189	P_{BAD} *lux att* φ80 gm^R
pSV202	pSV1-1L_0028	pSV190	P_{BAD} *att* λ gm^R
pSV203	pSV1-1L_0028	pSV183	P_{BAD} *lux att* HK022 spc^R
pSV204	pSV1-1L_0028	pSV184	P_{BAD} *lux att* P21 spc^R
pSV205	pSV1-1L_0028	pSV185	P_{BAD} *lux att* φ80 spc^R
pSV206	pSV1-1L_0028	pSV186	P_{BAD} *att* λ spc^R
pSV209	pSV1-1L_0003	pSV185	P_{BAD} *mCherry att φ80*
pSV218	pSV1-1L_0162	pSV190	P_{BAD} *mTurquoise att λ*

pSVM-1_076	pSV1-1L_0016 + pSV1-2L_0007 + pJM1-3R_004 + pSV1-4L_0004 + pSV1-5L_0014	pAGM8031	part of 3-step timer
pSVM-1_078	pSV1-1L_0018 + pSV1-2L_0007 + pJM1-3R_004 + pSV1-4L_0004 + pSV1-5L_0015	pAGM8031	part of 3-step timer
pSVM-1_168	pSV1-1L_0163 + pSV1-2L_0122 + pSV1-3L_0111 + pSV1-4R_0003	pAGM8031	ECF14/AS14 t2-switch, part1
pSVM-5_008	pSV1-5L_0092 + pSV1-6L_0007 + pSV1-7L_0008	pAGM8079	ECF14/AS14 t2-switch, part2
pSVM-5_009	pSV1-5L_0092 + pSV1-6L_0008 + pSV1-7L_0008	pAGM8079	ECF14/AS14 t2-switch, part2
pSVM-5_010	pSV1-5L_0092 + pSV1-6L_0009 + pSV1-7L_0008	pAGM8079	ECF14/AS14 t2-switch, part2
pSVM6_018	pSV1-6L_0006 + pSV1-7R_0002 + pSV1-1L_0088	pAGM8081	part of 3-step timer
pSVM6_019	pSV1-6L_0006 + pSV1-7R_0003 + pSV1-1L_0088	pAGM8081	part of 3-step timer
pSVM6_020	pSV1-6L_0006 + pSV1-7R_0004 + pSV1-1L_0088	pAGM8081	part of 3-step timer neg. control
pSVM6_021	pSV1-6L_0006 + pSV1-7R_0005 + pSV1-1L_0088	pAGM8081	part of 3-step timer neg. control
pSVM-mc_038	pSV1-1L_0028	pSVM-mc	P_{BAD} *lux*
pSVM-mc_074	pSV1-1L_0016 + pJM1-2L_0014 + pSV1-3L_0034	pSVM-mc	P_{BAD} *ecf28* du300 double term. du15 *lux*
pSVM-mc_111	pSV1-1L_0016 + pSV1-2L_0007 + pJM1-3R_002 + pSV1-4L_0004	pSVM-mc	ECF28-switch / 1-step timer
pSVM-mc_112	pSV1-1L_0018 + pSV1-2L_0007 + pJM1-3R_003 + pSV1-4L_0004	pSVM-mc	ECF32-switch / 1-step timer
pSVM-mc_113	pSV1-1L_0016 + pSV1-2L_0007 + pSV1-1R_0003	pSVM-mc	P_{BAD} *ecf28* du300 term. du15 *lux* (rev.)
pSVM-mc_116	du1 + pSV1-2L_0007 + pJM1-3R_003 + pSV1-4L_0004	pSVM-mc	Pecf32 *luxCDABE* reporter
pSVM-mc_117	pSV1-1L_0016 + pSV1-2L_0007 + pJM1-3R_003 + pSV1-4L_0004 + pSV1-5L_0014	pSVM-mc	2-step timer *ecf28* Pecf32
pSVM-mc_118	pSV1-1L_0018 + pSV1-2L_0007 + pJM1-3R_002 + pSV1-4L_0004 + pSV1-5L_0015	pSVM-mc	2-step timer *ecf32* Pecf28
pSVM-mc_120	pSV1-1L_0016 + pSV1-2L_0007 + pJM1-3R_003 + pSV1-4L_0004 + pSV1-5L_0016	pSVM-mc	2-step timer *ecf28* neg. control
pSVM-mc_122	pSV1-1L_0018 + pSV1-2L_0007 + pJM1-3R_002 + pSV1-4L_0004 + pSV1-5L_0017	pSVM-mc	2-step timer *ecf32* neg. control
pSVM-mc_133	pSV1-1L_0012 + pSV1-2L_0007 + pSV1-3R_0012 + pSV1-4L_0004 + pSV0-15_026	pSVM-mc	ECF14/AS14-switch
pSVM-mc_134	pSV1-1L_0029 + pSV1-2L_0007 + pSV1-3R_0013 + pSV1-4L_0004 + pSV0-15_027	pSVM-mc	ECF15/AS15-switch
pSVM-mc_135	pSV1-1L_0013 + pSV1-2L_0007 + pSV1-3R_0014 + pSV1-4L_0004 + pSV0-15_028	pSVM-mc	ECF16/AS16-switch

pSVM-mc_136	pSV1-1L_0030 + pSV1-2L_0007 + pSV1-3R_0015 + pSV1-4L_0004 + pSV0-15_039	pSVM-mc	ECF17/AS17-switch
pSVM-mc_137	pSV1-1L_0014 + pSV1-2L_0007 + pSV1-3R_0016 + pSV1-4L_0004 + pSV0-15_029	pSVM-mc	ECF20/AS20-switch
pSVM-mc_138	pSV1-1L_0031 + pSV1-2L_0007 + pSV1-3R_0017 + pSV1-4L_0004 + pSV0-15_030	pSVM-mc	ECF22/AS22-switch
pSVM-mc_139	pSV1-1L_0015 + pSV1-2L_0007 + pSV1-3R_0018 + pSV1-4L_0004 + pSV0-15_040	pSVM-mc	ECF26/AS26-switch
pSVM-mc_140	pSV1-1L_0032 + pSV1-2L_0007 + pSV1-3R_0019 + pSV1-4L_0004 + pSV0-15_031	pSVM-mc	ECF27/AS27-switch
pSVM-mc_141	pSV1-1L_0016 + pSV1-2L_0007 + pJM1-3R_002 + pSV1-4L_0004 + pSV0-15_041	pSVM-mc	ECF28/AS28-switch
pSVM-mc_142	pSV1-1L_0017 + pSV1-2L_0007 + pSV1-3R_020 + pSV1-4L_0004 + pSV0-15_032	pSVM-mc	ECF31/AS31-switch
pSVM-mc_143	pSV1-1L_0019 + pSV1-2L_0007 + pJM1-3R_004 + pSV1-4L_0004 + pSV0-15_042	pSVM-mc	ECF34/AS34-switch
pSVM-mc_144	pSV1-1L_0033 + pSV1-2L_0007 + pSV1-3R_021 + pSV1-4L_0004 + pSV0-15_033	pSVM-mc	ECF37/AS37-switch
pSVM-mc_145	pSV1-1L_0034 + pSV1-2L_0007 + pSV1-3R_0022 + pSV1-4L_0004 + pSV0-15_034	pSVM-mc	ECF38/AS38-switch
pSVM-mc_146	pSV1-1L_0012 + pSV1-2L_0007 + pSV1-3R_0012 + pSV1-4L_0004	pSVM-mc	ECF14-switch
pSVM-mc_147	pSV1-1L_0029 + pSV1-2L_0007 + pSV1-3R_0013 + pSV1-4L_0004	pSVM-mc	ECF15-switch
pSVM-mc_148	pSV1-1L_0013 + pSV1-2L_0007 + pSV1-3R_0014 + pSV1-4L_0004	pSVM-mc	ECF16-switch
pSVM-mc_149	pSV1-1L_0030 + pSV1-2L_0007 + pSV1-3R_0015 + pSV1-4L_0004	pSVM-mc	ECF17-switch
pSVM-mc_150	pSV1-1L_0014 + pSV1-2L_0007 + pSV1-3R_0016 + pSV1-4L_0004	pSVM-mc	ECF20-switch
pSVM-mc_151	pSV1-1L_0031 + pSV1-2L_0007 + pSV1-3R_0017 + pSV1-4L_0004	pSVM-mc	ECF22-switch
pSVM-mc_152	pSV1-1L_0015 + pSV1-2L_0007 + pSV1-3R_0018 + pSV1-4L_0004	pSVM-mc	ECF26-switch
pSVM-mc_153	pSV1-1L_0032 + pSV1-2L_0007 + pSV1-3R_0019 + pSV1-4L_0004	pSVM-mc	ECF27-switch
pSVM-mc_154	pSV1-1L_0017 + pSV1-2L_0007 + pSV1-3R_020 + pSV1-4L_0004	pSVM-mc	ECF31-switch
pSVM-mc_155	pSV1-1L_0019 + pSV1-2L_0007 + pJM1-3R_004 + pSV1-4L_0004	pSVM-mc	ECF34-switch
pSVM-mc_156	pSV1-1L_0033 + pSV1-2L_0007 + pSV1-3R_021 + pSV1-4L_0004	pSVM-mc	ECF37-switch
pSVM-mc_157	pSV1-1L_0034 + pSV1-2L_0007 + pSV1-3R_0022 + pSV1-4L_0004	pSVM-mc	ECF38-switch
pSVM-mc_180	pSV1-1L_0006	pSVM-mc	P_{tet} *lux*

pSVM-mc_182	pSV1-1L_0011 + pSV1-2L_0007 + pSV1-3R_0011 + pSV1-4L_0004	pSVM-mc	ECF11-switch
pSVM-mc_183	pSV1-1L_0011 + pSV1-2L_0007 + pSV1-3R_0011 + pSV1-4L_0004 + pSV0-15_025	pSVM-mc	ECF11/AS11-switch
pSVM-mc_184	pSV1-1L_0011 + pSV1-2L_0007 + pSV1-3R_0011 + pSV1-4L_0004 + pAD1-5L_0034	pSVM-mc	ECF11/AS11 t1-switch
pSVM-mc_185	pSV1-1L_0011 + pSV1-2L_0007 + pSV1-3R_0011 + pSV1-4L_0004 + pAD1-5L_0035	pSVM-mc	ECF11/AS11 t2-switch
pSVM-mc_205	pSV1-1L_0016 + pICH54022 + pSV1-3L_0034	pSVM-mc	P_{BAD} *ecf28* du2 du15 *lux*
pSVM-mc_216	du1 + pSV1-2L_0007 + pSV1-3R_0011 + pSV1-4L_0004	pSVM-mc	Pecf11-*luxCDABE* reporter
pSVM-mc_217	du1 + pSV1-2L_0007 + pSV1-3R_0012 + pSV1-4L_0004	pSVM-mc	Pecf12-*luxCDABE* reporter
pSVM-mc_218	du1 + pSV1-2L_0007 + pSV1-3R_0013 + pSV1-4L_0004	pSVM-mc	Pecf15-*luxCDABE* reporter
pSVM-mc_219	du1 + pSV1-2L_0007 + pSV1-3R_0014 + pSV1-4L_0004	pSVM-mc	Pecf16-*luxCDABE* reporter
pSVM-mc_220	du1 + pSV1-2L_0007 + pSV1-3R_0015 + pSV1-4L_0004	pSVM-mc	Pecf17-*luxCDABE* reporter
pSVM-mc_221	du1 + pSV1-2L_0007 + pSV1-3R_0016 + pSV1-4L_0004	pSVM-mc	Pecf20-*luxCDABE* reporter
pSVM-mc_222	du1 + pSV1-2L_0007 + pSV1-3R_0017 + pSV1-4L_0004	pSVM-mc	Pecf22-*luxCDABE* reporter
pSVM-mc_223	du1 + pSV1-2L_0007 + pSV1-3R_0018 + pSV1-4L_0004	pSVM-mc	Pecf26-*luxCDABE* reporter
pSVM-mc_224	du1 + pSV1-2L_0007 + pSV1-3R_0019 + pSV1-4L_0004	pSVM-mc	Pecf27-*luxCDABE* reporter
pSVM-mc_225	du1 + pSV1-2L_0007 + pJM1-3R_002 + pSV1-4L_0004	pSVM-mc	Pecf19-*luxCDABE* reporter
pSVM-mc_226	du1 + pSV1-2L_0007 + pSV1-3R_0020 + pSV1-4L_0004	pSVM-mc	Pecf31-*luxCDABE* reporter
pSVM-mc_227	du1 + pSV1-2L_0007 + pJM1-3R_004 + pSV1-4L_0004	pSVM-mc	Pecf18-*luxCDABE* reporter
pSVM-mc_228	du1 + pSV1-2L_0007 + pSV1-3R_0021 + pSV1-4L_0004	pSVM-mc	Pecf39-*luxCDABE* reporter
pSVM-mc_229	du1 + pSV1-2L_0007 + pSV1-3R_0022 + pSV1-4L_0004	pSVM-mc	Pecf38-*luxCDABE* reporter
pSVM-mc_263	pSV1-1L_0140	pSVM-mc	P_{BAD}-*lux* (RBS st3)
pSVM-mc_264	pSV1-1L_0141	pSVM-mc	P_{BAD}-*lux* (RBS st4)
pSVM-mc_265	pSV1-1L_0142	pSVM-mc	P_{BAD}-*lux* (RBS st5)
pSVM-mc_266	pSV1-1L_0143	pSVM-mc	P_{BAD}-*lux* (RBS st7)
pSVM-mc_267	pSV1-1L_0144	pSVM-mc	P_{BAD}-*lux* (RBS st11)
pSVM-mc_268	pSV1-1L_0145	pSVM-mc	P_{BAD}-*lux* (RBS wk2)
pSVM-mc_269	pSV1-1L_0146	pSVM-mc	P_{BAD}-*lux* (RBS wk4)
pSVM-mc_270	pSV1-1L_0147	pSVM-mc	P_{BAD}-*lux* (RBS wk5)
pSVM-mc_271	pSV1-1L_0148	pSVM-mc	P_{BAD}-*lux* (RBS wk6)
pSVM-mc_272	pSV1-1L_0149	pSVM-mc	P_{BAD}-*lux* (RBS wk7)
pSVM-mc_274	pSV1-1L_0151	pSVM-mc	P_{BAD}-*lux* (RBS wk11)
pSVM-mc_294	du1 + pSV1-2L_0007 + pSV1-3R_0045 + pSV1-4L_0004	pSVM-mc	Pecf12-*ccdB*

pSVM-mc_297	du1 + pSV1-2L_0007 + pJM1-3R_0048 + pSV1-4L_0004	pSVM-mc	Pecf19-*ccdB*
pSVM-mc_298	du1 + pSV1-2L_0007 + pJM1-3R_0049 + pSV1-4L_0004	pSVM-mc	Pecf18-*ccdB*
pSVM-mc_299	du1 + pSV1-2L_0007 + pSV1-3R_0050 + pSV1-4L_0004	pSVM-mc	Pecf39-*ccdB*

Table 9.5. Level M parts and synthetic circuits. CRIMoClo and MoClo-encoded Level M parts and synthetic circuits. The genetic constructs are listed in alphabetical order. Internal name abbreviations: (pSV) generated by Stefano Vecchione; (pAD) generated by Angelika Diehl, (pJM) generated by Julia Manning**.** The internal names of the level 1 parts used as well as the original names of the CRIMoClo and MoClo destination vectors, in which the parts are encoded, and a description of the constructs is indicated.

Level P synthetic circuits			
Internal name	Donor	Destination vector	Description
pSV056	pSVM-mc_182	pSV016	ECF11-switch for chromosomal int.
pSV057	pSVM-mc_146	pSV016	ECF14-switch for chromosomal int.
pSV058	pSVM-mc_147	pSV016	ECF15-switch for chromosomal int.
pSV059	pSVM-mc_148	pSV016	ECF16-switch for chromosomal int.
pSV060	pSVM-mc_149	pSV016	ECF17-switch for chromosomal int.
pSV061	pSVM-mc_150	pSV016	ECF20-switch for chromosomal int.
pSV062	pSVM-mc_151	pSV016	ECF22-switch for chromosomal int.
pSV063	pSVM-mc_152	pSV016	ECF26-switch for chromosomal int.
pSV064	pSVM-mc_153	pSV016	ECF27-switch for chromosomal int.
pSV065	pSVM-mc_111	pSV016	ECF28-switch for chromosomal int.
pSV066	pSVM-mc_154	pSV016	ECF31-switch for chromosomal int.
pSV067	pSVM-mc_112	pSV016	ECF32-switch for chromosomal int.
pSV068	pSVM-mc_155	pSV016	ECF34-switch for chromosomal int.
pSV069	pSVM-mc_156	pSV016	ECF37-switch for chromosomal int.
pSV070	pSVM-mc_157	pSV016	ECF38-switch for chromosomal int.
pSV071	pSVM-mc_180	pSV004	P_{tet} *lux (for chromosomal int.)*
pSVPmc_009	pSVM-1_076 + pSVM6_018	pICH82094	3-step timer *ecf28 ecf32* Pecf34
pSVPmc_010	pSVM-1_076 + pSVM6_020	pICH82094	3-step timer *ecf28 ecf32* neg. control
pSVPmc_011	pSVM-1_078 + pSVM6_019	pICH82094	3-step timer *ecf32 ecf28* Pecf34

pSVPmc_012	pSVM-1_078 + pSVM6_021	pICH82094	3-step timer *ecf32 ecf28* neg. control
pSVP-mc_025	pSVM-1_168 + pSVM-5_008	pICH82094	ECF14/AS14 t2-switch with fluorophores
pSVP-mc_026	pSVM-1_168 + pSVM-5_009	pICH82094	ECF14/AS14 t2-switch with fluorophores
pSVP-mc_027	pSVM-1_168 + pSVM-5_010	pICH82094	ECF14/AS14 t2-switch with fluorophores
pSVP-mc_028	pSV118	pICH82094	PL_{O-1} *lux*

Table 9.6. Level P synthetic circuits. CRIMoClo and MoClo-encoded Level P synthetic circuits. The genetic constructs are listed in alphabetical order. Internal name abbreviations: (pSV) generated by Stefano Vecchione. The internal names of the level M parts used as well as the original names of the CRIMoClo and MoClo destination vectors, in which the parts are encoded, and a description of the constructs is indicated.

Oligonucleotides		
Name	Nucleotide sequence (5' → 3')	Description
GF0006	AAATgaagacatGAGGACGGTACGCGACTG	LacI rev mismach 2
GF0007	AAATgaagacatCCTCATGGGAGAAAATAATAC	LacI fw mismach 3
GF0008	AAATgaagacatagtaTTATCCGCTCACAATTCC	LacI rev
GF0010	AAATGAAGACATAGTAGCCCAAAAAACGGGTATG	PBAD rev
GF0011	AAATgaagacataATGCGTAAAGGAGAAGAAC	Gfp mut3 fw
GF0012	AAATgaagacatGATCTCTCTTTTCGTTGG	Gfp mut3 rev mismach
GF0013	AAATgaagacatGATCACATGGTCCTTCTT	Gfp mut3 fw mismach
GF0014	AAATgaagacataagcAACAGGAGTCCAAGCTCA	Gfp mut3 rev
GF0019	AAATGAAGACGAGCTTCTCGGTACCAAATTCCAGAAAAGAGGCCTCCCGAA AGGGGGGCCTTTTTTCGTTTTGGTCCCGCTATGTCTTCTAAA	L3S2P21 fw
GF0020	TTTAGAAGACATAGCGGGACCAAAACGAAAAAAGGCCCCCCTTTCGGGAGG CCTCTTTTCTGGAATTTGGTACCGAGAAGCTCGTCTTCATTT	L3S2P21 rev
GF0021	AAATGAAGACGAGCTTCTCGGTACCAAATTCCAGAAAAGAGACGCTTTCGA GCGTCTTTTTTCGTTTTGGTCCCGCTATGTCTTCTAAA	L3S2P11 fw
GF0022	TTTAGAAGACATAGCGGGACCAAAACGAAAAAAGACGCTCGAAAGCGTCTC TTTTCTGGAATTTGGTACCGAGAAGCTCGTCTTCATTT	L3S2P11 rev
GF0025	GTTTAAACCACTTCGTGCAGAA	Level 1 seq fw
GF0026	CGTTTTTAATGTACTGGGGTGG	Level 1 seq rev
GF0027	GAGTCAGTGAGCGAGGAA	Level 0 seq fw
GF0028	GTGCCACCTGACGTCTAA	Level 0 seq rev
GF0032	AAATgaagacatAGGACAGCTCATGTTATATCC	LacI rev mismach 1

GF0033	AAATgaagacatTCCTCGGTATCGTCGTATC	LacI fw mismach 2
GF0034	AAATgaagacatGCGCTTATGACAACTTGA	PBAD FW fusion
GF0035	AAATgaagacatggagGTCTAGGGCGGCGGATTT	pLacI-term t1 fw
GF0037	AAATgaagacatCGAATTGTCGAGGGAAAG	pLacI_rev_fusion
GF0038	AAATgaagacatCCATCACGGAAAAAGGTT	PTet-TetR fw
GF0039	AAATgaagacatagtaTTCACTTTTCTCTATCACTG	PTet-TetR rev
GF0040	AAATgaagacataATGGTTTCCAAGGGCGAG	mCherry fw
GF0041	AAATgaagacataagcCCGACGTTATTTGTACAGC	mCherry rev
GF0042	AAATgaagacataATGAGCAAAGGTGAAGAAC	mVenus fw
GF0043	AAATgaagacataagcGTTTATTTATACAGTTCGTCCA	mVenus rev
GF0046	ggagGGGATACCAGAAACAAAAAAAGGGGAGCGGTTTCCCGCTCCCCTTCAATAATTGG	L3S3P00_araC_fw_ggag
GF0047	gcgcCCAATTATTGAAGGGGAGCGGGAAACCGCTCCCCTTTTTTTGTTTCTGGTATCCC	L3S3P00 araC rev
GF0048	ggagTTTTGTTATCAATAAAAAAGGCCCCCCGTTAGGGAGGCCTTATTGTTCGTC	L3S1P13 tetR fw
GF0049	atggGACGAACAATAAGGCCTCCCTAACGGGGGGCCTTTTTTATTGATAACAAAA	L3S1P13 tetR rev
GF0050	ttcgATAAATGTGAGCGGATAACATTGACATTGTGAGCGGATAACAAGATACTGAGCACATCAGCAGGACGCACTGACC	PL-lacO1 fw
GF0051	agtaGGTCAGTGCGTCCTGCTGATGTGCTCAGTATCTTGTTATCCGCTCACAATGTCAATGTTATCCGCTCACATTTAT	PL-lacO1 rev
GF0058	TACTAAAAATAAGGAGGAAAAAAA	RBS st8 fw
GF0059	CATTTTTTTTTCCTCCTTATTTTT	RBS st8 rev
GF0060	GCTTCCAATTATTGAAGGCCTCCCTAACGGGGGGCCTTTTTTTGTTTCTGGACTCCC	L3S3P21 fw
GF0061	AGCGGGGAGTCCAGAAACAAAAAAAGGCCCCCCGTTAGGGAGGCCTTCAATAATTGG	L3S3P21 rev
GF0062	GCTTCCAATTATTGAAGGCCGCTAACGCGGCCTTTTTTTGTTTCTGGACTCCC	L3S3P22 fw
GF0063	AGCGGGGAGTCCAGAAACAAAAAAAGGCCGCGTTAGCGGCCTTCAATAATTGG	L3S3P22 rev
GF0064	GCTTCTCGGTACCAAAGACGAACAATAAGACGCTGAAAAGCGTCTTTTTTCGTTTTGGTCC	L3S2P55 fw

GF0065	AGCGGGACCAAAACGAAAAAAGACGCTTTTCAGCGTCTTATTGTTCGTCTTTGGTACCGAG	L3S2P55 rev
GF0066	AAATgaagacatGCTATCTTCGGTATCGTCG	LacI fw2 mm GCTA
GF0067	AAATgaagacatTAGCTCATGTTATATCCCGCC	LacI rev2 mm TAGC
GF0068	AAATgaagacatATCTTCATGGGAGAAAATAA	lac I fw3 mm ATCT
GF0069	AAATgaagacatAGATGGTACGCGACTGGG	lac I rev3 mm AGAT
GF0070	GCTGGTGGCAGGATATATTG	cPCR lev M-P-L2lc fw
GF0071	GATAAACCTTTTCACGCCCT	cPCR lev M-P-L2lc rev
GF0078	GGTCTCATGCCTTGTCTTCTGTCAGACCAAGTTTACTC	Level P backbone fw
GF0079	TTCGTGTCCCTTGTCTTCGTCACAGCTTGTCTGTAAG	Level P backbone rev
GF0080	GAAGACAAGGGACACGAAGTGATCCGTTTAAAC	Level M fw Gibson
GF0081	CAGAAGACAAGGCATGAGACCACAGAGTGTTCAACCCC	Level M rev Gibson
GF0086	AAATGAAGACATGGAGAATAGGCGTATCACGAGG	PECF fw universal
GF0087	AAATGAAGACATAGTACGGAAATTGACAGGATCC	PECF rev universal
GF0088	AAATGAAGACATAATGATGAGCGATAGTCCG	ECF11_987 fw
GF0090	AAATgaagacataATGAATGATACCGCAGCAG	ECF14_1324 fw
GF0091	AAATgaagacataagcCTTATGCGCTTGTACCACC	ECF14_1324 rev
GF0092	AAATGAAGACATAATGACCCAGACCCCGAAAG	ECF15_436 fw
GF0093	AAATGAAGACATAAGCTCCTTATGCTGCGGTCATAC	ECF15_436 rev
GF0094	AAATGAAGACATAATGCAGCGTACCAATAGC	ECF16_3622 fw
GF0095	AAATGAAGACATAAGCAAGCTTGGATCCTTAACGATC	ECF16_3622 rev
GF0096	AAATgaagacataATGGCACGTGTTAGCGGTG	ECF17_1691 fw
GF0097	AAATgaagacataagcAAGCTTGGATCCTTAACGGG	ECF17_1691 rev
GF0098	AAATGAAGACATAATGAATGAAACCGATCCTGATC	ECF20_992 fw
GF0099	AAATGAAGACATAAGCTCCTTACGGTTTGCGACG	ECF20_992 rev
GF0100	AAATgaagacataATGCCGCAGCAGACCGAT	ECF22_4450 fw
GF0101	AAATgaagacataagcCCGCAAGCTTGGATCCTT	ECF22_4450 rev
GF0102	AAATGAAGACATAATGAATGATCTGGACCCG	ECF26_4464 fw
GF0103	AAATGAAGACATAAGCCCTTAGCTTTTTTCTTCCAGC	ECF26_4464 rev

GF0104	AAATGAAGACATAATGGCAGGCGGTGCAAG	ECF27_4265 fw
GF0105	AAATGAAGACATAAGCGATCCTTATGCGCGACCA	ECF27_4265 rev
GF0106	AAATGAAGACATAATGTTTGATAGCCTGCGC	ECF28_1088 fw
GF0107	AAATGAAGACATAAGCGATCTCAGTGGTGGTGGTG	ECF28_1088 rev
GF0108	AAATgaagacataATGGATACCCAAGAAGAACAG	ECF31_34 fw
GF0109	AAATgaagacataagcGCTTGGATCCTTATTCATCATC	ECF31_34 rev
GF0110	AAATGAAGACATAATGACCGAAATTCATCTGCA	ECF32_1122 fw
GF0111	AAATGAAGACATAAGCCCTTAGCTAAAAACGCTCTG	ECF32_1122 rev
GF0112	AAATgaagacataATGAATACCCGTACCCGT	ECF34_1384 fw
GF0113	AAATgaagacataagcGCTTGGATCCTTAAACACAGG	ECF34_1384 rev
GF0114	AAATgaagacataATGGCAAGCGATAAAGAACTGG	ECF37_2513 fw
GF0115	AAATgaagacataagcCAAGCTTGGATCCTTACAGGG	ECF37_2513 rev
GF0116	AAATgaagacataATGCCGGTTATTGCACCG	ECF38_1322 fw
GF0117	AAATgaagacataagcTCCTTATGCCGGTGCTTC	ECF38_1322 rev
GF0132	AAATGAAGACATAAGCCTTGGATCCTTACAGCTGTTC	ECF11_987 rev
GF0133	AAATGAAGACATGGAGTTCACCTCGAGGCCTC	PECF 11
GF0134	AAATGAAGACATAATGACTAAAAAAATTTCATTCA	Lux fw
GF0135	AAATGAAGACATCCTCATTCCGTCATGA	Lux rev
GF0136	AAATGAAGACATGAGGCCGTTGCAACGATT	Lux fw 2
GF0137	AAATGAAGACATATGACATCAGACTGGAAGAG	Lux rev 2
GF0138	AAATGAAGACATTCATGCCATTTCTTAAAG	Lux fw 3
GF0139	AAATGAAGACATAAGCTCAACTATCAAACGCTTCGG	Lux rev 3
GF0158	GCTTCTCTACCAAAGGTCA	Dummy 0-11 fw
GF0159	AGCGTGACCTTTGGTAGAG	Dummy 0-11 rev
GF0174	AAATgaagacatggagAGTCACGTGGCCTCCAGT	Du300 0-1 fw
GF0175	AAATgaagacatagtaCCACCACTCCGAGCGTTA	Du300 0-1 rev
GF0176	AAATgaagacaatactTAGTGGAGTTGGTGGCCC	Du300 0-2 fw
GF0177	AAATgaagacatatggGCAAAGCGGCCTTCACTC	Du300 0-2 rev
GF0178	AAATgaagacatccatAAGGAGATGCTGCTGCAGG	Du300 0-3 fw

GF0179	AAATgaagacatcattACTAAGCGTCCATCCGCA	Du300 0-3 rev
GF0180	AAATGAAGACATAATGTCTGGGAGTGAAGTGGCC	Du300 0-4 fw
GF0181	AAATGAAGACATACCTTACAGCGACCATCCGCTC	Du300 0-4 rev
GF0182	AAATGAAGACATAGGTACAGGAGTTATGGGGCCC	Du300 0-5 fw
GF0183	AAATGAAGACATCGAACAGAAGCGACCGTCCCCT	Du300 0-5 rev
GF0184	AAATGAAGACAATTCGGAGTGGGGTGGCCAACAA	Du300 0-6 fw
GF0185	AAATGAAGACATAAGCAATGTGAGCGACCCGCCA	Du300 0-6 rev
GF0186	AAATgaagacatgcttAGGAGTATGGTGGCCTGC	Du300 0-7 fw
GF0187	AAATgaagacaataccGAGCAGCGTCCTCCCACC	Du300 0-7 rev
GF0196	tactCGCACAGTGAGGGTC	Du15bp 0-2 fw
GF0197	atggGACCCTCACTGTGCG	Du15bp 0-2 rev
GF0198	ccatACTTGGTCGTTCGGC	Du15bp 0-3 fw
GF0199	cattGCCGAACGACCAAGT	Du15bp 0-3 rev
GF0200	AATGTCTACCGACACGAAC	Du15bp 0-4 fw
GF0201	ACCTGTTCGTGTCGGTAGA	Du15bp 0-4 rev
GF0202	AGGTTCCTACCAGAGGTCT	Du15bp 0-5 fw
GF0203	CGAAAGACCTCTGGTAGGA	Du15bp 0-5 rev
GF0204	TTCGAGTACTTTCAGAATC	Du15bp 0-6 fw
GF0205	AAGCGATTCTGAAAGTACT	Du15bp 0-6 rev
GF0206	gcttAAGTGACGCTTATTA	Du15bp 0-7 fw
GF0207	taccTAATAAGCGTCACTT	Du15bp 0-7 rev
GF0208	ggtaTGGACTTCGACATGG	Du15bp 0-8 fw
GF0209	agcgCCATGTCGAAGTCCA	Du15bp 0-8 rev
GF0210	GGAGACAACGTCACGACGA	Du15bp 0-14 fw
GF0211	CATTTCGTCGTGACGTTGT	Du15bp 0-14 rev
GF0212	AATGATCACCGACGCCGTT	Du15bp 0-15 fw
GF0213	AAGCAACGGCGTCGGTGAT	Du15bp 0-15 rev
GF0244	AAATgaagacataATGAACAAACACCCGGAT	As11_987 fw
GF0245	AAATgaagacataagcTCCTTACGGATACAGACC	As11_987 rev
GF0246	AAATgaagacataATGAGCGGTAGCCGTCC	As14_1324 fw
GF0247	AAATgaagacataagcAGGGATCCTTAACGCAGC	As14_1324 rev
GF0248	AAATgaagacataATGGCACAGAGCACCGAAC	As15_436 fw
GF0249	AAATgaagacataagcGATCCTTATTTACCGGTGCC	As15_436 rev
GF0250	AAATgaagacataATGATGAAAACCGATGAACT	As16_3622 fw
GF0251	AAATgaagacataagcCCTTACCAACGCAGCAG	As16_3622 rev
GF0252	AAATgaagacataATGACACCGGAACGTTTTG	As20_992 fw

GF0253	AAATgaagacataagcTCCTTACTGTTCTGCTTC	As20_992 rev
GF0254	AAATgaagacataATGGAACTGGACGATATG	As22_4450 fw
GF0255	AAATgaagacataagcGGATCCTTAATCACGCTG	As22_4450 rev
GF0256	AAATgaagacataATGACAGGTCATCCGGATG	As27_4265 fw
GF0257	AAATgaagacataagcGGATCCTTAGCTACGTGC	As27_4265 rev
GF0258	AAATgaagacataATGAACAAAGAAAAACTGAG	As31_34 fw
GF0259	AAATgaagacataagcTCCTTAACCACGTTTCAC	As31_34 rev
GF0260	AAATgaagacataATGAGCAGCGCACCGG	As37_2513 fw
GF0261	AAATgaagacataagcTCCGCCAAAACAGGGATC	As37_2513 rev
GF0262	AAATgaagacataATGTCCGATGGTAATGATG	As38_1322 fw
GF0263	AAATgaagacataagcTCCTTATGCACCGCTACC	As38_1322 rev
GF0264	GCTTCCAATTATTGAACACCCTTCGGGGTGTTTTTTTGTTTCTGGTCACCC	L3S3P11 fw
GF0265	AGCGGGGTGACCAGAAACAAAAAAACACCCCGAAGGGTGTTCAATAATTGG	L3S3P11 rev
GF0266	GCTTCCAATTATTCAAGACGCTTAACAGCGTCTTTTTTTGTTTCTGGTCACCC	L3S3P23 fw
GF0267	AGCGGGGTGACCAGAAACAAAAAAAGACGCTGTTAAGCGTCTTGAATAATTGG	L3S3P23 rev
GF0268	GCTTCTCGGTACCAAATTCCAGAAAAGACACCCGAAAGGGTGTTTTTTCGTTTTGGTCC	L3S2P24 fw
GF0269	AGCGGGACCAAAACGAAAAAACACCCTTTCGGGTGTCTTTTCTGGAATTTGGTACCGAG	L3S2P24 rev
GF0270	GCTTGACGAACAATAAGGCCGCAAATCGCGGCCTTTTTTATTGATAACAAAA	L3S1P22 fw
GF0271	AGCGTTTTGTTATCAATAAAAAAGGCCGCGATTTGCGGCCTTATTGTTCGTC	L3S1P22 rev
GF0272	GCTTTTTTCGAAAAAAGGCCTCCCAAATCGGGGGGCCTTTTTTTATAGCAACAAAA	L3S1P47 fw
GF0273	AGCGTTTTGTTGCTATAAAAAAAGGCCCCCCGATTTGGGAGGCCTTTTTTCGAAAA	L3S1P47 rev
GF0274	GCTTTTCCAGAAAAGACACCCTAACGGGTGTTTTTTCGTTTTTGGTCACCC	L3S3P45 fw

GF0275	AGCGGGGTGACCAAAAACGAAAAAACACCCGTTAGGGTGTCTTTTCTGGAA	L3S3P45 rev
GF0276	GCTTCTCGGTACCAAACCAATTATTGATGACGCTGAAAAGCGTCATTTTTTGTTTCGGTCC	L3S2P44 fw
GF0277	AGCGGGACCGAAACAAAAAATGACGCTTTTCAGCGTCATCAATAATTGGTTTGGTACCGAG	L3S2P44 rev
GF0278	GGAGCCCCTGGCGCCCCTT	du15 0-1 fw
GF0279	AGTAAAGGGGCGCCAGGGG	du15 0-1 rev
GF0349	GGAGGGGAGTCCAGAAACAAAAAAAGGCCGCGTTAGCGGCCTTCAATAATTGG	L3S3P22 RC 0-1 fw
GF0350	AGTACCAATTATTGAAGGCCGCTAACGCGGCCTTTTTTTGTTTCTGGACTCCC	L3S3P22 RC 0-1 rev
GF0353	TACTGGGCTCCTGGCCTGC	L3S3P31 RC 0-1 fw
GF0354	CATTGCAGGCCAGGAGCCC	L3S3P31 RC 0-1 rev
GF0363	AAATgaagacataATGACCATGCCGCTGCG	AS17_1691 fw
GF0364	AAATgaagacatAAGCGGATCCTTACAGGCTACGC	AS17_1691 rev
GF0365	AAATgaagacATAATGAAAGATATCGATGAAAGC	AS26_4464 fw
GF0366	AAATgaagacATAAGCGGATCCTTAACGCCAAT	AS26_4464 rev
GF0367	AAATgaagacATAATGGATGATCTGCAGTTT	AS28_1088 fw
GF0368	AAATgaagacATAAGCGGGATCCTTAGATAAAGGT	AS28_1088 rev
GF0369	AAATgaagacATAATGGGTCATGTTCATCCG	AS34_1384 fw
GF0370	AAATgaagacATAAGCGGGATCCTTAATTACCGC	AS34_1384 rev
GF0406	AAATgaagacATcgaaGCTACCAACCAGATCGC	As11_987 trunc1 rev
GF0407	AAATgaagacATcgaaAACCACATTATCATTCACCG	As11_987 trunc2 rev
GF0408	AAATgaagacATcgaaACCAACTTCATGAATACGAAAACC	AS14_1324 trunc2 rev
GF0409	AAATgaagacATcgaaATCACTATCACCACCACCAG	AS14_1324 trunc2 rev
GF0410	AAATgaagacATcgaaATGAACGGCTGCCAGCAG	AS17_1691 trunc1 rev
GF0411	AAATgaagacATcgaaCGGACTCAGACCGCTTGC	AS17_1691 trunc2 rev
GF0412	AAATgaagacATcgaaACCTGCATAACGGCTCC	AS20_992 trunc1 rev
GF0413	AAATgaagacATcgaaCTGCTGGGCTGCTG	AS20_992 trunc2 rev
GF0414	AAATgaagacATcgaaGCTGCTACGAACGG	AS22_4450 trunc rev
GF0415	AAATgaagacATcgaaGGTTGCCGGTGC	AS26_4464 trunc 1 rev

GF0416	AAATgaagacATcgaaGCTGGTCTGCGGAC	AS26_4464 trunc 2 rev
GF0417	AAATgaagacATcgaaACGACCCGGACCTGTG	AS27_4265 trunc1 rev
GF0418	AAATgaagacATcgaaCAGAGGCGGTTCTGCTG	AS27_4265 trunc2 rev
GF0419	AAATgaagacATcgaaCTGATGCTGGCTCAG	AS28_1088 trunc1 rev
GF0420	AAATgaagacATcgaaCAGCTGCTGACGC	AS28_1088 trunc2 rev
GF0421	AAATgaagacATcgaaTTTTTTACGATATTCTGCTTTC	AS31_34 trunc1 rev
GF0422	AAATgaagacATcgaaATTTGCGGTCTGATCG	AS31_34 trunc2 rev
GF0423	AAATgaagacATcgaaCTGGCTACCACGAACAC	AS34_1384 trunc1 rev
GF0424	AAATgaagacATcgaaGCTGCTTTCACGCAGAC	AS34_1384 trunc2 rev
GF0425	AAATgaagacATcgaaCGGTTCACCAGGCGGACG	AS37_2513 trunc1 rev
GF0426	AAATgaagacATcgaaTTTTTTACGTGCCAGTGCTGC	AS37_2513 trunc2 rev
GF0427	AAATgaagacATcgaaTTTACGTGCACGACGTG	AS38_1322 trunc rev
GF0431	ttcggtGATTACAAGGATGACGACGATAAGGACTATAAGGACGATGATGACAAG GACTACAAAGATGATGACGATAAATAG	Oligo-FLAG-tag fw
GF0432	aagcCTATTTATCGTCATCATCTTTGTAGTCCTTGTCATCATCGTCCTTATAGTC CTTATCGTCGTCATCCTTGTAATC	Oligo-FLAG-tag rev
GF0448	tactAAAAAAAAATAAGGAGGAA	RBS st3 fwd
GF0449	cattTTCCTCCTTATTTTTTTTT	RBS st3 rev
GF0450	tactAAAAAAAATAAGGAGGAAA	RBS st4 fwd
GF0451	cattTTTCCTCCTTATTTTTTTT	RBS st4 rev
GF0452	tactAAAAAAATAAGGAGGAAAA	RBS st5 fwd
GF0453	cattTTTTCCTCCTTATTTTTTT	RBS st5 rev
GF0454	tactAAAAATAAGGAGGAAAAAA	RBS st7 fwd
GF0455	cattTTTTTTCCTCCTTATTTTT	RBS st7 rev
GF0456	tactATAAGGAGGAAAAAAAAAA	RBS st11 fwd
GF0457	cattTTTTTTTTTTCCTCCTTAT	RBS st11 rev
GF0458	tactAAAAAAAAAGGAA	RBS wk2 fwd
GF0459	cattTTCCTTTTTTTTT	RBS wk2 rev
GF0460	tactAAAAAAAGGAAAA	RBS wk4 fwd
GF0461	cattTTTTCCTTTTTTT	RBS wk4 rev
GF0462	tactAAAAAAGGAAAAA	RBS wk5 fwd
GF0463	cattTTTTTCCTTTTTT	RBS wk5 rev
GF0464	tactAAAAAGGAAAAAA	RBS wk6 fwd
GF0465	cattTTTTTTCCTTTTT	RBS wk6 rev
GF0466	tactAAAAGGAAAAAAA	RBS wk7 fwd
GF0467	cattTTTTTTTCCTTTT	RBS wk7 rev
GF0470	tactAAAGGAAAAAAAAAA	RBS wk11 fwd
GF0471	cattTTTTTTTTTTCCTTT	RBS wk11 rev
GF0512	GGCATCACGGCAATATAC	P1 λ colony PCR primer

GF0513	TCTGGTCTGGTAGCAATG	P4 λ colony PCR primer
GF0514	ATCGCCTGTATGAACCTG	P1 P21 colony PCR primer
GF0515	TAGAACTACCACCTGACC	P4 P21 colony PCR primer
GF0516	GGAATCAATGCCTGAGTG	P1 HK022 colony PCR primer
GF0517	GGCATCAACAGCACATTC	P4 HK022 colony PCR primer
GF0518	CTGCTTGTGGTGGTGAAT	P1 ϕ80 colony PCR primer
GF0519	TAAGGCAAGACGATCAGG	P4 ϕ80 colony PCR primer
GF0521	ACGAGTATCGAGATGGCA	P3 colony PCR primer
GF0524	TCATGTTTGACAGCTTATCAC	Lt3 terminator fw
GF0525	GAAGTTCCTATACTTTCTAGAGAATAGGAACTTCGGAATAGGAACTGCCATG GGACAAAATTGAAATC	pAH68 rev + FRT
GF0526	GAAGTTCCTATACTTTCTAGAGAATAGGAACTTCGGAATAGGAACTACCGAC CGATACAATGATG	pAH81 rev + FRT
GF0527	GATTTTTCTCTTCTTGCGCT	pAH120-1 rev point mutation (delete bpiI site)
GF0528	ACCTTGCGCTAATGCTCTG	pAH120-2 fw
GF0529	GAAGTTCCTATACTTTCTAGAGAATAGGAACTTCGGAATAGGAACTGCCATG GCATCACAGTATC	pAH120-2 rev + FRT
GF0530	GAAGTTCCTATACTTTCTAGAGAATAGGAACTTCGGAATAGGAACTCCCGTG CGAATCAGAAAT	pAH153 rev + FRT
GF0531	TAATTCCCATGTCAGCCG	R6K ori fw
GF0532	CAAGATCCGGCCACGATG	R6K ori rev
GF0533	ATTTAAATGGCGCGCCTTAC	chloramphenicol fw
GF0534	CTACCTGTGACGGAAGATC	chloramphenicol rev
GF0535	GAAGTTCCTATTCCGAAGTTCCTATTCTCTAGAAAGTATAGGAACTTCGTCTC CCCATGCGAGAGT	rgnB fw + FRT
GF0536	ACTGGCCACGCAAAAAGG	rgnB rev
GF0537	CACATTGCGGACGTTTTTAATG	MoClo M-P mcs+ori fw
GF0538	CTCTTAGGTTTACCCGCC	MoClo M-P mcs+ori rev
GF0539	CACTGATCAGTGATAAGCTGTCAAACATGACTCTTAGGTTTACCCGCCAATA TATCCTGT	bridging MCS+att
GF0540	AGGAACACTTAACGGCTGACATGGGAATTAGAAGTTCCTATACTTTCTAGAG AATAGGAACTTCG	bridging att+r6k
GF0541	GGCGTAAGGCGCGCCATTTAAATCAAGATCCGGCCACGATGCGTC	bridging R6K+cm
GF0542	CTAGAGAATAGGAACTTCGGAATAGGAACTTCCTACCTGTGACGGAAGATCA CTTCGC	Bridging CM+rgnb
GF0543	CCCAGTACATTAAAAACGTCCGCAATGTGACTGGCCACGCAAAAAGGCCATC C	bridging rgnB+MCS

GF0671	GGAGCGCGAGGCGGCGCCC	du15 0-12 fw
GF0671	GGAGCGCGAGGCGGCGCCC	du15 0-12 fw
GF0672	ATGGGGGCGCCGCCTCGCG	du15 0-12 rev
GF0672	ATGGGGGCGCCGCCTCGCG	du15 0-12 rev
GF0673	AATGCCGGGGGCGTTCCGC	du15 0-13 fw
GF0673	AATGCCGGGGGCGTTCCGC	du15 0-13 fw
GF0674	CGAAGCGGAACGCCCCCGG	du15 0-13 rev
GF0674	CGAAGCGGAACGCCCCCGG	du15 0-13 rev
GF0675	GGAGCCCGAACGCCCCGTA	du15 0-16 fw
GF0676	AGCGTACGGGGCGTTCGGG	du15 0-16 rev
GF0677	GGAGaagagtttgtagaaacgcaaaaaggccatccgtcaggatggccttctgcttaatttgatg	rrnB T2 RC in 0-1 fw
GF0677	GGAGAAGAGTTTGTAGAAACGCAAAAAGGCCATCCGTCAGGATGGCCTTCT GCTTAATTTGATG	du15 0-16 fw
GF0678	AGTAcatcaaattaagcagaaggccatcctgacggatggccttttgcgtttctacaaactctt	rrnB T2 RC in 0-1 rev
GF0678	AGTACATCAAATTAAGCAGAAGGCCATCCTGACGGATGGCCTTTTTGCGTTT CTACAAACTCTT	du15 0-16 rev
GF0679	GCTTCATCAAATAAAACGAAAGGCTCAGTCGAAAGACTGGGCCTTTCGTTTT ATCTGTTGTTTGTCGGTGAACGCTCTCCTGAGTAGGACAAATCTGCACATCA AATTAAGCAGAAGGCCATCCTGACGGATGGCCTTTTTGCGTTTCTACAAAC	rrnB T2 RC in 0-1 fw
GF0680	AAGAAGTTTGTAGAAACGCAAAAAGGCCATCCGTCAGGATGGCCTTCTGCTT AATTTGATGTGCAGATTTGTCCTACTCAGGAGAGCGTTCACCGACAAACAAC AGATAAAACGAAAGGCCCAGTCTTTCGACTGAGCCTTTCGTTTTATTTGATG	rrnB T2 RC in 0-1 rev
GF0805	CGCATCGTGGCCGGATCTTGACAGCTAAAACAATTCATCCAG	kanamycin fw + backbone overlap
GF0807	GTGATCTTCCGTCACAGGTAGGAAG	CRIMoClo backbone fw
GF0808	CTTCCTACCTGTGACGGAAGATCACCCTCACCCCAAAAATGGC	kanamycin rev + backbone overlap
GF0856	CGCATCGTGGCCGGATCTTGTCCGACGAATAGAGTAAC	gentamicin fw + backbone overlap
GF0858	CGCATCGTGGCCGGATCTTGACCTGATAGTTTGGCTGTGAGC	spectionomycin fw + backbone overlap
GF0945	ACTCTTCCTTTTTCAATATTATTGAAGC	CRIMoClo backbone fw KM promoter
GF0947	AATATTGAAAAAGGAAGAGTATGGGGGAAGCGGTGATC	spectionomycin rev + backbone overlap
GF0949	AATATTGAAAAAGGAAGAGTATGTTACGCAGCAGCAAC	gentamicin rev + backbone overlap
GF0971	AGCAACTTAAATAGCCTCTAAGG	P2 colony PCR primer
GF0998	AAATgaagacataATGCAGTTTAAGGTTTACAC	ccdb fw
GF0999	AAATgaagacataagcCTTAATTATATTCCCCAGAAC	ccdb rev

Table 9.7. Oligonucleotides used in this study.

9.2 Supplementary Figures

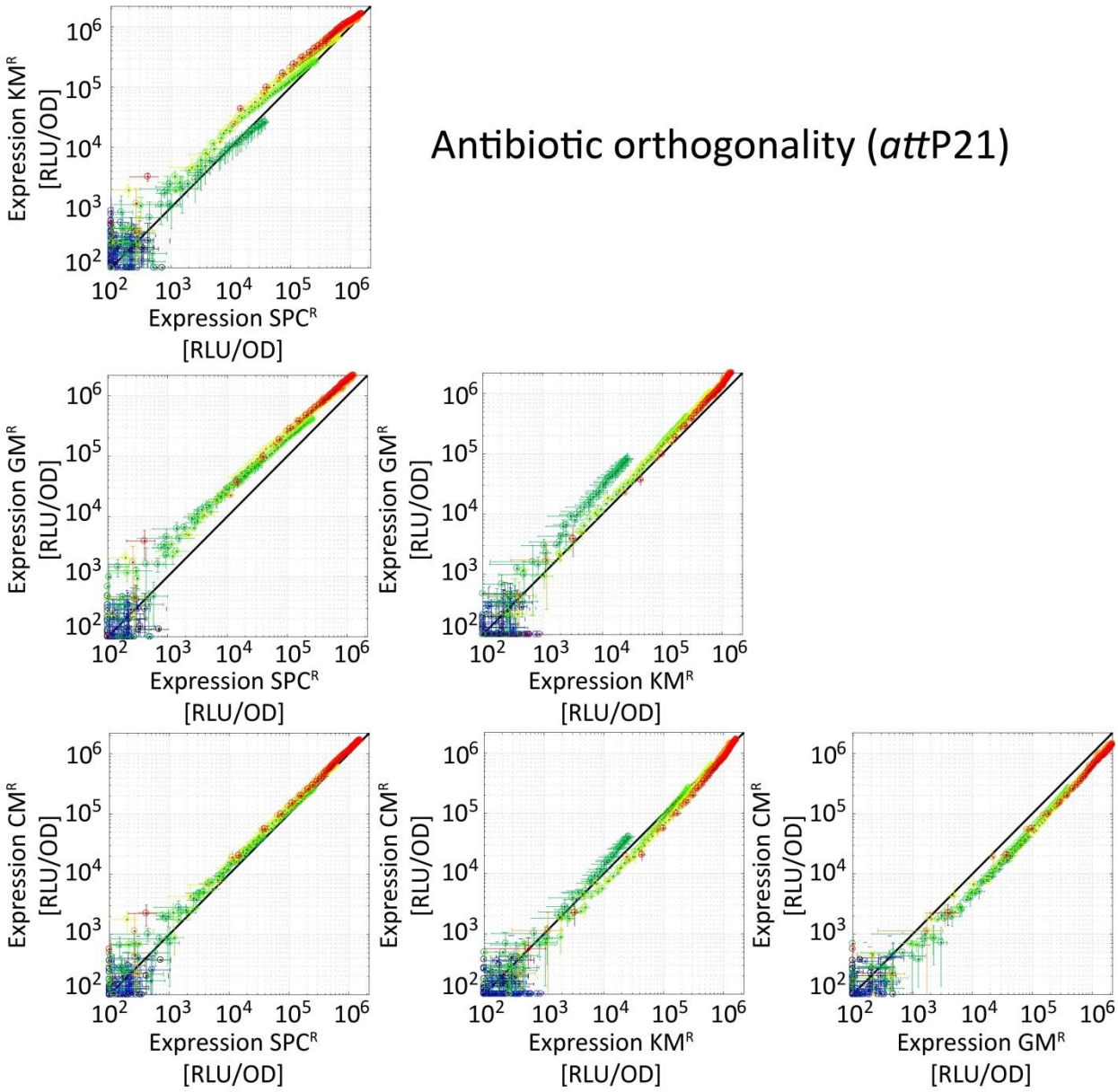

Figure 9.1. Antibiotic orthogonality CRIMoClo vectors (P21 *att* site). Orthogonality of reporter gene expression between resistance cassettes used for integration in the phage P21 *att* site. Correlation graphs between luciferase activities obtained from P_{BAD}-*lux* integrated into att_{P21}, using CRIMoClo plasmids with four indicated resistance cassettes (chloramphenicol, kanamycin, spectinomycin, gentamicin). All data indicate averages from at least two independent biological assays and error bars denote standard deviations.

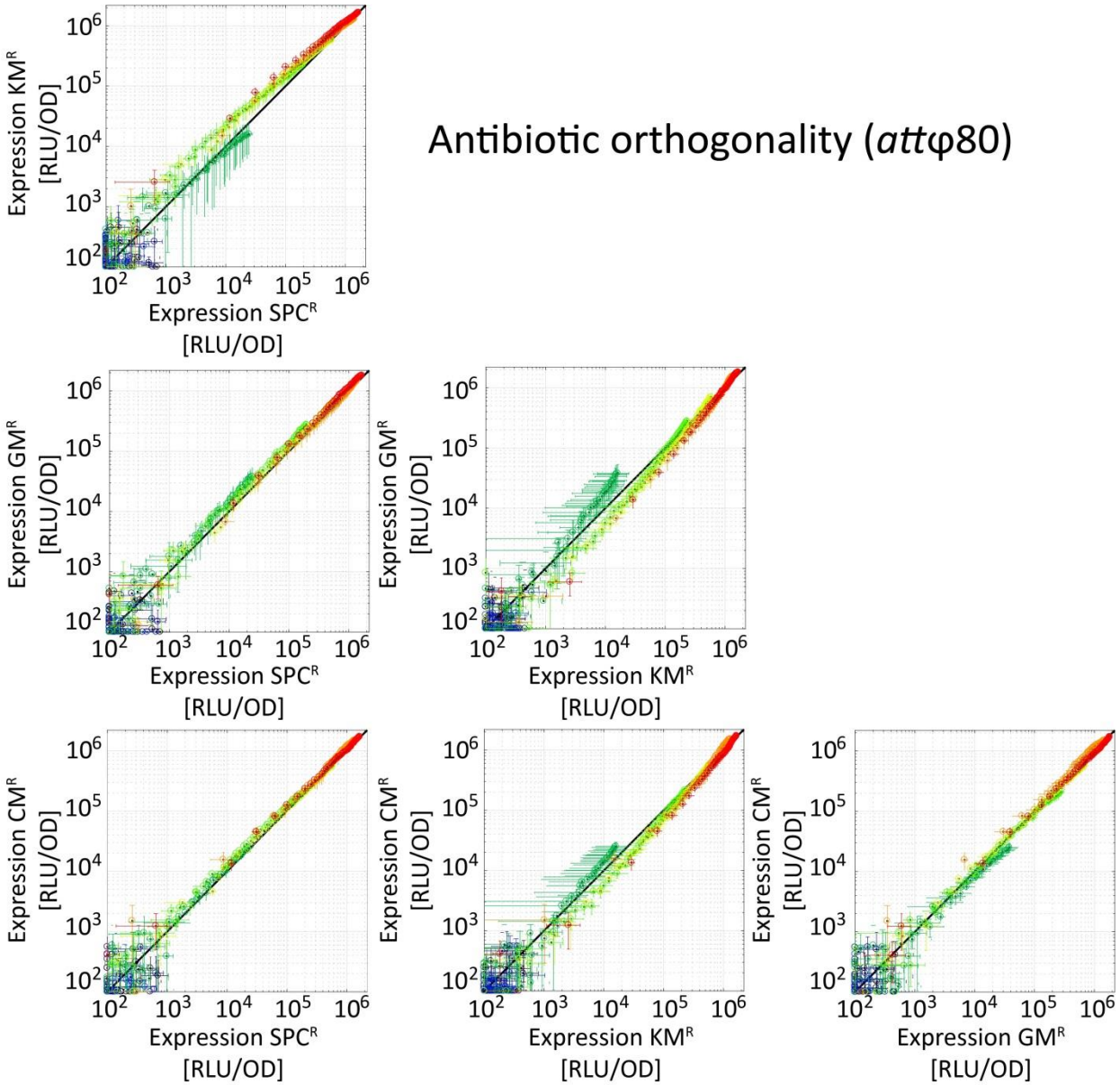

Figure 9.2. Antibiotic orthogonality CRIMoClo vectors (ϕ80 *att* site). Orthogonality of reporter gene expression between resistance cassettes used for integration in the phage ϕ80 *att* site. Correlation graphs between luciferase activities obtained from P_{BAD}-*lux* integrated into $att_{\phi 80}$, using CRIMoClo plasmids with four indicated resistance cassettes (chloramphenicol, kanamycin, spectinomycin, gentamicin). All data indicate averages from at least two independent biological assays and error bars denote standard deviations.

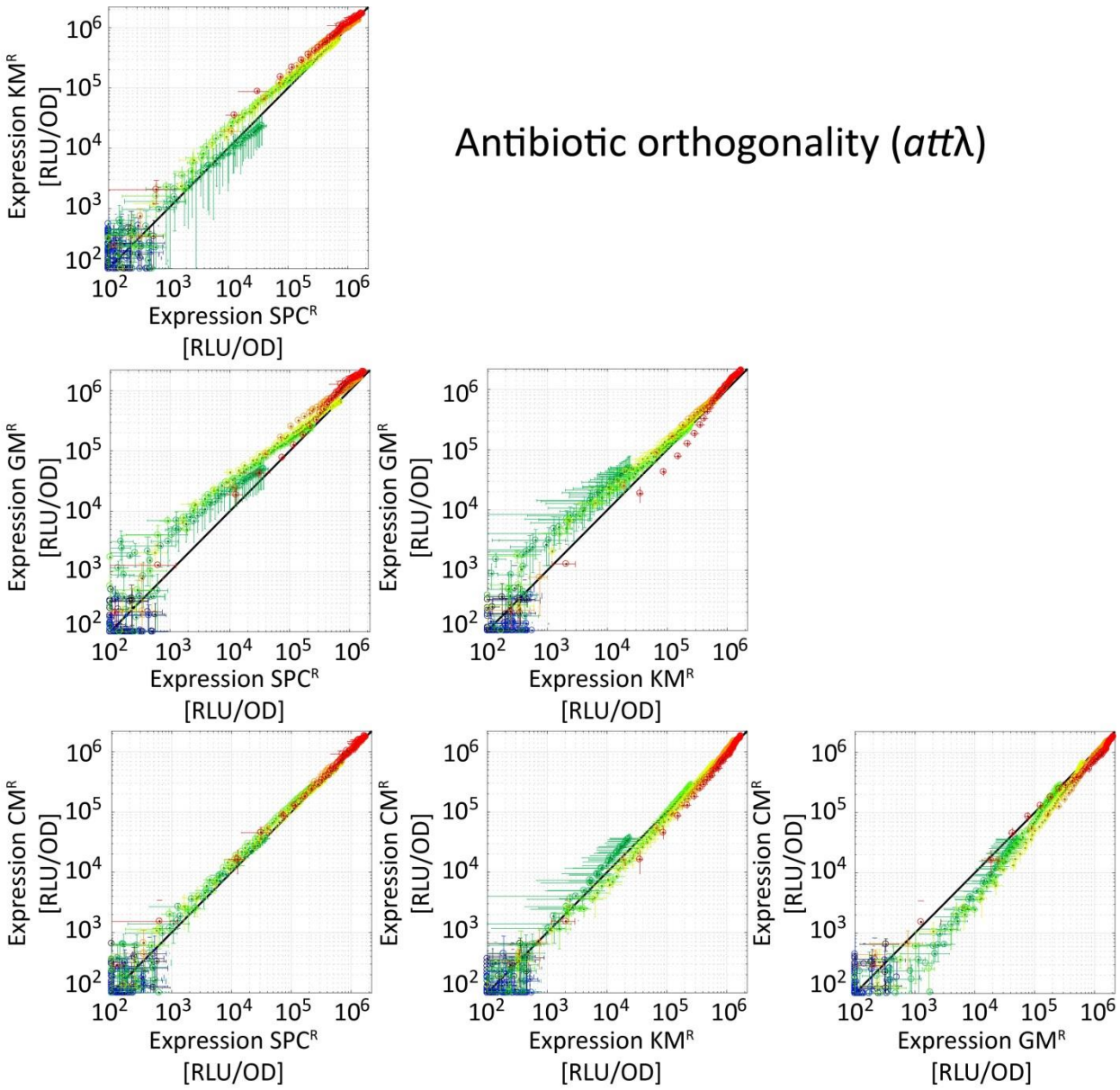

Figure 9.3. Antibiotic orthogonality CRIMoClo vectors (λ *att* site). Orthogonality of reporter gene expression between resistance cassettes used for integration in the phage λ *att* site. Correlation graphs between luciferase activities obtained from P_{BAD}-*lux* integrated into att_{λ}, using CRIMoClo plasmids with four indicated resistance cassettes (chloramphenicol, kanamycin, spectinomycin, gentamicin). All data indicate averages from at least two independent biological assays and error bars denote standard deviations.

9.3 List of Figures

9.4 List of Tables

9.5 List of abbreviations

Amp^R	Ampicillin resistance
ATc	Anhydrotetracycline
AS	Anti-σ
Cm^R	Chloramphenicol resistance
Ch. int.	Chromosomal integration
CPEC	Circular Polymerase Extension Cloning
CRIM	Conditional-replication, integration, modular
ECF σ	Extracytoplasmic function σ
Gm^R	Gentamicin resistance
Km^R	Kanamycin resistance
LCR	Ligase cycling Reaction
MoClo	Modular Cloning
Nal^R	Nalidixic acid resistance
OD	Optical density
Ori	Origin of replication
OE-PCR	Overlap extension polymerase chain reaction
PCR	Polymerase Chain Reaction
RFU	Relative fluorescent units
RLU	Relative luminescence units
RBS	Ribosome Binding Sequence
S/D	Shine-Dalgarno
Spc^R	Spectinomycin resistance
Str^R	Streptomycin resistance
TU	Transcription unit
TF	Transcriptional factor
TSS	Transformation and storage solution